

**Differential Proteome Analysis of Human Lung Epithelial Cells
Following Exposure to Aromatic Volatile Organic Compounds**

Dissertation
zur Erlangung des akademischen Grades
„doctor rerum naturalium“
(Dr. rer.nat.)
in der Wissenschaftsdisziplin „Ernährungswissenschaft/Toxikologie“

eingereicht an der
Mathematisch-Naturwissenschaftlichen Fakultät
der Universität Potsdam

von
Nora Mörbt

Potsdam, Juni 2010

This work is licensed under a Creative Commons License:
Attribution - Noncommercial - Share Alike 3.0 Germany
To view a copy of this license visit
<http://creativecommons.org/licenses/by-nc-sa/3.0/de/>

Published online at the
Institutional Repository of the University of Potsdam:
URL <http://opus.kobv.de/ubp/volltexte/2010/4925/>
URN <urn:nbn:de:kobv:517-opus-49257>
<http://nbn-resolving.org/urn:nbn:de:kobv:517-opus-49257>

Contents

List of Abbreviations	III
1 General Introduction	1
1.1 Volatile Organic Compounds	1
1.2 Bioactivation and Health Effects of Aromatic VOCs	3
1.3 Toxicoproteomics	5
1.4 Objectives	8
2 Methodology	10
2.1 Cell Culture	10
2.1.1 A549 Cell Line	10
2.1.2 Seeding on Transwell Inserts and Cell Exposure to Aromatic VOCs	11
2.1.3 Cell Harvesting and Preparation of Total Soluble Protein Fractions	12
2.2 Gas Chromatographic Analysis of VOC Atmospheres	13
2.3 Cytotoxicity Measurements	13
2.4 Proteomic Studies	14
2.4.1 SDS-PAGE	14
2.4.2 Two-dimensional Gel Electrophoresis (2-DE)	15
2.4.3 Differential Protein Phosphorylation	17
2.4.4 Quantitative Image Analysis	17
2.4.5 Western Blotting (Target Validation, Apoptosis)	18
2.4.6 Protein Identification	20
2.4.7 Detection of Styrene 7,8 Oxide Protein Adducts	20
2.5 Quantitative PCR	22
2.6 ROS Measurement	22
2.7 List of used Chemicals and Devices	22
3 Development of the Toxicoproteomics Approach for the VOC Lung Cell Model	27
3.1 Introduction	27
3.1.1 The A549 Cell Exposure Setup	27
3.1.2 Monitoring VOC Atmospheres	29
3.2 Results	30
3.2.1 Adaption of Existing Exposure Setup to Proteomics Approach	30
3.2.2 Proteome Map of the A549 Cell Line	31
3.2.3 Characterization of Applied VOC Atmospheres	33
3.3 Discussion	35
4 Toxicoproteomics of Styrene Exposure	38
4.1 Introduction	38
4.1.1 Styrene - Sources of Human Exposure	38
4.1.2 Toxicokinetics of Styrene	39
4.1.3 Toxicodynamics of Styrene	41
4.1.4 Effects of Styrene on Cellular Proteins	43
4.2 Results	44
4.2.1 Styrene Toxicity in the Cell Model	44

4.2.2	Differential Protein Expression in 2-DE	45
4.2.3	Styrene Exposure Modulates Oxidative Stress Proteins	47
4.2.4	Styrene Exposure May Stimulate an Inflammatory Process	49
4.2.5	Styrene Affects Abundance of Cell Death-Related Proteins	49
4.2.6	Styrene, Metabolic Changes and Protein Quality Control	50
4.2.7	Differential Phosphorylation Patterns in 2-DE	50
4.2.8	Validation of 2-DE Results on Protein and Transcript Level	54
4.2.9	Induction of Oxidative Stress Markers	57
4.2.10	Formation of Reactive Oxygen Species	58
4.2.11	Identification of Styrene Oxide Protein Adducts	59
4.3	Discussion	64
5	Toxicoproteomics of Mono- and 1,2-Dichlorobenzene Exposure	79
5.1	Introduction	79
5.1.1	Mono- and 1,2-Dichlorobenzene – Sources of Human Exposure	79
5.1.2	Toxicokinetics of Monochloro- and 1,2-Dichlorobenzene	80
5.1.3	Toxicodynamics of Monochloro- and 1,2-Dichlorobenzene	82
5.1.4	Effects of Chlorinated Benzenes on Proteins	84
5.2	Results	86
5.2.1	Toxicity of Monochloro- and 1,2-Dichlorobenzene in A549 Cells	86
5.2.2	Differential Protein Expression in 2D DIGE	86
5.2.3	Differential Phosphorylation Patterns in 2-DE	95
5.2.4	Validation of 2-DE Results	98
5.3	Discussion	99
6	Common Mechanisms of Aromatic VOCs on Cellular Protein Expression	109
7	Summary	116
	Zusammenfassung	118
	References	121
8	Appendix	i
	Publications and Conference Contributions	xii
	Erklärung zur Dissertation	xiii
	Danksagung	xiv
	Lebenslauf	xv

List of Abbreviations

1,2-DCB	1,2-Dichlorobenzene
1D	One-dimensional
2D	Two-dimensional
2-DE	Two dimensional electrophoresis
8-'OH-dG	8-hydroxydeoxyguanosine
aa	Amino acid
ACLY	ATP-citrate synthase
ACN	Acetonitrile
AGW	Arbeitsplatzgrenzwert
AKR	Aldo-keto reductase
ALDH3A1	Aldehyde dehydrogenase 3A1
amu	Atomic mass unit
ANX	Annexin
APS	Ammoniumperoxodisulfate
AR	Aldose reductase
Asp	Aspartic acid
BAT	Biologischer Arbeitsstoff-Toleranzwert
BLV	Binding limit value
BLVRA	Biliverdin reductase A
BSA	Bovine serum albumin
BTEX	Benzene, Toluene, Ethylbenzene, Xylene
C, Cys	Cysteine
CAPS	N-cyclohexyl-3-aminopropanesulfonic acid
CB	Monochlorobenzene
CBB	Coomassie brilliant blue
cDNA	Complementary desoxyribonucleic acid
CHAPS	3-[(3-Cholamidopropyl)dimethylammonio]-1-propanesulfonate
CLIC1	Chloride intracellular channel protein 1
COPD	Chronic obstructive pulmonary disease
CYP	Cytochrome P450
D	Aspartic acid
DCB	Dichlorobenzene
DCC	Dichlorocatechol
DCFH-DA	Dichlorofluorescein diacetate
DCP	Dichlorophenol
DDB1	DNA-damage binding protein 1
DDT	Dichlorodiphenyltrichloroethane
DIGE	Differential in gel electrophoresis
DJ-1	Protein DJ-1 (gene name PARK7)
DMF	Dimethylformamide
DMSO	Dimethyl sulfoxide
DNA	Desoxyribonucleic acid
dNTP	Desoxynucleotide triphosphate
DTE	Dithioerythrol
DTT	1,4-Dithiothreitol
E	Glutamic acid
EDTA	Ethylenediaminetetraacetic acid
EEF2	Elongation factor 2
EH	Epoxide hydrolase
EPA	Environmental Protection Agency (U.S.)
ESI	Electron spray ionization
EZR	Ezrin
FACS	Fluorescence activated cell sorting

FAD	Flavin adenine dinucleotide
FCS	Fetal calf serum
G6PD	Glucose-6-phosphate-1-dehydrogenase
GAPDH	Glyceraldehyde-3-phosphate dehydrogenase
GDI	GDP dissociation inhibitor
Glu	Glutamic acid
GSH	Glutathione (reduced form)
GSSG	Glutathione (oxidized form)
H, His	Histidine
HCCA	α -cyano-4-hydroxy cinnamic acid
HEPES	4-(2-hydroxyethyl)-1-piperazineethanesulfonic acid
HNRNPC	Heterogeneous nuclear ribonucleoprotein C
HO-1	Heme oxygenase 1
HRP	Horseradish peroxidase
HSP	Heat shock protein
IDH	Isocitrate dehydrogenase
IEF	Isoelectric focusing
I κ B- α	Inhibitory protein alpha
IL	Interleukin
IPG	Immobilized pH-gradient
IRES	Internal ribosome entry site
K	Lysine
kDa	Kilo Dalton
LC	Liquid chromatography
LDH	Lactate dehydrogenase
LMNB2	Lamin B2
Lys	Lysine
MAK	Maximum Work Place Level
MALDI	Matrix-assisted laser desorption ionization
MCP-1	Monocyte chemoattractant protein-1
MS	Mass spectrometry
MSN	Moesin
MW	Molecular weight
NAC	N-acetyl cysteine
NADPH	Nicotinamide adenine dinucleotide phosphate
NF- κ B	Nuclear factor kappa B
NIF3L1	NIF3-like protein 1
NL	Non linear pH-gradient
NM23-H1	Nucleoside diphosphate kinase A
NOEC	No observed effect concentration
NPM	Nucleophosmin
OSHA	Occupational Safety & Health Administration
PAGE	Polyacrylamide gel electrophoresis
PB-PK	Physiologically based pharmacokinetic model
PBS	Phosphate-buffered saline
PCBs	Polychlorinated biphenyls
PCNA	Proliferating cell nuclear antigen
PCR	Polymerase chain reaction
PDCD6IP	Programmed cell death 6-interacting protein
PDI	Protein disulfide isomerase
PEL	Permissible exposure limit
Pen/Strep	Penicillin/streptomycin
PGD	6-phosphogluconate dehydrogenase
PHB	Prohibitin
pI	Isoelectric point
PMPCB	Mitochondrial-processing peptidase subunit beta

ppb	Parts per billion
ppm	Parts per million
PPP	Pentose phosphate pathway
PRDX	Peroxiredoxin
PRMT1	Protein arginine N-methyltransferase 1
PTM	Posttranslational modification
RAB2A	Ras-related protein Rab-2A
RACK1	Nucleotide-binding protein subunit beta-2-like 1 (Receptor of activated protein kinase C1)
RKIP	Phosphatidylethanolamine-binding protein 1 (Raf-1 kinase inhibitor protein)
RNA	Ribonucleic acid
ROS	Reactive oxygen species
RPL5	60S ribosomal protein L5
rpm	Rounds per minute
RPMI	Cell culture medium, developed at Roswell Park Memorial Institute
RPS7	40S ribosomal protein 7
RPSA	40S ribosomal protein SA
RT	Room temperature
RT-PCR	Reverse transcriptase polymerase chain reaction
RUVBL2	RuvB-like 2
SARS	Seryl-tRNA synthetase
SDHA	Succinate dehydrogenase
SDS	Sodium dodecyl sulfate
Secys	Selenocysteine
SEM	Standard error of the mean
Ser	Serine
SO	Styrene 7,8 oxide
SOD	Superoxide dismutase
STRAP	Serine-threonine kinase receptor-associated protein
TALDO	Transaldolase
TBS-T	TRIS-buffered saline containing Tween 20
TCA	Trichloroacetic acid
TEMED	Tetramethylethylenediamine
Thr	Threonine
TNF α	Tumor necrosis factor alpha
TOF	Time of flight mass analyzer
TPT1	Translationally-controlled tumor protein
TRIS	Tris (hydroxymethyl)-aminomethan
TRK	Technische Richtkonzentration
TRR1	Thioredoxin reductase 1
Trx	Thioredoxin
TUBB	Tubulin beta chain
TVOC	Total volatile organic compounds
Tyr	Tyrosine
U	Selenocysteine
UGDH	UDP-glucose 6-dehydrogenase
VDAC2	Voltage-dependent anion-selective channel protein 2
v/v	Volume/Volume
Vh	Volt hours
VOC	Volatile organic compound
w/v	Weight/volume
WDR1	WD-repeat-containing protein 1
XIAP	X-linked inhibitor of apoptosis
XRCC5	ATP-dependent DNA helicase 2 subunit 2

1 *General Introduction*

Changes in life style, accompanied by prolonged times spent indoors and the widespread usage of products containing volatile organic compounds (VOC), have lead to a general human exposure to these chemicals in work places or homes being suspected to contribute to the growing incidence of environmental diseases over the last decades. Since especially the causal molecular mechanisms for the development of these disorders are not completely understood, the overall objective of this thesis was to investigate VOC-mediated molecular effects on human lung cells *in vitro* with a focus on altered protein expression. Besides others, the presented effects on cellular proteins may be involved in impaired health in VOC-exposed human beings.

In this introductory chapter, an overview will be given on human exposure to VOCs, their biotransformation, toxicity as well as the proposed underlying molecular mechanisms. In a further section, the used proteomic techniques will be introduced as powerful tools to identify molecular targets of chemical-induced cellular toxicity. Finally, the major objectives within the scope of this thesis will be summarized.

1.1 *Volatile Organic Compounds*

VOCs are aliphatic or aromatic hydrocarbons characterized as having a high vapor pressure such that, under normal conditions, a significant amount of the compound vaporizes and enters the atmosphere. In general, boiling points of these substances are in the range of 50-260°C. The overwhelming majority of the VOCs that is commonly found in occupational or non-occupational environments are terpenes, aldehydes and alkanes as well as monocyclic aromatic hydrocarbons such as benzene, ethylbenzene, toluene, xylene (collectively BTEX), styrene and chlorinated benzenes (Jia *et al.*, 2007; Kinney *et al.*, 2002). However, more recent studies observed a gradual shift in solvent use from aromatics to other solvents, typically alcohols (Hofmann *et al.*, 2008; Samoto *et al.*, 2006).

Classical anthropogenic sources of VOCs are motor vehicle exhausts, agricultural chemicals such as pesticides and emissions from chemical plants that produce these VOCs or related compounds. For an increasing number of volatile compounds, national authorities regularly specify the maximum exposure limits at work places in order to avoid health risks for workers. In the U.S., the Occupational Safety and Health Administration adopts the Permissible Exposure Limit (PEL); in Germany, the Arbeitsplatzgrenzwert (AGW) is assigned by the German Federal Ministry of Labor and Social Affairs. The AGW has been introduced in 2005 in order to define a new health-based occupational limit in contrast to the formerly used different values: MAK – Maximale Arbeitsplatzkonzentration, BAT – Biologischer Arbeitsstoff-Toleranzwert and TRK - Technische Richtkonzentration. In addition, the European Union presents binding limit values (BLV) for exceptionally toxic substances

becoming directly valid in the member states. A selection of current VOC exposure limits is presented in Table 1-1.

Table 1-1 Occupational exposure limitations for selected VOCs

VOC	AGW ^a	PEL-TWA ^d
Formaldehyde	0.3 ppm ^b	0.75 ppm
Toluene	50 ppm	200 ppm
Benzene	1 ppm ^c	1 ppm
Chlorobenzene	10 ppm	75 ppm
1,4-Dichlorobenzene	1 ppm	75 ppm
Styrene	20 ppm	100 ppm

^a Arbeitsplatzgrenzwert (AGW) values extracted from GESTIS Substance Database, <http://www.dguv.de/ifa/de/gestis/stoffdb/index.jsp>

^b Recommendation of former MAK (Maximale Arbeitsplatzkonzentration) -Commission

^c EU binding limit value (BLV) according to guideline 2004/37/EG

^d Permitted exposure limit – time-weighted average (PEL-TWA) for 8 h a day, 5 d a week, <http://www.osha.gov>

Not only work places but also consumer products (paints, cleaning agents, printer's ink, furniture, carpets) and building material may contain a high number of different VOCs (Cooke, 1991; Davis *et al.*, 2007; Kwon *et al.*, 2008; Samet *et al.*, 1987; Steinemann, 2009). During a monitoring campaign, the total volatile organic compound (TVOC) concentrations in German dwellings ranged between 33 and 1600 µg/m³ with a median of 289 µg/m³ (Hippelein, 2004) in contrast to outdoor air concentrations that are at least 2-5 times lower (Kinney *et al.*, 2002; Rehwagen *et al.*, 2003). In standard households in the U.S. or in Germany, single VOC concentrations up to 20 µg/m³ have been reported (Arif *et al.*, 2007; Herbarth *et al.*, 1998). For more information on human exposure to compounds studied in this thesis (styrene and chlorinated benzenes) see sections 4.1.1 and 5.1.1, respectively.

A study funded by the German Federal Environment Agency (UBA) assessed 2,663 datasets with more than 300,000 single measurements of VOC concentrations in occupational and non-occupational settings from 2002 to 2006. In this investigation, mean total volatile organic compound levels (TVOC) were found to be about 500 µg/m³. Aldehydes, alkanes and aromatics were the most abundant substance classes. The VOCs that were detected in at least 90% of indoor environments comprised toluene, m, p-xylene, 1-butanol, hexanal, propanal, nonanal, ethylbenzene, 1,2,4 trimethylbenzene, acetaldehyde, formaldehyde and limonene (Hofmann *et al.*, 2008).

Of note, the specific pattern of indoor VOCs changes over time with the development and the distribution of new VOC-containing products and the use of modern sampling and quantification techniques (Hofmann *et al.*, 2008). In older surveys using passive sampling in the 1980/90s, especially aromatic VOCs (~50% of TVOC) and alkanes (~26% of TVOC) had been detected in indoor environments. In contrast, the recent analysis yielded a much

broader spectrum of VOCs with four main substance classes: aldehydes (~17% of TVOC), esters of mono- or dihydric alcohols (~13% of TVOC), aromatics (~12% of TVOC) and terpenes (~11% of TVOC) (Hofmann *et al.*, 2008). Moreover, human activities like redecoration or smoking have a large impact on VOC concentrations in the indoor environment (Kinney *et al.*, 2002; Wallace *et al.*, 1987; Wieslander *et al.*, 1997a).

Stimulated by the increasing evidence of VOC-induced health disorders (see section 1.2) over the last decades, strategies have been developed to ameliorate indoor air quality in work places and homes. Strict threshold values for occupational exposure (see Table 1-1) have been adopted by national authorities and the amount of VOCs that may be added to consumer products has been limited. As an example, the former German MAK value for multiple VOCs has been diminished several times. Further, since 2004, the European Decopaint Directive 2004/42/EC limits the VOC-content in interior paints and vanishes as well as paints for automobile industry. Moreover, in order to avoid environmental contamination from chemical plants, VOCs and related compounds are in most cases produced in closed circuits. Fortunately, between 1990 and 2003, German atmospheric VOC-emissions that are to a significant part caused by automobile exhausts, decreased by 60% (UBA, 2005). As a result of all these efforts, a clear downward tendency for VOC concentrations in apartments has been reported (Hofmann *et al.*, 2008; Rehwagen *et al.*, 2003).

1.2 *Bioactivation and Health Effects of Aromatic VOCs*

The major route of human exposure to VOCs is via inhalation. Due to their lipophilic character, most VOCs are easily absorbed in the conducting zone of the lung (trachea, bronchi and bronchioles) and more importantly, through the epithelium consisting of type I and -II pneumocytes lining the gas exchanging alveoli (Altraja *et al.*, 2009). The overwhelming part (50-70%) of inhaled aromatic VOCs is retained in the alveoli while the residual compounds diffuse across the capillary endothelium into the pulmonary blood (Csanady *et al.*, 2003; Filser *et al.*, 1993; Fustinoni *et al.*, 1998; Heinrich-Ramm *et al.*, 2000).

Once absorbed, most aromatic VOCs are rapidly metabolized by human cells in order to form better water-soluble metabolites that subsequently may be excreted more efficiently via the bile, feces or urine (Heinrich-Ramm *et al.*, 2000). Especially the halogenated aromatic VOCs are strongly lipophilic with a certain capacity to concentrate in fat deposits throughout long-term exposures (Croute *et al.*, 2000). In general, the metabolism of VOCs is highly active in liver cells (supplied with VOCs via the blood stream) but was also detected in lung tissue (Guengerich, 1995; Sheets *et al.*, 2004). As a first step (so-called Phase I), cytochrome P450 (CYP) monooxygenase enzymes that are expressed in most lung cells e.g. bronchial and bronchiolar epithelium, Clara cells, type II pneumocytes, and alveolar macrophages activate various of VOCs to reactive metabolites such as epoxides that may

form adducts with cellular macromolecules such as DNA or proteins. During this oxidative metabolism, NADPH is consumed in a stoichiometric manner, diminishing the cell's reduction equivalents. In human pulmonary tissues, CYP1A1, 1B1, 2A6, 2A13, 2B6, 2E1, 2F1 and 3A5, 2S1, 4B1 have been detected. Less conclusive results have been obtained concerning CYP2C, 2D6 and 3A4 (Bieche *et al.*, 2007; Castell *et al.*, 2005; Zhang *et al.*, 2006). In general, human CYP 2E1 is the most active CYP in oxidizing low molecular weight compounds such as benzene and chlorinated benzenes. Furthermore, CYP1A1 and 1A2 showed relatively high enzymatic activities toward the lower chlorinated benzenes (1,2-dichlorobenzene, 1,4-dichlorobenzene, 1,2,4-trichlorobenzene) and CYP3A4 toward the higher chlorinated benzenes (1,2,3,5-tetrachlorobenzene, pentachlorobenzene) (Bogaards *et al.*, 1995). In addition, human lung cells also express Phase II (conjugation) enzymes such as epoxide hydrolase, UDP-glucuronyl transferase (e.g. UGT1A) and glutathione S-transferase (e.g. GST-P1), which largely detoxify the formed reactive Phase I metabolites (Castell *et al.*, 2005). VOCs are excreted mainly as conjugates with glycine, sulfuric acid, and glucuronic acid (Heinrich-Ramm *et al.*, 2000). For detailed information on the bioactivation of styrene and chlorinated benzenes, see section 4.1.2 and 5.1.2, respectively.

Toxic intermediates or conjugates of VOC metabolism have been related to environmental and occupational diseases. Organic solvents are well-known for their ability to interact with and to accumulate in biological membranes causing damage and alteration of function of integral membrane proteins (Escuder-Gilabert *et al.*, 2008; McDermott *et al.*, 2008; Tähti, 1992; Urban, 2004). Acute exposure to aromatic VOCs (upper mg range) causes symptoms like nausea, dizziness, vertigo and unconsciousness by a nonpolar narcosis mode of toxic action (Merz, 2004; Singer, 1990). In response to subacute exposure (lower mg range), irritation of mucous membranes such as of the nose, throat, eyes are reported as well as chesty coughs. Further, chronic exposure to aromatic VOCs has been linked to disorders of the central nervous system such as mental and neuropsychological disorders, motor incoordination but also hepatotoxicity, nephrotoxicity and different types of cancer in humans and laboratory animals (Gerin *et al.*, 1998; Merz, 2004).

Especially the “sick building syndrome” defined by WHO in 1982, and the “toxic encephalopathy”, that has been accepted as occupational disease in Germany in 1997, are in the focus of VOC-induced health effects (EPA, 1991; Merz, 2004). The „sick building syndrome“ describes situations in which building occupants experience acute health and comfort effects that appear to be linked to time spent in a building, but no specific illness or cause can be identified. Typical symptoms are irritation of eyes, nose, throat and the skin, headache, lack of concentration, nausea, fatigue, depression and sleeping disorders. In contrast, “toxic encephalopathy” has been observed predominantly among painters or automobile mechanics and has been directly linked to VOC exposure at their work places.

This disease is characterized by mental and neuropsychological disorders, headache, lack of concentration, nausea, fatigue, depression and sleeping disorders (Merz, 2004).

It has further been shown in epidemiologic studies that the long-term exposure at lower concentrations, as occurring indoors, as well as renovation activities can also add up in affecting the immune system, especially in susceptible groups like children (Herberth *et al.*, 2009; Lehmann *et al.*, 2001; Lehmann *et al.*, 2002a; Lehmann *et al.*, 2002b; Mendell, 2007). Elevated concentrations of VOCs in the indoor air have been shown to be associated with asthma and respiratory diseases of children (Diez *et al.*, 2000; Diez *et al.*, 2003; Rumchev *et al.*, 2004; Ware *et al.*, 1993) and adults (Pappas *et al.*, 2000; Wieslander *et al.*, 1997a). For more information on health effects induced by exposure to styrene and chlorinated benzenes see sections 4.1.3 and 5.1.3, respectively.

In vitro, a large diversity of aromatic compounds including benzene, mono- and 1,2-dichlorobenzene have been identified as inducers of glucose-related protein 78 (Croute *et al.*, 2002). One hypothesis is that VOCs interact with cellular proteins, lead to thiol oxidation, protein-protein disulfide bonding, and destabilize protein structures (Ait-Aissa *et al.*, 2000; Voellmy, 1996) what may be responsible for the induction of heat shock protein synthesis (Meyer *et al.*, 1995; Neuhaus-Steinmetz *et al.*, 1997). Further, cellular toxicity occurs when VOCs or their electrophilic metabolites form adducts with cellular proteins thereby disrupting protein structure and/or function, which secondarily causes damage to submembrane organelles, metabolic pathways, or cytological processes. Since many VOCs and their metabolites are electrophilic neurotoxicants, it has been assumed that protein adduct formation may also be a critical step in the neuropathogenic processes initiated by exposure to VOCs (Lopachin *et al.*, 2005). Up to now, VOC adduction has been identified predominantly for highly abundant proteins of body fluids such as hemoglobin and serum albumin. Further information on known interactions of VOCs with proteins will be given when introducing each of the used VOCs in sections 4.1.4 and 5.1.4.

1.3 Toxicoproteomics

In general, the functionality of a cell is defined predominantly by the proteins that are present together with their abundance. Although these proteins are based on mRNA precursors, post-translational modifications (PTMs) such as phosphorylation and environmental interactions make it especially for low abundance proteins impossible to predict abundance based on gene expression analysis alone (Hirsch *et al.*, 2004; Vlaanderen *et al.*, 2010). This is underlined by studies performed by Anderson *et al.*, 1997 and Tian *et al.*, 2004. Both research groups reported a rather moderate correlation coefficient of only 0.4-0.5 between mRNA and protein abundances in mammalian cells.

The total set of proteins expressed by a genome in a cell, tissue, or organism at a given time is defined as “proteome”, a term that was first used in 1994 (Wetmore *et al.*, 2004; Wilkins *et al.*, 1996) and that is a hybrid of the two terms “protein” and “genome”. In contrast to the genome, the proteome is highly variable over time, between cell types and in response to the environment. Thus, analyzing the changes (“differential expression”) in a proteome provides insights into the complex role proteins have in biological systems (Hirsch *et al.*, 2004; Vlaanderen *et al.*, 2010). When proteomic techniques are used for global protein measurements in toxicology testing and research this is called “toxicoproteomics”. This research field aims to improve mechanistic understanding of how specific exposures alter protein expression, protein behavior and response to cause injury and disease. Thus, one of the major tenets of toxicoproteomics is that specific patterns of protein changes can comprise a consistent “signature” of toxicity that is robust enough to be observed in spite of variations in biology and experimental design. However, specific descriptions of such toxicity signatures and so-called “biomarkers” are at an early stage in the field of toxicoproteomics (Merrick *et al.*, 2009). Nevertheless, proteomic investigations have been successfully used to study lung toxicity of compounds such as fuels (Witzmann *et al.*, 2007), formaldehyde (Yang *et al.*, 2005), 1-nitronaphthalene (Wheelock *et al.*, 2005), benzene and hydroquinone (Li *et al.*, 2006).

According to (Merrick *et al.*, 2009), there are several aims of (toxico)proteomic analyses: 1) to achieve maximal coverage of the proteome in each sample, 2) to complete analysis at high throughput, 3) to produce an accurate quantitative protein measurement, 4) to deliver data and interpretable results in a timely period, and 5) to use discovery-oriented, open platforms (Merrick *et al.*, 2009). Thereby, the focus of proteomics applications can range from global protein analysis via approaches like “shotgun proteomics” (MacCoss *et al.*, 2002; Wolters *et al.*, 2001) where researchers strive for maximum number of protein identifications to a more discrete level of protein analysis often termed “targeted proteomics” (Dongre *et al.*, 2001) using subproteomes (Cordwell *et al.*, 2000) such as organelles (Dreger, 2003) or signaling pathways (Ping, 2003; Wetmore *et al.*, 2004). However, the most often applied type of proteomic study is the so-called “expression proteomics” approach (Graves *et al.*, 2002). This strategy that was also used in the present thesis compares protein abundances between different conditions. Combined with bioinformatics and identification tools, the detected differentially expressed proteins may be related to distinct biochemical pathways and may be considered as candidate biomarkers for certain exposure effects (Gündel, 2009). Finally, the resulting differential protein pattern may indicate directions for more specific investigations (Hirsch *et al.*, 2004).

In this thesis, total soluble protein of A549 cell line was separated using a classical proteomic technique: the two-dimensional polyacrylamide gel electrophoresis. This high-

resolution protein separation technique was first reported in 1975 (Klose, 1975; O'Farrell, 1975; Scheele, 1975). It enables quantification of protein species following two-dimensional separation, first by charge using isoelectric focusing (IEF) and then by mass using SDS-PAGE. Despite the non-complete coverage of the proteome, the resolution of modern 2-DE techniques allows detection and quantification of up to 3,000 protein spots per gel, representing as many protein species. By their specific electrophoretic mobility and isoelectric point, they reveal information about posttranslational modifications, besides the mere identity of the protein itself, which can be missed by peptide-based "shotgun" approaches. Although 2D gel electrophoresis has biophysical limits that constrain resolution of proteins at the extremes of pH, hydrophobicity, and mass, it is still an extremely versatile separation technique that readily couples with mass spectrometry to form the most widely used proteomics platform by research laboratories (Berth *et al.*, 2007; Merrick *et al.*, 2009; Wetmore *et al.*, 2004).

A major challenge of proteomic analysis is the wide concentration range of proteins that exists in most tissues and that is often referred to as a "large dynamic range" that often exceeds 6 or 7 orders of magnitude. For example, albumin is very abundant at concentrations of mg/ml in serum while other bioactive proteins such as cytokines are found at pg/ml levels, creating a dynamic range of >100-fold (Wetmore *et al.*, 2004). This requires the development of sensitive technologies that can detect a wide range of proteins in samples from different origins. Besides classical staining methods like silver staining or colloidal Coomassie staining, fluorescent staining is often the most sensitive means of protein detection. A famous but costly method that was also applied in the present thesis is the 2D differential in gel electrophoresis (DIGE). Protein samples to be compared are labeled with one of the fluorescent cyanine dyes Cy2 (internal standard), Cy3 (control sample) or Cy5 (treated sample) before two-dimensional protein separation is performed. Labeled samples are mixed together and are analyzed on the same gel. This procedure minimizes spot editing errors from electronic alignment of different gels, since each dye (sample) is read at a different wavelength on the same gel (Merrick *et al.*, 2009; Vlaanderen *et al.*, 2010; Wetmore *et al.*, 2004). After warping (electronic alignment) of stained proteins in 2D gels by image analysis software, intensities of identical protein spots are compared among treatment groups and a ratio ("expression ratio") is calculated for each protein using specialized software with integrated statistical tests. In this thesis, the software package Delta 2D 3.6/4.0 has been used as it allows excellent data/image handling (Berth *et al.*, 2007).

Finally, differential expression analysis of a given exposure scenario provides a pattern of regulated protein species that have to be identified subsequently. A common method is to digest the protein (that was cut from the 2D gel) by proteases with highly reproducible cleavage sites e.g. trypsin and to identify the amino acid sequence of the

resulting peptides by mass spectrometry (MS). In this thesis, peptides were identified using two different mass spectrometers, either a MALDI (Matrix-assisted laser desorption ionization) ion source coupled to a time-of-flight (TOF) mass analyzer or a nano liquid chromatography (LC) system combined with an iontrap MS system. In contrast to the MALDI/TOF machine, the latter system consists of an electrospray ionization (ESI) source and a nano LC column providing further separation of applied peptides according to their physicochemical properties. Ultimate protein identification is obtained by correlating the MS data with sequence databases (for further details see section 2.4.6). A review on proteomic techniques and their application in lung disease was published by Hirsch *et al.*, 2004.

In recent years, more than 10,000 manuscripts that present results of proteomic assays have been published. However, many of these initial studies have not been accompanied by any validating analyses using an independent protein quantification method such as ELISA, Western blot, immunohistochemistry or functional assays (Merrick *et al.*, 2009). Since this validation step is essential to reduce the possibility that the initial finding was an artifact of the used technology, in this thesis validation experiments will be included.

1.4 Objectives

Although the adverse health effects of the acute exposure of lung tissue to volatile organic compounds (VOCs) have been characterized, only few data are available on the exact molecular causes of VOC-induced health effects. Therefore, International Union of Pure and Applied Chemistry (IUPAC) recommended further “studies on the issue of biochemical (e.g., protein/DNA adducts) and biological effect markers for VOC exposure” in order to improve the interpretation of induced health effects (Heinrich-Ramm *et al.*, 2000).

Cellular stress in response to VOCs is proposed to be triggered by different mechanisms of toxicity, among which impaired protein function seems to be a common link (Ait-Aissa *et al.*, 2000). Differential expression of single proteins has been reported but effects on complex protein networks (proteome) have not been investigated. However, this information is indispensable when trying to ascertain a mechanism for VOC action on the cellular level and establishing preventive strategies, especially for those working in industrial environments where VOC exposure is significant.

Thus, the overall objective of this thesis was the characterization of molecular effects of aromatic VOCs in a human lung cell model with a focus on the modulation of the cellular proteome at VOC concentrations comparable to exposure scenarios below current occupational limits.

For this study, the alveolar epithelial cell line A549 has been chosen as a famous *in vitro* model when studying lung cell toxicity of airborne contaminants. These cells possess various typical properties of alveolar epithelial type II cells, are competent of metabolizing

VOCs (see section 3.1.1) and emitting markers for inflammatory reactions (Fischäder *et al.*, 2008; Roder-Stolinski *et al.*, 2008a). A previously developed two phase (air/liquid) exposure system that had been successfully applied in the Department of Environmental Health of the Helmholtz-Centre for Environmental Research, Leipzig, allows the most direct exposure of A549 cells to VOCs. Using this model, the aromatic compounds monochlorobenzene, styrene, and m-xylene caused a modulated release of inflammatory mediator proteins such as interleukins 6 and 8 and monocyte attractant protein 1 (MCP-1), even at lower concentration ranges (100 and 10 $\mu\text{g}/\text{m}^3$) by activation of the NF- κB and the p38 MAP kinase pathways (Fischäder, 2006; Roder-Stolinski *et al.*, 2008a; Roder-Stolinski *et al.*, 2008b).

However, for the investigations carried out in this thesis, the two-phase model had to be modified according to the requirements of proteomic techniques. Subsequently this model should be used to characterize effects of the aromatic compounds styrene, monochlorobenzene and 1,2-dichlorobenzene that are typical air contaminants found in occupational but also non-occupational environments on the cellular proteome.

The specific research goals are introduced, results are presented and discussed in three different **chapters (3-5)** leading to a final conclusion on common mechanisms of proteotoxic effects of the tested aromatic VOCs (**Chapter 6**). Chapters are preceded by a section including all methods applied (**Chapter 2**).

In detail, the main objectives of this thesis include:

- Adaption of the available A549 air/liquid exposure setup to the proteomics approach (**Chapter 3**) involving:
 - the characterization of VOC partitioning between culture medium and gas phase,
 - the establishment of cell culture, exposure and proteomic techniques,
 - the creation of an A549 reference proteome map.
- Toxicoproteomics investigation using the modified exposure setup for styrene (**Chapter 4**) and chlorinated benzenes (**Chapter 5**), subdivided in:
 - the assessment of cell toxicity,
 - the detection of differential protein expression and phosphorylation at moderate VOC concentrations by two-dimensional gel electrophoresis (2-DE),
 - the validation of 2-DE results using independent methods,
 - the identification and characterization of styrene 7,8 oxide protein adducts.

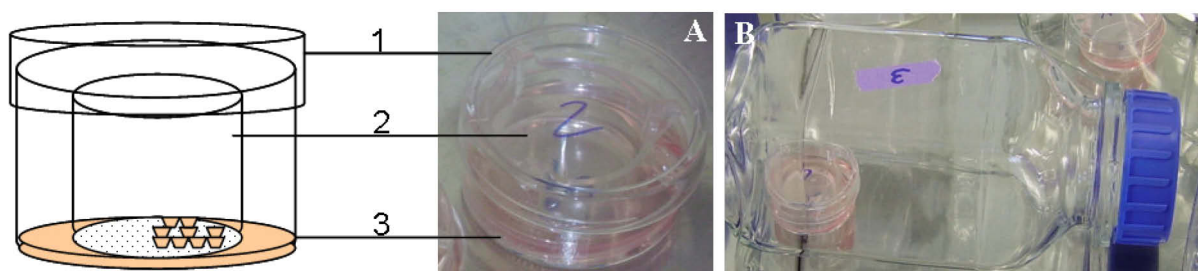
2 Methodology

2.1 Cell Culture

2.1.1 A549 Cell Line

Human lung epithelial cells (A549, ATCC No. CCL-185) were used for experiments on volatile organic compounds. A549 cells are type II human respiratory epithelial cells derived from a lung tumor explant of a 58 year old Caucasian male in 1972. Cells are growing adherently as a monolayer with a doubling time of approximately 48-60 h.

All cell culture work was performed with sterile tools and on sterile surfaces using a clean bench. Passages 3-20 were used for exposure experiments. Monthly mycoplasma testing as well as measurement of cellular viability for each cell splitting insured intact and healthy cell cultures. Cell culture and exposure was performed applying a modified procedure of G. Fischäder (Fischäder, 2006; Fischäder *et al.*, 2008). Using this model, cells attached to cell culture inserts were exposed apically to VOCs directly via the gas phase and were simultaneously nourished via the membrane pores of the transwell (Figure 2-1A, Figure 3-1). The transwell inserts used here contain an inorganic (aluminium oxide) Anopore membrane providing low protein binding and high solvent resistance.



1 Lid of petri dish. 2 Transwell insert with Anopore membrane (pores 0.2 μm) and attached cells nourished through membrane pores. 3 Petri dish filled with cell culture medium.

Figure 2-1 Cell culture model. A: Transwell inserts B: Cell exposure to VOC in flasks

Splitting. A549 cells were cultured in RPMI 1640 medium (including 5% heat-inactivated FCS) at 37°C and 5% CO₂ in cell culture flasks in a water-saturated atmosphere. After 2-3 days, cell culture media was removed and cells were washed with 5-10 ml of warm PBS. The solution was removed and 2 ml of a trypsin/EDTA solution were added to the cells. All cells were detached following an incubation for three minutes at 37°C. Cell detachment was verified using a light microscope. 2 ml of RPMI 1640 including 5% FCS and 1% Penicillin/Streptomycin (Pen/Strep) were added to the cell suspension in order to stop tryptic digestion of proteins. The suspension was centrifuged in a 15 ml tube for 5 min at 170 x g, the exhausted medium was removed and the cells were thoroughly resuspended in 1 ml of fresh pre-warmed RPMI including 5% FCS and 1% Pen/Strep. Afterwards, RPMI/5% FCS and 1% Pen/Strep was added to a final volume of 10 ml. Following resuspension, 20 μl of the

cell suspension were mixed with 20 μl of Trypan blue solution. After 5 min, 10 μl out of the mixture were used for cell counting using a hemocytometer plate. Cell numbers within four 1 mm^3 squares were recorded. The total number was divided by four and multiplied by two (because of dilution with Trypan blue), then multiplied by 10,000 to obtain the number of cells per milliliter. The percentage of dead (blue-stained) cells was calculated. For all cell experiments, starting cultures had a viability of at least 95%. The volume of cell suspension corresponding to one million cells was calculated and added together with 15 ml of pre-warmed RPMI medium including 5% FCS and 1% Pen/Strep in a prepared T75 flask.

2.1.2 Seeding on Transwell Inserts and Cell Exposure to Aromatic VOCs

Seeding. In the last passage prior to the exposure experiment, the cells were adapted to RPMI 1640 medium supplemented with only 2.5% FCS and 1% Pen/Strep for 2 days. Then, cells were detached and counted as described above. Transwell inserts (2.3 cm diameter, pore size 0.2 μm) containing a transparent Anopore membrane were used for culture and subsequent exposure to volatile organic compounds. For each transwell insert, one well of a 6-well cell culture plate was filled with 2.5 ml of pre-warmed RPMI/2.5% FCS and 1% Pen/Strep. The transwell insert was placed in the well using sterile tweezers, while taking care to avoid the formation of air bubbles below the membrane. The cell suspension was diluted to a concentration of 200,000 cells/ml. Within each insert, 1 ml of cell suspension was spread evenly over the surface of the membrane. Cells were allowed to attach to the membrane and form a monolayer (70% confluent) at 37°C for three consecutive days before starting exposure to the volatile organic compounds.

Cell exposure. Shortly before starting cell exposure, cells were checked under the light microscope for normal growth, cell shape and absence of contaminations. Upper and lower medium phase were discarded and the inserts were transferred to petri dishes (35x10 mm) containing 2 ml of fresh exposure medium, a mixture of one part CO_2 -independent cell culture medium including 2 mM N-acetyl-L-alanyl-L-glutamine and 1% BME amino acid cocktail and one part RPMI 1640, supplemented with 1% Pen/Strep. Three petri dishes (containing transwell inserts) were placed in each of the pre-warmed wide-necked glass flasks (600 ml volume). Following a 15 min cell adaption period, 10 μl of the respective serial dilution of the VOC stock solution (freshly dissolved in methanol) was applied to the inside of the neck of the glass flask avoiding contact to petri dishes (Table 2-1). As an example for the cell exposure to 10^{-1} g/m^3 VOC, the stock solution was diluted 1:100 with methanol and 10 μl were added to the flask. Immediately after adding the VOC, the glass flasks were tightly closed and incubated for 24 h (or 1 h for phosphorylation experiments) at 37°C (Figure 2-1B). Only in the highest of the applied concentrations, more than 10 μl of the original VOC and in addition 10 μl solvent were applied to the flasks (Table 2-1). For controls, 10 μl of the solvent were used. All samples were set up as triplicates. The use of closed

glass flasks ensured a sealed exposure system with a stable gaseous atmosphere, which was confirmed later experimentally by gas chromatographic measurements.

Table 2-1 Preparation scheme for VOC solutions

	Stock solution	10² g/m³	10¹ g/m³	Lower than 10¹ g/m³
Styrene	662 µl styrene + 338 µl methanol	66.2 µl styrene + 10 µl methanol	6.6 µl methanol + 10 µl stock	10 µl serial dil. stock
Chlorobenzene (CB)	544 µl CB + 456 µl methanol	54.4 µl CB + 10 µl methanol	5.4 µl methanol + 10 µl stock	10 µl serial dil. stock
1,2-Dichlorobenzene (1,2-DCB)	465 µl 1,2-DCB + 535 µl methanol	46.5 µl 1,2-DCB + 10 µl methanol	4.6 µl methanol + 10 µl stock	10 µl serial dil. stock

2.1.3 Cell Harvesting and Preparation of Total Soluble Protein Fractions

Following exposure (see details above), cells of each transwell insert were washed once with 1 ml cold PBS and harvested using 1.5 ml trypsin/EDTA (applied to both sides of the transwell membrane) for 10 min at 37°C. Cell suspensions of the three transwell inserts exposed in one glass bottle (see details above) were pooled in a 15 ml tube, centrifuged at 2,000 x g for 3 min and the pellets were washed thoroughly 3 times in ice cold PBS. Afterwards, cell pellets were lysed in 300 µl of 20 mM HEPES, pH 7.2, including 10% glycerol, 1% Triton X 100, 1 mM EDTA, 0.5% proteinase inhibitor cocktail and 1.25% benzonase on ice for 30 min, sonicated 3 times for 30 sec (duty cycle 40%, output control 3) and centrifuged 15 min at 13,000 x g. The pellets were discarded and lysates frozen and stored at -80°C in a fresh tube.

Protein concentration (about 1-2 mg/ml) of the soluble protein fraction was determined using Bio-Rad's DC (detergent compatible) Protein Assay (based on the Lowry method) and BSA dissolved in the used cell lysis buffer as a protein standard. The assay was performed in triplicates in 96-well plates according to the manufacturer's recommendations. Lysis buffer was tested for cross-reactivity with the Lowry dye solution. No interaction was observed when all samples and standards were diluted to a final concentration of 0.5 x lysis buffer. Optical density was measured at 750 nm with Biolog MicroStation plate reader. Standard protein data were imported into Excel and a linear best fit line was created. Protein concentrations of lysates were calculated from this curve. Finally, the volume corresponding to 5 µg of total soluble protein of each sample was subjected to SDS-PAGE and loading of equal protein amounts was confirmed after staining by visual inspection.

2.2 Gas Chromatographic Analysis of VOC Atmospheres

Styrene concentrations were measured by automated headspace gas chromatography with a Varian 3800 gas chromatograph equipped with a CP SIL 5 CB capillary column (film thickness, 0.12 μm ; ID, 0.25 mm; length, 25 m) and a flame ionization detector.

Following the cellular exposure to VOCs above described, glass flasks were opened and petri dishes containing transwells were quickly removed from the flasks. 1 ml of cell culture medium was aspirated from beneath of each transwell and added to a 20 ml glass vial containing 9 ml of 1.6 mM H_2SO_4 . Glass vials were thoroughly sealed. Triplicate samples were stored in the refrigerator until measured. The samples were incubated for 30 min at 70°C in an agitator (rotation regime 250 rpm for 5 s and no rotation for 2 s) prior to analysis, and 1 ml of each sample's headspace was injected. The chromatographic conditions were as follows: injector temperature, 250°C, split 1:50, detector temperature, 260°C and an oven temperature program consisting of 70°C for 2 min, followed by an increase at a rate of 10°C min^{-1} up to 90°C and then followed by a further increase at a rate of 60°C min^{-1} until 220°C was reached. Helium (1 ml min^{-1}) was used as a carrier gas. For calibrations, seven diluted standards of styrene (45 $\mu\text{g/l}$ – 4.5 mg/l), monochlorobenzene (55 $\mu\text{g/l}$ – 5.5 mg/l) and 1,2-dichlorobenzene (64.9 $\mu\text{g/l}$ – 6.49 mg/l) prepared from stock solutions were treated in the same way as the samples. The stock solutions were prepared in pure methanol. Styrene, monochlorobenzene and 1,2-dichlorobenzene exhibited the following retention times: 3.05, 2.70 and 4.44 min, respectively.

The mean partition coefficients at each time point were calculated by dividing the corresponding VOC concentrations of the culture medium by the assumed VOC concentration in the atmosphere of the exposure system. This is illustrated in the following example: It was assumed that the application of 1 g of VOC to a volume of one cubic meter of atmosphere yielded an exposure concentration of 10⁰ g/m³. If the gas chromatographic analysis of the liquid phase (sampled following a certain exposure period) revealed a concentration of 20 mg/l, the partition coefficient at the sampling time point would be 20 mg/l divided by 10⁰ g/m³ resulting in a partition coefficient of 2.

2.3 Cytotoxicity Measurements

Trypan blue exclusion. Before VOC exposure, cell viability and cell numbers were recorded by Trypan blue exclusion as described in chapter 2.1.1. Numbers of detached as well as freely floating dead cells could be determined following centrifugation at 170 x g for 3 min and resuspension in 20 μl cell culture medium (RPMI 1640 containing 2.5% FCS). The supernatant (cell-free cell culture medium) was used for lactate dehydrogenase leakage estimation (described below). The number and viability of attached cells was assessed

following trypsinization as described in 2.1.1 and 2.1.3 but using 200 μ l instead of 10 ml fresh culture medium.

Lactate dehydrogenase release. Membrane integrity was measured using the Cytotoxicity Detection Kit. Leakage of lactate dehydrogenase (LDH) from VOC exposed cells was estimated in culture medium of exposed cells according to the recommendations of the supplier. As a positive control (performed in duplicate), all cells from a transwell insert treated with solvent only were lysed by adding 50 μ l of the provided lysis buffer below the transwell insert, liberating a maximum amount of LDH from the cells. For all samples and controls, 100 μ l cell culture supernatant were centrifuged at 170 x g for 3 min, added to a well of a 96-well plate and incubated with 100 μ l of the freshly prepared dye/catalyst mixture for 30 min in the dark at room temperature. The reaction was stopped by addition of 50 μ l of stop solution and the optical density at 500 nm was measured immediately in triplicates using a 96-well plate reader. Values of solvent controls were subtracted. LDH release of exposed cells was expressed as percentage of available cellular LDH (lysis control).

2.4 *Proteomic Studies*

2.4.1 *SDS-PAGE*

Ceramic and glass plates of the Hoefer casting system were thoroughly cleaned with 70% ethanol solution. 1 mm thick and 10 x 10 cm large polyacrylamide/bisacrylamide gels were used for preparative/analytical one-dimensional gel electrophoresis. Separating and collecting gel solutions were prepared according to Table 2-2 with doubly distilled water. APS and TEMED were added just before pouring. When the gel cassette was filled with the separating gel, 1 ml of water-saturated 2-butanol was pipetted on top of the separating gel, thereby ensuring an even surface of the polymerizing gel. Onto the solidified and rinsed (doubly distilled water) separating gel, the solution for the stacking gel and the comb (10 wells) were added. After 30 min of polymerization, the comb was removed and the wells were rinsed. Protein samples of up to 200 μ g protein were diluted with the respective volume of a 5x concentrated Lämmli sample buffer. After heating at 95°C, samples were centrifuged and applied to the wells of the gel as well as 3 μ l of the unstained PageRuler protein ladder. Electrophoresis was started with 10 mA per mini-gel on the Hoefer SE 260 Mighty Small II system for 20 min followed by the protein separation at 20 mA per mini-gel for approximately 90 min.

Table 2-2 Preparation of polyacrylamide gels

	Separating gel		Collecting gel	
	Mini gel	Large gel	Mini gel	Large gel
Total Volume [ml]	10	40	5	10
Water [ml]	3.35	13.4	3.05	6.1
1.5 M TRIS/HCl, pH 8.8 [ml]	2.5	10	-	-
0.5 M TRIS/HCl, pH 6.8 [ml]	-	-	1.25	2.5
10% (w/v) SDS [μ l]	100	400	5	10
30% (w/v) Acrylamide ^a [ml]	4	16	0.65	1.3
10% (w/v) APS [μ l]	75	300	37.5	75
TEMED [μ l]	7.5	30	7.5	15

^a A ready-made 30% acrylamide/bisacrylamide solution (AppliChem) was used.

2.4.2 Two-dimensional Gel Electrophoresis (2-DE)

For two dimensional gels quantified by **Coomassie staining** (styrene experiment), 200-300 μ g protein from each protein extract (prepared from cultures in transwell inserts, see details in paragraph 2.1.3) were precipitated with 5 volumes of cold acetone (100%) at -20°C for 15 min. The precipitates were centrifuged at 20,000 x g for 15 min. Obtained pellets were air dried and resuspended in 135 μ l (7 cm IPG strips) or 400 μ l (18 cm IPG strips) of DeStreak rehydration solution containing 0.5% IPG-buffer 3-10 NL. Samples were shaken for 10 min and centrifuged at 20,000 x g for 30 min at 20°C. The supernatant containing the soluble proteins was applied to the wells of a rehydration tray. IPG strips (7 cm or 18 cm, pH range 3-10 NL; GE Healthcare) were rehydrated overnight in this solution. Strips were electrofocused at 20°C and a maximum of 50 μ A/strip using an Ettan IPGphor 3 isoelectric focusing unit according to the following protocols:

Table 2-3 Isoelectric focusing protocols

Steps	IPG strips, 3-10 NL, 7 cm	IPG strips, 3-10 NL, 18 cm
Step 1, hold	300 V, 2 h	300 V, 6 h
Step 2, gradient	1000 V, 1 h	1000 V, 6 h
Step 3, gradient	5000 V, 2 h	8000 V, 3 h
Step 4, hold	5000 V, 1.5 h	8000 V, 11 h

After focusing, strips were rinsed with doubly distilled water and equilibrated for 15 min with 20 mg/ml DTE and proteins were subsequently alkylated for 15 min in 25 mg/ml iodoacetamide. For this, both reagents were dissolved in equilibration buffer containing 6 M urea, 30% glycerol, 4% SDS, 50 mM TRIS/HCl and traces of bromophenol blue. Finally, strips were fixed with 1% agarose on 12% polyacrylamide separating gels (see paragraph

2.4.1). Electrophoresis was started with 10 mA per gel for 20 min followed by the protein separation at 20 mA per mini-gel on the Hoefer SE 260 Mighty Small II system for approximately 90 min. For large gels, second dimension separations were performed on the PROTEAN II xi/XL system at 6 mA per gel overnight until the dye front reached the bottom of the gel. Gels were rinsed in doubly distilled water and stained with colloidal Coomassie G250 according to (Neuhoff *et al.*, 1988), scanned using an Image scanner II and dried between cellophane sheets.

DIGE (Differential in Gel Electrophoresis). For differential in gel electrophoresis using fluorescent cyanine dyes, 150 µg protein of cells exposed to CB and 1,2-DCB (prepared according to paragraph 2.1.3) were precipitated with cold acetone at -20°C for 15 min, and the precipitates were centrifuged at 20,000 x g for 15 min. The pellets were resuspended in 30 µl of DIGE labeling buffer (30 mM TRIS/HCl pH 9.0, 7 M Urea, 2 M Thiourea, 4% CHAPS). Solubilization of the precipitate was facilitated by sonication for 30 seconds. Two thirds (i.e., 100 µg protein in 20 µl) of the samples were labeled separately using the fluorescent cyanine dyes (Cy3 for control samples and Cy5 for treated samples, 200 pmol in water-free DMF/100 µg protein). The remaining 50 µg (10 µl) of all samples were pooled to generate a single internal standard and labeled with Cy2. All labeling reactions were carried out for 30 min on ice in the dark and stopped with 1 µl of 10 mM lysine per 100 µg of protein for 10 min. For each DIGE gel, 100 µg of the labeled sample (20 µl) and control (20 µl) were pooled in a new tube with 100 µg of labeled internal standard (20 µl) to be run on a single two-dimensional gel. A 0.3 µl aliquot of this mixed protein solution was separated via SDS-PAGE (according to paragraph 2.4.1) in order to verify the labeling efficiency. 340 µl of DeStreak rehydration solution containing 0.5% IPG-buffer 3-10 NL were added to the protein solution (60 µl). Samples were shaken for 10 min and insoluble material removed by centrifugation at 20,000 x g for 30 min at 20°C. The supernatant was applied to the wells of a rehydration tray. IPG strips (18 cm, pH range 3-10 NL; GE Healthcare, Freiburg, Germany) were rehydrated overnight and focused using an Ettan IPGphor 3 isoelectric focusing unit as listed in Table 2-3. Strips were equilibrated and a second dimension performed as described in paragraph 2.4.2. During all stages of the work, light exposure was carefully avoided.

Image acquisition. Immediately after electrophoresis, DIGE gels were rinsed in doubly distilled water and scanned using the Ettan DIGE Image Scanner with the following excitation/emission filter settings (Cy2: 480 nm/530 nm; Cy3: 540 nm/595 nm; Cy5: 635 nm/680 nm) at 100 µm resolution. Scanner settings and resulting image quality were evaluated using Image Quant software, whereby the fluorescence intensities of the most intense spot and the background were compared. The exposure time was adjusted to a value that allowed the most intense spot to reach a grey value close to the maximum but

without achieving saturation. After fluorescent signal detection, gels were stained with Colloidal Coomassie G250 according to Neuhoff *et al.*, 1988, scanned with an Image scanner II and dried between cellophane sheets.

2.4.3 *Differential Protein Phosphorylation*

Differential protein phosphorylation was detected following cell exposure to styrene, monochlorobenzene or 1,2-dichlorobenzene (at exposure to 10^0 g/m³ and 10^{-4} g/m³) for 1 h (see paragraph 2.1.2). Following exposure, cells of three transwell inserts were washed twice with 1 ml of ice cold PBS, lysed directly on the membranes of the inserts using 300 μ l of the lysis buffer (see paragraph 2.1.3) and pooled in one tube. Lysates were stored at -70°C after freezing in liquid nitrogen.

Experiments were performed three times including controls exposed to methanol for 1 h. Preparation of the protein extract, protein estimation, isoelectric focusing and second dimension separation were carried out as mentioned above using 200 μ g of total soluble protein for 7 cm IPG strips (pH 3-10 NL) on 10 x10 cm mini-gels. During all stages of the work light exposure was carefully avoided. Immediately after the electrophoretic run, gels were incubated in 100 ml of fixation solution (50% methanol, 10% acetic acid) for 30 min. Gels were stored in fresh fixation solution overnight at 4°C. In the next morning gels were washed 3 times with 100 ml of doubly distilled water for 10 min and incubated (with continuous shaking) for 90 min in 50 ml of the Pro Q Diamond Phosphoprotein Gel stain (Molecular Probes) in the dark. Afterwards, gels were incubated 3 times for 30 min in 100 ml of destain solution (75% (v/v) doubly distilled water, 20% (v/v) acetonitrile, 5% 1 M sodium acetate solution (pH 4.0)). Before gel scanning on Ettan DIGE Image Scanner, gels were rinsed twice for 10 min in doubly distilled water. Scanner settings were: excitation/emission filters 540 nm/595 nm, exposure of 0.4 s per pixel, pixel size 100 μ m. Afterwards, gels were washed again in water and exposed overnight to 50 ml SYPRO Ruby protein gel stain (BIO-RAD Laboratories GmbH). The total-protein stain was removed and the gels were destained for 30 min in a solution of 10% methanol and 7% acetic acid. Gels were rinsed with doubly distilled water and scanned using the same fluorescence scanner and the following settings: excitation/emission filters: 480 nm/595 nm, exposure of 1.0 s per pixel.

2.4.4 *Quantitative Image Analysis*

Gel images were analyzed using the Delta 2D Version 3.6/4.0 software (Decodon GmbH, Greifswald, Germany; (Berth *et al.*, 2007)).

Coomassie stained images. In the first step of analysis, Coomassie-stained gel pictures were manually connected by warping vectors using the all-to-one strategy (all images are warped to one central image). Later, a fusion gel was created including all gels of the experiment. Automatically detected spots were manually edited and transferred to all gel

pictures. Spot volumes (integrated staining intensity) were normalized to the total protein amount on each gel (excluding the biggest spots representing ~ 5% of total intensity from the normalization). Relative volumes of the spots were determined. Mean relative volumes of identical spots on triplicate gels (for styrene concentration of 10 g/m³: duplicate gels) were calculated and divided by the mean relative volume of the corresponding spots in the controls (4 replicates), yielding the expression ratio. Differentially expressed proteins were identified using the following parameters: expression ratio lower than 0.666 or higher than 1.5 and a value of $p < 0.05$, as obtained by the software's integrated Student's t-test.

Cyanine fluorescent dyes. DIGE gel images originating from CB/1,2-DCB exposures were quantitatively analyzed in Delta 2D version 3.6/4.0 software in a similar way with the following changes: Only the pictures of the internal standard needed to be connected, resulting in a lower number of warping artifacts. In addition to the normalization to the total protein amount on each gel, relative volumes of the spots were determined in comparison to the same spots intensity in the internal standard channel (Cy2) on each gel. Differentially expressed proteins were identified using the following parameters: expression ratio lower than 0.77 or higher than 1.3 and a t-test value of $p < 0.05$. An expression ratio of 1.3 has been successfully used by several research groups for the detection of differentially expressed proteins using fluorescent dyes.

Pro Q Diamond and SYPRO Ruby. Phosphostain images (see paragraph 2.4.3) were also quantitatively analyzed in Delta 2D version 3.6 software (Decodon GmbH, Greifswald, Germany; (Berth *et al.*, 2007). First, all SYPRO Ruby images were warped manually and overlaid with the corresponding Pro Q Diamond signals of the identical gels. A fusion gel (of all Pro Q Diamond images) was created. Detected spots were manually edited and retransferred to all the Pro Q Diamond images for subsequent protein identification. Spot volumes were normalized as already described above. Differentially expressed proteins were identified using the following parameters: expression ratio lower than 0.77 or higher than 1.3 and a t-test value of $p < 0.05$.

2.4.5 Western Blotting (Target Validation, Apoptosis)

Target validation. Western blotting was mainly used to validate potential targets of VOC exposure. Cells were lysed as described in paragraph 2.1.3. 5 or 20 µg of protein extract were used for SDS-PAGE on 12% mini-gels (see paragraph 2.4.1). 20 µg of total soluble protein were used for every lane in Western blots specific for SOD1 and HSPB1 (HSP27), whereas only 5 µg of total soluble protein were used for every lane in Western blots specific for VDAC2. Gels were electro-blotted using tank blotting on Optitran BA-S83 Reinforced Nitrocellulose (Whatman) for 2 h at 100 V and 12°C in CAPS buffer (10 mM CAPS, pH 11, 10% methanol). Protein bands were stained with Ponceau S. Blotting efficiency was controlled by staining the gels with CBB G250. Membranes were incubated for 1 h in 5%

skimmed milk in TBS including 0.1% Tween 20 (TBS-T), washed three times 10 min in TBS-T and incubated overnight in the respective primary antibody dilution, containing 2% skimmed milk (or BSA for anti-SOD1) in TBS-T. HSP27-specific monoclonal mouse antibody (#2402, Cell Signalling Technology, 1:1,000), VDAC2-specific polyclonal rabbit antibody (IMG-5817A, Imgenex, 1:1,000) and polyclonal rabbit anti-SOD1 (#1926, Epitomics, 1:5,000) were used for overnight incubation of membranes. After successive washing steps in TBS-T, the horseradish peroxidase-conjugated secondary antibody (goat anti-mouse (#A4416, Sigma-Aldrich) or goat anti-rabbit antibody (#170-6515, Bio-Rad Laboratories) was added and incubated for 1.5 h at RT. Chemiluminescence signal was measured using Amersham ECL Advance Western Blotting detection kit (GE Healthcare) and a FluorChem™ 8900 imager (Alpha Innotech). All measurements were normalized to beta-actin signals obtained by using monoclonal anti- β -actin antibody (Sigma-Aldrich, clone AC-74, 1:5,000 in 2% milk) on the same immunoblots after stripping at 70°C for 30 min (62.5 mM TRIS/HCl, pH 6.7, 2% SDS, 100 mM freshly added 2-mercaptoethanol). Immunoblot signals were quantified using the freely available Image J software (<http://rsbweb.nih.gov/ij/index.html>).

Antioxidant treatment. In a second validation experiment, oxidative stress protein expression (in the presence of styrene) was detected with and without cell treatment with the antioxidant N-acetylcysteine (NAC). For these experiments, cells were cultured on transwell inserts and NAC was added to cell exposure medium at a final concentration of 10 mM for the whole exposure time of 24 h. The protein concentration of cell lysates was estimated and 10 μ g of total soluble protein were used for each gel lane in mini-gels. The detection and analysis of human glutathione transferase P1 (monoclonal mouse anti-human GST P1 antibody, #MC-411, Kamiya Biomedical Company, 1:2,000) and human heme oxygenase 1 (polyclonal rabbit anti-human HO-1, #Ab3470, Abcam, 1:2,000) were performed as specified before.

Apoptosis signaling. 10 μ g of all cell lysates used for the DIGE experiment (CB-, 1,2-DCB-treated and controls) were analyzed for caspase 3 cleavage (activation). Protein extracts were separated using SDS-PAGE on 12% gels (see section 2.4.1). Gels were electro-blotted by tank blotting on Nitrocellulose for 1.5 h at 100 V and 12°C in CAPS buffer (10 mM CAPS, pH 11, 10% methanol). For verification of transfer to the membrane, protein bands were stained with Ponceau S. Membranes were incubated for 1 h in 5% skimmed milk in TBS-including 0.1% Tween 20 (TBS-T), washed three times for 10 min in TBS-T and incubated overnight in caspase 3-specific polyclonal rabbit antibody (#9662, Cell Signaling Technology, 1:1,000) or Cleaved caspase 3-specific polyclonal rabbit antibody (#9661, Cell Signaling Technology, 1:1,000). After successive washing steps in TBS-T, the horseradish peroxidase-conjugated secondary antibody (goat anti-rabbit antibody, # 170-6515, Bio-Rad Laboratories, 1:2000) was added and incubated for 1.5 h at RT. Chemiluminescence

signal was measured using Amersham ECL Advance Western Blotting detection kit and a FluorChem™ 8900.

2.4.6 Protein Identification

In general, proteins whose expression was significantly altered (see section 2.4.4) were cut from dried gels whereas significantly regulated proteins detected in the Phospho-2-DE experiment were cut from wet Coomassie stained gels. Peptides obtained via tryptic proteolysis were identified by mass spectrometry.

Tryptic digestion was carried out using porcine trypsin as described by Benndorf and co-workers (Benndorf *et al.*, 2007). The extracted peptides were either spotted on a MALDI anchor chip target using HCCA matrix (0.6 mg/ml) and analyzed using a Bruker Ultraflex III or were separated by reversed-phase nano-LC (LC1100 series; column: Zorbax 300SB-C18, 3.5 μ m, 150 x 0.075 mm; eluent: 0.1% formic acid, 0-60% ACN) and analyzed by tandem mass spectrometry (LC/MSD TRAP XCT mass spectrometer, Agilent Technologies). Database searches were carried out using the MS/MS ion search (MASCOT, <http://www.matrixscience.com>) against all entries of the UniProtKB/TrEMBL database (<http://www.uniprot.org>) with the subsequent parameters: trypsin digestion, up to one missed cleavage, fixed modifications: carbamidomethyl (C), and with the following variable modifications: oxidation (M), peptide tolerance: \pm 1.2 Da, MS/MS tolerance: \pm 0.6 Da and peptide charge: +1, +2 and +3. Proteins were specified as unambiguously identified if the Mowse score was higher than 100 and at least 2 different peptides ($p < 0.05$) were used for identification. Molecular weight and *pI* of the identified protein were cross-checked with the gel position of the excised spot. When a significant difference between experimental and theoretical *pI* and/or molecular weight was noticed, the protein has been analyzed for possible protein isoforms or posttranslational modifications that could explain the observed shift using UniProtKB/TrEMBL database and NetPhos 2.0 Server (Blom *et al.*, 1999; Zhu *et al.*, 2005) or PhosphoSitePlus (www.phosphosite.org). Isoelectric points and molecular weight listed in tables were estimated using the ProtParam tool on www.expasy.com.

2.4.7 Detection of Styrene 7,8 Oxide Protein Adducts

For detection of proteins covalently modified by styrene 7,8 oxide (SO), a recently developed antibody was used (Chung *et al.*, 2006; Yuan *et al.*, 2007).

Preparation of SO protein adducts. SO BSA adducts were used as a positive control in Western blots and for peptide analysis by MS. These SO BSA adducts were prepared using a procedure published by Yuan *et al.*, 2007 with slight modifications: BSA (Albumin Fraction V, #1120180025, Merck) was dissolved in PBS. BSA (final concentration of 55 mg/ml) and SO (final concentration of 7.5 mM diluted in DMSO) were mixed at a ratio of 4:1 (v/v) in a total volume of 2 ml. The solution was incubated overnight under continuous

shaking and dialyzed using a Slide-A-lyzer Dialysis Cassette (10,000 MWCO, Pierce Biotechnology) three times against one liter of doubly distilled water for 45 min. Untreated BSA was used as a negative control.

Detection of SO protein adducts. A549 cells were exposed to 10^2g/m^3 of styrene for 24 h and lysed together with control cells they were lysed (see sections 2.1.2, 2.1.3). 50 μl of the exposed cell culture medium were acetone precipitated. The lysates (200 μg , in duplicates) were analyzed on SDS-PAGE as well as on 7 cm, 3-10 NL 2-DE Western blots (for details see 2.4.1, 2.4.2, 2.4.5). Nitrocellulose membranes were stained with Ponceau S and scanned, then blocked with 5% milk for 1h and incubated in rabbit SO-adduct-specific antiserum #1043 (1:1,000, kindly provided by Jiang Zheng, University of Washington, Seattle) in 2% milk overnight at 4°C . Membranes were washed three times with TBS-T and were incubated in secondary antibody solution containing 2% milk for 1.5 h. 2-DE chemiluminescence images of control and styrene exposed lysates were analyzed using Delta 2D 3.6 software (Decodon GmbH). Protein spots that were detected with much higher intensity were excised from CBB stained 2-DE gels that had been run in parallel and prepared from the same sample as the immunoblots. Prior to spot identification on the CBB gel, the Ponceau S (total protein) staining picture of the membrane which was very similar to the CBB picture of the corresponding gel, had to be matched with the (SO-adduct-specific) chemiluminescence detection picture of the same membrane using Delta 2D 3.6 software. Protein identification was carried out twice.

MS analysis of modified proteins. Covalent modification of proteins was analyzed by nano-HPLC/nano-ESI MS. 2-DE Spots (ID104, Proteome map Figure 3-2) of SO-modified proteins (identified with SO-specific antibody) as well as a band of 5 μg of prepared styrene-oxidized BSA (see preparation of SO-adducted BSA above) were cut from CBB stained gels. A band of 5 μg of untreated BSA and 2-DE spots (ID104) cut from a control gel served as negative controls. Tryptic digest and identification of the spots were carried out as described above using nano-HPLC/ESI-MS. Extracted peptides were reconstituted with 50 μl of 0.1% formic acid, 3% acetonitrile (ACN). 8 μl of 0.1% formic acid, 3% ACN were added to 2 μl of the reconstituted peptides (the remaining volume was stored at -20°C) for further dilution. The peptide solution was added to a 96-well plate. The injection volume was set to 8 μl . Identification of SO-modified peptides of thioredoxin reductase 1 (isoform 5) were carried out using BioTools 3.0 and Sequence Editor (Bruker Daltonik) using the subsequent parameters: trypsin digestion, up to one missed cleavage, variable modifications: oxidation (M), styrene 7,8 oxide (Asp, Glu, His, Lys or Secys, Cys), peptide tol.: ± 1.2 Da, MS/MS tol.: ± 0.6 Da and peptide charge: +1, +2 and +3.

2.5 Quantitative PCR

Potential VOC targets identified by proteomic methods were validated using quantitative PCR. mRNA extraction was performed with the MagNA Pure LC system, using the MagNA Pure LC mRNA Isolation Kit I (Roche) according to the manufacturer's protocol for cultured cells. cDNA synthesis was performed using the AMV reverse transcriptase according to the manufacturer's specifications (Promega). Reverse transcription products were amplified using a LightCycler 2.0 system and a Fast Start DNA SYBR Green Kit according to the manufacturer's instructions (Roche). Primers and standards for voltage-dependent anion-selective channel protein 2, superoxide dismutase 1 and heat shock protein beta (HSP27) as well as the amplification protocol were obtained from Search-LC (Heidelberg). For the housekeeping genes β 2-microglobulin and GAPDH, 2 μ l of the cDNA were amplified (see primer sequence in paragraph 2.7) in a 20 μ l reaction volume that contained 3 mM MgCl₂ and 0.5 μ M of both sense and anti-sense primers. After an initial denaturation step for 10 min at 95°C, amplification was performed during 40 cycles using a touch-down PCR protocol with 10 s denaturation at 95°C, annealing for 10 s at 68°C with an incremental decrease of 0.5°C during the first 20 cycles, and elongation for 16 s at 72°C. Relative transcript concentrations were determined by performing linear regression for a dilution series of the respective standards. Obtained expression levels were normalized versus the housekeeping genes, and changes in expression levels are given relative to the untreated controls.

2.6 ROS Measurement

To further strengthen the hypothesis of increased cellular formation of reactive oxygen species (ROS) by exposure to styrene, their internal concentration using 2'-dichlorofluorescein diacetate has been measured. A549 cells were grown for 24 h in transwell inserts (1 cm, 100,000 cells/insert) supported by a 24-well plate (Roder-Stolinski *et al.*, 2008b). Cells were rinsed with PBS (with Ca²⁺ and Mg²⁺) and incubated with 50 μ M of 2',7'-dichlorofluorescein diacetate (2',7' DCFH-DA, Sigma-Aldrich, stock solution in DMSO) for 30 min at 37°C. Cells were washed again, stimulated with 1 ng/ml rh-TNF α (AL-ImmunoTools) and exposed to styrene (10⁻² g/m³), methanol (control) or CdCl₂ (25 μ M, positive control) for 2 h. After a subsequent wash, cells were detached using trypsin for 3 min and resuspended in 250 μ l of PBS supplemented with 2.5% of FCS. Intracellular generation of reactive oxygen species was quantified by measuring the fluorescence of oxidatively converted DCFH using a BD FACS Calibur™ (at 488/525 nm) and Cellquest software. Experiments were performed in triplicates.

2.7 List of used Chemicals and Devices

All chemicals, which are not mentioned in the following, were purchased from the companies Merck (Darmstadt, Germany), Sigma-Aldrich (Deisenhofen, Germany) as well as Carl Roth

GmbH & Co (Karlsruhe, Germany) in p. a. quality. All solutions have been prepared with distilled water.

Cell Culture and Exposure to VOCs

6-well Cell Culture Plates; 96-well Cell Culture Plates	Nunc
Bacillol Plus Solution	Bode Chemie
BME Amino Acid Cocktail; N-Acetyl-L-Alanyl-L-Glutamine	Biochrom
Cell Culture Flask T25/T75/T150	Nunc
Cell Culture Inserts (2.5 cm diameter, pore size 0.2 µm)	Nunc
CO ₂ -independent Cell Culture Medium	Gibco Invitrogen Corp
EDTA; Trypan-Blue	Sigma-Aldrich
Fetal Calf Serum	Biochrom
Glycerol; Triton X 100	Merck
HEPES; Benzonase	Merck
Human Lung Epithelial Cells (A549, ATCC No. CCL-185)	LGC Promochem
Methanol	Merck
MycoAlert Mycoplasma Detection Kit	Lonza
PBS Dulbecco w/o Ca, Mg	Biochrom
Penicillin/Streptomycin	Invitrogen Corporation
Petri Dishes (35x10 mm)	Corning Costar
Proteinase Inhibitor Cocktail for Mammalian Cells	Sigma-Aldrich
rh-TNFα	AL-ImmunoTools
RPMI 1640 Medium HEPES-buffered	Biochrom
Styrene; Chlorobenzene; 1,2-Dichlorobenzene	Merck
Trypsin-EDTA	PAA
Wide-necked Glass Flasks (600 ml volume)	Duran Group

Measurement of VOC Atmospheres

Styrene; Chlorobenzene; 1,2-Dichlorobenzene	Merck
Methanol	Merck
20 ml GC Glass Vials	Hewlett Packard

Cytotoxicity Measurements

Cytotoxicity Detection Kit	Roche
Trypan Blue	Sigma-Aldrich

Gel Electrophoresis

2-Mercaptoethanol; Methanol	Merck
Acetic acid; Ethanol	Merck
Acetone; Glycerol; Glycine,	Merck
Acetonitrile; Sodium acetate	Merck
Acrylamide/Bisacrylamide-Solution (30%)	AppliChem
Ammoniumperoxodisulfate (APS); Dimethylsulfoxide (DMSO)	Carl Roth
Ammoniumsulfate	Carl Roth

BSA (Albumin Fraction V), #1120180025	Merck
Cellophane Sheets	Bio-Rad Laboratories
Colloidal Coomassie G250, Bromophenol Blue	Merck
CyDye DIGE Fluor, Minimal Labeling Kit (5 nmol)	GE Healthcare
DC Protein Assay	Bio-Rad Laboratories
DeStreak Rehydration Solution; IPG-Buffer 3-10 NL	GE Healthcare
Dimethylformamide (water-free); Lysine	Sigma-Aldrich
Dithiothreitol; Triton X 100	Sigma-Aldrich
Dual Gel Caster SE245	Hoefler
Immobiline Dry Strip Reswelling Tray	GE Healthcare
IPG Immobiline DryStrip (18 cm or 7 cm, pH range 3-10 NL)	GE Healthcare
N,N,N',N'-Tetramethylethylenediamine (TEMED)	Merck
Page Ruler Protein Ladder, prestained	Fermentas
Pro Q Diamond Phosphoprotein Gel stain	Molecular Probes
Rehydration tray; Paper wicks; DryStrip Cover Fluid	GE Healthcare
Sodiumdodecylsulfate; TRIS	Carl Roth
SYPRO Ruby Protein Gel Stain	Bio-Rad Laboratories
Thiourea; 1,4- Dithioerytritol; Urea; CHAPS; Iodoacetamide	GE Healthcare

Mass Spectrometry

96-well plate, Polypropylene	Agilent Technologies
Ammoniumsulfate	Carl Roth
Dimethylsulfoxide	Carl Roth
Formic acid; Acetonitrile; Methanol; Ethanol	Merck
HCCA matrix (2.5 mg/ml); Ammonium bicarbonate	Sigma-Aldrich
MTP Anchor Chip Target 0.6; Steel Target	Bruker-Daltonik
Phosphoric acid	Merck
Porcine Trypsin	Promega
Slide-A-lyzer Dialysis Cassette (10,000 MWCO)	Pierce Biotechnology
Styrene 7,8 oxide #77950	Sigma-Aldrich
Styrene; BSA (Albumin Fraction V) #1120180025	Merck
ZipTip C18, Pipette Tips	Millipore

Western Blot

2-Mercaptoethanol; N-acetylcysteine; CAPS	Sigma-Aldrich
BSA; TRIS/Base, Methanol	Merck
ECL Advance Western Blotting detection kit	GE Healthcare
Gel Blotting Paper, Sodiumdodecylsulfate	Carl Roth
Goat Anti-Mouse HRP-Conjugated, #A4416	Sigma-Aldrich
Goat Anti-Rabbit HRP-Conjugated, #170-6515	Bio-Rad Laboratories
Mouse Monoclonal Anti-Human GST P1, #MC-411	Kamiya Biomedical
	Comany
Mouse Monoclonal Anti- β -Actin Antibody, Clone AC-74	Sigma-Aldrich
Mouse Monoclonal HSP27-Specific Antibody, #2402	Cell Signalling Technology

Non-Fat Dry Milk Powder	Bio-Rad Laboratories
Optitran BA-S83 Reinforced Nitrocellulose	Whatman
Page Ruler Protein Ladder, prestained	Fermentas
Ponceau S	Merck
Rabbit Polyclonal Anti-Human HO-1, #Ab3470	Abcam
Rabbit Polyclonal anti-SOD1, #1926	Epitomics
Rabbit Polyclonal Caspase 3 Antibody, #9662	Cell signalling technology
Rabbit Polyclonal Cleaved Caspase 3 Antibody, #9661	Cell signalling technology
Rabbit Polyclonal SO-adduct-specific Antiserum, #1043	Jiang Zheng, University of Washington, Seattle, US
Rabbit Polyclonal VDAC2-Specific Antibody, IMG-5817A	Imgenex
Sodium Chloride; TRIS; Tween 20	Carl Roth
Tank Blot Cassette TE22	Hofer

Quantitative PCR

10x Taq Buffer	Promega
AMV Reverse Transcriptase	Promega
Fast Start DNA SYBR Green Kit	Roche
MagNA Pure LC mRNA Isolation Kit I	Roche
Primer and Standards for VDAC2, HSP27, SOD1	Search-LC
Primer β 2-Microglobulin	GenExpress
Sense: 5'-GATGAGTATGCCTGCCGTGTG-3'	
Antisense: 5'-CAATCCAAATGCGGCATCT-3'	
Primer GAPDH	GenExpress
Sense: 5'-GGCATGGACTGTGGTCATGAG-3'	
Antisense: 5'-TGCACCACCAACTGCTTAGC-3'	
Taq DNA Polymerase	Promega

FACS (Reactive Oxygen Species Measurement)

2',7'-Dichlorodihydrofluorescein diacetate (2',7' DCFH2-DA)	Sigma-Aldrich
Cadmium chloride	Sigma-Aldrich

Used Electronic Devices

BD FACS Calibur	Becton Dickinson
Bruker Ultraflex III Mass Spectrometer	Bruker-Daltonics
Centrifuge 1-15 , Rotor 12124	Sigma-Aldrich
Centrifuge 3K30, Rotor 12154-H	Sigma-Aldrich
Centrifuge Mikro 22 R, Rotor 1400 RPM	Hettich
Centrifuge Rotina 46R, Rotor 002129, 4624	Hettich
Centrifuge ZK 380, Rotor 220.59 V	Hermle
Electrophoresis Power Supply EPS 600	Amersham Biosciences
ELISA-Reader Synergy HT	Bio-Tek

Ettan DIGE Image Scanner	Amersham Biosciences
Ettan IPGphor 3 Isoelectric Focusing Unit	GE Healthcare
FluorChem 8900 Imager	Alpha Innotech
Gel Air Dryer	Bio-Rad Laboratories
Image scanner II	Amersham Biosciences
Incubator BBD 6220	Heraeus
Laminar Flow Clean Bench	Hera Safe
LC-Column: Zorbax 300SB-C18, 3.5 µm, 150 x 0.075 mm	Agilent Technologies
Light Microscope AXIOVERT 40C	Zeiss
LightCycler 2.0 system	Roche
MagNA Pure LC System	Roche
Micro Plate Reader MicroStation	Biolog
Minicell Power Pack P20 Power Supply	Biometra
Nano-LC/MSD TRAP XCT Mass Spectrometer (LC1100 series)	Agilent Technologies
Precision Balance MC1	Sartorius
PROTEAN II xi/XL System	Bio-Rad Laboratories
SE260 Mighty Small II Deluxe Mini Vertical Electrophoresis Unit	Hoefer
Shaker	Pharmacia Biotech
Speedvac SC110	Savant
TE22 Mighty Small Tank Transfer	Hoefer
Thermomixer Comfort	Eppendorf
Ultrasonic bath Transsonic 470/H	Elma
Ultrasonic homogenizer	B. Braun
Varian 3800 Gas Chromatograph	Varian, Palo Alto, USA
CP SIL 5 CB Capillary Column (0.12 µm; ID, 0.25 mm; length, 25 m)	
Flame Ionization Detector	
Water Bath	Julabo TW 20

Software

BLAST (Basic Local Alignment Search Tool)	NCBI (National Center for Biotechnology Information)
Cellquest software	BD Biosciences
Delta 2D 3.6/4.0	Decodon GmbH
Flex Control, Flex Analysis, Bioltools, and Sequence editor	Bruker-Daltonics
Image J (http://rsbweb.nih.gov/ij/index.html)	National Institutes of Health
Image Quant	GE Healthcare
Mascot search engine (www.matrixscience.com)	Matrix Science
NetPhos 2.0 Server (http://www.cbs.dtu.dk/services/NetPhos)	Center for Biological
Sequence Analysis	
PhosphoSitePlus	www.phosphosite.org
PyMOL Molecular viewer	DeLano Scientific
STRING 8.3 (Search Tool for the Retrieval of Interacting Genes/Proteins, http://string-db.org/)	CPR, EMBL, SIB, KU, TUD and UZH
UniProtKB/TrEMBL	EBI, SIB, PIR

3 *Development of the Toxicoproteomics Approach for the VOC Lung Cell Model*

3.1 *Introduction*

3.1.1 *The A549 Cell Exposure Setup*

The toxicity of aromatic VOCs has been studied for a long time. Mostly animal models were applied identifying major toxic metabolites of acute exposure scenarios. Strikingly, the biotransformation of aromatic VOCs was reported to be quite different in humans and rodents yielding a different profile of ultimate metabolites and thereby different clinical symptoms. For humans, only little information is available on the effects arising from low concentrations of VOCs (see 1.1) as occurring in ambient air. Epidemiologic studies hint at the development of inflammatory processes and allergies (see section 1.2) although the mechanism behind is not fully understood.

One possible explanation for the observed toxicity would be impaired protein function such as reduced enzyme activity due to modulation of expression or formation of covalent binding of proteins or their active metabolites (Shen *et al.*, 2009; Yuan *et al.*, 2007). Indeed, interactions of VOC metabolites with serum proteins have been identified, while consequences thereof are still unknown (see 4.1.4). In addition, *in vitro* studies provided evidence, that the expression of intracellular proteins such as heat shock proteins are modulated in their expression by VOCs as well (see 4.1.2). However, up to now, no comprehensive investigations have been undertaken to identify the extent and the means by which aromatic VOCs interact with the complex network of cellular proteins of human lung cells.

In vitro models are mainly employed to help investigate fundamental mechanisms underlying *in vivo* findings. The employment of a human lung cell line combined with proteomic tools (see section 1.3) may provide further insights into the molecular interactions of VOCs with cellular proteins. Furthermore, the usage of this *in vitro* model offers a controllable and reproducible means being of great importance when proteomic techniques are applied. Subsequently, models that are more complex such as primary cells or animal models may be used to evaluate the identified mechanisms.

The human epithelial cell line A549, which originated from a human lung carcinoma and is routinely used as an *in vitro* model of human pulmonary cuboidal epithelium has been chosen (Rothen-Rutishauser *et al.*, 2005; Stearns *et al.*, 2001). Among a variety of airway epithelial cells and cell lines tested, human alveolar cells especially A549 have been proposed as the most convenient cell type to be used for developing tests for respiratory immunotoxicity assessment (Roggen *et al.*, 2006).

A549 cells are derived from alveolar epithelial type II cells, the progenitor cells for type I epithelial cells (Sheets *et al.*, 2004). Despite their malignant nature (see section 2.1.1), it was shown that A549 possess typical properties of alveolar epithelial type II cells. They contain membrane-bound lamellar bodies used for the storage of surfactant proteins and have pronounced cytoplasmic extensions (Rothen-Rutishauser *et al.*, 2005; Young *et al.*, 2001). Moreover, the expression of the epithelial sodium channel has been reported with biophysical properties similar to those found in alveolar epithelial type II cells in primary culture (Lazrak *et al.*, 2000). Furthermore, A549 cells express multi drug resistance-associated proteins MRP 1 and 3 (Stehfest *et al.*, 2006) as well as most of the major constitutive and inducible CYP forms found in lung epithelial cells including 1A1, 1B1, 2B6, 2C8-19, 2E1, 3A5, and 3A7. CYP2E1 expression has been established in several studies, while CYP2F1 and CYP4B1 mRNAs have not been detected in A549 but have been found in whole lung tissue. Hence, A549 cells possess metabolic activities toward xenobiotics such as shown for benzene, albeit with lower activity than in the human lung (Hukkanen *et al.*, 2000; Sheets *et al.*, 2004).

In most cell culture settings, the cells are immersed in culture medium what does not reflect the physiological condition of lung epithelial cells. Under physiological conditions, these cells are exposed to air, separated from it only by a very thin liquid lining layer with a surfactant film at the air-liquid interface. In this study, A549 epithelial cells were grown on microporous membranes in a two chamber (air/liquid) system (see Figure 2-1 and section 2.1.2), that has been established and successfully applied by the Department of Environmental Immunology (Helmholtz-Centre of Environmental Research, Leipzig (Fischader *et al.*, 2008; Lehmann *et al.*, 2008; Roder-Stolinski *et al.*, 2008b) for the analysis of VOC-induced immunomodulation. After the formation of a confluent monolayer, the apical medium phase is discarded and the cells are exposed to VOCs (see 2.1.2). It has been reported that culturing epithelial cells on permeable supports leads to an increased differentiation (Adler *et al.*, 1990; Handler *et al.*, 1989). The morphology of A549 cells cultured in air/liquid models on microporous membranes has been studied with confocal laser scanning and transmission electron microscopy. Under these culturing conditions, the cells form a distinct polarized monolayer, express tight junctions and develop transepithelial electrical resistance. Enough surfactant phospholipids are produced and released at the apical side of the air-exposed A549 cells to reach a surface tension as low as in the airways (Blank *et al.*, 2006; Chuang *et al.*, 2009; Rothen-Rutishauser *et al.*, 2005). Despite the fact that no *in vitro* model can reflect the situation in human lung, A549 cells cultured in an air/liquid model are a useful tool to study basic molecular effects of VOCs on cellular protein expression. In fact, previous experiments with this experimental setup confirmed the ability of

A549 cells to secrete cytokines in response to low concentrations of VOCs (Fischader *et al.*, 2008; Hetland *et al.*, 2001).

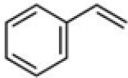
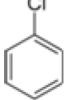
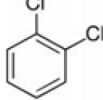
*Because most proteomic techniques have to meet other requirements (such as higher cell numbers, low salt content) than the immunologic analyses mentioned beforehand do, the available cell exposure system needed to be adapted for the toxicoproteomic experiments of this thesis. Finally, a further aim was to create the first extensive standard 2D reference map for the A549 cell line in order to avoid repeated mass spectrometric identification of the same proteins, making proteomic studies faster, easier and less expensive as proposed by (Wu *et al.*, 2005).*

3.1.2 Monitoring VOC Atmospheres

When studying the toxicity caused by exposure of volatile chemicals to cells, it is essential to monitor the prevalent concentration in the test atmosphere. In tightly closed systems, as applied here, volatile compounds distribute between air and liquid phase depending on their physicochemical properties until a state of equilibrium is established. The partitioning of the compound can be assessed by measuring the concentration of the volatile substance in the liquid phase after a certain incubation time. Finally, the so-called “partition coefficient”, defined as the concentration ratio of a volatile compound distributed between a liquid phase and a gas phase, can be derived (see calculation in section 2.2).

All three compounds studied here are volatile at room temperature and are important representatives of the aromatic class of VOCs that occur in occupational and non-occupational environments. 1,2-dichlorobenzene, shows the lowest water solubility, the highest octanol/water partition coefficient and the lowest vapor pressure, as these parameters are dependent on the degree of chlorination (Table 3-1).

Table 3-1 Physicochemical properties of styrene, monochlorobenzene and 1,2-dichlorobenzene.

	Styrene^a	Monochlorobenzene^a	1,2-Dichlorobenzene^b
CAS.-No.	108-90-7	100-42-5	95-50-1
			
Molecular mass	104.14 g/mol	112.56 g/mol	147.0 g/mol
Density (20°C)	0.906 g/cm ³	1.1058 g/cm ³	1.3048 g/cm ³
Vapor pressure (20°C)	666 Pa	1560 Pa	160 Pa ^c
Octanol-water partition coefficient	891	692	2398
Water solubility (25°C)	310 mg/l	466 mg/l	156 mg/l
Conversion factors (25°C, 101.3 kPa)	1 ppm = 4.33 mg/m ³ 1 mg/m ³ = 0.23 ppm	1 ppm = 4.70 mg/m ³ 1 mg/m ³ = 0.22 ppm	1 ppm = 6.00 mg/m ³ 1 mg/m ³ = 0.17 ppm

^a U.S. EPA, OPPT Chemical Fact Sheets, <http://www.epa.gov/opptintr/chemfact/>

^b OECD, Screening Information Datasets, Initial Assessment Report 1,2-dichlorobenzene, 2001

^c Material safety data sheet, <http://msds.chem.ox.ac.uk/DI/1,2-dichlorobenzene.html>

For this thesis, the exposure atmospheres of the three aromatic VOCs styrene, monochlorobenzene and 1,2-dichlorobenzene should be characterized in the beforehand described in vitro model in order to ensure stable and reproducible exposure conditions.

3.2 Results

3.2.1 Adaption of Existing Exposure Setup to Proteomics Approach

The available cell exposure model that was established by the Department of Environmental Immunology (Helmholtz-Centre of Environmental Research, Leipzig (Fischader *et al.*, 2008; Lehmann *et al.*, 2008; Roder-Stolinski *et al.*, 2008b) needed to be modified for the toxicoproteomic experiments of this thesis. The use of transwell inserts allows the most direct exposure of the cells to the volatile organic compounds (VOC) styrene, monochlorobenzene and 1,2-dichlorobenzene via the gas phase. The cells are nourished through membrane pores from the basal side while being exposed directly to the gas phase (VOC) above them (see Figure 2-1). For the proteomics investigations, the relatively small transwell inserts (growth surface 2.6 cm²) of the established model were replaced by inserts with a 4 times larger surface area, providing a higher protein yield. In addition, instead transwells with opaque polycarbonate membranes, inserts with a transparent inorganic Anopore membrane were chosen in order to monitor changes in cell shape or attachment as well as contamination events and to minimize protein binding. No surface coating was necessary for culturing and exposure of A549 cells. 3 days after seeding of 250,000 cells on each transwell, the cells formed a monolayer (Figure 3-1 A and B). In comparison to flask cultures, cell shape was more three-dimensional. Vitality was comparable with flask cultures and did not decrease when culture medium was taken off the upper compartment and cells were cultured for three more days on the Anopore membrane.

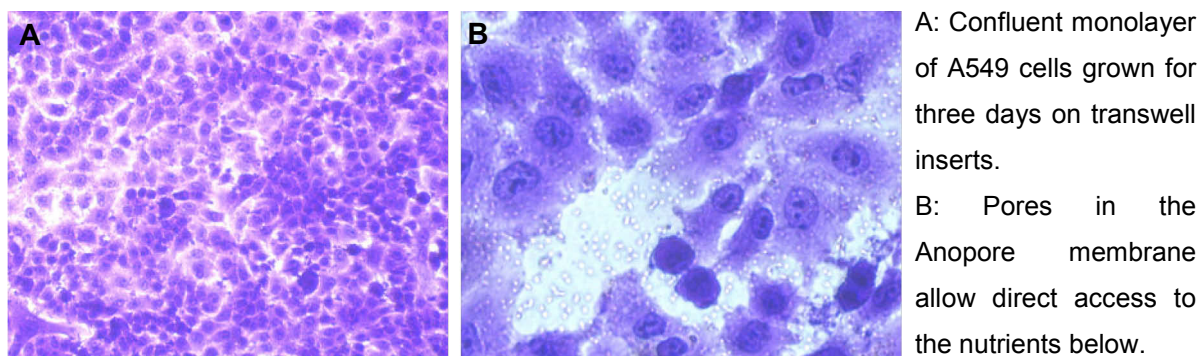


Figure 3-1 Phase contrast microscopic images of A549 cells grown on transwell inserts and stained with methyl violet.

From each transwell, about 150 µg of total soluble protein were obtained. Cells from 3 transwells exposed together in one flask produced enough protein to perform two-dimensional gel electrophoresis (2-DE) and use the remaining protein for validation

experiments. A protein amount of 250 μg was found to be adequate for a Coomassie staining approach whereas for CyDye-labeled proteins 150 μg were sufficient for quantitative analysis. The spot pattern was highly similar for both the staining methods as investigated for a set of control samples. Greater differences in positions of the same spots using the two detection methods in one gel were observed for low molecular weight proteins (< 10 kDa) that were excluded in the expression experiments.

In the beginning, using transwell inserts for cell culturing and exposure resulted in a small number of highly abundant proteins on the 2-DE pattern compared to a high number of spots on 2D gels prepared from flask cultures of the same cell line. It was found that proteins such as serum albumin contained in the culture medium additive FCS appeared to bind to the culture membrane to a much higher extent than to the culture flasks and were subsequently dissolved when cells were lysed on the membranes using typical urea-containing 2-DE lysis buffers. Therefore, cell culture and lysis protocols were modified. Cell culture was performed in cell culture media with reduced (final concentration 2.5%) FCS concentration. Together with trypsinization instead of direct lysis and repeated washing steps of the cells, high-resolution proteome patterns (see Figure 3-2) could be obtained that was essentially needed for quantitative proteome analysis.

3.2.2 *Proteome Map of the A549 Cell Line*

As described above, an existing lung cell exposure system was adapted for a proteomic approach to identify proteins differentially expressed following exposure to VOCs. Since the used human lung epithelial cell line A549 is the most common model to test pollutant effects to lung cells, a 2-DE reference map was created from all identified protein spots in order to support future studies (see Figure 3-2). In total, 1,380 protein spots with a molecular weight of 15-150 kDa and isoelectric points from 3-10 have been detected using colloidal Coomassie staining. 266 of these spots (labeled with ID numbers) were identified by tryptic digest and mass spectrometric analysis of the peptides (see Table 8-1 in the appendix). The presented proteome map is the first of this cell line to comprise such a large number of identified proteins.

Molecular weight and isoelectric point (pI) of the identified proteins were crosschecked with the gel position of the excised spots. When a significant difference between experimental and theoretical pI and/or molecular weight was noticed, the protein has been analyzed for possible protein isoforms or posttranslational modifications that could explain the observed shift. Known isoforms or PTMs were extracted from UniProtKB/TrEMBL database whereas possible phosphorylation sites have been predicted by NetPhos 2.0 Server (Blom *et al.*, 1999). Both are given for proteins labeled with an asterisk in Table 8-1 and are discussed in section 3.3.

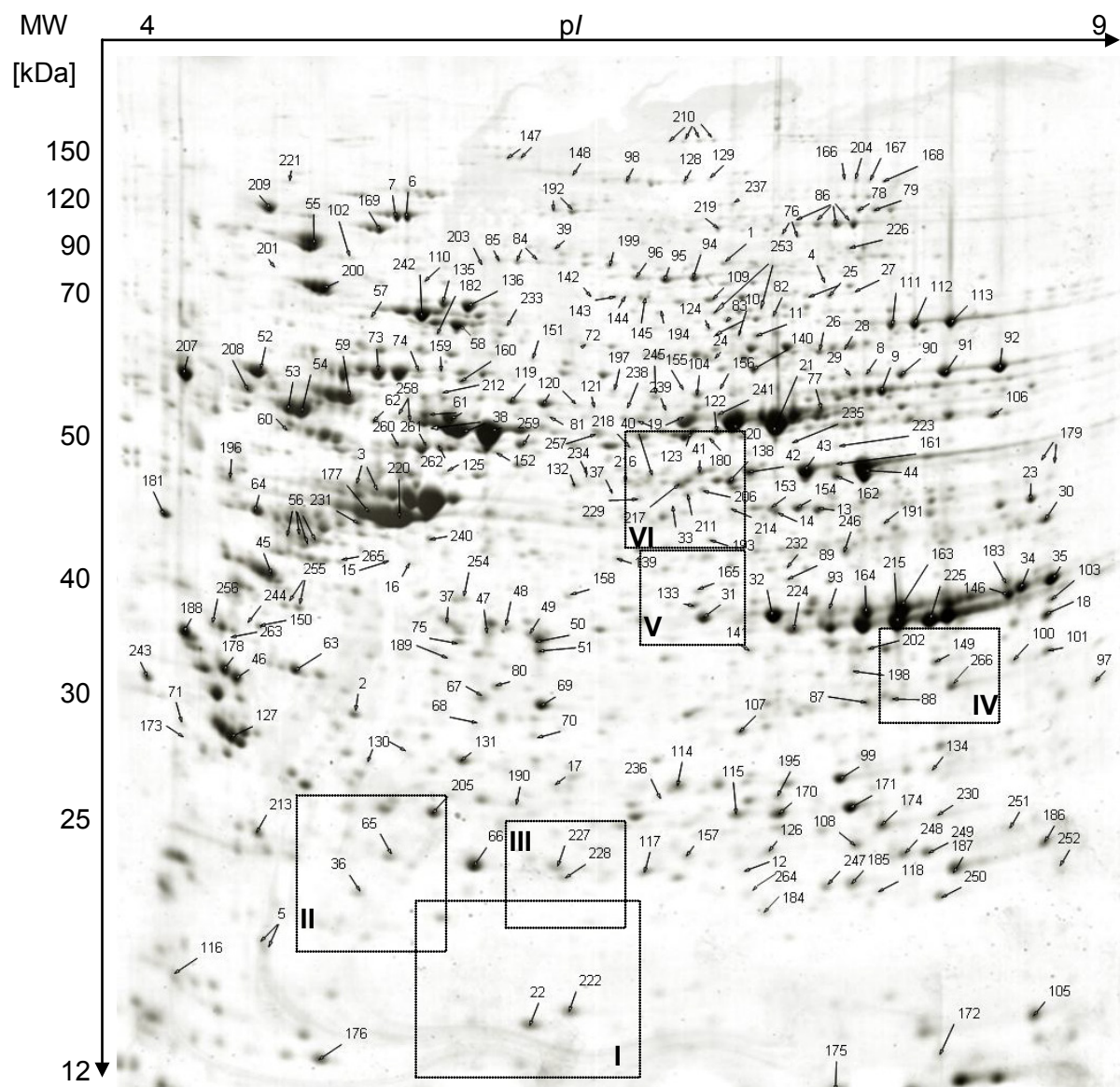


Figure 3-2 Proteome map of the A549 cell line cultured on transwell inserts. 500 μ g of total soluble protein were separated by 2-DE (18 cm IPG strips, 3-10 NL, 12% acrylamide/bisacrylamide). Marked squares I-VI are shown in detail in Figure 4-3. Mass spectrometric identification data for all spots labeled with ID numbers are listed in Table 8-1.

3.2.3 Characterization of Applied VOC Atmospheres

Studying the toxicity of volatile compounds requires the knowledge of the prevalent exposure concentrations and their stability over time. Thus, the cell's actual exposure to the applied VOCs, styrene, monochlorobenzene (CB) or 1,2-dichlorobenzene (1,2-DCB), was estimated by monitoring the distribution of the respective substance between air and medium phase. VOC concentrations in cell culture medium were analyzed in triplicates using headspace gas chromatography (see paragraph 2.2) after 4 and 24 h of cell exposure to 10^{-1} g, 10^0 g, 10^1 g and 10^2 g VOC/m³ gas atmosphere. These concentrations correspond to 23 – 23,000 ppm of styrene, 22 – 22,000 ppm of CB and 17 – 17,000 ppm of 1,2-DCB.

Exposure to 10^{-1} - 10^2 g/m³ of styrene, CB or 1,2-DCB resulted in medium concentrations of 0.2 – 75.5 mg/l (1.9 - 725.3 μ M), 0.19 – 105.23 mg/l (1.7 - 934.4 μ M) and 0.2 – 52.6 mg/l (1.4 - 357.5 μ M), respectively. VOC medium concentrations for both time points are listed in Table 3-2 and are displayed in Figure 3-3.

Table 3-2 VOC concentrations measured by headspace gas chromatography in cell culture medium following 4 or 24 h of cell exposure.

Exposure	Styrene		Monochlorobenzene		1,2-Dichlorobenzene	
	[μ M]		[μ M]		[μ M]	
	4 h	24 h	4 h	24 h	4 h	24 h
10^2 g/m ³	725.3 \pm 40.0	572.5 \pm 3.0	934.4 \pm 55.2	528.5 \pm 22.6	357.5 \pm 12.7	319.5 \pm 14.3
10^1 g/m ³	267.6 \pm 3.1	191.8 \pm 1.6	163.7 \pm 3.7	135.3 \pm 0.8	194.0 \pm 4.0	127.2 \pm 1.6
10^0 g/m ³	28.8 \pm 0.2	19.6 \pm 0.4	22.3 \pm 1.1	16.2 \pm 0.5	27.0 \pm 1.2	14.1 \pm 0.5
10^{-1} g/m ³	2.7 \pm 0.0	1.9 \pm 0.0	2.2 \pm 0.0	1.7 \pm 0.0	2.7 \pm 0.0	1.4 \pm 0.0

For all tested VOCs, the measured medium concentrations following 24 h exposure were in average about 30% lower than the values measured after a 4 h exposure period. In contrast, methanol (solvent) concentrations in cell culture medium did not vary significantly between both time points. No VOCs (besides methanol) were detected in cell culture medium of control cells that was not exposed to other VOCs than the solvent. Increased solvent (methanol) volumes resulted in slightly increased VOC concentrations in the medium. As analyzed for styrene in a cell-free model system, the VOC concentration in the liquid phase following a 24 h exposure period did not change significantly when water or PBS was used instead of culture medium.

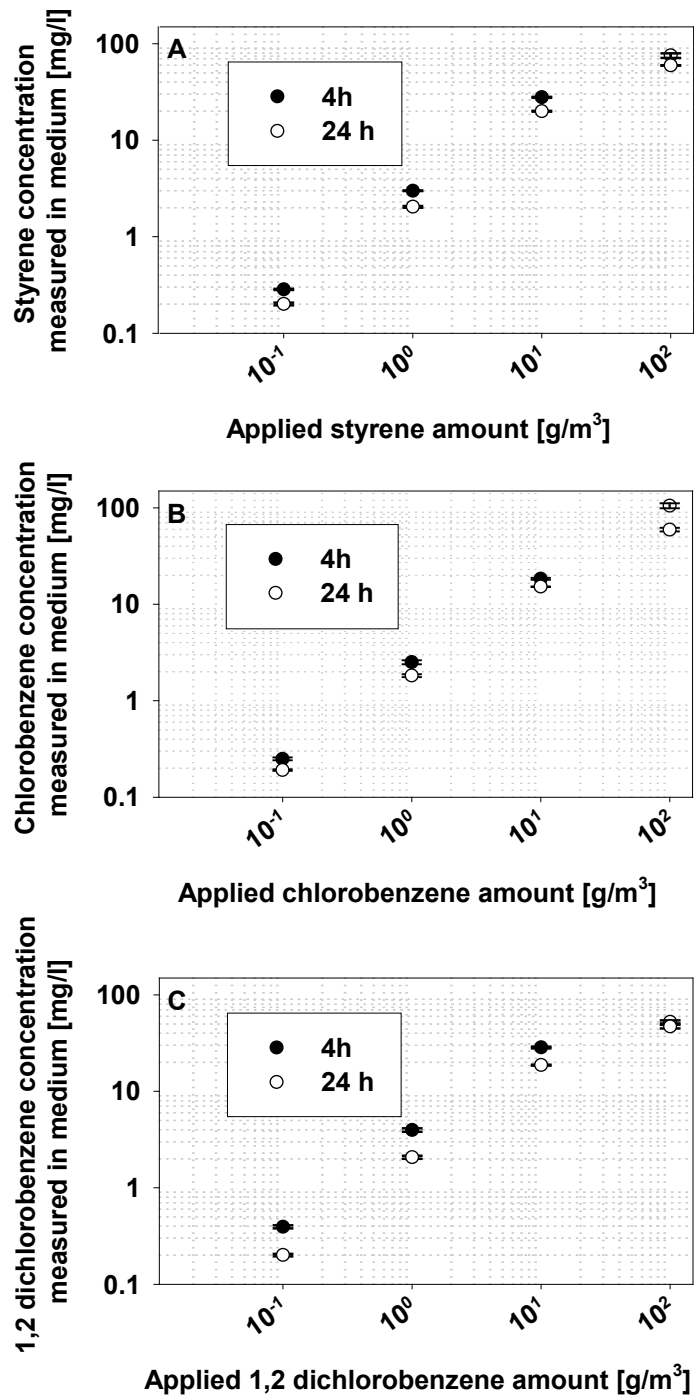


Figure 3-3 VOC concentrations in cell culture medium following cell exposure (4 h or 24 h) to styrene, monochlorobenzene or 1,2-dichlorobenzene. Cell culture medium was analyzed using headspace gas chromatography. Data are shown as mean of triplicates + SEM.

The mean partition coefficients ($c_{\text{medium}}/c_{\text{gas}}$) were calculated as described in section 2.2 for exposure concentrations of 10^{-1} g, 10^0 g and 10^1 g/m³ from measured medium concentrations and applied VOC amounts (see Table 3-3). In general, partition coefficients after 24 h treatment were lower than following 4 h treatment. As a rough trend, partition coefficients increased with decreasing exposure levels.

Table 3-3 Calculated partition coefficients ($c_{\text{medium}}/c_{\text{gas}}$). VOC concentrations in liquid phase (cell culture medium) were measured by headspace gas chromatography.

Exposure	Styrene		Monochlorobenzene		1,2-dichlorobenzene	
	4 h	24 h	4 h	24 h	4 h	24 h
10^1 g/m ³	2.79	2.00	1.84	1.52	2.85	1.87
10^0 g/m ³	3.00	2.04	2.51	1.82	3.97	2.08
10^{-1} g/m ³	2.84	2.01	2.50	1.91	3.93	2.01

3.3 Discussion

The existing exposure setup using transwell inserts for cell culture was successfully adapted for the application in proteomic approaches. In the beginning, a major problem was the strong binding of proteins from the culture medium to the insert's membrane. This resulted in a small number of highly abundant bovine proteins in the 2-DE pattern in contrast to the high number of human protein spots on 2D gels that were obtained when using flask cultures of the same cell line. Finally, a modified cell culture protocol provided a high-resolution (1,380 spots) proteome pattern.

However, the additional, extensive washing steps that were introduced in order to remove adhering serum proteins may have affected the cell's protein turnover/cell signaling. A procedure using antibodies to eliminate highly abundant (culture medium) proteins from cell lysates would also be useful. However, this approach was not applied in order to avoid a loss of less abundant proteins that might be bound to the abundant ones. Binding of small proteins, protein fragments and peptides to albumin or other highly abundant proteins (Zolotarjova *et al.*, 2005) can result in significant losses of less abundant species that are potential biomarkers (Linke *et al.*, 2007).

The collected identification data for 266 protein spots are in good agreement with the limited proteome data on A549 cells available in the literature. Myung and colleagues published proteome maps of chaperones for 10 cancer cell lines, including a map containing 35 spots from A549 cells (Myung *et al.*, 2004). The spot pattern is quite similar to the proteome map presented here. 22 protein spots are overlapping between the two analyses. For these spots, all presented identifications confirmed the earlier data whereas the remaining 13 spots identified by Myung and coworkers were not covered by the here presented map. Furthermore, (Forbus *et al.*, 2006), published a map of 89 nuclear proteins of

the A549 cell line. As could be expected, the nuclear spot pattern deviates significantly from the total soluble protein pattern published here.

For most protein spots, observed/experimental molecular weight and/or *pI* is very close to the predicted values extracted from UniProtKB/TrEMBL database. Posttranslational modifications, especially known and predicted phosphorylations (Blom *et al.*, 1999) could explain the significant *pI* shifts for spots with ID38, ID71, ID150, ID243, ID244 and ID259-61. For database entries of ID73, ID74 and ID119-21, Zhu *et al.* published similar experimental differences in *pI* as noticed in this study. The observed shifts were correlated to protein modifications. The modifications that cause such shifts include truncations and deletions that are often observed in cancer cells or phosphorylations that can shift the *pI* by several pH units. Large changes in the *pI* are often observed for proteins with a *pI* above 7.0 upon phosphorylation, whereas little change is observed for proteins with a *pI* of approximately 5.0 (Zhu *et al.*, 2005). Molecular weight and/or *pI* shifts for spots of ID104, ID245 and ID189 could be assigned to the occurrence of specific isoforms and were confirmed by peptide mass fingerprint analysis.

Monitoring the VOC concentrations in cell culture medium over the exposure period revealed a relatively stable distribution of the three VOCs between the air and the liquid phase in the cell culture exposure system. Calculated partition coefficients correspond well with published data, even though available data were mostly acquired in cell-free systems. Gargas and Andersen determined a partition coefficient ($C_{0.9\%NaCl}/C_{gas}$) of 1.41 ± 0.47 for styrene and 2.81 ± 0.07 for monochlorobenzene (Gargas *et al.*, 1989). Sato and Nakajima published a styrene partition coefficient (C_{aqua}/C_{gas}) of 4.68 ± 0.31 (Sato *et al.*, 1979). Further data on partitioning between cell culture medium and air are available for monochlorobenzene and 1,2-dichlorobenzene. Croute and colleagues found partition coefficients (C_{medium}/C_{gas}) of 4.66 and 3.38, respectively (Croute *et al.*, 2002). As investigated for styrene in this thesis, the distribution between air and liquid phase was not significantly affected when varying the salt content of the liquid phase. Thus, differences in partitioning in literature data may not be determined by the ingredients of the used liquid phases but by varying analytical equipment and exposure systems. McIntosh and Heffron provided evidence that cellular material added to a final concentration of 250 μ g protein per ml does not affect the partitioning in the studied two-phase system (buffer/air and medium/air) for dichloromethane, toluene and xylene (McIntosh *et al.*, 2000). However, it is interesting to note that the partition coefficients for the referred VOCs are higher by at least a factor of 10 when assessed in blood/air models (Gargas *et al.*, 1989; Sato *et al.*, 1979), pointing to enhanced storage in lipophilic compartments such as cell membranes.

The presented partition coefficients together with the relatively small medium phase (6 ml versus 600 ml gas phase) in the exposure system ensured that the applied VOC

concentrations remained stable during the experiments and cellular VOC exposure could occur mainly via the gas phase, thus mimicking cell exposure in the lungs. Slightly decreasing VOC concentrations in the culture medium concomitant with unchanged medium methanol concentrations over exposure time hint at VOC binding to culturing material and/or cellular metabolism of VOCs. In a cell-free experiment, no significant difference in VOC concentrations of the liquid phase was detected when PBS or water were used instead of protein-containing cell culture medium, demonstrating that no prominent VOC binding to culture medium proteins as for example, albumin occurred. Protein binding of activated VOCs such as styrene-oxide may be more probable.

4 *Toxicoproteomics of Styrene Exposure*

4.1 *Introduction*

4.1.1 *Styrene - Sources of Human Exposure*

Among the non-halogenated substances, styrene, of which 14 million tons are produced per year in the European Union, is one of the most important contaminants released from indoor sources. According to the Toxics Release Inventory, styrene was listed 16th among total reported air emissions (EPA, 2007). Moreover, approximately 21 million tons of styrene were consumed worldwide in 2000, a 50% increase since 1993 (Kolstad *et al.*, 1995).

Typical sources of emissions are factories producing styrene, polystyrene, plastics, synthetic rubber, and resins or boatbuilding facilities. Furthermore, styrene is released from motor vehicle emissions, stack emissions from waste incineration and wood smoke emissions as well as effluents from chemical, textile, latex, and coal gasification plants. General workplace styrene concentrations range from 89 $\mu\text{g}/\text{m}^3$ to $1.5 \times 10^6 \mu\text{g}/\text{m}^3$. It was estimated that approximately 300,000 workers at 22,000 facilities are exposed to styrene. The highest potential exposure occurs in the reinforced-plastics industry, where workers are exposed to high air concentrations and have dermal contact to liquid styrene. It has been estimated that heavily exposed workers in this industry in Finland might be exposed to up to 3 g of styrene per day (ATSDR, 2007).

Since 1987, the German threshold limit value for occupational exposure, called "Maximale Arbeitsplatzkonzentration" (MAK) and more recently Arbeitsplatzgrenzwert (AGW), for styrene is 20 ppm ($\sim 100 \text{ mg}/\text{m}^3$) while in the United States the current permissible exposure limit (PEL) for styrene is 100 ppm. This means that a worker should not be exposed to more than an average of 20 versus 100 ppm styrene via inhalation during a regular work day and without respiratory protection.

In addition, styrene evaporates from building materials (carpets, floor tiles, insulation), office copiers, and consumer products (disinfectants, plastics, paint, cigarettes) and contributes significantly to indoor air pollution (Crump, 1995). Average styrene emission rate from new carpets is $0.4 \mu\text{g}/\text{minute}/\text{m}^2$ (Hodgson *et al.*, 1993) and $2.3 \mu\text{g}/\text{minute}/\text{m}^2$ (Schaeffer *et al.*, 1996) from carpet cushioning material. Moreover, 18 μg of styrene has been detected in one cigarette (IARC, 1979). Printer operation was reported to cause test chamber concentrations of $380 \mu\text{g}/\text{m}^3$ (Kagi *et al.*, 2007). For photocopiers, emission rates averaged 3,300 $\mu\text{g}/\text{hour}$ (Leovic *et al.*, 1996).

Thus, the most likely mode of exposure for the general population is by inhalation of indoor air (EPA, 1985; Fleming-Jones *et al.*, 2003) where levels of styrene are in the range of 0.1– 50 $\mu\text{g}/\text{m}^3$. Based on the EPA estimate that a person spends 20.4 hours/day indoors inhaling about 17 m^3 mean indoor air (EPA, 1989), typical indoor exposure levels to styrene

may range from 1.7 to 850 µg/day. In contrast, outdoor air concentrations are small (0.28 to 20 µg/m³) (ATSDR, 2007). U.S. Environmental Protection Agency proposed a Reference Concentration of 1 mg/m³ (0.23 ppm) for styrene inhalation as an estimate of a daily exposure to the human population that is likely to be without an appreciable risk of deleterious effects during a lifetime (EPA, 1999). Additional human exposure may occur from ingestion of styrene-containing food. Styrene is a natural component of cheese, roasted nuts, dried legumes, fried chicken, cooked pork (Takeoko *et al.*, 1988; Tang *et al.*, 1983; Tang *et al.*, 2000), but concentrations are often very low, except for cinnamon, with concentrations up to 40,000 ppb (Tang *et al.*, 2000). Moreover, styrene may enter packaged foods by migration from polystyrene food containers and packaging materials, with concentrations ranging from <100 to >3,000 ppm, but common levels being much lower (5–30 ppb) (EPA, 1985; Tang *et al.*, 2000). Based on estimated food consumption rates, Tang *et al.*, 2000 reported an estimated annual general population exposure to styrene ranging from 0.8 to 4.5 mg/person from food. Finally, an estimated annual total (by food and inhalation) styrene exposure of 6.7–20.2 mg was derived. Smokers and those eating a high proportion of foods packaged in polystyrene may also have higher exposure to styrene, with the amounts estimated by smoking more than doubling the normal estimated exposure to styrene. In addition, workers with long-term employment at photocopy centers may also be exposed to high concentrations (Tang *et al.*, 2000).

4.1.2 Toxicokinetics of Styrene

Absorption of styrene mainly occurs through inhalation. In the conducting zone of the lung (trachea, bronchi and bronchioles), the gaseous styrene is partly absorbed during inhalation and is desorbed again during exhalation (Johanson *et al.*, 1992). The portion of styrene not being absorbed reaches the alveolar zone where the steady state between tissue and gas phase is immediately achieved. More than 90% of inhaled styrene is retained while the residual compound diffuses across the capillary endothelium into the pulmonary blood (Csanady *et al.*, 2003; Filser *et al.*, 1993; Fustinoni *et al.*, 1998). Only 0.7–4.4% of the amount of styrene absorbed in the lungs is exhaled unchanged (IARC, 1994b). Absorption of styrene from the gut is rapid, leading to the assumption that contact with styrene contaminated food or water will result in significant absorption. In contrast, dermal absorption of styrene is low compared to other routes (ATSDR, 2007; Wieczorek, 1985).

Inhalation studies with both, humans and animals, resulted in the widespread distribution of styrene with the highest concentration in adipose tissue (ATSDR, 2007). Styrene has been detected in blood (0.4 µg/l), exhaled breath (0.7–1.6 µg/m³), breast milk, and adipose tissue (8–350 ng/g) of the general population (Antoine *et al.*, 1986; EPA, 1986, 1987; Pellizzari *et al.*, 1982). The high octanol/water partition coefficient of styrene of 891 (log Po/w = 2.95) (Hansch *et al.*, 1995) suggests partitioning to fat tissues. Reported partition

coefficient between different body tissues (4100 for fat, 84-154 for other organs and 59 for blood) and air confirmed this hypothesis (Droz *et al.*, 1983; IARC, 1994b). However, styrene does not accumulate to high levels, because of its fast metabolism and effective elimination (EPA, 1984; Kenaga, 1980). Half-life of styrene in human blood is only a few minutes (Vodicka *et al.*, 2003).

Although inhalation is the most important route of styrene exposure, metabolic conversion takes place predominantly in the liver. In liver and lung, metabolism of styrene is activated by cytochrome P450 (CYP) to styrene 7,8-oxide (SO) with other alternative routes e.g. formation of styrene 3,4 oxide (see Figure 4-1) (Boogaard *et al.*, 2000; Manini *et al.*, 2002; Vodicka *et al.*, 2006). However, human pulmonary tissue is not particularly effective in metabolizing styrene to SO. In human lung microsomes, a styrene metabolism of 0.0065 nmol/min/mg protein, which is about 100-fold lower than the activity in rat microsomes, was reported (Nakajima *et al.*, 1994). Similarly, human liver metabolizes styrene to a lower rate than in rodents. Only CYP 2E1 was clearly assigned so far. However, human CYP1A2, 1A6, 2B6, 2C8, 2C9, 2D6, 2F1, 3A3, 3A4, 3A5 and 4B1 metabolize styrene *in vitro* with the highest metabolic rate for CYP2B6 and 2E1/2F1 (Nakajima *et al.*, 1994). Saturation of metabolism occurs between 100 and 200 ppm of styrene (Prieto-Castello *et al.*, 2010). Genetic polymorphisms of CYP2B6, CYP2D6 and glutathione S transferase P1 have been related to susceptibility to the metabolism of styrene in humans (Wang *et al.*, 2009)

SO is fairly reactive and has a short half life *in vivo* (Phillips *et al.*, 1994). In mammals, detoxification of SO is mainly realized by either epoxide hydrolysis leading to the formation of styrene glycol and the excretion of mandelic, phenylglyoxylic, benzoic and hippuric acid or glutathione conjugation resulting in the excretion of mercapturic acids (see Figure 4-1) (Csanady *et al.*, 2003; Sumner *et al.*, 1997; Vodicka *et al.*, 2006). Epoxide hydrolase (EH) is very active in both, human lung and nasal tissue, removing any small amounts of SO (Vodicka *et al.*, 2006) accounting for 95% of the absorbed dose (Prieto-Castello *et al.*, 2010). In addition to this pathway, the formation of phenylacetaldehyde, -ethanol, phenylacetic and -aceturic acid was observed with 5% of total metabolic activity. No more than trace amounts of GSH conjugates or ring-opened metabolites occur in humans exposed to styrene. As in humans, the EH pathway accounts for the greatest percentage removal of SO in rodents, but in contrast, the use of GSH conjugation is also an important metabolic pathway for removal of SO (Cruzan *et al.*, 2002).

In mice, there are four metabolic pathways with a different metabolic capacity: a) EH metabolism of SO resulting in styrene glycol and acidic metabolites (50%); b) SO conjugation with glutathione, excretion of mercapturic acids (30%); c) Formation of phenylacetaldehyde, -ethanol, phenylacetic and -aceturic acid (15%) and d) Oxidation of the benzene ring, formation of 4-vinylphenol (5%) (Figure 4-1). In rats, only the first three of the four pathways

have been reported, accounting for 70, 25 and 5% of styrene metabolism, respectively (Cruzan *et al.*, 2002).

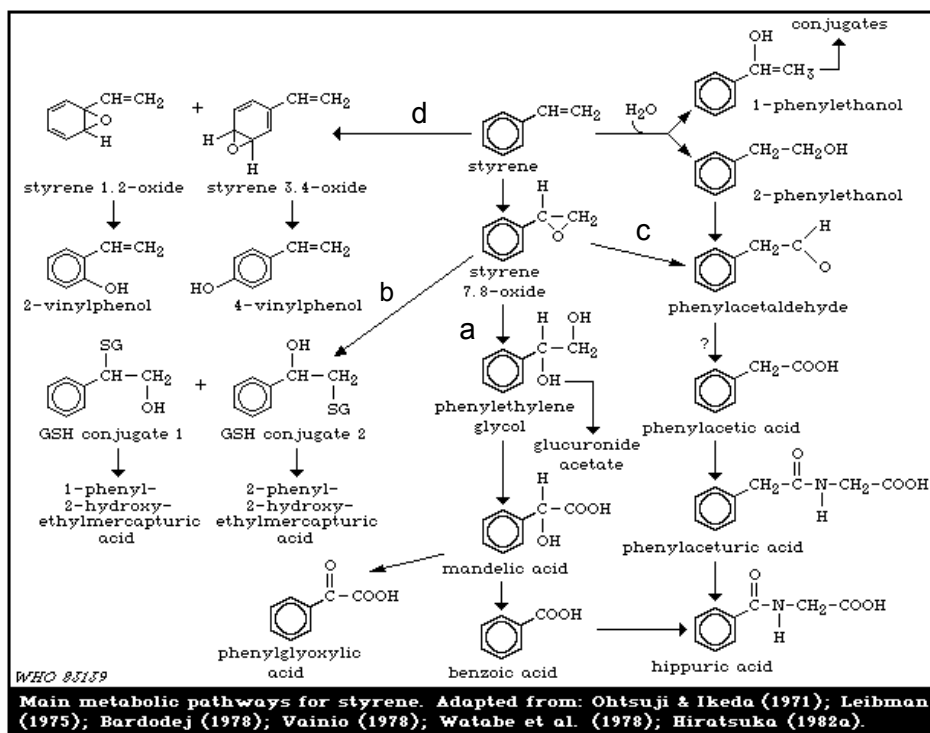


Figure 4-1 Main metabolic pathways for styrene in humans and rodents. The figure has been adapted from EHC, 1983.

4.1.3 Toxicodynamics of Styrene

Various toxic effects have been observed in experimental animals after exposure to styrene: hepatotoxicity, pneumotoxicity, neurotoxicity and reproductive toxicity (Bond, 1989; IARC, 1994b; Sumner *et al.*, 1997). Numerous studies have demonstrated marked differences in toxicity between rats and mice to styrene exposure, especially by inhalation. Mice are particularly sensitive to respiratory tract and hepatic toxicity from styrene. Styrene 7,8 oxide (SO), the major metabolite, induced forestomach tumors in rat and mice (Phillips *et al.*, 1994). Furthermore, in a chronic inhalation study with mice, a significant increase in late life lung tumors at 40-160 ppm for males and at 20-160 ppm in females was detected. In contrast to mice, rats tolerated up to 1000 ppm via inhalation for 2 years showing only slight nasal olfactory lesions (Cruzan *et al.*, 2002).

However, in humans, there is inadequate evidence for the carcinogenicity of styrene (Gerin *et al.*, 1998; Hirasawa *et al.*, 2005; IARC, 1994a). Epidemiologic studies revealed a weak connection to cancers of rectum and prostate (Gerin *et al.*, 1998). Furthermore, significant excess of malignant lymphoma have been observed among styrene-exposed workers. No clear increase in risk for congenital malformations among children of styrene-exposed women or of women married to styrene-exposed men has been reported (IARC, 1994a). Nevertheless, the International Agency for Research on Cancer lists styrene as a

possible human carcinogen (group 2b) and SO as a probable human carcinogen (group 2a) (Gerin *et al.*, 1998; Hirasawa *et al.*, 2005; IARC, 1994a).

The carcinogenic potential of styrene and SO is closely related to the fact that epoxides and epoxide-forming compounds can interact with biological macromolecules e.g. proteins or DNA. These primary DNA lesions may cause alterations in DNA ultra structure finally resulting in DNA strand breaks and mutations. The most prominent binding sites are the 7-position of guanine, the most nucleophilic center in the DNA molecule, or the 1-substituted adenine (Timbrell, 1998). SO-DNA adducts were found in urine and lungs of mice exposed to styrene via inhalation (750 or 1500 mg/m³). Styrene in blood, guanine DNA adducts in lungs and urinary excretion of these adducts increased with exposure while no guanine adducts were detected in liver (Vodicka *et al.*, 2006). 1-SO-adenine DNA adducts have been found in styrene exposed (mean 170.6 ± 114.5 mg/m³) lamination workers raising a high level of concern of cancer risk associated with occupational exposure (Melnick, 2002; Vodicka *et al.*, 2003).

The SO burden in different species is not correlated with the tumors. SO burden in bronchial epithelium was same in mice at 20 ppm (tumors) and in rats at 1000 ppm (no tumors). Moreover, styrene-induced GSH depletion is high in mice and low in rats and humans where SO burden is lower at the same styrene air concentrations as well (Kaufmann *et al.*, 2005). Further studies in mice revealed that SO exposure causes a significant increase in proliferation of Clara cells in bronchi and terminal bronchioles combined with glutathione depletion in bronchiolar epithelium. Thus, Clara cells, that are metabolically highly competent, were supposed to be the primary target for styrene-induced toxicity in murine lungs. It was concluded, that the carcinogenicity of styrene and SO might be a consequence of a weak genotoxic activity *in vivo* combined with a strong cell-proliferating activity (Kaufmann *et al.*, 2005; Phillips *et al.*, 1994). Finally, it was suggested that the human lung is incapable of generating sufficient SO to achieve the bronchiolar concentration produced in rodents, thus, respiratory tract effects caused by SO in rodents are not relevant for human risk assessment (Cruzan *et al.*, 2002).

Chronic styrene exposure to humans causes irritation of skin, eyes and the respiratory tract at low doses, whereas chronic bronchitis and obstructive pulmonary changes are reported at high concentrations (>100 mg/m³). Electroencephalographic, dopaminergic, functional and psychiatric impairments have been noted mostly at concentrations about 100 ppm (IARC, 1994b). Furthermore, occupational exposure with styrene was reported to cause behavioral deficits such as memory loss, fatigue and mood swings (Hirasawa *et al.*, 2005).

4.1.4 Effects of Styrene on Cellular Proteins

Formation of protein covalent binding with xenobiotics or their active metabolites has been recognized for a long time as a possible mechanism of chemical toxicity, especially for epoxides. Thus, cellular protein modification by SO was suggested to play an important role in styrene toxicity (Shen *et al.*, 2009). SO-modified proteins, such as albumin, hemoglobin and globin, have been detected in animals and humans after exposure to styrene (Teixeira *et al.*, 2007; Yeowell-O'Connell *et al.*, 1996). In rats, a linear dose response relationship for serum protein adducts was observed at low exposures to styrene or SO, while with increasing SO doses, a higher than proportional increase in the level of alkylation of hemoglobin was seen (Yuan *et al.*, 2007). For serum proteins, SO-adduction has been studied in more detail. Within amino acids and proteins SO alkylates nucleophilic sites including the cysteine sulphhydryl group, histidine imidazole, aspartic and glutamic groups as well as carboxylic groups in lysine. For individual amino acids cysteine showed superior reactivity (Basile *et al.*, 2002; Yuan *et al.*, 2007).

Apart from the studies on serum proteins, little is known about the interaction of SO with cellular proteins (Yuan *et al.*, 2007). Styrene epoxidation and covalent binding of SO to cellular proteins was reported for rat nasal mucosa samples incubated with 1-5 mM styrene. Nevertheless, the identities of the detected proteins have not been elucidated so far (Yuan *et al.*, 2007).

Since epidemiological studies provided evidence for impaired health caused by low-dose exposure to styrene (Diez *et al.*, 2000; Diez *et al.*, 2003), *in vitro* exposure models for the detailed analysis on the molecular level have been developed (Fischäder *et al.*, 2008; Lehmann *et al.*, 2008). Results from these studies point to pro-inflammatory effects of styrene mediated by the production of altered patterns of immune-modulating cytokines such as increased levels of the monocyte chemoattractant protein-1 (MCP-1) (Fischäder, 2006; Roder-Stolinski *et al.*, 2008b) which was also observed in mice (Diodovich *et al.*, 2004). This chemokine is known to induce T-cell differentiation toward a Th2 phenotype, with the consequence of an enhanced susceptibility to allergic hyperreactivity (Fischäder, 2006). Moreover, inhalation of styrene (100 ppm) potentiated murine interleukin 4, 5 and 13 production, resulting in increased immunoglobulin E levels and inflammatory reaction. Thus, styrene is supposed to act as immune response modifier, contributing to asthma exacerbation (Ban *et al.*, 2006). Furthermore, it was found out recently that styrene vapors (75 ppm) initiate the murine sensory irritation response through electrophile-sensitive TRPA1 receptor detection of their CYP450 metabolites (Lanosa *et al.*, 2010).

In addition to pro-inflammatory proteins, recent studies provide evidence for styrene-induced modulation of stress response proteins such as heat shock proteins, metallothioneins, superoxide dismutase 1, heme oxygenase 1 as well as apoptosis-related

proteins (Dare *et al.*, 2002; Feltens *et al.*, 2010; Harvilchuck *et al.*, 2009a; Harvilchuck *et al.*, 2009b; Roder-Stolinski *et al.*, 2008b; Vettori *et al.*, 2005; Yang *et al.*, 2008).

In order to obtain an extensive understanding of styrene-caused proteotoxic effects, styrene-induced differential expression and differential phosphorylation of total soluble proteins have been studied in human lung epithelial cells (A549). In addition, intracellular adduction of proteins with styrene oxide has been investigated.

4.2 Results

4.2.1 Styrene Toxicity in the Cell Model

Cell toxicity of styrene for human lung epithelial cells (A549) exposed directly via the gas phase has been monitored. Total cell number and cell viability were measured by Trypan blue exclusion after 24 h of exposure. The total cell number decreased to 69.6% relative to control cells following exposure to 10^2 g/m³ styrene. With decreasing styrene concentration total cell number reached 77.4% (10^1 g/m³, 0.19 mM) and 88.1% (10^0 g/m³, 0.019 mM) relative to control cells (data not shown).

Control cells showed a high viability (92-94%) under the exposure conditions (no serum supplementation, growth on membrane inserts, trypsinization). Viability of exposed cells, as assessed by Trypan blue, decreased with increasing concentration of styrene to 40% upon exposure to 10^2 g/m³ (Figure 4-2 A).

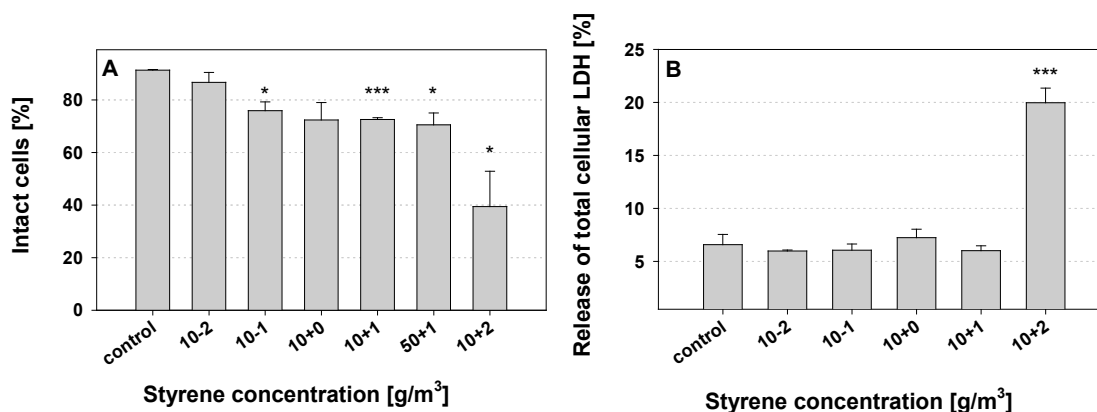


Figure 4-2 Cell toxicity of styrene exposure (24 h) on A549 cells was estimated using Trypan blue exclusion (A) and lactate dehydrogenase (LDH) release (B). LDH release is normalized versus total LDH as estimated by a lysis control. Data are shown as mean of triplicates + SEM. * $p < 0.05$, ** $p < 0.01$, *** $p < 0.001$.

Membrane damage was assessed by measuring lactate dehydrogenase (LDH) release into the cell culture medium (Figure 4-2 B). LDH release within 24 h increased up to 20% of total cellular LDH (estimated by lysing all cells of a transwell insert) compared to control cultures (only 6% of LDH_{total}) when cells were exposed to 10^2 g/m³ styrene. No membrane damage could be detected when exposing cells to lower concentrations.

From the collected toxicity data, a No Observed Effect Concentration (NOEC) of 10^{-2} g/m³ has been derived following a 24 h exposure in this experimental setup.

4.2.2 *Differential Protein Expression in 2-DE*

In this study, five styrene concentrations (10^{-3} g, 10^{-2} g, 10^{-1} g, 10^0 g and 10^1 g/m³) have been applied for differential protein expression analysis in gel replicates. Using 10^{-2} g (2.3 ppm) and 10^{-3} g styrene/m³ (0.23 ppm), cells were exposed to concentrations that are in the range of concentrations of indoor ambient air e.g. in working places. Quantification of the expression of about 1,380 protein spots of A549 cells with pI between 3 and 10 was done by Delta 2D 3.6 software. The reproducibility of the gels was confirmed by cluster analysis, by which the comparisons between the different samples and the controls showed a clear clustering according to the experiments (clustering dendrograms are shown in Figure 8-1 in the appendix). Significantly regulated protein species are listed in Table 4-1 and a subset is displayed in more detail in Figure 4-3 and Figure 4-4.

In total, 71 protein species with altered expression (by a factor of 1.5 or more, $p < 0.1$) have been detected, 51 being induced (71.8% of all differentially expressed spots) and 20 being repressed. 64 of the listed protein spots displayed a difference with higher significance ($p < 0.05$) in at least one of five styrene concentrations between 10^1 g and 10^{-3} g/m³. Thus, only 4.64% of all quantified protein spots (64 of 1380) showed differential expression (by a factor of 1.5 or more, $p < 0.05$) following cell exposure to styrene. A total of 24 protein spots were significantly ($p < 0.05$) changed (factor > 1.5) by at least two, 13 protein spots by at least three of the five different styrene concentrations. The highest number of protein expression changes was observed for the two highest styrene concentrations applied. Following exposure to 10^1 g/m³, 17 proteins were up- and 7 were downregulated. When applying 10^0 g/m³, 22 proteins were significantly up- and 7 were downregulated. Using lower concentrations less differentially expressed proteins (10^{-1} g/m³: 6 up, 7 down; 10^{-2} g/m³: 9 up, 8 down; 10^{-3} g/m³: 12 up, 5 down) have been observed.

Some proteins changed their expression in a roughly concentration-dependent manner, e.g. transaldolase, moesin, thioredoxin reductase 1 or protein DJ-1. However, for most regulated protein spots no direct correlation between expression and exposure concentration has been observed. The strongest upregulation was observed for 60S ribosomal protein L5 (5-fold control level), the strongest downregulation for tumor rejection antigen (one fifth of control level).

Differentially expressed proteins were assigned to their major role (see Table 4-1) within the cell, based on their main functions listed in the UniProtKB/TrEMBL database as well as in existing scientific literature. According to this grouping, identified proteins with modulated expression after exposure to styrene are involved in five different cellular processes such as oxidative stress regulation (16 proteins), inflammation (4 proteins), cell

death signaling (16 proteins), protein quality control (7 proteins) and metabolism (12 proteins) (see Table 4-1). The fundamentals of the applied protein grouping including references and their derived biological significance being the basis for further validation experiments presented in this chapter are discussed in section 4.3.

Table 4-1 Identified protein spots of differentially expressed proteins following exposure to styrene

ID ^{a)}	Protein involved in process	Accession ^{b)}	Exposure-dependent expression level ^{c)}				
			10 ⁻³	10 ⁻²	10 ⁻¹	10 ⁰	10 ¹
Oxidative stress							
2	Chloride intracellular channel protein 1	O00299			1.38°	2.50***	
13	Isocitrate dehydrogenase	O75874					1.51°
22	Superoxide dismutase [Cu-Zn]	P00441	1.51**		1.72*		
77	Glucose-6-phosphate 1-dehydrogenase	P11413			1.50*		
93	Aldose reductase	P15121				2.26*	
99	Phosphoglycerate mutase 1	P18669				1.56°	1.61°
104	Thioredoxin reductase 1	Q16881				1.38*	1.57*
110	NADH-ubiquinone oxidoreductase 75 kDa subunit	P28331					1.63*
123	Aldehyde dehydrogenase 3A1	P30838	1.31*	1.40*		1.46**	1.70**
133	Transaldolase	P37837	1.58°	1.73°		2.29**	2.37*
161	6-phosphogluconate dehydrogenase	P52209				2.71**	1.80°
165	Biliverdin reductase A	P53004	1.60**				1.88**
184	Peroxiredoxin-1	Q06830	1.68°				
190	Peroxiredoxin-4	Q13162			0.58°	0.72°	
216	GDI2 protein	Q6IAT1				1.57*	
217	GDI2 protein	Q6IAT1				1.36°	1.72*
228	Protein DJ-1	Q99497	1.67*	1.86°	1.91*		1.99*
Inflammation							
36	Heat shock protein beta 1	P04792			0.37**		0.40*
109	Moesin	P26038			1.34°	1.59**	2.05**
211	Annexin A7	Q5T0M6	1.92***			2.31**	1.98***
224	Annexin A2	Q8TBV2				1.64°	1.64*
Cell death signaling							
27	Lamin-A/C	P02545	0.64°	0.64*			
28	Lamin-A/C	P02545		0.59*			
31	Annexin A1	P04083				2.11*	1.65°
2x38	Vimentin	P08670	1.75-1.90*				
59	Vimentin	P08670		1.50*			
60	Vimentin	P08670			1.48*		
63	Annexin A5	P08758			1.76*		1.22*
68	Annexin A4	P09525					1.55*
70	Annexin A4	P09525	1.86°				
94	Ezrin	P15311	1.96*			1.73*	2.38**
100	Voltage-depend. anion-selective channel protein 1	P21796					0.42°
149	Voltage-depend. anion-selective channel protein 2	P45880		0.57*	0.47***		0.58**
150	60S ribosomal protein L5	P46777		2.24*		2.06*	2.11°
176	Eukaryotic translation initiation factor 5A-1	P63241	1.51**	2.04*		2.77*	
177	Actin, cytoplasmic 2	P63261		0.60*			
182	Lamin-B2	Q03252	0.64**	0.62**		0.79*	0.72**
213	Tumor protein translationally controlled 1	Q5W0H4			2.82***		
219	PDCD6IP protein	Q6NUS1					1.87**
222	Nucleoside diphosphate kinase	P15531	1.51°		1.68°	1.84**	
241	Pre-mRNA-processing factor 19	Q9UMS4					1.57*
244	60S ribosomal protein L5	P46777		4.70°		5.02***	
Protein quality control							
160	T-complex protein 1 subunit theta	P50990				0.33*	
180	T-complex protein 1 subunit beta	P78371		1.38°		1.32°	2.10°
201	Heat shock 70kDa protein 4	Q2TAL4	5.25**				
203	Eukaryotic translation initiation factor 4B	Q4G0E3	0.34°		0.26*	0.26*	0.19*
206	Proteasome 26S non-ATPase subunit 11	Q53FT5				1.54**	
209	Tumor rejection antigen (Gp96) 1	Q5CAQ5	0.44°	0.21*		0.26*	
243	Ribosomal protein S3a	Q6NXR8		0.44°	0.69°	0.36*	0.58°

Second part of Table 4-1

ID ^{a)}	Protein involved in process	Accession ^{b)}	Exposure-dependent expression level ^{c)}				
			10 ⁻³	10 ⁻²	10 ⁻¹	10 ⁰	10 ¹
Metabolism							
19	Retinal dehydrogenase 1	P00352	1.41 [°]	1.57*			1.76 [°]
39	Gelsolin	P06396				2.27*	
40	Alpha-enolase	P06733	1.41*	1.45**		1.80**	
41	Alpha-enolase	P06733	1.77*			2.36*	2.06*
42	Alpha-enolase	P06733	1.99*	2.28*	1.33*	2.67**	2.07*
43	Alpha-enolase	P06733		1.55*		2.56**	
44	Alpha-enolase	P06733	1.57*		1.77**		
57	Laminin subunit beta-1	P07942				0.38*	
47	L-lactate dehydrogenase B chain	P07195	0.56*				
48	L-lactate dehydrogenase B chain	P07195		0.60*	0.50*		
50	L-lactate dehydrogenase B chain	P07195	0.46*				
2x76	Glycogen phosphorylase	P11216	0.64*		0.55*	0.32**	0.45**
106	ATP synthase	P25705		0.56*			
125	Cytochrome b-c1 complex subunit 1, mitochondrial	P31930			0.55*	0.66 [°]	
126	HNRPH1 protein	P31943		1.24*		1.60**	0.61*
128	Kinesin-1 heavy chain	P33176		1.66*			
129	Kinesin-1 heavy chain	P33176		2.39*			
143	Glycyl-tRNA synthetase	P41250				1.50*	
145	Glycyl-tRNA synthetase	P41250				1.76*	
223	Elongation factor 2b	Q8TA90	2.03*	2.44**	0.64 [°]	1.37*	2.75***

a) For spot IDs see proteome map in Figure 3-2

b) Uni-Prot Accession from www.uniprot.org

c) Expression level (exposed *versus* control) following exposure to styrene (10⁻³ to 10¹ g/m³). [°] p<0.1, * p<0.05, ** p<0.01, *** p<0.001

Only significant expression changes are listed. Mass spectrometric identification data are found in the appendix (Table 8-1)

4.2.3 Styrene Exposure Modulates Oxidative Stress Proteins

Intriguingly, several redox-sensitive proteins susceptible to styrene exposure have been differentially expressed. Except peroxiredoxin-4, all proteins of this group showed increased expression, especially following exposure to higher styrene concentrations. The induction of common oxidative stress markers such as superoxide dismutase [Cu-Zn], biliverdin reductase A and thioredoxin reductase 1 has been observed. DJ-1 protein was induced significantly at 3 of 5 styrene concentrations. In addition, key enzymes of the pentose phosphate pathway involved in the regeneration of reducing equivalents (NADPH) such as transaldolase 1 (TALDO1), 6-phosphogluconate dehydrogenase (PGD), glucose-6-phosphate 1-dehydrogenase and cytosolic isocitrate dehydrogenase have been identified. Transaldolase and aldehyde dehydrogenase 3A1 showed significantly increased expression at 4 of 5 exposure levels. Furthermore, expression of aldose reductase (AR) and chloride intracellular channel protein 1, a redox-sensitive ion channel, has been found to be doubled when cells were exposed to 10⁰ g/m³ styrene. Further explanations on the relevance of the observed effects will be given in section 4.3. In conclusion, the early molecular response of the cells in this model seems to be governed by an oxidative stress response.

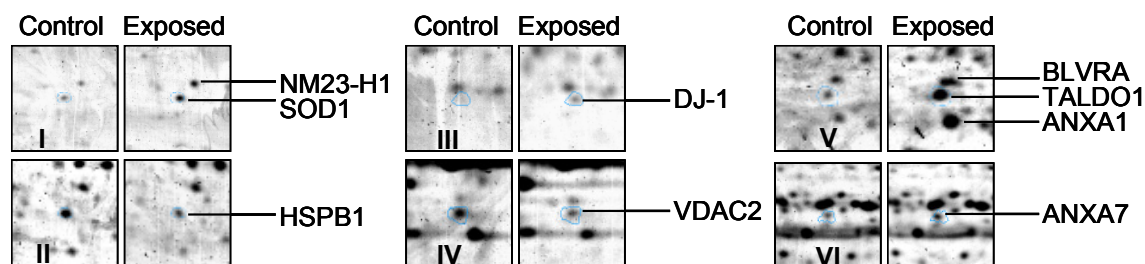


Figure 4-3 Examples of gel image regions of differentially expressed proteins following styrene exposure. 250 μ g of total soluble protein of the A549 cell line were separated by 2-DE (18 cm IPG strips 3-10 NL, 12% acrylamide/bisacrylamide) and quantitatively analyzed. Abbreviations are gene names. Explanations are found in Figure 4-4. Differential expression areas are highlighted in the A549 proteome map (see Figure 3-2).

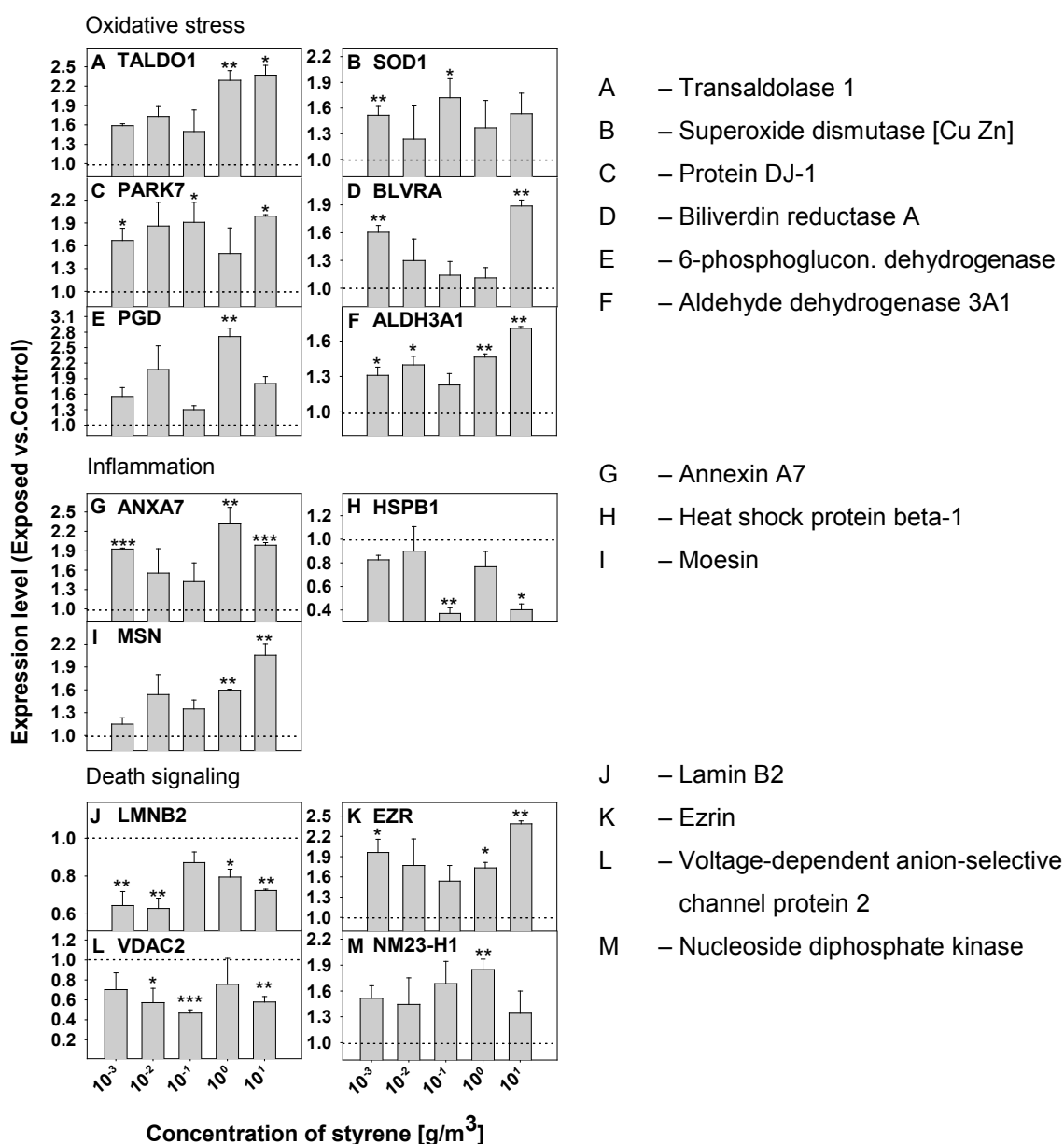


Figure 4-4 Profiles of proteins displaying changes in expression after cellular (A549) exposure to styrene. Expression levels are spot volumes relative to spot volumes of control (see dotted line), given as means + SEM of 2-4 replicates. Abbreviations are gene names. * $p < 0.05$, ** $p < 0.01$, *** $p < 0.001$.

4.2.4 *Styrene Exposure May Stimulate an Inflammatory Process*

As expected from epidemiologic studies, styrene exposure also affects expression of proteins linked to inflammatory processes. The observed doubling ($p < 0.01$) in expression of annexin A7 at concentrations of 10^1 and 10^0 g/m^3 as well as 10^{-3} g/m^3 may be indicative for stimulated secretion of lung surfactant that delimitates lung injury during non-infectious and inflammatory challenge. Furthermore, heat shock protein B1 (HSPB1) expression was decreased to a level of about 40% (relative to the control) at 10^1 g/m^3 as well as at 10^{-1} g/m^3 styrene. A two-fold increased expression of moesin, an important molecule for leukocyte adhesion during inflammation, was observed. Peroxiredoxin 4 expression was limited to 58% relative to the control level when cells were exposed to styrene at a concentration of 10^{-1} g/m^3 . Further explanations on the relevance of the observed effects will be given in section 4.3.

4.2.5 *Styrene Affects Abundance of Cell Death-Related Proteins*

From the observed effects, clues for the modulation of cell death-related proteins have been derived. Nucleoside diphosphate kinase A (NM23-H1), an apoptosis-inducing DNase, showed increased expression at all styrene concentrations, reaching levels of up to 185% relative to control cells at a concentration of 10^1 g/m^3 ($p < 0.01$). Annexin A1 expression, known for its involvement in apoptosis signaling, was increased at several concentrations, with a more than doubled expression when cells were exposed to 10^0 g/m^3 of styrene. The programmed cell death 6-interacting protein, also known as ALG-2/AIP-complex, is supposed to play a modulating role at the interface between cell proliferation and cell death. The protein was also upregulated when cells were exposed to 10^1 g/m^3 styrene. In contrast, voltage-dependent anion-selective channel protein 2 (VDAC2) showed significantly decreased expression when exposed to styrene at three concentrations (10^{-2} g/m^3 , 10^{-1} g/m^3 , 10^1 g/m^3). Reduced levels of VDAC2 make cells more susceptible to apoptotic death. Furthermore, several different lamins, known to undergo proteolysis during apoptosis, revealed reduced expression in the presence of styrene. Translation initiation factor eIF-5A, playing a role in apoptosis, was significantly upregulated at three styrene concentrations, including the lowest one of 10^{-3} g/m^3 . Increased intensity of two protein spots identified as 60S ribosomal protein L5 (RPL5) was observed at all concentration levels. RPL5 was recently linked to apoptosis signaling. Further explanations on the relevance of the observed effects will be given in section 4.3. In summary, these data provide evidence that styrene, besides oxidative stress, also induces apoptotic pathways.

4.2.6 Styrene, Metabolic Changes and Protein Quality Control

A relatively high number (7) of proteins that can be connected to protein quality control, such as t-complex protein 1, tumor rejection antigen, proteasomal and ribosomal proteins were differentially altered in expression following styrene exposure as well as proteins involved in the cellular metabolism (12), such as glycyl-tRNA synthetase and glycogen phosphorylase. Further explanations on the relevance of the observed effects will be given in section 4.3.

4.2.7 Differential Phosphorylation Patterns in 2-DE

It is widely accepted, that one third of all proteins in eukaryotic cells are phosphorylated at any given time (Wu *et al.*, 2005). The combination of 2-DE and phospho-specific Pro Q Diamond staining was successfully employed for analyzing changes in protein phosphorylation, enabling the identification of kinase/phosphatase targets with a detection sensitivity of 0.1 fmol of mono-phosphorylated proteins. It allows for the detection of general protein phosphorylation states at Tyr-, Ser-, or Thr-residue(s) with a strong correlation between the observed fluorescence signal and the number of phosphates per protein (Jin *et al.*, 2006; Orsatti *et al.*, 2009).

Thus, in addition to the applied total protein staining, this phospho-specific dye was used in the 2-DE experiment for the analysis of changes in this post translational modification induced by styrene (Figure 4-5) and chlorinated benzenes (see section 5.2.3). 200 µg of total soluble protein of A549 cells were separated by 2-DE (7 cm IPG strips, pH 3-10 NL), and phosphoproteins (Figure 4-5 A) as well as total protein (B) were stained using Pro Q Diamond and SYPRO Ruby, respectively. Both images of the same gel are overlaid in C (A in blue and B in orange). Comparing the staining patterns of Pro Q Diamond and SYPRO Ruby on the same 2D gel, only a limited number of overlapping protein spots can be found (black spots in Figure C). In most cases, highly abundant protein spots (high intensity in B) do not show intense phospho-specific staining. Thus, many phosphorylated proteins were of low abundance as also observed by Jin *et al.*, 2006 for human blood monocyte proteins. Strikingly, most protein spots with high intensity for the phospho-specific dye are located in the gel part of proteins with acidic isoelectric points. This phenomenon will be discussed in section 4.3.

Pro Q Diamond Phosphoprotein stain enabled the detection of differential protein phosphorylation following styrene treatment (10^{-4} g/m³ and 10^0 g/m³). Differential expression of phosphoproteins following one hour of styrene treatment is displayed in Figure 4-5 D, where areas 1-8 (as indicated in Figure A) are compared between gels of styrene-treated and untreated control cells. Overall, 28 protein spots detected by phospho-specific fluorescence staining showed significantly (at least $p < 0.1$) altered phosphorylation (Table 4-2). Most protein spots (26 out of 34) detected indicated reduced intensity compared to the corresponding spots in control cells. Only 14 protein spots changed their intensity after

exposure to the low styrene concentration (10^{-4}g/m^3), whereas 20 protein spots were detected with modified intensity following cell exposure to 10^0g/m^3 of styrene.

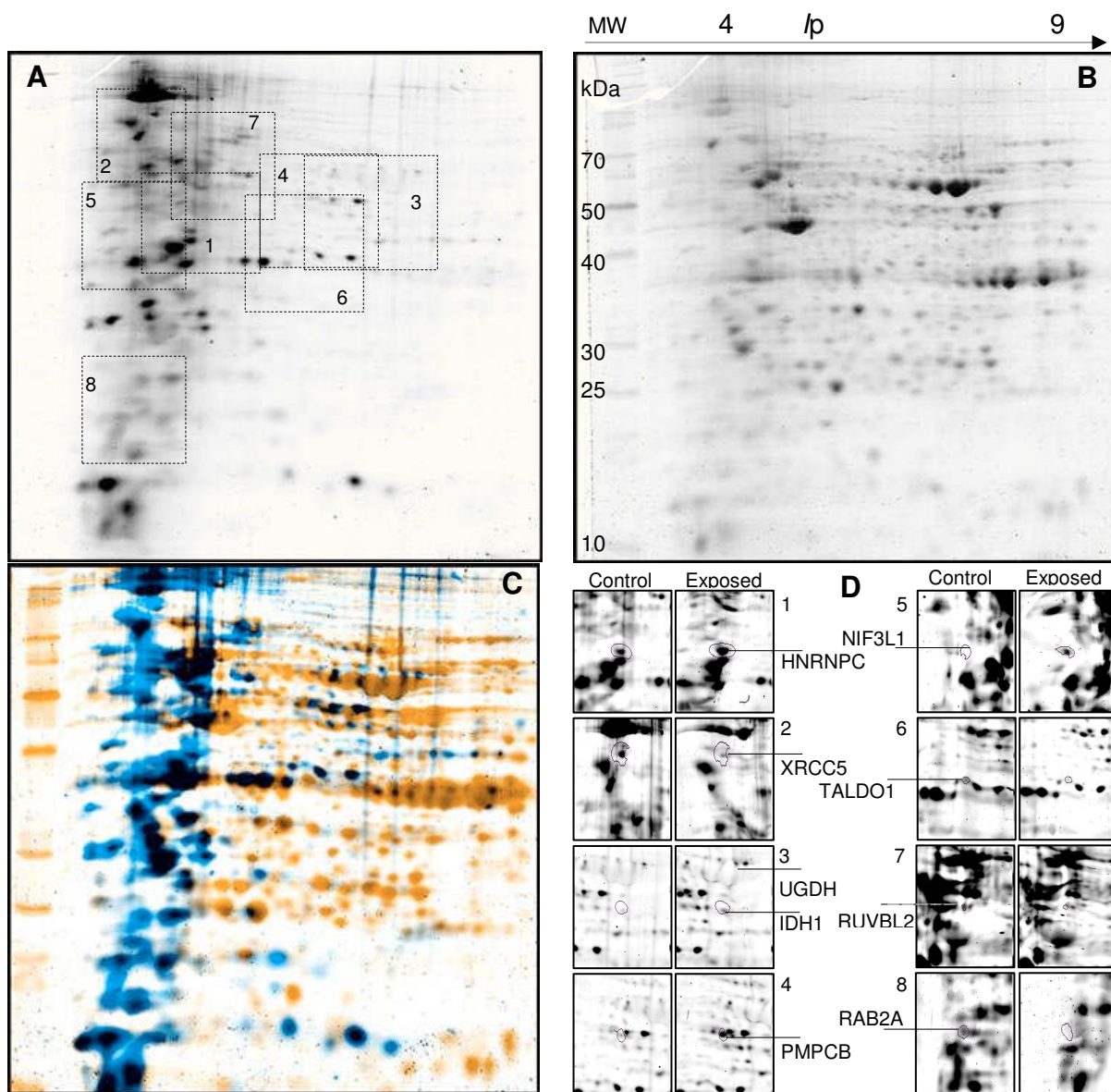


Figure 4-5 Pro Q Diamond Phosphoprotein stain enables detection of differential protein phosphorylation following styrene treatment. 200 μg of total soluble protein of A549 control cells were separated by 2-DE (7 cm IPG strips, pH 3-10 NL) and phosphoproteins (A) as well as total proteins (B) were stained using Pro Q Diamond and SYPRO Ruby, respectively. Both images of the same gel are overlaid in C (A shown in blue, B shown in orange). Differential expression of phosphoproteins following one hour of styrene treatment is displayed in more detail in D. Enlargements 1-8 are also labeled in A. Given abbreviations are gene names. Full protein names are found in Table 8-4 in the appendix. The underlying quantification data are listed in Table 4-2. Mass spectrometric identification data are found in the appendix in Table 8-2.

The greatest induction of phosphorylation was detected for NIF3-like protein 1, which showed a more than 7-fold increase with respect to the intensity of controls and was the only protein with amplified intensity after treatment of A549 cells with the lower styrene concentration. In contrast, 7 protein spots, identified as UDP-glucose 6-dehydrogenase, isocitrate dehydrogenase, ATP citrate synthase, heterogeneous nuclear ribonucleoprotein C1/C2 (two spots), programmed cell death 6-interacting protein and mitochondrial-processing peptidase, were detected with significantly higher phospho-specific intensity following exposure to the higher concentration of styrene.

The strongest repression of phosphorylation occurred for Ras-related protein RAB2A, which was detected with only one fifth of its intensity compared to controls. Six protein spots displayed decreased staining after treatment with both styrene concentrations: heat shock 70 kDa protein 4, proliferating cell nuclear antigen, 14-3-3 protein theta, 40S ribosomal protein S7, glyceraldehyde-3-phosphate dehydrogenase as well as aspartate aminotransferase. DNA-damage binding protein 1 (DDB1) showed a 4 times lower phospho-specific fluorescence. A spot, identified as transaldolase 1 (TALDO1) showed only half the phosphorylation intensity in response to the low styrene (10^{-4} g/m³) concentration compared to the level displayed by control cells. The spot has a slightly higher molecular weight and lower isoelectric point than the two main transaldolase spots that show a high phospho-specific staining but no differential phosphorylation following styrene treatment (see Figure 4-5 D, enlargement 6). In contrast, in the total protein approach TALDO1 (key enzyme of the PPP) showed increased expression for 4 of 5 styrene concentrations.

Nearly all identified proteins are well-known phosphoproteins (listed as such in the UniProtKB/TrEMBL database) or have at least predicted phosphorylation sites (in PhosphoSitePlus; www.phosphosite.org). The only protein identified here, for which no phosphorylation site has been known or predicted is the thioredoxin domain-containing protein 5, that showed only one fifth of its normal phospho-specific intensity in styrene-treated cells.

Six of the proteins showing differential phosphorylation were also detected earlier in the total proteomic approach where Coomassie staining was used to map differences in protein expression (see Table 4-1). For isocitrate dehydrogenase and programmed cell death 6-interacting protein (PDCD6IP) that showed increased phosphorylation, protein expression was also found to be increased. Alpha-enolase, transaldolase 1 and heat shock protein 70 kDa protein 4 as well as vimentin showed reduced phosphorylation but increased protein expression. A detailed discussion of views from the literature with respect to the detected protein phosphorylation events and derived biological fundamentals is presented in section 4.3.

Table 4-2 Differentially expressed phosphoproteins following one hour treatment with styrene

Spot	Identification ^{a)}	Accession ^{a)}	Expression level ^{b)}	
			10 ⁰ g/m ³	10 ⁻⁴ g/m ³
P1	DNA damage-binding protein 1	Q16531		0.25**
P2	Heat shock 70 kDa protein 4	P34932	0.53°	0.35**
P3	Isocitrate dehydrogenase [NADP] cytoplasmic	O75874	2.00*	
P4	ATP-dependent DNA helicase 2 subunit 2	P13010	0.30°	
P5	Protein disulfide-isomerase	P07237	0.52*	
P6	UDP-glucose 6-dehydrogenase	O60701	2.50*	
P7	Vimentin	P08670	0.50***	
P8	Thioredoxin domain-containing protein 5	Q8NBS9	0.20*	
P9	RuvB-like 2	Q9Y230		0.39°
P10	Actin, cytoplasmic 1	P60709	0.51°	
P11	40S ribosomal protein SA	P08865	0.34*	
P12	ATP-citrate synthase	P53396	1.98°	
P13	Glyceraldehyde-3-phosphate dehydrogenase	P04406	0.51°	0.33**
P14	Mitochondrial-processing peptidase subunit beta	O75439	3.19*	
P15	Heterogeneous nuclear ribonucleoproteins C1/C2	P07910	2.03°	
P16	Heterogeneous nuclear ribonucleoproteins C1/C2	P07910	2.23*	
P17	NIF3-like protein 1	Q9GZT8		7.56**
P18	Proliferating cell nuclear antigen	P12004	0.40°	0.47°
P19	14-3-3 protein epsilon	P62258		0.27**
P20	14-3-3 protein theta	P27348	0.35*	0.43**
P21	Proteasome subunit alpha type-3	P25788		0.65°
P22	Programmed cell death 6-interacting protein	Q8WUM4	1.79°	
P23	Aspartate aminotransferase, cytoplasmic	P17174	0.33*	0.39*
P24	Aldo-keto reductase family 1 member B10	O60218		0.40°
P25	Ras-related protein Rab-2A	P61019	0.19°	
P26	40S ribosomal protein S7	P62081	0.33°	0.20°
P27	Alpha-enolase	P06733		0.37°
P28	Transaldolase	P37837		0.48*

a) Uni-Prot Accession from www.uniprot.org

b) Expression level (exposed versus control) following exposure to styrene. ° p<0.1, * p<0.05, ** p<0.01, *** p<0.001. Only significant expression changes are listed. Mass spectrometric identification data are found in the appendix (Table 8-2)

4.2.8 Validation of 2-DE Results on Protein and Transcript Level

From each of the three important biological pathways, oxidative stress, death signaling and inflammation, which were affected by styrene treatment, one protein has been selected to validate 2-DE quantification results by an independent method: superoxide dismutase 1 (SOD1), voltage-dependent anion-selective channel protein 2 (VDAC2) and heat shock protein beta 1 (HSPB1). Using SDS-PAGE and immunoblot for detection of all three proteins from samples obtained after exposure to styrene at concentrations of 10^0 g/m³ and 10^{-4} g/m³, the results from 2-DE have been confirmed (Figure 4-6). Applying 5-20 μ g of total soluble protein, a slight (10-20%) but non-significant change in expression has been detected at the concentration of 10^0 g/m³ styrene for all three proteins (expression normalized versus beta-actin from the same sample). In the cells exposed to the lower concentration of styrene (10^{-4} g/m³), a significant ($p < 0.05$) increase in expression of SOD1 (174% of control) and a decrease in expression of VDAC2 (47% of control) and HSPB1 (57% of control) has been observed, similar to what was found in the 2-DE analysis (see Figure 4-4, Table 4-1).

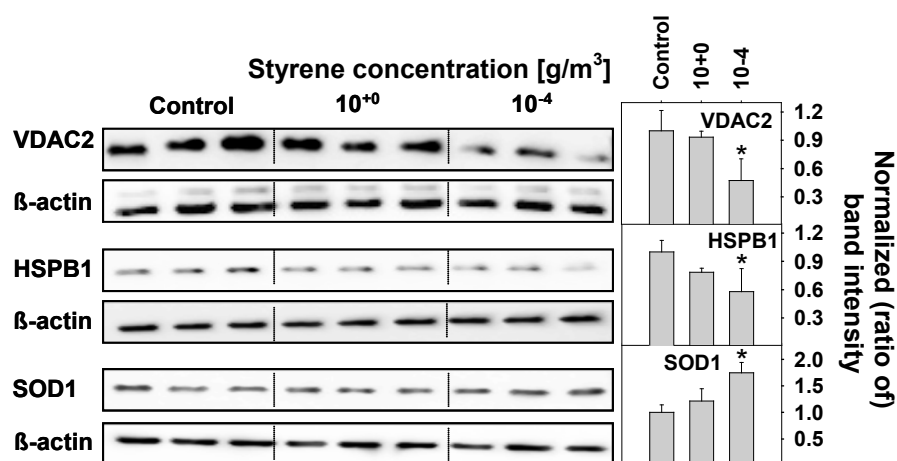


Figure 4-6 Western blot analysis of A549 cell lysates confirms differential protein expression of superoxide dismutase 1 (SOD1), voltage-dependent anion-selective channel protein 2 (VDAC2) and heat shock protein beta 1 (HSPB1) following cell exposure to styrene. 20 μ g of total soluble protein were used for every lane in Western blots against SOD1 and HSPB1, whereas only 5 μ g of total soluble protein were used for every lane in the Western blots against VDAC2. Beta-actin signals of every lane were used for normalization. Changes in band intensity (arbitrary units) are given relative to the control and calculated as mean of triplicates + SEM. * $p < 0.05$.

In a second validation step, quantitative PCR has been employed to estimate relative transcript concentrations of the earlier confirmed styrene targets voltage-dependent anion-selective channel protein 2 (VDAC2), superoxide dismutase 1 and heat shock protein beta (HSPB1). Initially, the relative transcript fluctuation of two typical housekeeping genes, β 2-microglobulin and glyceraldehyde-3-phosphate dehydrogenase (GAPDH), over exposure time was investigated in styrene-treated (10^0 g/m³ or 10^{-4} g/m³) and control cells (Figure 4-7). Total transcript copies of GAPDH varied depending on styrene concentration and exposure time. The copy number decreased about 20% within the first 10 h of exposure (solvent) in control cells. In styrene-treated cells, GAPDH copies decreased to a lowest level of 55% (10^0 g/m³) to 40% (10^{-4} g/m³) compared to control cells in this time period (Figure 4-7 A). After a 24 h exposure, control cell expression of GAPDH increased for the first time, contrary to both styrene-treated cell populations in which copy numbers were still reduced and able to catch up with those of control cells only after 46 h.

The number of β 2-microglobulin transcript copies (see Figure 4-7 B) increased for control and treated cells over time, as expected for a real housekeeping gene when cell numbers rise and thus mRNA transcription is enhanced. Expression in styrene-treated cells was about 20% lower than in control cells for most time points, except after a 10 h exposure to 100 g/m³, where the transcript copies of the treated cells surpassed the level of control cells by about 15%. As these results indicated that overall GAPDH expression (transcripts) seems to be affected by the supposedly innocuous methanol exposure of control cells as well as by styrene treatment, the obtained VDAC2, SOD1 and HSPB1 expression was normalized versus the housekeeping gene β 2-microglobulin.

VDAC2 expression decreased significantly following styrene treatment, from a level that was higher than in control cells to the lowest expression level of about 60% for both styrene treatments (Figure 4-7 C). The decrease in relative expression was more pronounced with the higher styrene concentration, but reached its minimum only after a 24 h exposure period, whereas for the lower styrene concentration, minimal expression of VDAC2 was observed after a 10 h treatment. After 46 h of treatment, both cell populations expressed approximately the same amount of VADC2 as control cells.

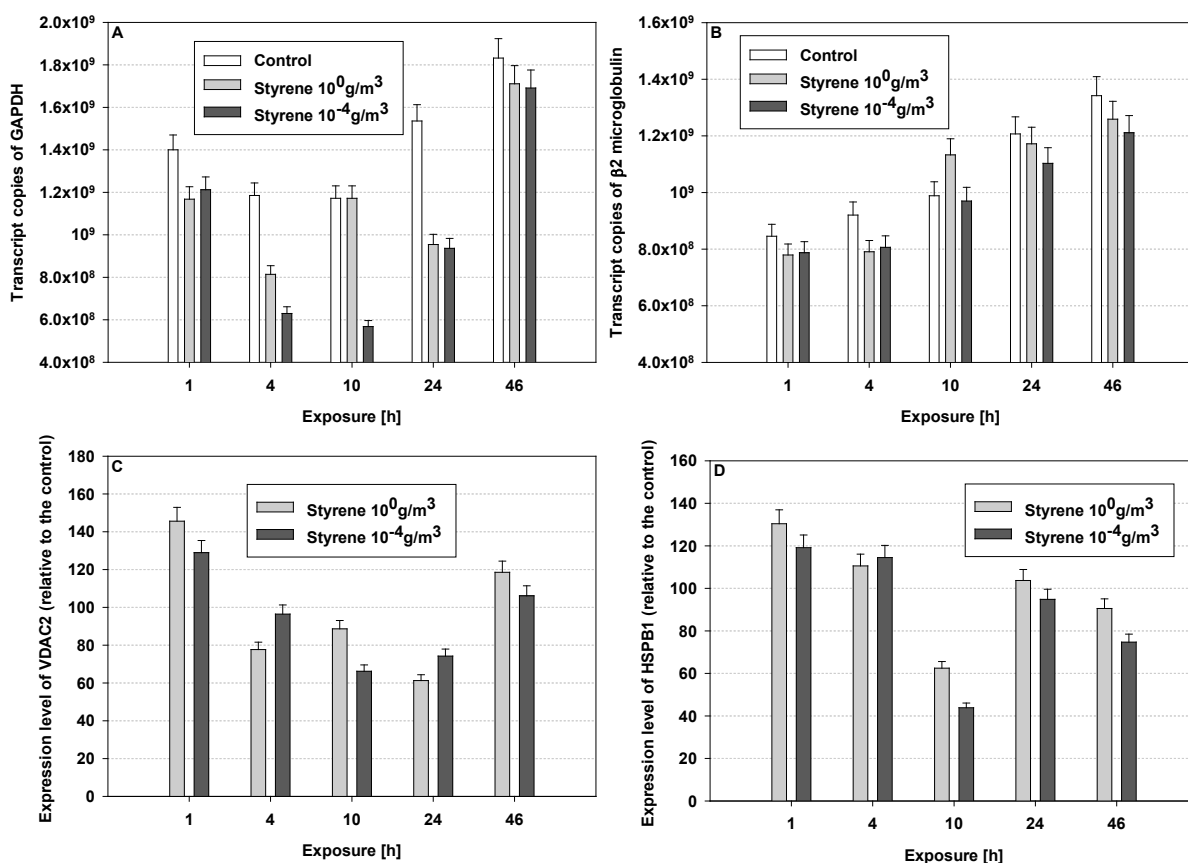


Figure 4-7 Quantitative PCR confirms differential expression of VDAC2 and HSPB1 following styrene treatment. Transcript fluctuation of two typical housekeeping genes, GAPDH (A) and β2-microglobulin (B), over time (1-46 h) was investigated in styrene-treated and control cells. Relative transcript expression of voltage-dependent anion-selective channel protein 2 (VDAC2, C) and heat shock protein beta (HSPB1, D) over time in styrene-treated cells. Obtained VDAC2 and HSPB1 expression levels are normalized versus the housekeeping gene β2-microglobulin and changes in expression levels are given relative to the untreated controls. All data are calculated as mean of triplicates + SEM

HSPB1 expression seemed to decrease in styrene-exposed cells compared to solvent-treated control cells. A significantly reduced transcript concentration was noticed for both styrene concentrations after 10 h of exposure, with an expression level of 60% for 10⁰g/m³ and 40% for 10⁻⁴g/m³ relative to control cells. However, considering the other time points as well, it is difficult to derive a straightforward relationship between the presence of styrene and HSPB1 expression. No real dependency on styrene concentration was observed for HSPB1 and VDAC2 mRNA expression. Furthermore, for SOD1, no significant differential transcript expression was detected - mRNA expression following both treatments was comparable to that in control cells.

4.2.9 Induction of Oxidative Stress Markers

In an additional experiment, the protein expression of two typical oxidative stress markers, heme oxygenase 1 (HO-1) and glutathione S transferase P (GST P1), has been analyzed by immunoblotting using lysates obtained from styrene-treated cells (10^{-4} - 10^{-2} g/m³). Expression of both proteins was normalized against beta-actin expression, using the same sample lane. Applying 10 µg of total soluble protein, both markers showed a more than two-fold increased expression (Figure 4-8) following exposure to the three different styrene concentrations when compared to solvent-treated controls.

Simultaneous treatment of the cells with the antioxidant N-acetylcysteine (NAC, 10 mM final) significantly inhibited the induction of stress proteins caused by styrene exposure. GST P1 expression for all three styrene concentrations reached levels of control cells (no styrene, no NAC). HO-1 expression following treatment with styrene was only moderately reduced by the presence of NAC, a significant decrease occurring only for the lowest of the applied styrene concentrations. Whereas NAC treatment also significantly reduced GST P1 expression in control cells (solvent-treated), no prominent effect of NAC on HO-1 in control cells was observed. Surprisingly, for both enzymes, both effects (induction by styrene and repression by NAC) were not directly correlated with styrene concentration.

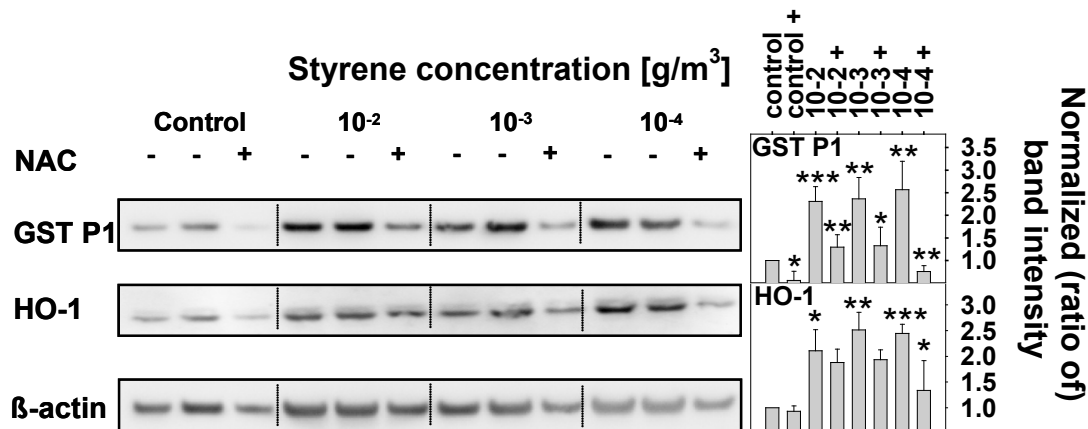


Figure 4-8 Treatment of cells with the antioxidant N-acetylcysteine (NAC, 10 mM final) inhibited increased expression of stress proteins heme oxygenase 1 (HO-1) and glutathione S transferase 1 (GST P1) caused by styrene exposure. 10 µg of total soluble protein were loaded on each lane. Beta-actin signals of every lane were used for normalization. Changes in band intensity (arbitrary units) are given relative to the control and calculated as mean of triplicates + SEM. * $p < 0.05$, ** $p < 0.01$, *** $p < 0.001$.

4.2.10 Formation of Reactive Oxygen Species

From the observed induction of oxidative stress marker proteins in styrene-treated A549 cells, the hypothesis of enhanced cellular formation of reactive oxygen species (ROS) in response to styrene exposure has been derived. To further strengthen this assumption, the cellular ROS concentration has been measured by monitoring the ROS-dependent, intracellular conversion of 2',7'-dichlorofluorescein to its fluorescent, oxidized counterpart 2',7'-dichlorodihydrofluorescein diacetate (DCF). Upon styrene exposure (10^{-2}g/m^3 for 2 h), a distinct increase in fluorescence levels that is reflected by the shift of the fluorescence distribution curve towards higher intensities compared to the untreated control, was observed (Figure 4-9). The effect was even stronger than the one observed for the positive control, the incubation of the cells with 25 μM cadmium chloride, a well known inducer of oxidative stress (Yano *et al.*, 2005). These results clearly demonstrate that formation of reactive oxygen species is specifically induced by styrene treatment.

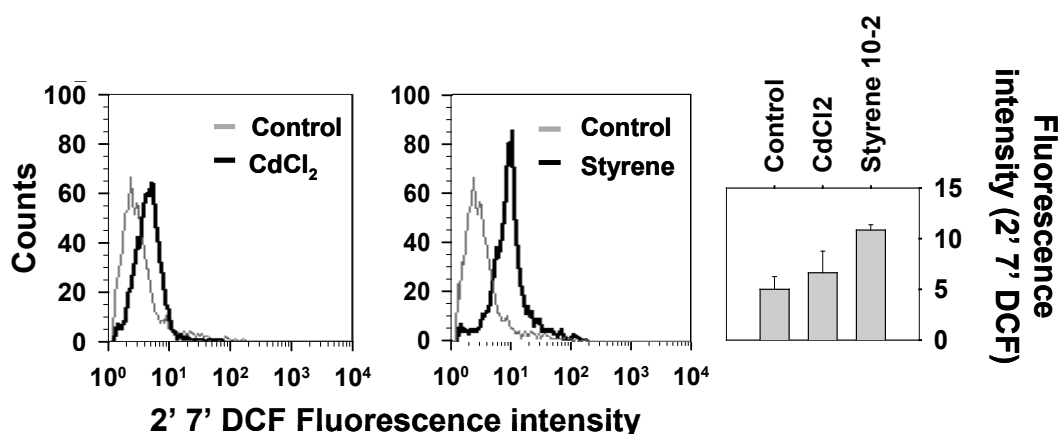


Figure 4-9 Analysis of reactive oxygen species (ROS) formation following exposure to styrene (10^{-2}g/m^3) or cadmium chloride (25 μM) for 2 h in A549 cells. Cells were analyzed for ROS levels by FACS analysis using 2',7'-dichlorodihydrofluorescein diacetate. ROS levels from one representative experiment as well as the quantification of three independent experiments (mean and standard error of fluorescence intensities) are shown. Cadmium chloride was used as a positive control.

4.2.11 Identification of Styrene Oxide Protein Adducts

As mentioned before (see section 4.1), metabolic styrene activation by CYP450 leads to S- and R-forms of styrene 7,8 oxide (SO). SO-modified proteins, such as albumin and hemoglobin, have been detected in animals and humans after exposure to styrene (Teixeira *et al.*, 2007; Yeowell-O'Connell *et al.*, 1996). Formation of protein covalent binding with xenobiotics or their active metabolites has long been recognized as a possible mechanism of chemical toxicity, especially for epoxides (Shen *et al.*, 2009). In this thesis, the focus was laid on the analysis of the total soluble proteins. For detection of SO-adduction to proteins, immunoblotting with the SO-specific antibody #1043 (Chung *et al.*, 2006; Yuan *et al.*, 2007) and finally mass spectrometry have been used to validate potentially modified proteins.

As a positive control, SO-modified BSA was prepared according to the protocol of Yuan *et al.* (Yuan *et al.*, 2007) with minor modifications (see 2.4.7). Figure 4-10 A shows a total protein stain (Ponceau S) image of applied medium control (5 µg; lane 1), styrene-treated BSA (50 ng; positive control; lane 2) and non-treated BSA (5 µg; negative control; lane 3). In Figure 4-10 B the SO-specific antibody was used in Western blotting, yielding a very strong signal in the lane of the positive control (SO-treated BSA, lane 2), whereas only a low background signal has been observed in the negative control lane (untreated BSA, Figure 4-10 B, lane 3) as well as in the lane of the culture medium control (Figure 4-10 B, lane 1). As a previous experiment had shown, 5 µg of the positive control sample resulted in an intense chemiluminescence signal. Thus, for the gel shown here, the sample was diluted and only 1% of the protein amount of the negative control was applied to the gel.

Using lysates (100 µg) from styrene-exposed (10^2 g/m³) and non-exposed A549 cells for SO-specific standard (Figure 4-10, lane 5 and 4, respectively) and 2-DE Western blots (Figure 4-10 C/D), several significantly altered spots could be detected, even in the presence of an unexpectedly high number of non-specifically staining proteins in the control. Especially in the high molecular weight region (>72 kDa), important differences in the chemiluminescence signal of lysates of styrene-treated (lane 5) and control cells (lane 4) were noticed.

In the following, 2-DE Western Blot analysis was performed with the same cell lysates. Comparing the 2-DE signals of control (Figure 4-10 C) and styrene-exposed cells (D), two main areas (see circles) of significantly altered spots became apparent. Surprisingly, no intense signals above 80 kDa were located in styrene-treated lysates. In contrast, two “new” protein spots were detected at 40 kDa in the styrene-treated lysates. At 55-60 kDa, two spots that seemed to be isoforms were detected clearly in lysates of the exposed cells (Figure 4-10 D) but barely in control cell lysates (Figure 4-10 C).

Thus, the challenge was to identify the four protein spots that were detected with a much stronger signal in the lysates from styrene-treated cells by mass spectrometry. The

bigger one of the two spots at 40 kDa was identified as poly (rC)-binding protein 1, whereas the smaller spot could not be identified. Further research revealed that the bigger spot is identical to spot ID246 in the proteome map (Figure 3-2). At 55-60 kDa, both protein spots were identified as human thioredoxin reductase 1, and correspond to ID104 and ID245 in the proteome map. Identification data for IDs 246, 104 and 245 are found in Table 8-1 in the appendix.

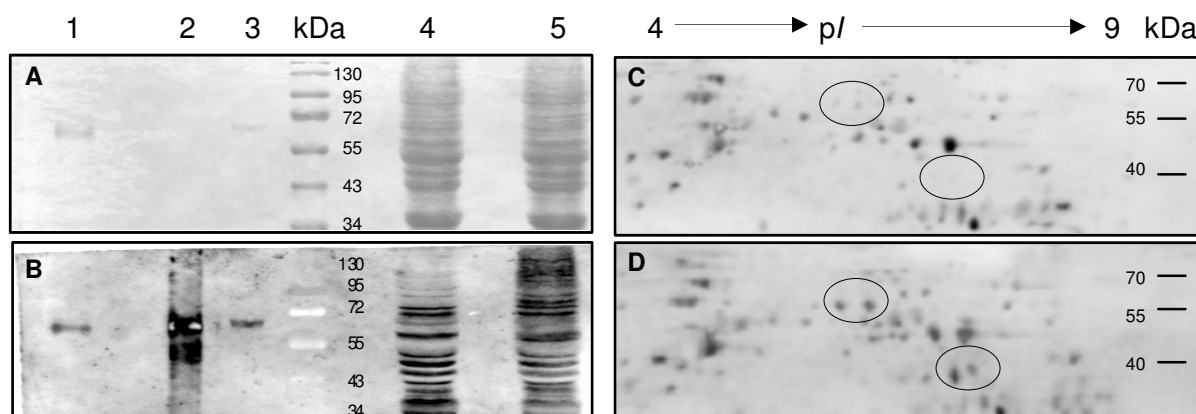


Figure 4-10 Western blot analysis of styrene 7,8 oxide (SO)-protein adduct formation following exposure of A549 cells to styrene (10^2 g/m^3). **Figure A** (total protein stain Ponceau S) and **B** (specific detection of protein adducts) prove the sensitivity of the antibody against the positive control (50 ng SO-modified BSA; lane 2) in contrast to low detection of untreated BSA (lane 3; 5 μg) and precipitated cell culture medium (lane 1). SO-modified proteins were detected by comparing patterns of lysates (100 μg protein) of styrene exposed (lane 5) and control (lane 4) cells. **C, D**: 2-DE Western blot of SO-protein adduct formation following exposure of A549 cells to styrene (10^2 g/m^3). The analysis of lysates (200 μg) of control (C) and exposed cells (D) revealed two main areas of differentially detected spot patterns (see circles).

In a second step, covalent SO-modification of detected proteins (and the positive control, SO-treated BSA) was analyzed by nano-HPLC/nano-ESI MS. 2-DE Spots (ID104, 245 and 246) of SO-modified proteins (identified with SO-specific antibody) as well as a band of 5 μg of prepared styrene-oxidized BSA (see preparation of SO-modified BSA in section 2.4.7) were cut from CBB stained gels. A band of 5 μg of untreated BSA and 2-DE spots (ID104, 245, 246) cut from a control gel served as negative controls.

Again, the specificity of the used immunoserum and therewith the specific detection of SO-modified proteins in 2-DE Western blots was demonstrated by mass spectrometric analysis of SO-modified BSA peptides. In total, for the prepared SO-treated BSA, 15 tryptic peptides with SO-adduction were identified and are listed in Table 4-3. SO-adduction occurred at cysteine (C), glutamic acid (E), aspartic acid (D), histidine (H) and lysine (K), as indicated in the amino acid sequences. For most of the peptides of the SO-treated BSA, the modified (labeled with an asterisk) and the unmodified state could be assigned. However, for the last four peptides of the list, only the SO-adducted peptide was detected. 5 of the observed modified BSA peptides are displayed in the BSA sum spectrum (m/z 300-1200) in Figure 4-12 A. In control cell lysates, only the corresponding unmodified peptides were observed.

Table 4-3 Detected SO-adducted peptides and their corresponding unmodified peptides for BSA.

Range ^a	Sequence	<i>m/z</i> ^b	Control peptides			SO-adducted peptides		
			<i>Mr</i> _{theo} ^c	Ion score	label ^d	<i>m/z</i> ^b	<i>Mr</i> _{theo} ^c	Ion score
35-44	FKDLGEEHFK	417.0	1248.6	29	1*	457.0	1368.6	36
360-371	RHPEYAVSVLLR	480.2	1438.1	43	2*	520.3	1558.9	51
66-75	LVNELTEFAK	582.1	1162.6	60	3*	642.0	1282.7	24
402-412	HLVDEPQNLIK	653.0	1304.7	53	4*	713.0	1424.8	31
438-451	VPQVSTPTLVEVSR	756.0	1510.8	53	5*	816.0	1630.9	51
569-580	TVMENFVAFVDK	699.9	1398.68	69	-	759.9	1518.7	47
437-451	KVPQVSTPTLVEVSR	820.1	1638.1	45	-	879.9	1758.9	33
469-482	MPCTEDYLSLILNR	n.o.	-	-	-	594.4	1786.9	110
508-523	RPCFSALTPDETYVPK	n.o.	-	-	-	648.4	1942.9	27
168-183	RHPYFYAPELLYYANK	n.o.	-	-	-	762.2	2284.1	45
529-544	LFTFHADICTLPDTEK	n.o.	-	-	-	657.4	1969.9	25

SO-adduction occurred at C, E, D, H, K as marked in the sequence. In some sequences, more than one adduct site was possible. In sequences labeled with an asterisk (*), both adducts were detected simultaneously. ^a Amino acids, ^b Detected mass charge ratio, ^c Theoretical mass, ^d Label used in Figure 4-12 A. For the last 4 peptides of the list only the SO-adducted peptide was detected. n.o.- not observed.

From the BSA sum spectra, extracted mass spectra were created with a retention time window of 5 min. Figure 4-12 B (*m/z* 400-550) and C (*m/z* 550-720) illustrate the formation of four styrene adducts by comparing the spectra from SO-treated and untreated BSA. For modified peptides, the mass shift of 120.1 amu (single charged ions), 60.0 amu (doubly charged ions) or 40.0 amu (triply charged ions) induced by the SO-adduct formation is obvious. Figure B presents the triply charged adducts labeled (in A) as 1* (aa 35-44, *m/z* 457.0) and 2* (aa 360-371, *m/z* 520.3) with a SO mass shift of 40 amu, whereas in C the doubly charged signals of peptides 3* (aa 66-75, *m/z* 642.0) and 4* (aa 402-412, *m/z* 713.0) cause a mass shift of 60 amu. The corresponding unmodified peptides 1 (*m/z* 417.0), 2 (*m/z* 480.2), 3 (*m/z* 582.1) and 4 (*m/z* 653.0), respectively, were detected in both, the treated and the control sample. Figure D (*m/z* 610-660) and E (*m/z* 690-740) show enlargements (retention time window 1 min) of Figure C.

As described above, alkylation of the proteins thioredoxin reductase 1 (TRR1) and poly (rC)-binding protein 1 by SO has been proven using the SO-specific antibody staining. Mass spectrometric analysis of tryptic peptides of spot ID246 (identified as poly (rC)-binding protein 1) from SO-treated cells revealed no hint at alkylation. In contrast, further analysis of ID104 and 245 (identified as TRR1) resulted in 3 SO-alkylated peptides, even though spectra quality as well as sequence coverage were inferior to the BSA sample. Candidate adducts are listed in Table 4-4. Mass spectrometric analysis of tryptic peptides revealed isoform 5 of TRR1, lacking amino acids 1-150 of the canonical sequence (isoform 1), as shown in Figure

4-11. Identified unmodified peptides are marked in red, whereas the SO-adducts (listed in Table 4-4) are highlighted in blue. Possible adduct sites are underlined.

Table 4-4 Detected SO-adducted peptides and their corresponding unmodified peptides for thioredoxin reductase 1.

Range ^a	Sequence	Control peptides			SO-adducted peptides		
		<i>m/z</i> ^b	<i>Mr</i> _{theo} ^c	Ion score	<i>m/z</i> ^b	<i>Mr</i> _{theo} ^c	Ion score
637-649	RSGASILQAG <u>C</u> U <u>G</u>	n.o.	-	-	724.5	1446.6	22
638-649	SGASILQAG <u>C</u> U <u>G</u>	n.o.	-	-	645.8	1290.4	14
203-218	WGLGGTCVNVG <u>C</u> IPKK	808.9 ^o	1616.7	101	602.9	1807.9	15

^oBoth cysteines were detected as being carbamidomethylated in the control peptide. SO-adduction occurred at C and U as marked in the sequence. In some sequences more than one adduct site was possible. ^a Amino acids ^bDetected mass charge ratio ^cTheoretical mass ^dLabel used in Figure 4-12 A. For the first two peptides of the list, only the SO-adducted peptide was detected. n.o. - not observed

Surprisingly, SO-adducts have been found at cysteines of both the reactive centers of TRR1, the redox-active disulfide bond (aa 209-214) and the selenocysteine (Secys) residue (aa 648) that is essential for catalytic activity. Evidence for the SO alkylation of Secys-648 is obtained by detection of the two peptides aa 638-649 and aa 637-649 (Figure 4-12 F-H). Figure F shows a sum spectrum (*m/z* 400-2000) of human TRR1 (ID104) peptides from styrene-treated lung epithelial cells. The two potential SO-adducted peptides are labeled and displayed in more detail in G and H (extracted mass spectra, retention time window 1 min). The doubly charged signals of TRR1 aa 638-649 (SGASILQAGCUG, C-terminally amidated, *m/z* 645.8, *Mr*_{theo} 1290.4, Δm 0.1 Da) and aa 637-649 (RSGASILQAGCUG, *m/z* 724.5, *Mr*_{theo} 1446.6, Δm 0.3 Da) are displayed, respectively. Both signals match a dual alkylation, one cysteine (C) or selenocysteine (U) by the reaction with SO (Δm 120.1 amu) and one with iodoacetamide (caused by 2-DE equilibration process with dithioerythrol).

```

1  MGCAEGKAVA  AAAPTELQTK  GKNGDGRRRS  AKDHHPGKTL  PENPAGFTST
51  ATADSRALLQ  AYIDGHSVVI  FSRSTCTRCT  EVKKLFSKSLC  VPYFVLELDQ
101  TEDGRALEGT  LSELAAETDL  PVVFKQQRKI  GGHGPTLKAY  QEGRLLQKLLK
151  MNGPEDLPKS  YDYDLIIIGG  GSGGLAAAKE  AAQYGKKVMV  LDFVTPTPLG
201  TRWGLGGTCV  NVGCIPKKLM  HQAALLGQAL  QDSRNYGWKV  EETVKHDWDR
251  MIEAVQNHIG  SLNWGYRVAL  REKKVVYENA  YGQFIGPHRI  KATNNKGKEK
301  IYSAERFLIA  TGERPRYLG  PGDKEYCISS  DDLFSLPYCP  GKTLVVGASY
351  VALECAGFLA  GIGLDVTVMV  RSILLRGFDQ  DMANKIGEHEM  EEHGKIFIRQ
401  FVPIKVEQIE  AGTPGRLRVV  AQTNSEEEII  EGEYNTVMLA  IGRDACTRKI
451  GLETGVKIN  EKTGKIPVTD  EEQTNVPYIY  AIGDILEDKV  ELTPVAIQAG
501  RLLAQRLYAG  STVKCDYENV  PTTVFTPLEY  GACGLSEEKA  VEKFGEENIE
551  VYHSYFWPLE  WTIPSRDNNK  CYAKICNTK  DNERVVGFHV  LGPNAGEVTQ
601  GFAAALKCGL  TTKQLDSTIG  IHPVCAEVFT  TLSVTKRSGA  SILQAGCUG

```

Figure 4-11 Sequence coverage of thioredoxin reductase 1 (isoform 1, aa 1-649). Mass spectrometric analysis revealed isoform 5, lacking amino acids 1-150 of the canonical sequence (isoform 1). Identified unmodified peptides are marked in red, whereas SO-adducts are highlighted in blue. Possible SO-adduct sites are underlined.

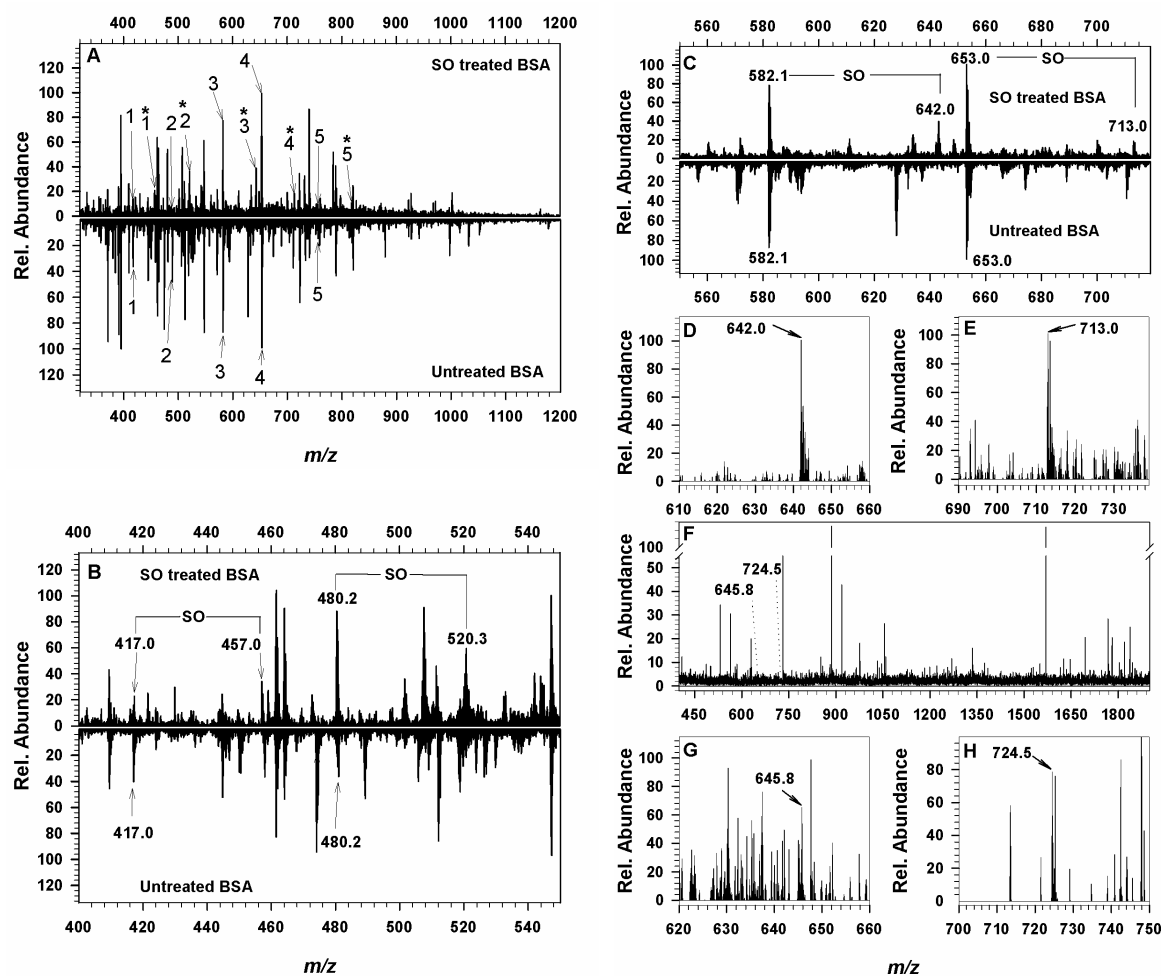


Figure 4-12 Mass spectrometric analysis of SO protein adducts. Sum spectra (A, F) and extracted mass spectra (B, C, D, E, G, H) of the nano-HPLC/ESI MS/MS analysis of SO-treated and untreated BSA (A-E) as well as SO-adducted thioredoxin reductase 1 (F-H).

A) BSA sum spectrum (m/z 300-1200). Several peptides were identified in the unmodified and SO-modified state (labeled with an asterisk) - solely detected in the spectrum of the treated BSA: 1- aa 35-44 m/z 417.0, $M_{r,theo}$ 1248.6, ion score 29; 1*- m/z 457.0, $M_{r,theo}$ 1368.6, ion score 36; 2- aa 360-371 m/z 480.2, $M_{r,theo}$ 1438.1, ion score 43; 2*- m/z 520.3, $M_{r,theo}$ 1558.9, ion score 51; 3- aa 66-75 m/z 582.1, $M_{r,theo}$ 1162.6, ion score 60; 3*- m/z 642.0, $M_{r,theo}$ 1282.7, ion score 24; 4- aa 402-412 m/z 653.0, $M_{r,theo}$ 1304.7, ion score 53; 4*- m/z 713.0, $M_{r,theo}$ 1424.8, ion score 31; 5- aa 438-451 m/z 756.0, $M_{r,theo}$ 1510.8, ion score 53; 5*- m/z 816.0, $M_{r,theo}$ 1630.9, ion score 51.

B (m/z 400-550), **C** (m/z 550-720)) Enlargements of extracted mass spectra (retention time window 5 min) of the SO-modified peptides annotated with 1*, 2* and 3*, 4* in A and the corresponding unmodified peptides are shown.

D, E) Enlargements of extracted mass spectra (retention time window 5 min) of the two modified peptides (shown in C). For modified peptides, the mass shift of 120.1 amu (single charged ions), 60.0 amu (doubly charged ions) or 40.0 amu (triply charged ions) induced by the SO-adduct formation was detected.

F) Sum spectrum (m/z 400-2000) of human thioredoxin reductase 1 from styrene-treated lung epithelial cells. Two possible SO-adducted peptides are labeled. (G and H) The doubly charged signals (extracted mass spectra, retention time window 1 min) of thioredoxin reductase 1 aa 638-649 (SGASILQAGCUG, C-terminally amidated, m/z 645.8, $M_{r,theo}$ 1289.5, Δm 0.1 Da) and aa 637-649 (RSGASILQAGCUG, m/z 724.5, $M_{r,theo}$ 1446.6, Δm 0.3 Da) are displayed, respectively. Both signals match to a dual alkylation, one Cys or Secys (U) by the reaction with SO (Δm 120.1 amu) and one with iodoacetamide.

4.3 Discussion

Styrene is a common toxic compound in indoor environments. While most inhabitants of industrial countries are exposed to it, styrene toxicity at lower concentrations is not well understood. The objective of this study was to investigate and characterize differential expression of proteins through short-term lung cell exposure to a broad range of styrene concentrations including those that may be encountered to indoors.

Initially, styrene toxicity has been assessed in the A549 transwell exposure system. Data obtained for the acute toxic concentration range provided the basis for the toxicoproteomic analyses. For the highest of the tested styrene concentrations (10^2 g/m³ corresponding to 0.5-0.7 mM), significant cell toxicity, characterized by a 30% decrease in cell number and a 50% reduction in cell viability, was observed in human lung epithelial cells by a 24 h exposure. Decreased cell numbers that were also observed for concentrations of 10^1 g/m³ and 10^0 g/m³, could either be the consequence of an observed cellular detachment at higher styrene concentrations, or diminished cell growth. From the collected toxicity data, the No Observed Effect Concentration (NOEC) of 10^{-2} g/m³ has been derived corresponding to approximately 0.2 μ M.

Compared to the results of this thesis, Croute et al. observed a stronger growth inhibition of 80-90% in studies employing A549 cells in exposure experiments over a longer period (4 days) using 1 mM ethylbenzene, xylene or monochlorobenzene. At lower concentrations, a similar growth inhibition (7-20%) was found (Croute *et al.*, 2002). Diodovich et al. demonstrated that after 24 and 48 h of exposure, styrene (0.8 mM) induced an increase in the necrosis of human mononuclear cord blood cells (Diodovich *et al.*, 2004). Similarly, in human neuroblastoma SK-N-MC cell line, a time and dose-dependent cytotoxicity (Trypan blue exclusion) was detected when cells were exposed to 0.3-1 mM of styrene 7,8 oxide (Dare *et al.*, 2002). In contrast to the results from human cells, various studies in mice showed that styrene inhalation (20-200 ppm) significantly enhanced the proliferation of Clara cells (in bronchi and bronchioles) but not in type II respiratory epithelial cells (Cruzan *et al.*, 1997; Green *et al.*, 2001; Kaufmann *et al.*, 2005).

Cellular protein expression was quantified employing 2-DE for a broad range of styrene concentrations including toxic ($>10^{-1}$ g/m³) and non-toxic concentrations (10^{-2} and 10^{-3} g/m³). A significant change in protein expression as well as protein phosphorylation patterns was observed following exposure to toxic as well as sub-toxic styrene concentrations. The greatest changes in expression in response to styrene exposure were found for proteins involved in the oxidative stress response as well as in cell death signaling pathways. Furthermore, several differentially expressed metabolic proteins and proteins with relatively little available information on protein functions or phosphorylation as e.g. NIF3-like protein 1

have been identified. Total protein expression was analyzed following a 24 h exposure period while changes in protein phosphorylation occur much faster and were detected in response to an exposure period of 1 h.

Comparing the staining patterns of phospho-specific and total protein signals in the same 2D gel revealed that in most cases, highly abundant protein spots did not show intense phospho-specific staining. Thus, many phosphorylated proteins were of low abundance as also observed by Jin *et al.*, 2006 using Pro Q Diamond stain for investigations in human blood monocyte proteins. Strikingly, in the 2D gels presented here, most protein spots with high intensity for the phospho-specific dye are located in the gel part of proteins with acidic isoelectric points (*pI*), similar to what was reported by Jin *et al.*, 2006. A possible explanation of this phenomenon may be provided by findings of Zhu *et al.*. They reported that phosphorylation of a protein induces a significant acidic shift on *pI* by introducing negative charge. The shift of *pI* for proteins with multiple phosphorylations was found to be cumulative. Thus, the observed shift is depending upon the protein and the amount of phosphorylation. Large changes (up to one pH unit) were observed for proteins with an expected *pI* above 7.0, whereas little change (0.2 pH units per phosphorylation) was noticed for proteins with a *pI* of 5.0 (Zhu *et al.*, 2005). Therefore, it is probable that proteins with *pI*s above 7.0 can easily be detected in the acidic part of the gel, especially when a phospho-specific stain is used.

In the following, a set of proteins detected with modulated expression and/or phosphorylation for which biological significance could be deduced from the scientific literature will be discussed. However, toxicoproteomics of styrene has not been investigated up to now, resulting in the absence of literature references stating a connection of styrene and differential protein expression.

Styrene exposure modulates cellular redox balance

Oxidative stress is a major cause of cell damage, cell death as well as inflammation. Lung cells, in particular alveolar epithelial type II cells are susceptible to injurious effects of oxidants. Amongst others, glutathione is an important protective antioxidant against free radicals and other oxidants. The glutathione redox cycle is crucial in maintaining intracellular homeostasis of reduced (GSH) and oxidized (GSSG) forms of glutathione that is critical for normal physiological processes. The system uses GSH as a substrate in the detoxification of peroxides such as H₂O₂ and lipid peroxides, generating GSSG, which is recycled to GSH by glutathione reductase in a reaction requiring NADPH that is synthesized predominantly in the Pentose Phosphate Pathway (Rahman *et al.*, 2000).

As mentioned above, cellular styrene exposure of lung epithelial cells could be correlated with differential expression of several redox-sensitive proteins e.g. induction of common oxidative stress markers. Expression of ***superoxide dismutase 1*** (SOD1), which

catalyzes the dismutation of the superoxide anion radical, was increased even at lower styrene concentrations. Earlier studies provided evidence that transgenic mice overexpressing SOD1 are partly protected when exposed to hyperoxic lung injury (White *et al.*, 1991). Thus, SOD1 is not only a marker protein for cellular oxidative stress but is actively involved in its modulation. Recently, Harvilchuck and colleagues described the effects of styrene on mice Clara cells, the epithelial progenitor cells of the small airways. They reported increased levels of SOD1 three hours following styrene exposure *in vitro* (Harvilchuck *et al.*, 2009b).

Increased expression of human **biliverdin reductase A** (BLVRA), exerting 3% of its total activity in lung cells and catalyzing the reaction of biliverdin to bilirubin, was observed following exposure to low as well as to high styrene concentrations. In the presence of biliverdin, which is supplied by heme oxygenase 1, an inducible stress protein (Slebos *et al.*, 2003; Slebos *et al.*, 2007), BLVRA is able to form a redox cycle that eliminates pro-oxidant species with concomitant consumption of NADPH (Baranano *et al.*, 2002). Baranano *et al.* reported the depletion of cellular bilirubin, a potent cytoprotectant, in RNA interference experiments targeting BLVRA, resulting in augmented tissue levels of reactive oxygen species and cell death (Baranano *et al.*, 2002). Furthermore, Ahmad *et al.* identified BLVRA as a leucine zipper-like DNA-binding protein that functions in transcriptional activation of heme oxygenase-1 by oxidative stress events (Ahmad *et al.*, 2002).

Thioredoxin reductase 1 (TRR1), is a key element in the control of the cellular redox state (Burke-Gaffney *et al.*, 2005), pivotal for the NADPH-dependent reduction of thioredoxins (Trx), and thus for returning oxidized cysteines of cellular proteins to their reduced state. Furthermore, it has been suggested that the TRR1/Trx system affects cellular processes by regulating the activity of transcription factors such as p53, NF- κ B, Sp-1, and HIF1- α , leading to changes in gene expression (Gorreta *et al.*, 2005). In the experiments of this thesis, enhanced expression of TRR1 was detected when cells were exposed to higher styrene concentrations. Similar to the obtained results, increased TRR1 expression was recently reported for A549 cells exposed to monochlorobenzene (Feltens *et al.*, 2010). Moreover, TRR1-styrene oxide adducts (later on discussed) have been detected in styrene-exposed cells. In conclusion, imbalance of the TRR1/Trx system may be a molecular principle of styrene-induced toxicity in A549 cells.

DJ-1 protein that possibly functions as a redox-sensitive molecular chaperone and antioxidant in human pneumocytes, protecting cells against the effects of oxidative stress (Moore *et al.*, 2006) and **Chloride intracellular channel protein 1**, a redox sensitive ion channel and a member of the GST family (Singh *et al.*, 2006), were found to be induced by styrene as well.

Finally, doubled expression of **aldose reductase** has been measured. This protein is a member of the ald-keto reductase superfamily that catalyzes the NADPH-dependent reduction of a wide variety of carbonyl-containing compounds to their corresponding alcohols with a broad range of catalytic efficiencies (Martin *et al.*, 2006). **Aldehyde dehydrogenase 3A1**, which preferentially oxidizes aromatic aldehyde substrates (Estey *et al.*, 2007), showed increased expression at most exposure levels. One possible substrate in the human styrene metabolism may be the styrene 7,8 oxide metabolite phenylacetaldehyde.

Increased expression of **peroxiredoxin 1**, as observed here, was found in testis of styrene-treated rats (Han *et al.*, 2007).

In a second group of redox-related proteins, several enzymes of the pentose phosphate pathway (PPP) and TCA cycle have been detected. Both pathways are involved in the regeneration of reducing equivalents needed for the oxidoreductase reactions mentioned above. Recovery of glutathione (GSH), which is needed to protect cells from highly reactive oxygen species, from its oxidized form is completely dependent on NADPH produced by the PPP (Banki *et al.*, 1996; Rho *et al.*, 2005).

As a first example, the key enzyme of the non-oxidative branch of the PPP, **transaldolase 1** (TALDO1), showed enhanced expression in a styrene concentration-dependent manner. Metabolic consequences of TALDO1 deficiency were recently characterized by depletion of NADPH and GSH, lost mitochondrial transmembrane potential and reduced ATP/ADP ratio in liver cells (Hanczko *et al.*, 2009). Furthermore, Banki *et al.* proposed that GSH levels and sensitivity to apoptosis are regulated by changes in TALDO1 expression in human cells (Banki *et al.*, 1996). Moreover, a spot on the 2D gel identified as TALDO1 but located next to the two main TALDO1 spots, showed only half the phosphorylation intensity in a low styrene (10^{-4} g/m³) concentration. Lachaise and colleagues suggested that regulation of transaldolase activity is achieved by posttranslational modification of the protein. The researchers identified a complex set of transaldolase isoforms and postulated that the phosphorylation of specific isoforms could be correlated with the different enzymatic activities seen (Lachaise *et al.*, 2001).

From the oxidative branch of the PPP, **glucose-6-phosphate-1-dehydrogenase** (G6PD) and **6-phosphogluconate dehydrogenase** (PGD), both catalyzing the production of NADPH (see Figure 4-13), were found with increased expression in cells exposed to moderate or high styrene levels. G6PD was identified as the rate-limiting enzyme of the PPP. Kozar *et al.* observed stimulation of the PPP including PGD during the recovery period from acute lung injury and concluded that both the PPP and the GSH system contribute to the recovery phase of oxidant-mediated lung injury (Kozar *et al.*, 2000). Shenton and Grant examined whether the expression of these enzymes was affected by the loss of gamma-glutamylcysteine synthetase (*gsh1*), the key enzyme for the *de novo synthesis* of GSH. They

observed elevated G6PD and PGD levels in the *gsh1* mutant during normal aerobic growth conditions indicating that, in the absence of GSH, cells try to compensate for the loss of reduction equivalents by upregulating the production of NADPH via the pentose phosphate pathway (Shenton *et al.*, 2003).

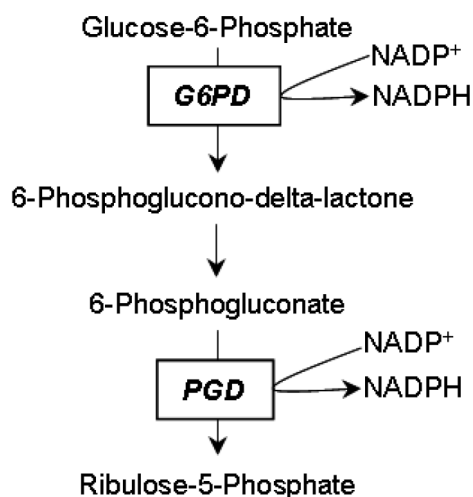


Figure 4-13 The oxidative branch of the pentose phosphate pathway (PPP) generates reducing equivalents. Glucose-6-phosphate 1-dehydrogenase (G6PD) and 6-phosphogluconate dehydrogenase (PGD) are key elements of the PPP. Both enzymes were induced by styrene exposure in A549 cells.

NADPH is also provided by **isocitrate dehydrogenase 1** (IDH1). Here, IDH1 expression as well as phosphorylation was significantly induced by styrene treatment. In contrast to the mitochondrial NAD-dependent isoform IDH3 that is involved in the TCA cycle, the metabolic functions of the NADP-dependent forms of the enzyme whose subcellular distribution varies depending upon tissues (Jennings *et al.*, 1994), are less well described. Lee *et al.* investigated the protective action of IDH1 against cytotoxicity induced by oxidative stress. They noticed a significantly higher ratio of oxidized glutathione to total glutathione in mice cells underexpressing IDH1. From this finding, the researchers concluded an essential role of IDH1 for efficient recycling of glutathione (Lee *et al.*, 2002), which in turn is required for the metabolism of xenobiotics such as styrene.

Finally, 2-DE results indicating stimulation of oxidative stress pathways were confirmed by additional experiments, validating the induction of oxidative stress markers superoxide dismutase 1 (SOD1), heme oxygenase 1 (HO-1) and glutathione S-transferase P1 (GST P1) on protein level employing Western blotting. SOD1 transcript levels, however, did not seem to be affected by styrene. Moreover, induction of HO-1 and GST P1 protein expression by styrene could be blocked by the antioxidant N-acetyl cysteine. To further strengthen the assumption of styrene-induced oxidative stress, the cellular ROS concentration has been determined. Upon styrene exposure, a distinct increase compared to the untreated control was observed. Taken together, these results clearly demonstrate that formation of reactive

oxygen species is specifically induced by styrene treatment what has been reflected in the differential expression/phosphorylation of redox-sensitive proteins.

In general, the results are in good accordance with recently published data of concurrent work of Harvilchuck *et al.* who studied styrene toxicity in mice. The researchers observed increases in reactive oxygen species (ROS) three hours after *in vitro* exposure of isolated lung (Clara) cells to styrene or styrene 7,8 oxide. ROS induction in Clara cells was also seen when styrene or styrene 7,8 oxide were intraperitoneally administered to the mice. In this case, in addition to the stimulated ROS formation, SOD1 expression was enhanced and lung DNA showed significant increases in oxidative damage as measured by 8-hydroxydeoxyguanosine (8'-OH-dG)-levels (Harvilchuck *et al.*, 2009b). Modest levels of ROS can lead to the formation of oxidatively damaged bases of the DNA, e.g., 8'-OH-dG, which can give rise to G to T transversions. Such mutations are believed to represent initiating events. Higher levels of ROS can lead to cell death either by apoptosis and/or necrosis (Burczynski *et al.*, 1999).

Styrene stimulates an inflammatory process via NF-kappa B activation

Subtle changes in the intracellular redox state such as the imbalanced TRR1/Trx system (discussed above) can also modulate nuclear factor-kappa B (NF- κ B) activity. This transcription factor plays a pivotal role in the expression of a wide range of genes involved in lung inflammation, such as interleukin-8 and granulocyte macrophage-colony stimulating factor (Lentsch *et al.*, 2000). Oxidants are able to cause phosphorylation and degradation of the NF- κ B inhibitors (I κ B). Liberated NF- κ B enters the nucleus and induces gene expression of inflammation- or immune response-related genes (Rahman *et al.*, 2000). Hence, it is meaningful that styrene exposure in addition to oxidative stress proteins also affected the expression of proteins linked to the inflammatory process.

Peroxiredoxin 4 expression was limited to 58% relative to the control level when cells were exposed to styrene. Jin *et al.* proposed that in human cells, peroxiredoxin 4 defines a redox-sensitive pathway that specifically regulates NF- κ B activity via I κ B- α phosphorylation. Interestingly, overexpression of peroxiredoxin 4 in HeLa cells resulted in suppression of TNF-dependent NF- κ B activation (Jin *et al.*, 1997). From this finding, it may be concluded that a decreased abundance (or activity) of peroxiredoxin 4, as observed in styrene-treated cells, promotes NF- κ B activation. Evidence for a connection between cell exposure to VOCs and the NF- κ B pathway was also confirmed by a study in which the induction of the NF- κ B and the p38 MAP kinase pathway, via a redox-specific mechanism, was shown after exposure to monochlorobenzene (Roder-Stolinski *et al.*, 2008a) or styrene (Roder-Stolinski *et al.*, 2008b).

Furthermore, expression of **heat shock protein B1** (HSPB1) was found to be decreased by styrene exposure according to 2-DE analysis. Subsequent validation experiments were able to confirm reduced protein copies as well as diminished HSPB1

mRNA transcripts. It had been shown previously that HSPB1 downregulation results in induction of NF-kappa B (NF- κ B) activity in a reporter assay and increased release of the pro-inflammatory cytokine interleukin 8 in human keratinocytes (Sur *et al.*, 2008). Additionally, HSPB1 siRNA increases basal and tumor necrosis factor alpha-mediated activation of the NF- κ B pathway in HeLa cells (Park *et al.*, 2003).

A perceived doubling in expression of **annexin A7** may be indicative for stimulated secretion of lung surfactant since annexin A7 promotes membrane fusion during exocytosis in alveolar type II cells (Caohuy *et al.*, 2001; Chander *et al.*, 2007). The ability of A549 cells to secrete surfactant proteins was confirmed by Rothen-Rutishauser *et al.*, 2005 and Chuang *et al.*, 2009. Increased lung surfactant protein secretion delimitates lung injury during non-infectious and inflammatory challenge (Casey *et al.*, 2005). A two-fold increased expression of **moesin**, that is an important molecule for leukocyte adhesion during inflammation, was observed following exposure to styrene. Recent studies have shown that moesin also regulates maintenance of alveolar structure and lung homeostasis (Hashimoto *et al.*, 2008). The involvement of oxidative stress in the development of inflammation has been studied *in vitro* and *in vivo*. One of the crucial regulatory mechanisms coupling oxidative stress to the release of inflammatory mediators from epithelial cells is the NF- κ B pathway that has been shown to be modulated by styrene (Roder-Stolinski *et al.*, 2008b).

Styrene affects abundance of apoptosis-related proteins

Apoptosis (programmed cell death) is a secondary response to DNA damage, with the biological goal of protecting multicellular organisms against a damaged cell that is controlled by the accumulation and phosphorylation of the tumor suppressor protein p53. p53, once phosphorylated, inhibits the cell cycle and activates pro-apoptotic genes such as BAX, BAK, NOXA and PUMA when DNA damage is extensive or the cellular repair efforts failed (Wang, 2001). The pro-apoptotic proteins finally activate initiator- and effector caspases (cysteine proteases) managing programmed protein and DNA degradation of the damaged cell resulting in cell death. In the experiments of this thesis, the following cell death-related proteins have been shown to be altered in their expression by styrene exposure in A549 cells.

In addition to its involvement in inflammatory processes, **HSPB1** also plays an important role in apoptosis signaling (Mehlen *et al.*, 1996). Pandey and colleagues were able to demonstrate for the first time that HSPB1 mediated the inhibition of cytochrome C-dependent activation of caspase 3 (Pandey *et al.*, 2000). Here, numerous proteins involved in cell death signaling displayed differential protein expression and/or phosphorylation following cellular styrene treatment. One prominent example is **annexin A1** which is known for its anti-inflammatory function as well as its involvement in the apoptotic and also the ERK repression pathway (Debret *et al.*, 2003). Increased expression of annexin A1 has been

detected at several styrene concentrations, with a more than doubled expression when cells were exposed to 10^0 g/m³. Interestingly, annexin A1 has been also proposed as a stress response marker in A549 cells by *Rhee et al.*, 2000.

Another enzyme, **nucleoside diphosphate kinase A** (NM23-H1), which has recently been identified as a granzyme A (GzmA)-activated, apoptosis-inducing DNase and which forms a part of the SET complex (*Fan et al.*, 2003; *Kaul et al.*, 2006), showed increased expression at all styrene concentrations. Cells with silenced NM23-H1 expression displayed resistance to GzmA-mediated DNA damage and cytolysis, while cells overexpressing NM23-H1 were more sensitive (*Fan et al.*, 2003).

Likewise, styrene exposure induced the **programmed cell death 6-interacting protein** (PDCD6IP protein) and its phosphorylation. PDCD6IP protein, also known as ALG-2/AIP-complex, is supposed to have a modulating role at the interface between cell proliferation and death (*Krebs et al.*, 2000). It belongs to a conserved family of proteins that have in common an N-terminal Bro1 domain and a C-terminal proline-rich domain, both of which mediate interactions with partner proteins (*Dejournett et al.*, 2007). Studies performed with mouse cells showed that overexpression of PDCD6IP protein may block apoptosis (*Mahul-Mellier et al.*, 2008). Moreover, *Schmidt et al.* proposed a model whereby Rous sarcoma oncogene Src antagonizes the effects of ALG-2/AIP by phosphorylation of its C-terminus, leading to the disruption of interactions with its target proteins (*Schmidt et al.*, 2005). In this context, PDCD6IP Tyr319 was shown to be both, a Src phosphorylation site and a docking site for the SH2 (Src homology 2) domain of Src (*Dejournett et al.*, 2007).

In contrast, **voltage-dependent anion-selective channel protein** (VDAC) **2** showed significantly decreased expression in the 2-DE when exposed to styrene. Protein quantification by immunoblotting as well as diminished transcript levels confirmed the 2-DE results. VDACS are mitochondrial membrane pores regulating the release of pro-apoptotic factors such as cytochrome C. VDACC2 is a candidate component of the permeability transition pore, supposed to participate in apoptotic cell death (*Cheng et al.*, 2003). This mitochondrial outer-membrane protein was shown to interact specifically with the inactive conformer of the multi-domain pro-apoptotic molecule BAK. Reduced levels of VDACC2, as observed here, make cells more susceptible to mitochondrial apoptosis by displacement of VDACC2 from BAK, thus enabling homo-oligomerization of BAK and release of cytochrome C from the mitochondria (*Cheng et al.*, 2003).

Of note, styrene-exposed A549 cells in the here discussed experiments also showed reduced levels as well as diminished phosphorylation of cytosolic **actin**. For actin, a high number of phosphorylation sites are known. *Papakonstanti et al.* reported actin phosphorylation by PAK1, resulting in the dissolution of stress fibers and redistribution of microfilaments (*Papakonstanti et al.*, 2002; *Sanders et al.*, 1999). Thus, the observed

diminished phosphorylation of actin in styrene-treated cells may cause enhanced stability of stress fibers. Increased actin-stability was supposed to prolong opening times of mitochondrial VDAC pores and thereby increasing the amount of ROS and cytochrome that will be released from mitochondria. These findings suggest that actin and its phosphorylation play an important role in cell death by regulating opening and closing of VDAC in eukaryotic cells (Gourlay *et al.*, 2005). In conclusion, the reduced levels of VDAC2 together with extended opening periods, due to lowered actin phosphorylation, could be causative for a stimulated apoptotic response in styrene-treated cells.

In line with a pro-apoptotic signaling event, several different **lamins**, known to undergo proteolysis during apoptosis, revealed reduced expression in the presence of styrene. Furthermore, phospho-specific intensity of **vimentin** from styrene-treated cells was only half as strong as when control cells were used. Vimentins are class-III intermediate filaments and are among the most prominent phosphoproteins in various cells. Their phosphorylation is enhanced during cell division, when vimentin filaments are reorganized (Eriksson *et al.*, 2004).

The **proliferating cell nuclear antigen** (PCNA) is involved in DNA replication and damage repair. PCNA function is controlled by phosphorylation of its Tyr 211 by epidermal growth factor receptor, which stabilizes its binding to chromatin. Increased PCNA Tyr 211 phosphorylation coincides with pronounced cell proliferation (Wang *et al.*, 2006). In this thesis, PCNA phosphorylation was significantly lower after both styrene treatments. Earlier, Prosperi *et al.* suggested that binding of PCNA to sites of DNA synthesis occurs after PCNA phosphorylation. In contrast, cells in early G1, G2 or M phases contain only basal levels of the DNA-bound form of the protein with a relatively low level of phosphorylation (Prosperi *et al.*, 1994). Thus, the here observed lower phosphorylation level of PCNA is in good accordance with the reported lower cell numbers in styrene-treated cells and may be indicative for an anti-proliferative effect of styrene that was also observed in previous studies (Croute *et al.*, 2002).

Differential protein phosphorylation measurement with Pro Q Diamond revealed two spots that were identified as **heterogeneous nuclear ribonucleoprotein C1/C2** (HNRNPC1/2) with a more than two-fold enhanced phosphorylation following cell exposure to the high styrene concentration. In contrast, with low-level exposure to styrene no significant modulation of phosphorylation was detected. For HNRNPC1/2, 14 possible serine phosphorylation sites are listed in the UniProtKB/TrEMBL database. Phosphorylation on Ser-260 and Ser-299 occurs typically in resting cells. Additional phosphorylation on Ser-253 and one on the serine residue in the poly-Ser stretch at position 238 are a known response to hydrogen peroxide stress (Stone *et al.*, 2003). Recently, Christian *et al.* identified a previously unknown regulatory cis-element within the coding region of p53 mRNA, which

interacts with HNRNPC1/C2, and they presented evidence for its involvement in the expression of p53 that can activate DNA repair, cell growth arrest or initiate apoptotic cell death. In detail, HNRNPC1 and C2 bound strongly and specifically, in a phosphorylation-dependent manner, at this site in response to DNA damage. Impaired binding of phosphorylated HNRNPC1/C2 significantly reduced p53 gene expression (Christian *et al.*, 2008). Thus, the here observed enhanced phosphorylation of HNRNPC1/C2 seems to be closely linked with stimulation of p53 expression and induction of apoptosis.

Translation initiation factor eIF-5A, a nucleocytoplasmic shuttle protein that stimulates the induction of apoptosis (Taylor *et al.*, 2007), was significantly upregulated at three styrene concentrations, including the relatively lowest one of 10^{-3} g/m³. Two protein spots, identified as **60S ribosomal protein L5 (RPL5)**, were upregulated in their expression at all concentration levels with great significance. However, RPL5 was recently identified as a substrate for death-associated protein kinase, a serine/threonine kinase whose contribution to cell death is well established (Bialik *et al.*, 2008).

DNA-damage binding protein 1 (DDB1) was detected with a 4 times reduced phospho-specific staining intensity. DDB1 is primarily located in the cytoplasm but in case of DNA damage, it translocates to the nucleus and accumulates at sites of damage (Groisman *et al.*, 2003). No information is available about its phosphorylation. Recently, Maddika and Chen confirmed the involvement of DDB1 in the phosphorylation-dependent protein degradation, a common mechanism for regulating protein stability (Maddika *et al.*, 2009).

ATP-dependent DNA helicase 2 subunit 2 (XRCC5) together with the 70 kDa subunit associates in a DNA-dependent manner with DNA-dependent protein kinases (by which XRCC5 is phosphorylated on serine residues). Altogether, the proteins form the DNA-dependent protein kinase complex DNA-PK (Chan *et al.*, 1999) and are required for the correct and efficient repair of DNA double-strand breaks (Gell *et al.*, 1999). Besides that, no additional information on the functional role of XRCC5 phosphorylation can be found. Here, the protein showed reduced phosphorylation which may correlate with a diminished ability of the cell to perform DNA repair.

Heat shock 70 kDa protein 4 (HSPA4) is predicted to be phosphorylated upon DNA damage (Rush *et al.*, 2005). However, here, it showed significantly reduced phospho-specific staining intensity at both styrene concentrations compared to controls while total protein expression was significantly enhanced. Induction of HSPA4 expression was also reported by Ait-Aissa *et al.* for a large number of organic compounds in HeLa cells (Ait-Aissa *et al.*, 2000).

RuvB-like 2 (RUVBL2) phosphorylation was also significantly repressed in styrene-treated cells. RUVBL2 forms a multimeric complex with RUVBL1 and is a component of the RNA polymerase II holoenzyme complex. It possesses single-stranded DNA-stimulated

ATPase and ATP-dependent DNA helicase (5' to 3') activity. Furthermore, it is a component of the NuA4 histone acetyltransferase complex, which is involved in transcriptional activation of select genes principally by acetylation of nucleosomal histones H4 and H2A (Kanemaki *et al.*, 1999; Wood *et al.*, 2000). Silencing RUVBL2 in human hepatocellular carcinoma cells reduced cell growth and increased apoptosis, as shown by DNA fragmentation and caspase 3 activity (Rousseau *et al.*, 2007). Moreover, Matsuoka *et al.* detected the protein in a phosphorylated state upon DNA damage. Thus, modulated phosphorylation of RUVBL2 and HSPA4 may be linked to apoptotic signaling (Matsuoka *et al.*, 2007).

In summary, these data provide evidence that styrene, besides oxidative stress and immunomodulation, also induces apoptotic pathways in A549 cells to a certain but lower extent. Recently, Harvilchuk and colleagues observed significant induction of oxidative stress combined with limited apoptosis in isolated murine Clara cells treated with styrene or SO (Harvilchuk *et al.*, 2009a; Harvilchuk *et al.*, 2009b). Furthermore, previous results stated that human blood or primary neural cells exposed to SO displayed apoptotic morphology, together with chromatin condensation and DNA cleavage by activated caspases (Boccellino *et al.*, 2003; Dare *et al.*, 2002; Marczyński *et al.*, 1997).

Styrene, metabolic changes and protein quality control

A relatively high number (7) of proteins that can be connected to protein quality control, such as ***t-complex protein 1, tumor rejection antigen***, proteasomal and ribosomal proteins were differentially altered in expression following styrene exposure. Protein quality control is a basic cellular phenomenon through which aberrant proteins become eliminated. Aberrant proteins can occur as waste products during de novo synthesis, or are caused by cellular stress. Protein quality control is ensured by various chaperones aiding proteins to achieve their proper conformation. The final step consists of polyubiquitination of aberrant proteins condemning them for degradation by proteasomes (Roth *et al.*, 2008). ***Protein disulfide isomerase (PDI)*** was detected with diminished phospho-specific staining intensity. Phosphorylation sites of the human PDIs have been reported, even though their relevance is not well understood. Regulation of isomerase activity by phosphorylation seems very probable; inhibition of its phosphorylation was hypothesized to either block or activate its ability to exchange disulfide bonds, with a corresponding impact on the folding and activity of target proteins (Herrmann, 2004).

40S ribosomal protein SA (RPSA) and ***40 S ribosomal protein 7*** (RPS7) were both diminished in phosphorylation by styrene treatment of the cells. RPSA is required for the assembly and/or stability of the 40S ribosomal subunit ensuring efficient mRNA translation whereas RPS7 plays an essential role in rRNA maturation. In general, it was reported that phosphorylation of ribosomal proteins is essential for translation regulation (Lekmine *et al.*, 2004; Sripathi *et al.*, 1987).

The members of the column labeled with the term “metabolism” are a heterogenic group consisting of metabolic enzymes, central cell signaling proteins such as 14-3-3 proteins, and proteins with so far unknown functions. Several authors emphasized the interrelation of oxidative stress as observed here with metabolic changes, although it remains challenging to explain this phenomenon (Kondoh *et al.*, 2007; Lelli *et al.*, 2005). Enhanced **ATP-citrate synthase** (ACLY) phosphorylation, as seen following styrene treatment in this work, was also observed by Migita *et al.* when they introduced a constitutively active protein kinase B (Akt) into cells, whereas dominant-negative Akt caused attenuation (Migita *et al.*, 2008). Furthermore, it is known that ACLY is phosphorylated by NM23 proteins on aspartic residues (Wagner *et al.*, 2000). Strikingly, the expression of the pro-apoptotic protein NM23-H1 was increased for all styrene treatments, as mentioned above.

Augmented phosphorylation of another enzyme, **UDP-glucose 6-dehydrogenase** (UGDH), was also caused by styrene. In bacteria, UGDH is activated via phosphorylation (Petranovic *et al.*, 2009). For human UGDH, however, no such information is available for the impact of this posttranslational modification.

Similarly, no information is available about the relevance of the observed more than 7-fold increased phosphorylation of **NIF3-like protein 1** (NIF3L1) phosphorylation. NIF3L1 is highly conserved in many organisms but its biological role is widely unknown.

Two **14-3-3 proteins**, epsilon and theta, were significantly reduced in their phosphorylation when A549 cells exposed to styrene. 14-3-3 proteins can bind a multitude of diverse signaling proteins, e.g. kinases, phosphatases, and receptors, usually by recognition of a phosphoserine or phosphothreonine motif. Subunits epsilon and theta are both homodimers. Currently, more than 100 14-3-3 ligands are known in the scientific literature. In general, 14-3-3 binding to ligands modulates the activity of the binding partner. Dubois *et al.* supposed that the regulation of 14-3-3-mediated protein complex formation may be controlled by the ratio of homo- and heterodimers in the cells, and by the phosphorylation of 14-3-3 targets as well as the phosphorylation of 14-3-3 itself (Dubois *et al.*, 1997).

Ras-related proteins (Rabs) are a ubiquitously expressed family of small (20–29 kDa) monomeric Ras-like GTPases. Family member **RAB2A** is essential for membrane trafficking in the early secretory pathway and associates with vesicular tubular clusters located between the endoplasmic reticulum and the cis-Golgi compartment. The protein showed significantly reduced phosphorylation when cells were exposed to a high styrene concentration (Grosshans *et al.*, 2006; Tisdale *et al.*, 2009).

The GDP dissociation inhibitors (GDIs) represent an important class of regulatory proteins in the functional cycle and recycling of Rab GTPases. Previous studies have demonstrated that GDI1 can operate with multiple Rab proteins. Furthermore, Shisheva *et al.*

reported general activity of **GDI2** in supporting Rab membrane release (Shisheva *et al.*, 1999). Here, GDI2 was significantly induced in expression.

Styrene causes formation of SO–protein adducts in the cells

In humans, mice and rat, styrene is mainly metabolized by cytochrome P450 monooxygenases to styrene 7,8 oxide (SO) (Cruzan *et al.*, 2002). This reaction leads to S- and R-forms of SO, which exerts its toxicity via DNA adduct formation (Harvilchuck *et al.*, 2009a). NADPH-dependent formation of an N-acetylcysteine conjugate derived from SO was identified in cell lysates incubated with styrene in the presence of N-acetylcysteine (Chung *et al.*, 2006).

SO-modified serum proteins, such as albumin and hemoglobin, have been detected in animals and humans after exposure to styrene (Teixeira *et al.*, 2007; Yeowell-O'Connell *et al.*, 1996) and are used as biomarkers for human styrene exposure. Apart from that, little is known about the interaction of SO with other proteins (Yuan *et al.*, 2007). Adduction of styrene to other cellular proteins has not been studied so far but could lead to further understanding of the molecular details of styrene-caused toxicity.

In the investigations of this thesis, the use of an antibody specific for SO-adducted proteins (developed and provided by J. Zheng, (Yuan *et al.*, 2007)) combined with 2-DE, Western blotting and mass spectrometric identification enabled us to detect candidates of SO-modified cellular proteins. The specificity of the immunoserum could be demonstrated with SO-adducted BSA. Finally, detected protein spots, identified as poly(rC) binding protein 1 and thioredoxin reductase 1 (TRR1), were analyzed together with SO-adducted BSA by mass spectrometry in order to specify the correct adduct sites.

SO-adduction on BSA was mainly detected on Cys, but also on Asp, Glu, His or Lys, as has been reported in earlier studies (Phillips *et al.*, 1994). Whereas for poly(rC) binding protein 1 the site of SO-adduction could not be identified, for TRR1 three candidate peptides were found. TRR1 is a member of the pyridine nucleotide-disulfide oxidoreductase family that has mechanistic and sequence identity with glutathione reductases, including a conserved CVNMG (aa 209-213) redox catalytic site. TRR1 catalyzes the NADPH-dependent reduction of the small redox protein thioredoxin, which in turn reduces oxidized cysteines on proteins and supplies reducing equivalents to thioredoxin peroxidases (Lee *et al.*, 2009). Thus, TRR1 is a key element in the control of the cellular redox state (Burke-Gaffney *et al.*, 2005). Surprisingly, following cell exposure to styrene, SO-adducts have been detected at cysteines of both the reactive centers of TRR1, the redox-active disulfide bond (aa 209-214) and the selenocysteine (Secys) residue (aa 648) that is essential for catalytic activity. This later redox-center is located on a flexible arm at the C-terminus of TRR1. The crystal structure in presence of the coenzymes NADP and FAD (flavin adenine dinucleotide) was solved by Fritz-Wolf *et al.* (see Figure 4-14).

During catalysis, reducing equivalents are transferred from the cofactor NADPH to FAD, then to the N-terminal active site cysteine residues [Cys-209, Cys-214] and from there to the flexible C-terminal part [cysteine Cys-647, Secys-648] of the other subunit to be finally delivered to a variety of substrates near the molecule's surface (Fritz-Wolf *et al.*, 2007; Mustacich *et al.*, 2000). From the presented results, direct evidence for the SO alkylation of Cys-647 and Secys-648 in the C-terminal redox center has been derived. The biological importance of these residues is underlined by the irreversible inhibition after alkylation of both, Cys-647 and Secys-648 (Nordberg *et al.*, 1998). The essential role of the selenocysteine in thioredoxin reductase 1 was demonstrated by further alkylation studies. With alkylation efficiency of >90% in Secys-648, enzyme activity was inhibited nearly completely (99%). Additional modification of the Cys-209, Cys-214 disulfide center was provoked under more severe alkylation conditions (Gorlatov *et al.*, 1998).

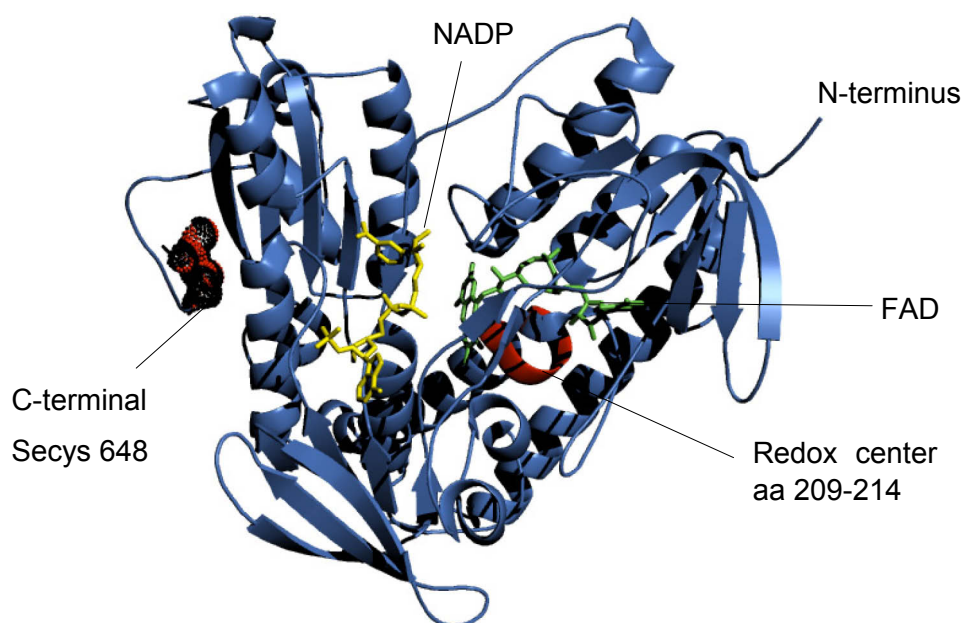


Figure 4-14 Crystal structure of human thioredoxin reductase 1 (aa 150-649; blue) in presence of the coenzymes FAD (green) and NADP (yellow). The crystal structure was solved by Fritz-Wolf *et al.* Both the reactive centers of TRR1, the redox-active disulfide bond (aa 209-214) and the selenocysteine residue (aa 648), located on a solvent-exposed flexible arm at the C-terminus, are colored in red. The image was generated using PyMol software.

As mentioned above, TRR1 was also detected with enhanced expression when cells were exposed to higher styrene concentrations. This effect together with its partial sequence identity with glutathione reductases and the observed Secys-648 SO alkylation provide further mechanistic understanding of a styrene-induced ROS formation in A549 cells. In detail, styrene-exposed cells may metabolize styrene to SO via CYP450 ultimately resulting in TRR1 protein adducts. SO-modulated TRR1 may show impaired enzyme activity thereby causing diminished recycling of oxidized thioredoxin (Trx_{ox}) and the accumulation of ROS such as H_2O_2 (Figure 4-15). Further downstream from these events, increased levels of ROS may be involved in protein misfolding and loss of function. Finally, higher levels of ROS

could lead to cell death by either apoptosis or necrosis as mentioned before (Singh *et al.*, 2006). Indeed, it has been reported that thioredoxin reductase is involved in the induction of apoptosis (Damdimopoulos *et al.*, 2004; Dammeyer *et al.*, 2008).

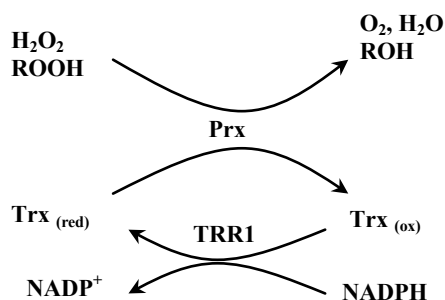


Figure 4-15 Antioxidative power of the thioredoxin reductase/thioredoxin system. TRR1 – thioredoxin reductase 1, Trx – thioredoxin, Prx – thioredoxin-dependent peroxidase (peroxiredoxin).

In conclusion, significant changes in abundance and phosphorylation of total soluble proteins of A549 cells following styrene exposure to non-cytotoxic concentrations have been observed. For most of the proteins, main cellular functions were assigned. However, for some proteins only basic information on their function is available, limiting the derivation of the biological relevance of the observed differential expression and/or phosphorylation. From the results, two main cellular pathways were identified that have been induced by styrene, the cellular oxidative stress response combined with cell death signaling. Validation experiments confirmed this hypothesis. Finally, styrene 7,8 oxide thioredoxin reductase protein adducts have been identified that may be involved in styrene-induced ROS formation and apoptosis.

5 *Toxicoproteomics of Mono- and 1,2-Dichlorobenzene Exposure*

5.1 *Introduction*

5.1.1 *Mono- and 1,2-Dichlorobenzene – Sources of Human Exposure*

As mentioned before (section 1.1), chlorinated benzenes are important representatives among the halogenated aromatic VOCs. In 1970, the annual production of chlorinated benzenes far surpassed the production of polychlorinated biphenyls (PCBs) which are known as ubiquitous pollutants. Since chlorinated benzenes have a chemical structure and properties similar to those of PCBs, it is important to direct attention to human exposure and environmental contamination by these compounds (Morita, 1977).

Due to their high vapor pressure, especially mono- and dichlorinated benzenes are released to the environment by evaporation ((Anonymous, 1988), see Table 3-1) but also significant amounts of chlorinated benzenes reach the aquatic environment via waste waters (Heinisch *et al.*, 2006). In 1995, 1,2-DCB emissions to water totaled 14.4 t, and to air, 20.5 t, based on a survey of 76 European sites (van Wijk *et al.*, 2004). In general, chlorinated benzenes biodegrade poorly and thus are significant environmental pollutants. Indirect entry into the environment is possible through biotic and abiotic degradation of more highly chlorinated benzenes (Hissink *et al.*, 1996).

Monochlorobenzene (CB), which makes up more than 50% of total production of all chlorobenzenes, is used for the synthesis of phenol, aniline, chloronitrobenzenes, diphenyl oxide, insecticides such as DDT and silicones. It is a solvent for adhesives, polishes, waxes, pharmaceutical products, natural rubber, and is used in heat transfer fluids in solar energy collectors (Guerin, 2008).

In 1988, 88,500 t were produced in Western Europe (Heinisch *et al.*, 2006). In plants involved in direct production and usage of CB, occupational exposure varied from 0.2 mg/m³ (0.04 ppm) to 488 mg/m³ (106 ppm) with a medium value at 5.5 mg/m³ (Kusters *et al.*, 1990; NIOSH, 1993). In order to protect human health, German Ministry of Labor and Social Affairs and the American Conference of Industrial Hygienists adopted a limit of 10 ppm for the occupational exposure to CB named Arbeitsplatzgrenzwert (AGW) and Threshold Limit Value (TLV), respectively. The current Permissible Exposure Limit (PEL) according to the Occupational Safety & Health Administration (OSHA) is 75 ppm (NIOSH, 1993).

Typical indoor air concentrations of CB in Germany are low (0.1-4 µg/m³) (Herbarth *et al.*, 1998; NIOSH, 1993). Higher indoor concentrations are reported from various cities in the USA ranging up to 72.5 µg/m³ (NIOSH, 1993). Outdoor air in the United States, in Germany

and in the Netherlands revealed mean CB concentrations of about 1.5-3 $\mu\text{g}/\text{m}^3$ (ATSDR, 1990; NIOSH, 1993).

Similarly to CB, **1,2-dichlorobenzene** (1,2-DCB) is widely used as an intermediate for the synthesis of dyes, agrochemicals, pharmaceuticals and paints. Moreover, 1,2-DCB is used in drain cleaners, as preservative for wood, in formulations for motor oil additives, lubricants and as industrial deodorizer (Whilhite *et al.*, 1990; Anonymous, 1988; NTP, 1985) as well as in components of dielectrics or heat insulations (Heinisch *et al.*, 2006).

In 1991, the Western European use of 1,2-DCB totaled 24,000 t. Occupational 1,2-DCB levels up to 8.5 ppm (51 mg/m^3) have been found in chlorobenzene factories (Howard, 1989). The American Conference of Governmental Industrial Hygienists (ACGIH) has assigned an occupational threshold limit value (TLV) of 25 ppm (150 mg/m^3) for a normal 8-hour workday and a 40-hour work week. Occupational Safety & Health Administration (OSHA) adopted a Permissible Exposure Limit of 50 ppm for 1,2-DCB. In 2001, the German MAK-value for 1,2-DCB was lowered to 10 ppm (60 mg/m^3).

1,2-DCB concentrations in ambient outdoor air are low and range from 0.01 ppb to 0.6 ppm. The average daily adult respiratory exposure is only 1.8 μg (ATSDR, 2006). This low exposure is a result of ambient indoor air concentrations below 1 $\mu\text{g}/\text{m}^3$ (0.17 ppb) due to limited use of 1,2-DCB in consumer products. General human exposure via drinking water and inhaled air is estimated as 2.5 mg per year (Howard, 1989).

In contrast to styrene, there are no natural sources of all three isomers of dichlorobenzenes as well as of monochlorobenzene (Anonymous, 1988). However, these compounds have been detected in drinking water, meat, eggs, fat, fruits, vegetables, fish and milk, albeit the levels in foods are generally low. Dietary intake of 1,2-DCB was estimated at 108 μg per person and year (ATSDR, 2006; OECD, 2005).

5.1.2 Toxicokinetics of Monochloro- and 1,2-Dichlorobenzene

In humans, **CB** exposure occurs primarily via inhalation of contaminated air. About 20-50% of the dose is absorbed via the lung and the gastrointestinal tract (ATSDR, 1990). A physiologically based pharmacokinetic model for CB predicted a blood concentration of 3.9 mM at the LC_{50} concentration of 2965 ppm for the rat as mammalian model species (ATSDR, 1990; DeJongh *et al.*, 1998).

Following absorption, CB is preferentially distributed to the adipose tissue reflecting the lipophilic nature of this compound. In rats, the following partition coefficients (see sections 2.2 and 3.1.2) between organs and air were determined: blood/air-59.4, fat/air-1277, liver/air- 86.1, muscle/air-34 (Gargas *et al.*, 1989). However, CB is not bioaccumulated to high levels and does not belong to the group of persistent organic compounds (Heinisch *et al.*, 2006; NIOSH, 1993). Only low amounts (1 - 9 ng/g) of CB were found in 98% of human

adipose tissue samples from all regions of the United States. In addition, CB was also detected in exhaled breath, urine (20 - 120 ng/l) and human breast milk (ATSDR, 1990).

Likewise, **1,2-DCB** is quickly and extensively absorbed through the gastrointestinal (> 90%) and the respiratory tract (60% of dose). Following absorption, 1,2-DCB is distributed throughout the body, but tends to be found in greatest levels in fat, kidney, liver and the urinary bladder (Anonymous, 1988; ATSDR, 2006). In Wistar rats, peak organ concentrations were measured 6 h following oral administration (5, 50 and 250 mg/kg) and then declined rapidly. 1,2-DCB was nearly completely absorbed and metabolized (Hissink *et al.*, 1996). In humans, exposed to 10 ppm (MAK-limit) for 8 h, 1,2-DCB concentrations of up to 182 µg/l blood and 18 µg/l erythrocytes are reported (Ardakani, 2007).

Measured 1,2-DCB concentrations in blood of the general “unexposed” population are below 3 ppb (ATSDR, 2006). The content in whole human milk range from 3 to 29 ppb while 38 µg of 1,2-DCB per kg fat were detected in adipose tissue (Howard, 1989; OECD, 2005). Bioaccumulation is only expected in tissues with high fat content during prolonged, continuous exposures (Anonymous, 1988) as observed in rats exposed to high concentrations of 250 mg/kg (Hissink *et al.*, 1996).

Metabolism of CB and 1,2-DCB is believed to occur mainly in the liver, but occurs at lower levels in other tissues, such as the kidney or lung (Fisher *et al.*, 1995). In mammals, CB and 1,2-DCB are oxidized mainly via a cytochrome P450 2E1 (or 3A1 in rats (Bogaards *et al.*, 1995)) monooxygenase-mediated reaction to active arene epoxides (Figure 5-1). Thereafter, the epoxide may either be conjugated with glutathione by glutathione S-transferase, with the formation of chloro-phenylmercapturic acids or it spontaneously rearranges to form 4-chlorophenol/2,3- or 3,4-dichlorophenol, or it is hydrated to dihydrodiols by epoxide hydrolase. The dihydrodiols of CB/1,2-DCB may be further dehydrogenated to 4-chlorocatechol/3,4- and 4,5-dichlorocatechol, respectively (ATSDR, 2006; Kumagai *et al.*, 1995; Kusters *et al.*, 1990; Nedelcheva *et al.*, 1998; Rietjens *et al.*, 1997).

While rats, mice and rabbits metabolize chlorinated arene epoxides mainly to mercapturic acids, in humans, preferentially dihydrodiols, phenols and catechols are formed. Resulting phenols are partly excreted unchanged, but mostly conjugated to glucuronides or sulfates (Kumagai *et al.*, 1995). In contrast to rats, in human urine, little to no phenylmercapturic acids were detected (Ardakani, 2007). Moreover, secondary metabolism of phenols/catechols may yield hydroquinones and benzoquinones. These compounds together with the epoxides are supposed to be responsible for the toxicity of chlorinated benzenes (ATSDR, 2006; Bogaards *et al.*, 1995; Nedelcheva *et al.*, 1998). In general, only small amounts (1–2%) of the dose leave the body in the feces or are exhaled (0.06-5 µg/m³) (ATSDR, 2006; Hissink *et al.*, 1996; OECD, 2005).

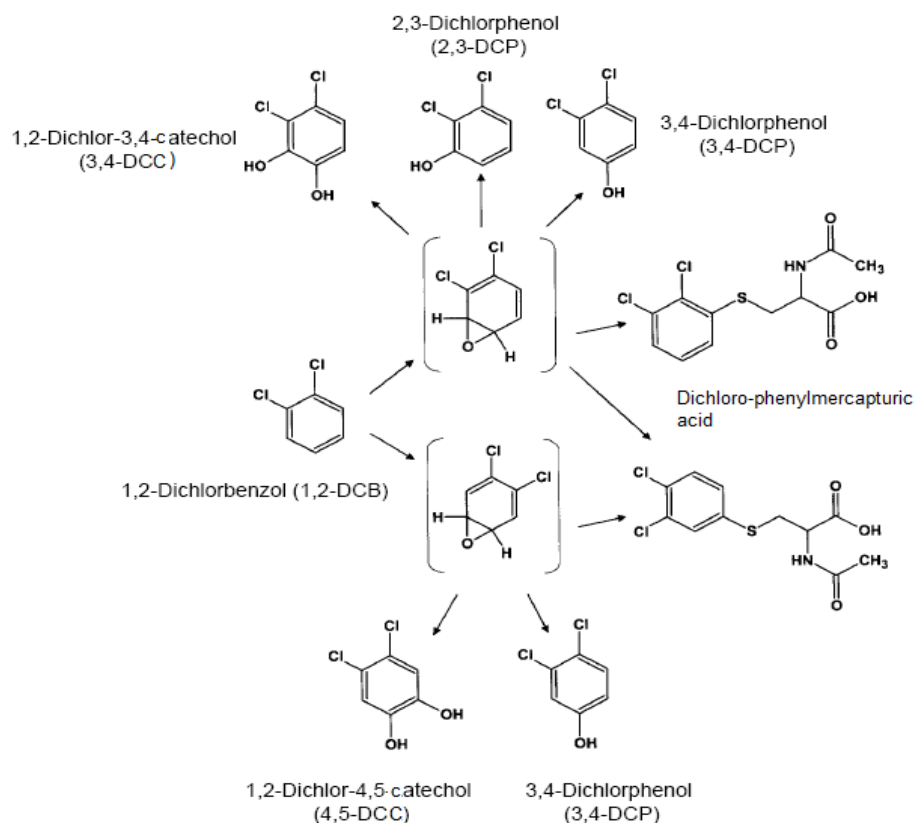


Figure 5-1 Metabolism of 1,2-dichlorobenzene. The figure was adapted from Ardakani *et al.*

5.1.3 Toxicodynamics of Monochloro- and 1,2-Dichlorobenzene

Halobenzenes are hepatotoxic in rodents and humans. Hepatotoxicity strongly correlates with hydrophobicity of compounds and arrangement of halogen substituents (Chan *et al.*, 2007). In a study comparing hepatotoxicity of different chlorinated benzenes in rats, 1,2-DCB and 1,2,4 trichlorobenzene produced the most severe hepatotoxic effects 72 h after intraperitoneal administration (den Besten *et al.*, 1991). 1,2-DCB was identified as a potent hepatotoxicant in most mammalian species (Hissink *et al.*, 1996; Kulkarni *et al.*, 1996). In rats and mice, acute exposure to 500 mg/kg of 1,2-DCB produced centrilobular necrosis of the liver and hepatocellular degeneration. Even at a dose of 120 and 250 mg/kg, necrosis of individual hepatocytes was observed (Ban *et al.*, 1998; NTP, 1985). In the above-mentioned comparative study, CB was considerably less hepatotoxic than all other chlorinated benzenes (den Besten *et al.*, 1991). However, when rats were exposed to CB via gavage in another study, an increased incidence of neoplastic nodules of the liver was observed (ARB, 1997).

Employing a physiologically based pharmacokinetic (PB-PK) model, human risk for 1,2-DCB induced hepatotoxicity was evaluated. It was predicted that the dose level needed to obtain the same toxic liver concentration of reactive epoxides as in rat can not be reached due to saturation of metabolism and a concomitant accumulation of 1,2-DCB in fat. Moreover, it appeared that at a dose level of 250 mg/kg, hepatic glutathione was completely

depleted after 10 h for man, whereas for the rat a maximum depletion of 75% was predicted after 15 h (Hissink *et al.*, 1997), supporting the idea of dissimilar mechanisms of toxicity in both species. Furthermore, evidence is presented suggesting that the formation of reactive benzoquinone metabolites rather than the traditional epoxides is linked to halogenated benzene-induced hepatotoxicity (den Besten *et al.*, 1994).

Chlorinated benzenes are suspected to affect mammalian leukocytes. Several U.S. citizens that used 1,2-DCB containing consumer products developed acute myeloblastic-/chronic lymphoid leukemia or proliferating myelosis (ACGIH, 1991). In agreement with these observations, chromosomal studies in laboratory animals exposed to 1,2-DCB revealed significant alterations in the leukocytes. Leucopenia was even observed in rats exposed for 4 h to 1,2-dichlorobenzene, at levels as low as the current occupational standard (OSHA, NIOSH) of 50 ppm (Brondeau *et al.*, 1990). A depletion of lymphocytes in the thymus and spleen and increased malignant histiocytic lymphoma were observed in rodents exposed to 500 mg/kg 1,2-DCB. In contrast, in a two-year gavage study, there was no evidence of carcinogenicity of 1,2-dichlorobenzene for rats or mice receiving 60 or 120 mg/kg per day (NTP, 1985). Moreover, high-dose exposure (750 mg/kg) of mice to monochlorobenzene was associated with peripheral lymphocytes genotoxicity. However, this solvent is not estimated to be a major hazard to bone marrow cells, even after repeated high-dose exposure (Vaghef *et al.*, 1995).

Because metabolism of halogenated benzenes yields a number of reactive metabolites such as electrophilic epoxides or benzoquinones, adduction of these metabolites to cellular macromolecules is a mechanism that may be responsible for observed genotoxic events (Rietjens *et al.*, 1997). In a study in rats and mice, 24 h following administration, 1,2-DCB was covalently bound to DNA, RNA and proteins of liver, kidney, lung and stomach. The covalent binding index to liver DNA was typical of carcinogens classified as weak initiators (Colacci *et al.*, 1990). In addition, metabolic activation of CB- and 1,2-DCB resulted in covalent binding to calf-thymus DNA. In a further study, guanine adducts were detected in the urine of monochlorobenzene-treated rats (Krewet *et al.*, 1989).

U.S. Environmental Protection Agency (EPA) and the International Agency for Research on Cancer (IARC) determined that 1,2-DCB as well as CB are not classifiable as to human carcinogenicity and categorized them in cancer weight-of-evidence group D/group 3 (ARB, 1997; ATSDR, 2006).

Because CB and 1,2-DCB can cross the blood–brain barrier, they are prone to act as neurotoxicants what has often been reported from occupational exposure to these compounds. In humans, vomiting, skin lesions, headaches, irritation of eyes, nose and the upper respiratory tract are reported following exposure to CB and 1,2-DCB (Von Burg, 1981). The air concentration level of 1,2-DCB where irritation to humans begins (threshold of

irritation) is between 15 and 30 ppm (OECD, 2005). In animals, short-term oral exposure caused sedation and disturbances of the central nervous system. However, the most frequent cause of death was respiratory depression (Escuder-Gilabert *et al.*, 2008).

Relationship between chronic indoor VOC exposure, respiratory and inflammatory diseases such as chronic obstructive pulmonary disease (COPD) and asthma has been established by several epidemiologic studies (Diez *et al.*, 2000; Diez *et al.*, 2003; Wieslander *et al.*, 1994; Wieslander *et al.*, 1997a; Wieslander *et al.*, 1997b). Especially in children and infants, exposure to VOCs including chlorinated benzenes significantly contributed to allergic sensitization mediated by a T cell polarization toward the type 2 phenotype (Herberth *et al.*, 2008).

Increased levels of pro-inflammatory cytokines such as TNF- α and IL-6 were detected in sera of 1,2-DCB-treated mice (Ban *et al.*, 1998). In accordance with that *in vitro* studies using human lung epithelial cells (A549) and peripheral blood mononuclear cells exposed to low levels of CB (100 and 10 $\mu\text{g}/\text{m}^3$) induced expression and release of the pro-inflammatory cytokine MCP-1 via the NF- κB - and the p38 MAP kinase pathways (Fischader *et al.*, 2008; Lehmann *et al.*, 2008; Roder-Stolinski *et al.*, 2008a). Even VOC-induced hepatotoxicity seems to be governed by increased secretion of inflammatory cytokines. Younis *et al.* reported that CB exposure to mice induced the release of cytokines and chemokines from hepatocytes in consequence stimulating Kupffer cell (liver macrophages) activity and the subsequent cascade of inflammatory events that leads to the progression of hepatocellular injury (Younis *et al.*, 2003).

5.1.4 Effects of Chlorinated Benzenes on Proteins

Covalent binding of reactive CB/1,2-DCB metabolites, especially epoxides and benzoquinones, to cellular proteins was reported, albeit the relative contribution of the quinones and the epoxides to the toxicity of halobenzenes is still unclear. Den Besten *et al.* suggested a key role for quinones in a microsomal system (den Besten *et al.*, 1992). Further studies with bromobenzene confirmed that secondary quinone metabolites are also involved in the alkylation of hepatic proteins. In fact, the majority of the protein-bound residues from bromobenzene was quinone-derived whereas only 0.5% accounted for epoxides (Hissink *et al.*, 1996; Slaughter *et al.*, 1991). Strikingly, in liver slices, CB hepatotoxicity was suppressed by supplementing 1% BSA (Fisher *et al.*, 1993), providing further evidence for an essential role of formed protein-adducts in the development of hepatotoxicity. Rats, treated with 1,2-DCB developed centrilobular necrosis of the liver accompanied by the formation of 4-hydroxynonenal protein adducts in the centrilobular regions indicating enhanced lipid peroxidation (Hoglen *et al.*, 1998).

Moreover, protein adducts of halobenzene derivatives are supposed to provoke thyroid toxicity. In rats, 1,2-DCB but not CB induced a reduction in plasma thyroxine levels that was

correlated with binding of the phenolic metabolites to the plasma transport protein for thyroxine, i.e., transthyretin (den Besten *et al.*, 1991). Finally, *in vitro* studies using whole blood from rats demonstrated binding of CB to hemoglobin (Beliveau *et al.*, 2000).

In a comparative study, the observed covalent binding of CB to microsomal proteins was by order of magnitude higher than that to DNA. Additionally, significant metabolic differences, that affect the formation of protein adducts, were reported for humans and laboratory animals. While human rates of metabolism of CB and 1,2-DCB to soluble metabolites were higher than that in mice and especially rat microsomes, in contrast, formation of covalently binding products was lowest in human, higher in rat and highest in liver microsomes of mice (Nedelcheva *et al.*, 1998).

Although no extensive *in vivo* or *in vitro* studies on affected protein expression caused by chlorinated benzenes are available, some reports indicate that these compounds modulate cellular protein expression. As mentioned before, CB and 1,2-DCB induced chemokine secretion from different cell types and tissues (Fischader *et al.*, 2008; Ban *et al.*, 1998; Lehmann *et al.*, 2008; Younis *et al.*, 2003). In mice subjected to a whole-body 4-h exposure to 1,2-DCB vapors, reduced staining for liver glucose-6-phosphatase was reported (De Ceaurriz *et al.*, 1988). Moreover, overexpression of stress proteins was studied in tumor-derived human cell lines (A549, HepG2) exposed for 4 days to a panel of aromatic VOCs via the culture medium. No significant change of expression level of HSP72 and HSP90 was observed by treatment with chlorinated benzenes. Conversely, a dose-dependent increase of GRP78 expression was induced by benzene (≥ 2 mM) and chlorinated pollutants including CB (≥ 500 μ M) and 1,2-DCB (≥ 50 μ M) (Crouté *et al.*, 2002).

Encouraged by the results on differential protein expression caused by styrene (presented in section 4) CB and 1,2-DCB have been used as model substances to investigate chlorination-mediated modulation of protein abundance and differential phosphorylation in lung epithelial cells in vitro. The results may improve the understanding of proteotoxic effects due to exposure to chlorinated aromatic VOCs that may contribute to impaired health.

5.2 Results

5.2.1 Toxicity of Monochloro- and 1,2-Dichlorobenzene in A549 Cells

Prior to the toxicoproteomic analysis of chlorinated benzenes, cell (A549) toxicity was estimated for a broad range of monochlorobenzene (CB) and 1,2-dichlorobenzene (1,2-DCB) concentrations by a 24 h exposure of the cells via the gas phase. Membrane damage (as a degree of cell viability) has been assessed by measuring cellular lactate dehydrogenase (LDH) release into cell culture media (according to section 2.3). LDH release within 24 h increased up to 65.6% and 73.8% of total cellular LDH (estimated by lysing all cells of a transwell insert) compared to control cultures (only 6% of LDH_{total}) when cells were exposed to 10^2 g/m³ of CB or 1,2-DCB, respectively (Figure 5-2). Only a weak increase in LDH release to 8.91% versus 9.63% could be detected when exposing cells to 10^1 g/m³ of CB or 1,2-DCB, respectively. No membrane damage was observed when exposing cells to lower concentrations. As presented in chapter 4, A549 control cells showed a high viability (92-94%) under exposure conditions (see paragraph 4.2.1).

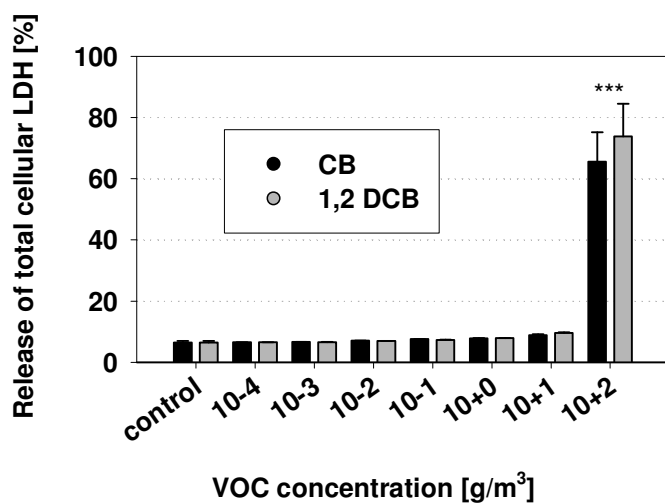


Figure 5-2 Toxicity of exposure to chlorinated benzenes (24 h) for A549 cells was estimated by release of lactate dehydrogenase (LDH). LDH release is normalized versus total LDH as estimated by a lysis control. Data are shown as mean of triplicates + SEM. *** $p < 0.001$

5.2.2 Differential Protein Expression in 2D DIGE

The effect of CB and 1,2-DCB exposure on differential protein expression of lung epithelial cells (A549) has been analyzed in 2D DIGE gel triplicates (Figure 5-3). Employing 10^{-2} g CB/m³ (2.2 ppm) and 10^{-3} g 1,2-DCB/m³ (0.17 ppm), environmentally relevant, but essentially non-toxic (see above) concentrations have been applied. In earlier results, these concentrations of CB were able to induce maximal secretion of monocyte chemoattractant protein 1 (MCP 1) and nuclear factor kappa B (NF- κ B) (Fischader *et al.*, 2008; Lehmann *et*

al., 2008; Roder-Stolinski *et al.*, 2008a), two major mediators of an inflammatory response, from A549 cells, leading to the hypothesis that even at these low concentrations, chlorinated benzenes are effective in modulating protein expression. However, the decision to use a 10-fold lower exposure concentration compared to CB is based on observations of Croute *et al.* (2000) in A549 cells stating that 1,2-DCB induced heat shock proteins with a 10-fold higher effectiveness.

Hence, the expression of about 860 protein spots of A549 cells with isoelectric points between 3 and 10 have been quantified using Delta 2D software. The reproducibility of the gels was confirmed by unsupervised cluster analysis, by which the comparisons between the different samples and the controls showed a clustering that was in line with the experimental setup (dendrograms are shown in Figure 8-2 in the appendix).

In general, more repressed protein spots have been observed than induced ones. 75.0% and 71.2% of all significantly ($p < 0.05$) altered protein spots showed reduced expression following cell exposure to 10^{-2} g/m³ CB and 10^{-3} g/m³ 1,2-DCB, respectively. Significantly regulated protein species are listed in Table 5-1 and a subset is displayed in more detail in Figure 5-4. Identification data are listed in Table 8-1. In some cases, several protein spots that were assigned to the same protein showed differential expression as listed in column 1 ("ID") of Table 5-1. In total, 52 versus 59 protein spots were detected with significantly ($p < 0.05$) altered expression (by a factor of 1.3) following cell exposure to 10^{-2} g CB or 10^{-3} g/m³ 1,2-DCB, respectively. Thus, 6.0% versus 6.9% of all quantified protein spots were modified in their expression following cell exposure to CB or 1,2-DCB, respectively. 15 protein spots were significantly ($p < 0.05$) regulated in the same direction for both compounds (CB and 1,2-DCB). Accepting a relaxed significance value of $p < 0.1$, 75 and 87 protein spots were altered in expression by CB and 1,2-DCB, respectively and 34 protein spots showed a similar expression change in response to both benzene derivatives. They account for 26.5% of all differentially expressed protein spots (128 in number) modulated by either CB, 1,2-DCB or both, and thus pointing to a common molecular response mechanism for both compounds. Furthermore, no protein spots have been detected that showed significant but inverse regulation in both treatments. 26 and 32 different proteins (detected as chains of up to 6 spots) have been identified displaying a difference in expression stronger than 1.3-fold ($p < 0.05$) at 10^{-2} g CB and 10^{-3} g/m³ 1,2-DCB, respectively. A total of 12 (for CB) versus 7 (for 1,2-DCB) proteins were significantly ($p < 0.05$) induced or repressed by a factor of two or more.

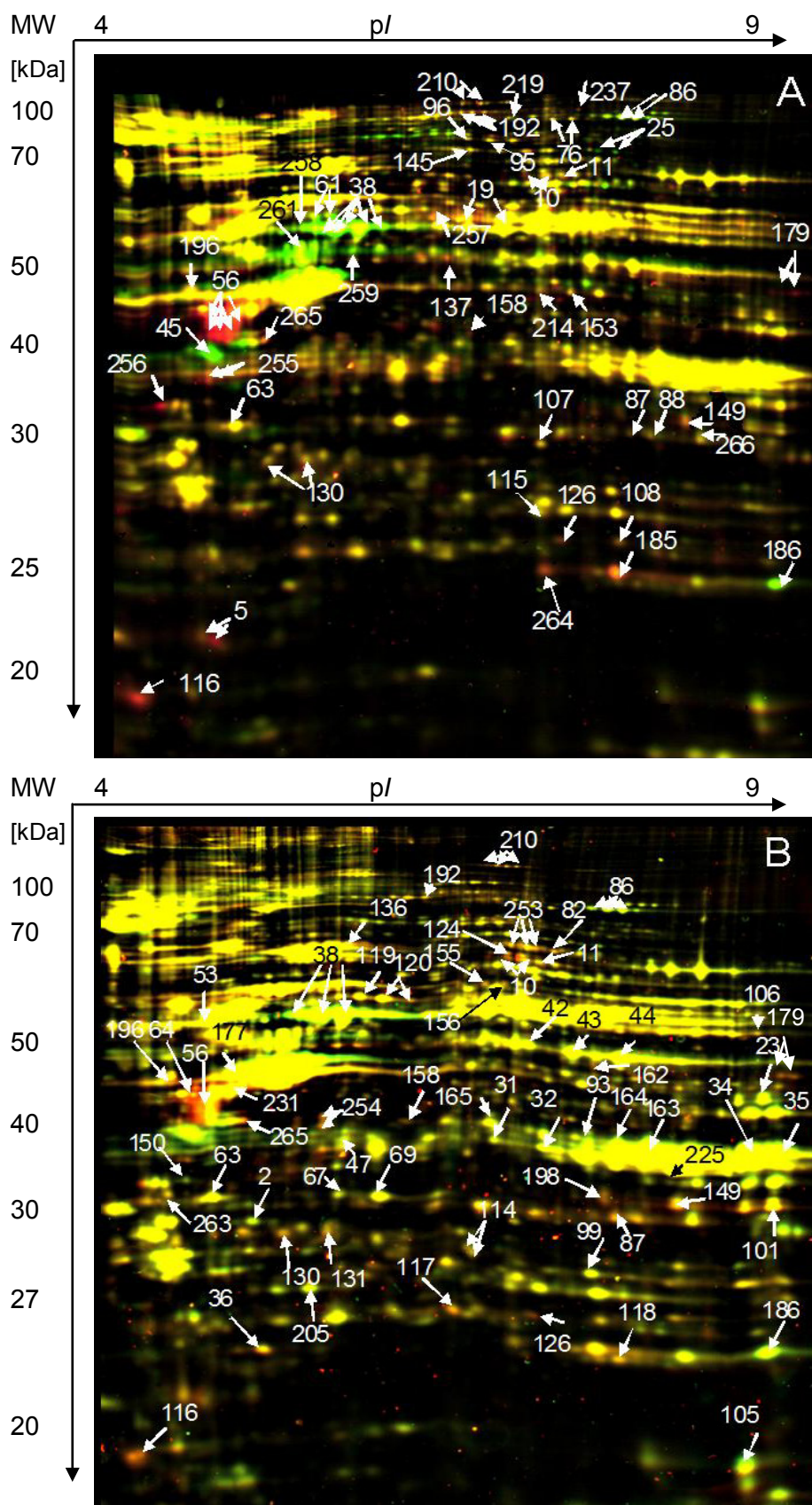


Figure 5-3 Differentially expressed protein spots in A549 cells following 24 h exposure to chlorinated benzenes. A) 10⁻² g/m³ monochlorobenzene B) 10⁻³ g/m³ 1,2-dichlorobenzene. Figures are overlays of fluorescent images of controls (in red) and treated cells (in green) that were analyzed in one 2-DE gel. 100 µg of total soluble protein were labeled with CyDyes and separated according to 2.4.2. For ID numbers and quantification, see Table 5-1. Mass spectrometric identification is listed in Table 8-1.

Table 5-1 Differentially expressed proteins following exposure to chlorinated benzenes

ID ^{a)}	Protein involved in process	Accession ^{b)}	Expression level ^{c)}	
			CB	1,2-DCB
Oxidative stress				
2	Chloride intracellular channel protein 1	O00299		1.54*
2x5	Cytochrome b5 type B precursor	O43169	0.15-0.38 ^{*/**}	
2x25	Lamin-A/C	P02545	1.99-3.68 ^{°/*}	
2x76	Glycogen phosphorylase	P11216	0.59-0.62*	
93	Aldose reductase	P15121		1.30*
99	Phosphoglycerate mutase 1	P18669		1.31 [°]
162	6-phosphogluconate dehydrogenase	P52209		1.39 [°]
163	Aldo-keto reductase family 1 member C2	P52895		1.82*
164	Aldo-keto reductase family 1 member C2	P52895		1.85*
165	Biliverdin reductase A	P53004		1.35*
185	Peroxiredoxin-1	Q06830	0.23 [°]	
186	Peroxiredoxin-1	Q06830	2.85*	2.36 [°]
264	Peroxiredoxin-1	Q06830	0.24 [°]	
Cell death signaling				
2x10	WD repeat-containing protein 1	O75083	0.56 ^{**}	0.39-0.58*
11	WD repeat-containing protein 1	O75083	0.63*	0.73*
31	Annexin A1	P04083		1.42 [°]
32	Annexin A1	P04083		1.54*
36	Heat shock protein beta-1	P04792		0.65*
6x38	Vimentin	P08670	2.35-4.35*	
45	Nucleophosmin	P06748	3.03*	
5x56	Heterogeneous nuclear ribonucleoproteins C1/C2	P07910	0.09-0.53 ^{*/**/**}	0.28-0.49 ^{*/**}
4x56	Heterogeneous nuclear ribonucleoproteins C1/C2	P07910		0.22-0.29*
63	Annexin A5	P08758		1.59 ^{**}
67	Annexin A4	P09525		1.31 [°]
69	Annexin A4	P09525		1.37 [°]
6x86	Elongation factor 2	P13639	1.75-1.91 [°]	1.45-1.79*
87	Electron transfer flavoprotein subunit alpha	P13804	0.60 [°]	0.59 [°]
88	Electron transfer flavoprotein subunit alpha	P13804	0.63*	
95	Ezrin	P15311	0.62*	
96	Ezrin	P15311	0.59*	
101	Voltage-dependent anion-selective channel protein 1	P21796		0.61 [°]
105	Cofilin-1	P23528		1.40 [°]
115	Peroxiredoxin 6	P30041	0.62 [°]	
117	Thioredoxin-dependent peroxide reductase	P30048		0.45 ^{**}
118	Phosphatidylethanolamine-binding protein 1	P30086		0.73 [°]
130	Prohibitin	P35232	0.60 ^{***}	0.74*
131	Prohibitin	P35232		0.66 ^{**}
149	Voltage-dependent anion-selective channel protein 2	P45880	0.57*	0.52 ^{***}
150	60S ribosomal protein L5	P46777		1.48 [°]
155	Seryl-tRNA synthetase	P49591		0.64*
156	Seryl-tRNA synthetase	P49591		0.63*
158	Isocitrate dehydrogenase, mitochondrial	P50213	0.40*	0.31*
177	Actin, cytoplasmic 2	P63261		0.57*
2x179	Elongation factor 1-alpha 1	P68104	0.14-0.18*	0.38-0.47 [°]
214	IDH1 protein	Q6FHQ6	0.65*	
219	PDCD6IP protein	Q8WUM4	0.64*	
231	Protein arginine N-methyltransferase 1	Q99873		0.33 ^{**}
2x254	Actin, cytoplasmic 1	P60709		0.37-0.40*
256	Proliferating cell nuclear antigen	P12004	0.23 [°]	
259	Elongation factor 1-alpha 1	P68104	2.23*	
261	Elongation factor 1-alpha 1	P68104	2.14*	
265	Heterogeneous nuclear ribonucleoproteins C1/C2	P07910	0.47 [°]	0.45*
266	Guanine nucleot.-bind. protein subunit beta-2-like 1	P63244	0.60 ^{**}	

Toxicoproteomics of Mono- and 1,2-Dichlorobenzene Exposure

ID ^{a)}	Protein involved in process	Accession ^{b)}	Expression level ^{c)}	
			CB	1,2-DCB
Protein quality control				
64	40S ribosomal protein SA	P08865		0.26*
107	Proteasome alpha 1	P25786	0.48**	
108	Proteasome subunit alpha type-2	P25787	0.51°	
2x114	Endoplasmic reticulum protein ERp29 precursor	P30040		0.68-0.71°/*
116	60S ribosomal protein L12	P30050	0.15*	0.38°
119	Protein disulfide-isomerase A3	P30101		0.74°
2x120	Protein disulfide-isomerase A3	P30101		0.71-0.76*
136	Stress-70 protein, mitochondrial	P38646		0.75*
205	Putative uncharacterized protein UCHL1	Q4W5K6		1.79*
Metabolism				
2x19	Retinal dehydrogenase 1	P00352	0.51-0.66°	
23	Phosphoglycerate kinase 1	P00558		1.73°
34	Glyceraldehyde-3-phosphate dehydrogenase	P04406		1.54°
35	Glyceraldehyde-3-phosphate dehydrogenase	P04406		1.43°
42	Alpha-enolase	P06733		1.39°
43	Alpha-enolase	P06733		1.68**
44	Alpha-enolase	P06733		1.64*
53	Tubulin beta chain	P07437		1.40**
2x61	Keratin, type II cytoskeletal 7	P08729	1.51*	
82	ATP-dependent DNA helicase 2 subunit 1	P12956		0.57**
106	ATP synthase subunit alpha, mitochondrial	P25705		0.65°
124	Succinate dehydrogenase flavoprotein	P31040		0.51*
126	Heterogeneous nuclear ribonucleoprotein H	P31943	0.37*	0.48°
137	Eukaryotic initiation factor 4A-III	P38919	0.62°	
145	Glycyl-tRNA synthetase	P41250	0.63*	
153	Elongation factor Tu	P49411	0.66*	
5x192	Neutral alpha-glucosidase AB	Q14697	0.44-0.53°/**	0.72°
196	Reticulocalbin 1 precursor	Q15293	0.52°	0.54*
198	Thiosulfate sulfurtransferase	Q16762		0.54*
4x210	Carbamoylphosphate synthetase I	Q5R208	0.52-0.54***	0.55-0.59*
225	Annexin A2	Q8TBV2		1.75°
237	2-Oxoglutarate dehydrogenase E1 component	Q9UDX0	0.39°	
3x253	Moesin	P26038		0.65-0.72*
3x255	Elongation factor 1-delta	P29692	0.36-0.60°/**	
257	Retinal dehydrogenase 1	P00352	0.53°	
2x258	G-rich sequence factor 1	Q12849	0.55-0.57°	
263	Tropomyosin alpha-1	P09493		0.71*

a) For spot IDs see map in Figure 5-3

b) Uni-Prot Accession from www.uniprot.org

c) Expression level (exposed *versus* control) following exposure to monochlorobenzene (10^{-2} g/m³) or 1,2-dichlorobenzene (10^{-3} g/m³). Only significant expression changes are listed. ° p<0.1, * p<0.05, ** p<0.01, *** p<0.001. Mass spectrometric identification data are found in the appendix (Table 8-1).

Differentially expressed proteins were assigned to their major role within the cell (see categories in Table 5-1) depending on their functions listed in the UniProtKB/TrEMBL database and in existing scientific literature. According to this grouping, identified proteins with modulated expression ($p < 0.05$) after exposure of A549 cells to CB or 1,2-DCB could be assigned to four different cellular processes, cell death signaling (21 proteins), oxidative stress regulation (8 proteins), protein quality control (7 proteins) and metabolism (15 proteins). The fundamentals of the applied grouping of the proteins including literature references and their derived biological significance are discussed in section 5.3.

In most cases, cellular exposure to chlorinated benzenes altered the expression of proteins linked to **cell death signaling**, possibly via an oxidative stress-related mechanism. Modulation of protein levels was observed mainly for pro-apoptotic and to a lesser extent for anti-apoptotic pathways. In the following, some examples thereof are given.

Pro-apoptotic regulation

A cluster of heterogeneous nuclear ribonucleoproteins C1/C2 (HNRNPC1/C2) showed a strong downregulation, the remaining levels reaching only 8.8% for CB ($p < 0.001$) and 21.6% for 1,2-DCB of the expression observed in control cells. A second well-known apoptosis marker, voltage-dependent anion-selective channel protein 2 (VDAC2), showed a more than 40% decreased expression when exposed to both chlorinated compounds ($p < 0.05$ for CB; $p < 0.001$ for 1,2-DCB). Cytoplasmic actin 2 expression was diminished to a level of 36%, whereas cytoplasmic actin 1 was limited to 58% of protein expression compared to controls when exposed to 1,2-DCB. Prohibitin displayed a reduction in expression of about 40% for CB ($p < 0.001$) and 35% for 1,2-DCB ($p < 0.01$). Expression of the nucleophosmin (NPM) protein was induced by more than three times compared to the control level in response to cellular exposure to CB ($p < 0.05$). Heat shock protein B1 (HSPB1) expression was decreased to a level of about 64% (relative to the control) at 10^{-3} g/m³ of 1,2-DCB ($p < 0.05$). Peroxiredoxin 3 was downregulated to a level of 45% ($p < 0.01$) by exposure to 1,2-DCB, whereas peroxiredoxin 6 expression fell to a level of 63% ($p < 0.1$) following CB exposure. 60S ribosomal protein L5 (RPL5) seemed to be upregulated in its expression, albeit with a low significance value ($p < 0.1$), when cells were exposed to 10^{-3} g/m³ 1,2-DCB. In addition, two protein spots identified as seryl-tRNA synthetase were detected with a more than 35% lowered expression ($p < 0.05$). Another protein hinting at a VOC-mediated induction of apoptosis is the guanine nucleotide-binding protein subunit beta-2-like 1, also called receptor of activated protein kinase C1 (RACK1), that showed a 40% reduced expression ($p < 0.01$) following cellular exposure to CB. Proliferating nuclear cell antigen (PCNA) expression was only affected in CB-treated cells. Here, cytosolic (IDH 1) and mitochondrial isocitrate dehydrogenase (IDH 3A) expression was depressed to a level of 64% and 39.5%,

respectively, for CB exposure and to a level of 30.5% (IDH 3A) for 1,2-DCB exposure compared to control cells. Finally, cofilin was induced when cells were treated with 1,2-DCB.

Anti-apoptotic regulation

The programmed cell death 6-interacting protein was downregulated when cells were exposed to CB ($p < 0.05$). In contrast, annexin A1 showed a more than 50% increased abundance when cells were exposed to 1,2-DCB. Significant ($p < 0.01$) repression of protein arginine N-methyltransferase 1 (PRMT1) has been observed down to a level of only 33% versus controls following exposure to 1,2-DCB. Two spots corresponding to the WD-repeat-containing protein 1 (WDR1/Aip1) showed a significant reduction in intensity to 56% ($p < 0.01$) and 39% ($p < 0.05$), respectively, after cell exposure to CB and 1,2-DCB. Two spots, located at the acidic region of the gel and identified as elongation factor 1 alpha (EEF1A1) showed a more than two-fold increased staining following A549 exposure to CB ($p < 0.05$). In contrast, two more spots, also identified as EEF1A1 and located at a similar molecular mass but in the basic region of the gel, were repressed more than factor 2 for both chlorinated compounds. Moreover, elongation factor 2 was also significantly induced in response to both volatile compounds. Furthermore, phosphatidylethanolamine-binding protein 1, also designated Raf-1 kinase inhibitor protein (RKIP), showed diminished expression following exposure to 1,2-DCB. Further explanations on the relevance of the observed effects will be given in section 5.3.

Additionally, several **redox-sensitive proteins** susceptible to CB or 1,2-DCB exposure have been assigned that were found to be regulated by styrene (see chapter 4). Increased expression (+34%, $p < 0.05$) of biliverdin reductase A (BLVRA) was observed following cell exposure to 10^{-3} g/m³ 1,2-DCB, though to a lower extent as the one observed for styrene exposure (+89%, $p < 0.01$). Chloride intracellular channel protein 1 (CLIC1), a redox-sensitive ion channel, was upregulated by 54% when the cells were exposed to 1,2-DCB while cellular expression reached 250% of control levels after exposure to a higher (10^0 g/m³) styrene concentration. And once more, enzymes of the pentose phosphate pathway (PPP) and of the xenobiotics metabolism displayed differential expression.

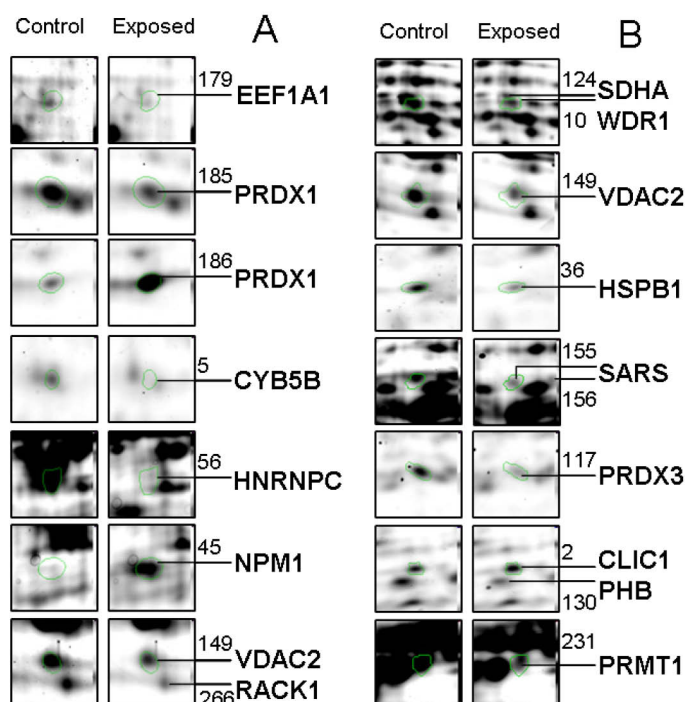


Figure 5-4 Examples of gel image regions of differentially expressed proteins following monochlorobenzene (A, 10^{-2} g/m³) and 1,2-dichlorobenzene (B, 10^{-3} g/m³) exposure. 100 μ g of total soluble protein of control and treated sample were separated by 2-DE (18 cm IPG strips 3-10 NL, 12% acrylamide/bisacrylamide) in one gel using DIGE fluorescent labeling. Abbreviations are gene names. An explanation is found in Figure 5-5. Given ID numbers are labeled in the DIGE map (see Figure 5-3).

In cells exposed to 10^{-3} g/m³ of 1,2-DCB, a spot corresponding to 6-phosphogluconate dehydrogenase (PGD) was detected with increased intensity (+50%) compared to control cells, albeit with lower significance ($p < 0.1$) than when upregulated by 10^1 g/m³ or 10^{-2} g/m³ of styrene. Aldose reductase expression was induced by 30% when cells were exposed to 1,2-DCB. Two spots of AKR1C2, also called trans-1,2-dihydrobenzene-1,2-diol dehydrogenase, showed 1.85 times the intensity of the control spots following exposure to 1,2-DCB. Glycogen phosphorylase expression decreased about 42% in CB-treated cells and two (ID 185, ID264) of the five spots identified as peroxiredoxin 1 in A549 proteome map were significantly reduced in expression, down to a remaining level of only one fourth of control cells. In contrast, ID186, the peroxiredoxin 1 spot with the most basic isoelectric point, was induced by more than factor of 2 in response to both chlorinated benzenes.

As might be expected, a relatively high number of proteins that can be connected to protein quality control (7), e.g. proteasomal proteins were differentially altered (all reduced in expression) following exposure to chlorinated benzenes. Furthermore, a fair number of proteins involved in cellular metabolism (15), such as glycyl-tRNA synthetase, glycogen phosphorylase or succinate dehydrogenase, were identified as well.

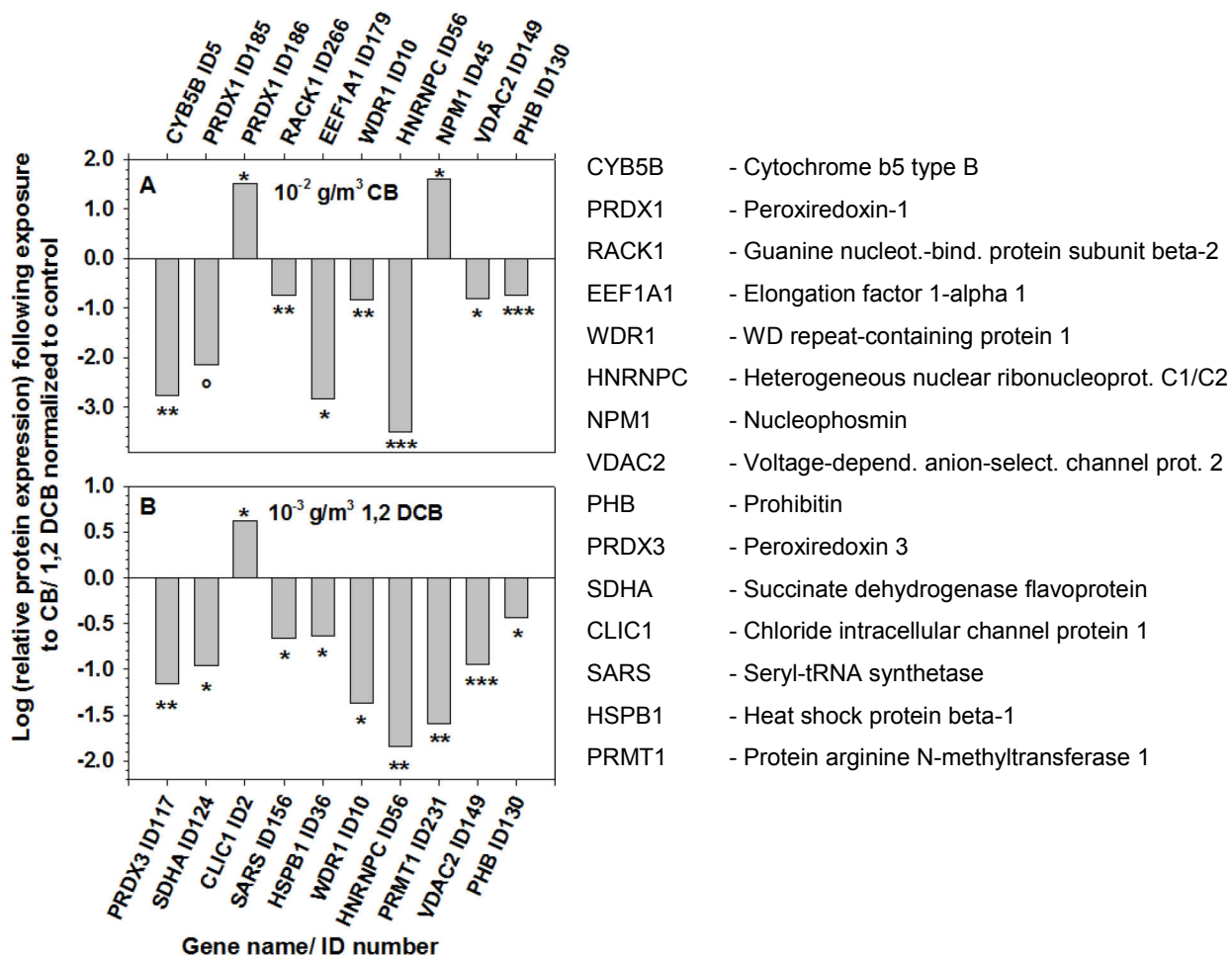


Figure 5-5 Profiles of proteins displaying changes in expression after cellular (A549) exposure to monochlorobenzene (A) or 1,2-dichlorobenzene (B). Expression levels (logarithmized to base 2) are spot volumes relative to spot volumes of the control, given as means of 3 replicates. Abbreviations are gene names. Given ID numbers (subsequent to gene name) are found in Table 5-1 together with quantification data. * $p < 0.05$, ** $p < 0.01$, *** $p < 0.001$.

5.2.3 Differential Phosphorylation Patterns in 2-DE

The combination of 2-DE and phospho-specific Pro Q Diamond staining had been successfully applied in previous studies for analyzing changes of protein phosphorylation, which enabled the identification of kinase/phosphatase targets with a detection sensitivity of 0.1 fmol of mono-phosphorylated proteins. It allows for the detection of general protein phosphorylation states at Tyr-, Ser-, or Thr-residue(s) with a strong correlation between the observed fluorescence signal and the number of phosphates per protein (Jin *et al.*, 2006; Orsatti *et al.*, 2009). Thus, in conjunction with total protein staining, this phospho-specific dye has been employed in the 2-DE analysis of the effects that chlorinated benzenes exert on A549 cells (Figure 5-6). 200 μg of total soluble protein were separated by 2-DE (7 cm IPG strips, pH 3-10 NL), and phosphoproteins as well as total protein were stained using Pro Q Diamond (colored in blue in Figure 5-6) and SYPRO Ruby (colored in red in Figure 5-6), respectively. As also observed for styrene treatment, most protein spots with high intensity for the phospho-specific dye are located in the gel part of proteins with acidic isoelectric points. A discussion on that phenomenon is found in section 4.3.

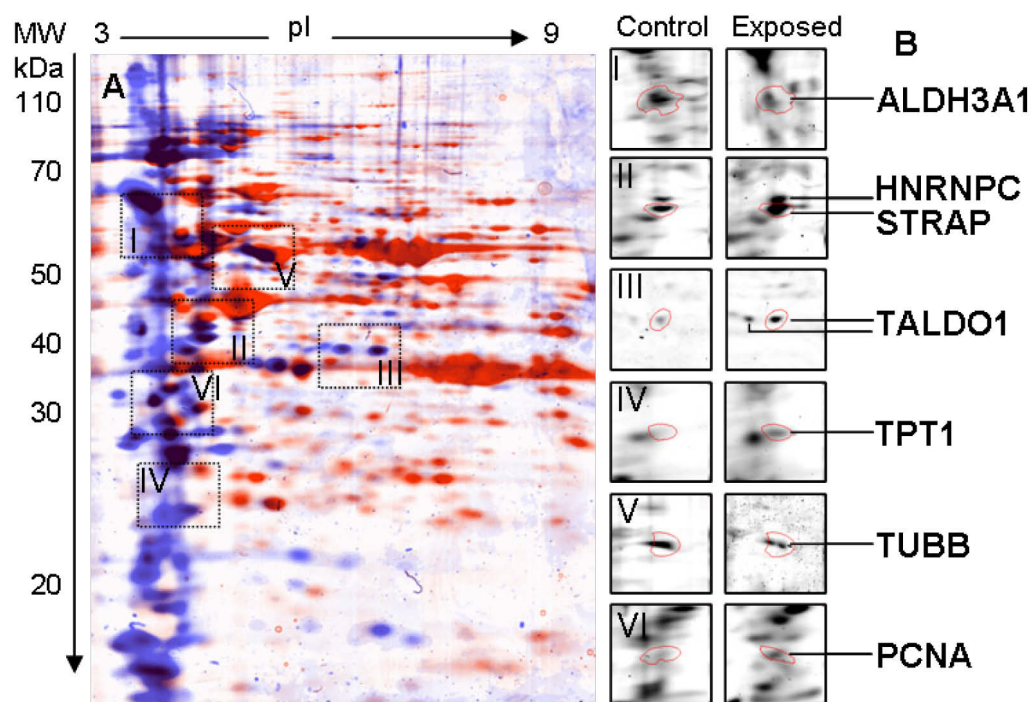


Figure 5-6 Phosphoproteome analysis of A549 cells following 1 h exposure to chlorinated benzenes. (A) Two-dimensional gel (200 μg of total soluble protein, 7 cm IPG strips) stained with phospho-specific Pro Q Diamond (in blue) and subsequently with total protein stain SYPRO Ruby (in red). Selected areas of differential phosphorylation are highlighted by squares. (B) Enlargements of marked areas from phosphostain image in A for exposed ($10^{-4}\text{g}/\text{m}^3$ and $10^0\text{g}/\text{m}^3$ CB or 1,2-DCB) and non-exposed cells. Detailed information on differential staining intensity of detected phosphoproteins is listed in Table 5-2. There, ID numbers are given in the column "Spot". Mass spectrometric identification data are found in the appendix (Table 8-3). Used abbreviations are gene names.

Pro Q Diamond phosphoprotein stain enabled the detection of differential protein phosphorylation following CB and 1,2-DCB treatment (both 10^{-4}g/m^3 and 10^0g/m^3). Differential staining of phosphoproteins following one hour of treatment with CB or 1,2-DCB is displayed in Figure 5-6 B, together with enlargements of (control) gel areas I-VI from Figure A compared to corresponding gel areas obtained from lysates of treated cells. Overall, 23 protein spots observed by phospho-specific fluorescence staining showed significantly ($p < 0.1$) altered intensities (Table 5-2). In contrast to the results from the styrene study, where most protein spots (26 of 34 spots) were detected with decreased intensity compared to the corresponding spots in control cells, for chlorinated benzenes most protein spots showed enhanced phospho-specific intensity. All identified proteins are well-known phosphoproteins (listed as such in UniProtKB/TrEMBL database) or have predicted phosphorylation sites (in PhosphoSitePlus; www.phosphosite.org).

In general, significance values were lower than those from the DIGE experiment. Only 9 protein spots were found to be regulated following 1,2-DCB exposure, whereas 19 protein spots were detected with modified intensities following cell exposure to CB. The greatest induction of phosphorylation was detected for serpin B6, which, for the higher 1,2-DCB concentration, showed more than 8-fold intensity of the controls. The highest number of modulated spots (13) was observed for the high CB concentration, whereas only 5 spots were detected with significantly altered phospho-specific staining for the high 1,2-DCB concentration. The strongest repression of phosphorylation occurred for a spot identified as tubulin beta chain, showing only one fourth of its original intensity. Seven protein spots displayed altered phosphorylation after treatment to both VOCs: serine-threonine kinase receptor-associated protein (STRAP), translationally-controlled tumor protein (TPT1), serpin B6, heterogeneous nuclear ribonucleoprotein C1/2 (HNRNPC1/2), alpha-enolase, adenosylhomocysteinase and tubulin beta chain (TUBB).

Eight of the proteins, showing altered phospho-specific intensity, were detected earlier in the total proteomic approach using CyDye staining (see DIGE results in Table 5-1). Alpha-enolase and annexin A5 were detected with increased phosphorylation in addition to the increased expression observed in the DIGE approach. In contrast, actin and elongation factor 1A1 showed reduced phosphorylation as well as reduced protein levels (see Table 5-1). Chlorinated benzenes enhanced phosphorylation of proliferating cell nuclear antigen, heterogeneous nuclear ribonucleoprotein C1/2 and cytochrome b5, whereas all three proteins were identified with decreased abundance using the CyDyes. A detailed discussion on the literature view of the phosphorylations of the detected proteins and their derived biological fundamentals is presented in section 5.3.

Furthermore, both spots of transaldolase (TALDO1) showed a more than doubled phosphorylation for the high CB (10^0g/m^3) concentration. The effect was also observed for

the high 1,2-DCB level, although with lower significance. Differential protein phosphorylation measurement with Pro Q Diamond revealed a 1.5 and 2.5-fold HNRNPC1/2 phosphorylation following cell exposure to a low (10^{-4} g/m³) and a high CB (10^0 g/m³) concentration, respectively. In contrast, for 1,2-DCB exposure, no significant phosphorylation modulation was detected. STRAP was the only protein found to be inversely regulated in CB and 1,2-DCB experiments. STRAP showed 2.3-fold increased phosphorylation in cells treated with the high concentration of CB (10^0 g/m³) and, at the lower concentration (10^{-4} g/m³), an increase of 1.7-fold, but with lower significance. In contrast to this, treatment with 1,2-DCB resulted in a reduction in STRAP phosphorylation to a level of 34% ($p < 0.1$). The phospho-specific spot belonging to elongation factor 1a was reduced to only half of its original signal following 1,2-DCB exposure.

Table 5-2 Differentially staining phosphoproteins following 1 h exposure to chlorinated benzenes

Spot	Identification ^{a)}	Accession ^{a)}	Expression level ^{b)}		Expression level ^{b)}	
			Chlorobenzene		1,2-dichlorobenzene	
			10^0 g/m ³	10^{-4} g/m ³	10^0 g/m ³	10^{-4} g/m ³
A (I)	Aldehyde dehydrogenase 3A1	P30838	0.55°			
B	Adenosylhomocysteinase	P23526	0.39°			0.40°
C (II)	Ser.-threon. kinase recept.-assoc. prot.	Q9Y3F4	2.35*		0.38°	
D (III)	Transaldolase	P37837	2.59°			
E (III)	Transaldolase	P37837	2.34*			
F	L-lactate dehydrogenase B chain	P07195	1.79°			
G	L-lactate dehydrogenase B chain	P07195	2.65°			
H	L-lactate dehydrogenase B chain	P07195	3.69°			
I (IV)	Translationally-controlled tumor protein	P13693	1.89°	1.60*		
J (VI)	Proliferating cell nuclear antigen	P12004	1.65°			
K	Serpin B6	P35237		4.83*	8.40°	6.43°
L (II)	Heterog. nuclear ribonucleoprot. C1/C2	P07910	2.47*	1.50°		
M	Aldo-keto red. family 1 member B10	O60218		2.08°		
N	Translationally-controlled tumor protein	P13693		1.47°		
O	Cytochrome b5 type B	O43169		1.85°		
P	Actin, cytoplasmic	P60709				0.37°
Q	Calreticulin	P27797		1.83°		
R	Alpha-enolase	P06733	1.94°		3.57**	
S	Annexin A5	P08758			2.08°	
T	Elongation factor 1-alpha 1	P68104				0.39°
U	Tubulin beta chain	P07437				3.20***
V	Tubulin beta chain	P07437	1.98*			
W (V)	Tubulin beta chain	P07437		0.36°	0.25°	0.30***

a) Uni-Prot Accession from www.uniprot.org

b) Expression level (exposed *versus* control) following exposure to monochlorobenzene or 1,2-dichlorobenzene. ° $p < 0.1$, * $p < 0.05$, ** $p < 0.01$, *** $p < 0.001$. Only significant expression changes are listed. Mass spectrometric identification data are found in the appendix (Table 8-3). Spots labeled as I-VI (see column "Spot") are displayed in Figure 5-6.

5.2.4 Validation of 2-DE Results

Modulation of cell death signaling was a common motif for quite a number of differentially expressed proteins in 2-DE analysis following treatment of A549 cells with chlorinated benzenes. Since caspase 3 is one of the key executioners of apoptotic signaling and since activation of caspase 3 requires the cleavage of the inactive zymogen (35 kDa) into the two active fragments p12 and p17, the level of the large fragment (17 kDa) after cell exposure to CB and 1,2-DCB has been determined. As clearly evident from Figure 5-7, treatment of A549 cells with 10^{-2} g/m³ CB or 10^{-3} g/m³ 1,2-DCB (as used in the DIGE approach) for 24 h induced the activation (cleavage) of caspase 3, resulting in the large active fragment (17 kDa). In contrast, no such band could be observed in control lysates. However, the amount of inactive caspase 3 (35 kDa) was not altered following treatment with chlorinated benzenes.

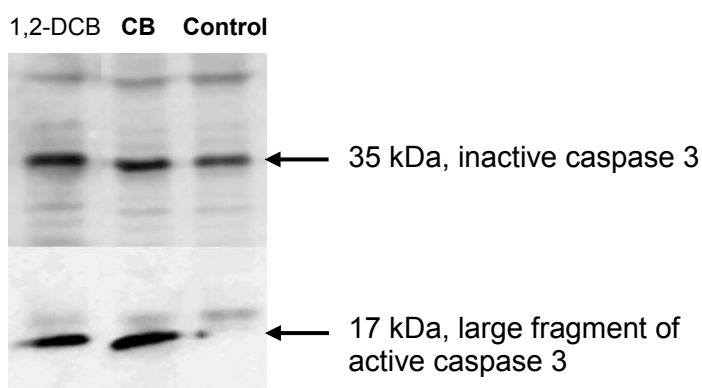


Figure 5-7 Detection of inactive (35 kDa) and cleaved (active, 17 kDa) caspase 3 by Western blotting in lysates of A549 cells treated for 24 h with 10^{-2} g/m³ monochlorobenzene or 10^{-3} g/m³ 1,2-dichlorobenzene. Each lane was loaded with 10 µg of total soluble protein from the samples of the DIGE approach. One out of three experiments is presented.

Within the scope of this study, no further experiments were performed on the validation of oxidative stress events in A549 cells following exposure to chlorinated benzenes. However, formation of reactive oxygen species and activation of oxidative stress marker proteins on transcript- as well as on protein level following cell exposure to monochlorobenzene were investigated and published by the Department of Environmental Immunology of the Helmholtz-Centre of Environmental Research, Leipzig (Feltens *et al.*, 2010). Results from this study, together with the here presented data, will be discussed in section 5.3.

5.3 Discussion

Similar to styrene, chlorinated benzenes are toxic compounds in indoor environments, albeit occurring at lower levels. While inhabitants and especially workers are exposed to them, toxicity at lower concentrations is not well understood. The objective of this study was to investigate and characterize differential expression of proteins, employing an *in vitro* system with short-term exposure of human lung cells to concentrations of lower chlorinated benzenes comparable to those found in work places.

Initially, cell membrane-associated toxicity of monochloro- (CB) as well as 1,2-dichlorobenzene (1,2-DCB) has been assessed in the A549 transwell exposure system. Knowledge of the acute toxic concentration range was the basis for the toxicoproteomic analysis aiming to identify early protein markers for toxicity. Reduction of cell membrane integrity (increased LDH-release) by 65% and 73% was caused in human lung epithelial cells (A549) by a 24 h exposure to 10^2 g/m^3 CB ($\sim 528 \text{ }\mu\text{M}$) and 1,2-DCB ($\sim 319 \text{ }\mu\text{M}$), respectively. In the study on effects of styrene exposure (presented in chapter 4), a lower cell membrane-associated toxicity of only 20% LDH_{total} at 10^2 g/m^3 ($\sim 572 \text{ }\mu\text{M}$) had been found. For styrene, as well as for CB and 1,2-DCB, no membrane damage could be detected when cells were exposed to concentrations lower than 10^1 g/m^3 . These results are in accordance with the ones of Younis *et al.*, who reported a more than 40% elevated LDH release caused by a 1.5 h exposure to 1,2-DCB (approx. $277 \text{ }\mu\text{M}$) in primary rat hepatocytes (Younis *et al.*, 2003). In general, primary cells are more sensitive to toxic compounds than cells derived from a stable cell line. On the other hand, metabolism (concomitant with activation) of most xenobiotics is generally assumed to be more pronounced in liver than in lung cells.

However, in a study by Croute *et al.* a significant growth inhibition (-17%) was observed in A549 cells that were exposed to only $100 \text{ }\mu\text{M}$ CB (comparable to 10^1 g/m^3 in this setup), albeit for the longer period of 4 days. Furthermore, a similar growth inhibition was detected with only $10 \text{ }\mu\text{M}$ of 1,2-DCB (comparable to 10^0 g/m^3 in this setup). Thus, for differential protein expression analysis, VOC concentrations have been applied that were even two orders of magnitude lower, definitely ensuring subtoxic levels. As shown by several researchers (Ait-Aissa *et al.*, 2000; Croute *et al.*, 2002; Croute *et al.*, 2000), *in vitro* toxicity of VOCs increases with the degree of chlorination which was also confirmed by the results that have been obtained with the A549 cells in the experimental setup of this thesis.

In comparison to the 2-DE styrene study (presented in chapter 4), where most proteins with altered expression were oxidative stress markers, chlorinated benzenes predominantly changed the abundance of cell death-associated proteins, in addition to or even possibly as a consequence of induced cellular oxidative stress. Furthermore, in contrast to styrene,

chlorinated benzenes induced a downregulation of most of the identified target proteins, hinting at protein degradation or even induced apoptotic proteolysis.

Chlorinated benzenes affect the abundance of apoptosis-related proteins

Apoptosis is a secondary response to DNA damage, with the biological goal of protecting multicellular organisms against a damaged cell that is controlled by the accumulation and phosphorylation of the tumor suppressor protein p53 via activation of pro-apoptotic genes such as BAK (Wang, 2001) as well as cysteine proteases (caspases) managing programmed protein and DNA degradation finally resulting in cell death. Here, the following pro-apoptotic proteins have been altered in expression in A549 cells exposed to chlorinated benzenes.

A set of proteins, modulated by chlorinated benzenes, was linked directly to caspase 3 activation, the central process of apoptotic cell death. **Heat shock protein beta 1** (HSPB1), which was significantly reduced in expression after styrene, CB and 1,2-DCB exposure, is an important component of caspase 3 activation (Mehlen *et al.*, 1996). Pandey and colleagues demonstrated that HSPB1 associates with caspase 3, but not Apaf-1 or caspase 9, and inhibits cytochrome c-dependent activation of caspase 3 (Pandey *et al.*, 2000). In addition, it has previously been shown that HSPB1 downregulation results in induction of NF-kappa B (NF-κB) activity when monitored via a reporter system and increases the release of the pro-inflammatory cytokine IL-8 in human keratinocytes (Sur *et al.*, 2008). Moreover, HSPB1 siRNA increases basal and tumor necrosis factor alpha-mediated activation of NF-κB pathway in HeLa cells (Park *et al.*, 2003). In accordance with the results of this thesis, the activation of the NF-κB pathway was reported for styrene- and CB-treated A549 cells (Roder-Stolinski *et al.*, 2008a; Roder-Stolinski *et al.*, 2008b).

Casas and colleagues provided evidence that **seryl-tRNA synthetase receptor-associated protein** (SARS) is a substrate of caspase 3 *in vitro* (Casas *et al.*, 2001). Thus, the lowered expression of SARS in response to 1,2-DCB may be caused through cleavage by activated caspase 3.

Peroxiredoxin 3 was downregulated during exposure to 1,2-DCB. Being a negative regulator of apoptosis, the protein becomes oxidized when apoptosis is starting, occurring within the same timeframe as increased mitochondrial oxidant production, caspase activation and cytochrome c release. It precedes other major apoptotic events including mitochondrial permeability transition and phosphatidylserine exposure, glutathione depletion, global thiol protein oxidation and protein carbonylation (Cox *et al.*, 2008).

Heterogeneous nuclear ribonucleoprotein C1/2 (HNRNPC1/2) is one of the well-known apoptotic markers detected in this study. As described above, HNRNPC1/2 showed a strong downregulation for CB and 1,2-DCB relative to its expression in control cells in the 2D DIGE analysis. Holcik and colleagues suggested that the proteolytic cleavage of HNRNPC1

and -C2 at the onset of apoptosis could be the reason for the attenuation of the synthesis of XIAP (X-linked inhibitor of apoptosis). XIAP is the most powerful and ubiquitous intrinsic inhibitor of apoptosis by virtue of its ability to block caspase activation. The researchers found out that cellular HNRNPC1 and -C2 levels correlate positively with the activity of the internal ribosome entry site (IRES) of XIAP mRNA *in vivo*. They observed that reduced levels of HNRNPC were followed by a reduction in XIAP IRES translation and finally provided evidence that HNRNPC1/2 bind to the XIAP IRES element, thus modulating XIAP translation (Holcik *et al.*, 2003).

Moreover, quantification of protein phosphorylation with Pro Q Diamond revealed a significantly enhanced phosphorylation of HNRNPC1/2 following cell exposure to low and high CB concentrations. Recently, Christian *et al.* identified a previously unknown regulatory cis-element within the coding region of p53 mRNA, which interacts with HNRNPC1/C2, and pointed out that this interaction is critical for the activation of p53 finally leading to apoptosis. They showed that HNRNPC1/2 bind strongly and specifically, in a phosphorylation-dependent manner, at this site in response to DNA damage and inhibition of transcription (Christian *et al.*, 2008). Overall, 14 possible HNRNPC1/2 phosphorylation sites (serine) are listed in the UniProtKB/TrEMBL database. Phosphorylation on Ser-260 and Ser-299 occurs typically in resting cells while phosphorylation on Ser-253 and on one serine residue in the poly-Ser stretch at position 238 is a known response to hydrogen peroxide stress (Stone *et al.*, 2003).

As mentioned when discussing styrene effects, **voltage-dependent anion-selective channel protein 2** (VDAC2) is a prominent indicator of apoptotic signaling. The protein showed a significantly decreased expression when exposed to both the chlorinated compounds. This mitochondrial outer-membrane protein, that was also limited in expression when cells were exposed to a wide range of styrene concentrations, interacts specifically with the inactive conformer of the multi-domain pro-apoptotic molecule BAK. Reduced levels of VDAC2 make cells more susceptible to apoptotic death (Cheng *et al.*, 2003). A linkage between oxidative stress, VDAC and **actin** depolymerization was proposed by Gourlay *et al.*, who postulated that the coupling of ROS release to actin function could be mediated via regulation of opening and closing of the VDACs, mitochondrial membrane pores regulating the release of pro-apoptotic factors such as cytochrome C (Gourlay *et al.*, 2005). As reported before in the context of styrene treatment, A549 cells showed lower levels as well as diminished phosphorylation of cytosolic actin. For actin, a high number of phosphorylation sites have been described. Papakonstanti *et al.* reported actin phosphorylation by PAK1, resulting in the dissolution of stress fibers and redistribution of microfilaments providing evidence that PAK1 can regulate the actin-myosin cytoskeleton by phosphorylating specific substrates, thereby modulating cell contractility (Papakonstanti *et al.*, 2002; Sanders *et al.*,

1999). Usually, during apoptosis, the major cytoskeletal filaments, microtubules, cytokeratin and actin, are degraded. A link between actin depolymerization and DNA degradation has recently been suggested. Although actin may be resistant to cleavage in some *in vivo* models, targeting of actin and other intermediate filaments was found to be responsible in part for the collapse of cell shape during the execution phase of apoptosis. In detail, degradation of actin filaments is suggested to disrupt required mechanical tension and lead to signals that may facilitate cell detachment (White *et al.*, 2001).

An additional pivotal regulator of the actin cytoskeleton in eukaryotes, being induced by 1,2-DCB, is **cofilin**. It was recently demonstrated that mitochondrial translocation of cofilin is an early step in the induction of apoptosis, and that overexpression of constitutively active cofilin can induce apoptosis. The protein promotes filament severing and depolymerization, facilitating the breakdown of existing filaments. Cofilin is also regulated by interaction with **WD-repeat containing protein 1** (WDR1), the mammalian homolog of actin interacting protein 1 (Aip1). Here, WDR1 expression was significantly reduced by CB and 1,2. Investigations of Kile *et al.* indicated that WDR1 is linked to apoptotic actin depolymerization process by binding a cofilin/actin complex (Kile *et al.*, 2007). However, only little information is available on WDR1 function in mammalian cells.

Another member of the WD-40 family of proteins, **guanine nucleotide-binding protein subunit beta-2** (RACK1), a 36-kDa homologue of the β subunit of G-proteins, shows specific binding to the active form of protein kinase C β isoforms and interacts with several other important signaling proteins, e.g. proteins from the Src kinase family (Mourtada-Maarabouni *et al.*, 2005). Conversely, overexpression of RACK1 in T cell lines resulted in resistance to dexamethasone- and ultraviolet-induced apoptosis. Downregulation of RACK1, as observed following 1,2-DCB exposure, abolishes resistance of the transfected cells to apoptosis. From these findings, it was suggested that RACK1 plays an important role in the intracellular signaling pathways that lead to apoptosis (Mourtada-Maarabouni *et al.*, 2005). In mammalian cells, RACK1 functions as an adaptor to favor PKC-mediated phosphorylation and subsequent activation of c-Jun NH₂-terminal kinase mitogen-activated protein kinase. Intriguingly, RACK1 is also a structural component of the 40S ribosomal subunit, and recent data suggest that it might be involved in the control of translation (Nunez *et al.*, 2009).

Furthermore, **serine-threonine kinase receptor-associated protein** (STRAP) showed a significantly increased phosphorylation in cells treated with a high concentration of CB. Contrarily, for the high concentration of 1,2-DCB a reduction in phosphorylation was detected. STRAP was recently identified as an interacting partner of apoptosis signal-regulating kinase 1 (ASK1). ASK1 phosphorylates STRAP at Thr₁₇₅ and Ser₁₇₉, suggesting a potential role for STRAP phosphorylation in ASK1-mediated regulation of apoptosis (Jung *et*

al., 2010). Furthermore, STRAP interacts with p53 via the pro-apoptotic protein NM23-H1, thereby positively regulating p53-induced apoptosis and cell cycle arrest (Jung *et al.*, 2007).

Further signs of stimulated pro-apoptotic events are provided by the observed strong induction of **nucleophosmin** (NPM) and reduced levels of **prohibitin** (PHB). NPM is a multifunctional protein that plays important roles in regulating cell proliferation and apoptosis. Induction of NPM protein expression was described in the human lung cell line H460 treated with different apoptosis-inducing agents (Lee *et al.*, 2005). In contrast, Dhar and colleagues observed a nucleophosmin-mediated suppression of apoptosis in skin epithelial cells (Dhar *et al.*, 2009). Fusaro and co-workers presented PHB as a potential tumor suppressor protein repressing the activity of the E2F transcription factors. Especially E2F1 is able to provoke apoptotic cell death by induction of pro-apoptotic genes, including Apaf-1 and p73. More specifically, PHB was found to bind to the pocket domain of Rb family members and contact E2F family members through the marked box domain. Prohibitin has been identified as inhibitor of apoptosis in at least two different scenarios: in camptothecin-induced as well as growth factor withdrawal-induced apoptotic signaling (Fusaro *et al.*, 2003).

Peroxiredoxin 6 expression decreased following CB exposure. In general; this is the peroxiredoxin isoform that is expressed at the highest level and its expression in lung epithelia exceeds that for other organs. The enzyme is highly inducible by oxidative stress in the lung, consistent with its predominant role in antioxidant defense (Schremmer *et al.*, 2007). Epithelial cells with diminished peroxiredoxin 6 expression showed higher ROS levels and were prone to apoptosis (Kubo *et al.*, 2010).

The programmed cell death 6-interacting protein (PDCD6IP protein), also known as ALG-2/AIP-complex, is supposed to have a modulating role at the interface between cell proliferation and cell death (Krebs *et al.*, 2000). The protein was downregulated when cells were exposed to CB, a result that is in contrast to the induction that was observed after styrene exposure. Studies performed with mouse cells showed that overexpression of PDCD6IP protein may block apoptosis (Mahul-Mellier *et al.*, 2008).

Furthermore, two spots, identified as **elongation factor 1 alpha** (EEF1A1) displayed reduced staining intensities in the presence of both chlorinated compounds. In addition, following 1,2-DCB exposure, the protein was detected with only half of the signal using the phospho-specific fluorescence dye when compared to control lysates. In accordance with these observations, several authors reported that EEF1A1 shows reduced expression as well as phosphorylation while cells undergo senescence (Byun *et al.*, 2009; Lamberti *et al.*, 2007; Panasyuk *et al.*, 2008). However, following CB treatment, in addition to the repressed spots of EEF1A1, two EEF1A1 spots have been detected in the acidic region (in contrast to the database prediction) of the DIGE gel with enhanced expression. Posttranslational modifications, e.g. phosphorylation (4 phosphotyrosine residues listed on UniProtKB/TrEMBL

database), could possibly explain the observed *pI* shift. As discussed in more detail in section 4.3, Zhu *et al.* reported that large *pI* shifts (up to one pH unit) were observed for proteins with an expected *pI* above 7.0, whereas little change (0.2 pH units per phosphorylation) was noticed for proteins with a *pI* of 5.0 (Zhu *et al.*, 2005). However, it is not clear if these results signify an up- or downregulation of the protein or simply a shift towards a heavily modified version of the protein, and how these modifications might relate to apoptotic signaling remains unclear.

60 S ribosomal protein L5 (RPL5), upregulated by 1,2-DCB and styrene, was recently identified as a substrate of death-associated protein kinase, a serine/threonine kinase whose contribution to cell death is well established (Bialik *et al.*, 2008). However, it is not clear why RPL5 expression was increased or what impact this increase might have in the context of apoptotic signaling.

Lee *et al.* investigated the protective action of cytosolic **isocitrate dehydrogenase 1** (IDH1) against cytotoxicity induced by oxidative stress. They noticed a significantly higher ratio of oxidized glutathione to total glutathione in cells underexpressing IDH1 and concluded an essential role of IDH1 for efficient recycling of glutathione (Lee *et al.*, 2002), which in turn is required for the metabolism of xenobiotics such as VOCs. Recent results of Lee *et al.* indicate that IDH1, in addition to the involvement in oxidative stress signaling, may play an important role in regulating apoptosis induced by different external signals. The co-workers reported that silencing of NADP(+)-dependent IDH1 expression (similar to the observed repression by CB) enhances apoptosis (Lee *et al.*, 2009). Concomitant to the downregulation of IDH1, CB affected the expression of the mitochondrial NAD(+)-dependent **isocitrate dehydrogenase 3A**. Further results suggest that reduced levels of mitochondrial isocitrate dehydrogenase sensitize cells to apoptotic cell death, presumably through the perturbation of the cellular redox status (Lee *et al.*, 2007).

The much lower expression of **proliferating cell nuclear antigen** (PCNA), indicating a reduced cell proliferation compared to untreated cells, may be explained by cells that are stressed by the presence of VOCs and undergo cell death (Bardales *et al.*, 1996). Recently, Tuck *et al.* observed airway epithelial cell apoptosis in the acute injury phase after exposure of mice to Cl₂. In the following repair phase, increased airway epithelial cell proliferation, measurable by increasing levels of immunoreactive proliferating cell nuclear antigen (PCNA), was recognized (Tuck *et al.*, 2008). Thus, in this setup, A549 cells do not show stimulated tissue repair as observed for hepatic cells of F344 rats when exposed to 1,2-DCB (Kulkarni *et al.*, 1996).

A549 exposure to chlorinated benzenes also caused anti-apoptotic signaling, although to a smaller extent. Examples thereof will be discussed in the following paragraphs.

Phosphatidylethanolamine-binding protein 1, a novel protein designated Raf-1 kinase inhibitor protein (RKIP), has been detected with reduced abundance in 1,2-DCB exposed cells. It negatively modulates mitogen-activated protein kinase cell signaling and is considered to play a pivotal role in regulating apoptosis. Overexpression of RKIP sensitizes tumor cells to chemotherapeutic drug-induced apoptosis (Altirriba *et al.*, 2009; Odabaei *et al.*, 2004). Loss of RKIP reduced the apoptotic response to drugs and favored proliferation (Chatterjee *et al.*, 2004; Woods Ignatoski *et al.*, 2008).

Annexin A1, induced by 1,2-DCB and styrene, is known for its anti-inflammatory function as well as its involvement in the ERK repression pathway and apoptosis (Debret *et al.*, 2003). The protein was also proposed as a stress response protein in A549 cells by Rhee *et al.* (Rhee *et al.*, 2000). However, recent findings reveal that, in addition, annexin A1 is an inducible endogenous inhibitor of NF-kappa B in human cancer cells and in mice (Zhang *et al.*, 2010b).

Finally, expression of **elongation factor 2** (EEF2) was induced following exposure to all three volatile compounds. This protein is considered as a powerful target of cancer therapy because inhibiting EEF2 causes the rapid arrest of protein synthesis and induces apoptosis (Wullner *et al.*, 2008).

Thus, for the chosen exposure time and concentrations, cells may have entered the early stages of the apoptotic pathway, even though no cell toxicity was observed. The results of the performed proteome analysis hint to a combination of a number of pro-apoptotic signals as well as cellular anti-apoptotic responses. Together with the presented caspase 3 activation (cleavage), these data provide evidence that chlorinated benzenes modulate cell death signaling, including caspase 3-mediated apoptosis, which is consistent with literature results. *In vitro* studies with metabolites of chlorinated benzenes (see section 5.1.2), in detail 4-chlorophenol, 2,4-dichlorophenol, 2,3,4-trichlorophenol induced apoptosis in L929 fibroblast cells (Chen *et al.*, 2004). In another investigation using human lymphocytes, caspase 3 expression was induced by several chlorinated catechols and phenols including the 1,2-DCB metabolite 4,5 dichlorocatechol in the range of 1-50 ppm (Michalowicz *et al.*, 2009). Moreover, human promyelocytic leukemia HL-60 cells have been analyzed for their protein expression in response to several aromatic VOCs (benzene, toluene, o-xylene, ethylbenzene, trichloroethylene and dichloromethane) using a whole human genome oligonucleotide microarray. Important apoptosis-related genes have been identified to be differentially expressed (Sarma *et al.*, 2010). Decreased cell viability, impaired DNA integrity and stress-induced apoptosis in A549 cells has been reported for aliphatic halogenated volatile compounds like halothane (Topouzová-Hristova *et al.*, 2007). Intensive expression of anti-apoptotic Bcl-2 protein during treatment has been demonstrated. The most prominent negative effect was the destruction of the lamellar bodies, the main storage organelles of

pulmonary surfactant, substantial for the lung physiology. Halothane applied at clinically relevant concentrations exerted genotoxic and cytotoxic effects on the alveolar cells *in vitro*, most likely as a consequence of stress-induced apoptosis, thus modulating the respiratory function.

However, it should be noted that most tumor cells such as A549 have adopted various mechanisms that interfere with the apoptotic signaling pathways and promote constitutive activation of cellular proliferation and survival pathways (Odabaei *et al.*, 2004).

Exposure to chlorinated benzenes modulates the cellular redox balance

Intriguingly, several redox-sensitive proteins susceptible to CB or 1,2-DCB exposure have been identified, some of which were also found to be regulated by styrene. Studies to explain the mechanism of toxicity of benzene and halogenated benzenes argue that the oxidative attack by cytochrome P450 results in the formation of electrophilic intermediates that are able to react with sulfhydryl groups, which concurrently leads to the depletion of reduced glutathione, which could then favor a pro-oxidant environment (Croute *et al.*, 2000). Thus, it has been suggested that exposure to VOCs such as BTEX or chlorinated benzenes generates oxidative stress.

Investigations of Burczynski *et al.* on exposure of HepG2 cells to a panel of aromatic hydrocarbons yielded a significant induction of the synthesis of **aldo-keto reductase 1C1/2** (AKR1C1/2) (Burczynski *et al.*, 1999). HepG2 exposure to a battery of ARE (anti-oxidant response element) inducers e.g. butylhydroquinone, 2,3-dimethoxynaphthalene-1,4-dione caused a 10-fold AKR1C1 expression at the RNA, protein and functional level (Penning *et al.*, 2007). Similarly, in the experiments of this thesis, an increase in AKR1C2, also called trans-1,2-dihydrobenzene-1,2-diol dehydrogenase, abundance has been detected in 1,2-DCB-treated cells. In detail, dihydrodiol dehydrogenase isoforms 1C1/2 oxidize aromatic trans-dihydrodiols to reactive and redox-active *ortho*-quinones which in turn cause an increased formation of reactive oxygen species (ROS) via a redox-cycling mechanism. However, human AKR1C subfamily members were also found to be induced by ROS (Burczynski *et al.*, 1999; Palackal *et al.*, 2002; Penning *et al.*, 2007) as reported also for **aldose reductase** (H₂O₂-inducible). Here, a higher abundance of aldose reductase, an enzyme which catalyzes the NADPH-dependent reduction of a wide variety of carbonyl-containing compounds to the corresponding alcohols (Martin *et al.*, 2006), could be detected when cells were exposed to styrene or 1,2-DCB, thereby pointing to an increased oxidative stress-related cellular reduction activity. Aldose reductase upregulation was supposed to be a risk factor in pulmonary disease (Jiang *et al.*, 2005).

One of the most impressive effects of chlorinated benzenes is illustrated by the altered expression of **peroxiredoxin 1** isoforms. From the five spots, identified as peroxiredoxin 1 in the A549 proteome map, two spots (ID185, ID264) were significantly reduced in expression

to a remaining level of one fourth of control cells by CB. Furthermore, ID186, the peroxiredoxin 1 spot with the most basic isoelectric point, was induced by more than a factor of 2 (compared to control cells) by both chlorinated benzenes after an exposure period of 24 h. This observation was quite unexpected.

In general, peroxiredoxin 1 is rapidly (for A549 within 10 min) inactivated upon oxidative stress by overoxidation of Cys₅₂ (active site) to Cys₅₂-SOH, Cys₅₂-SO₂H and Cys₅₂-SO₃H resulting in a shift to a more acidic pH (in 2-DE). This effect, however, is in contrast to the one observed for CB and 1,2-DCB, which implies a shift towards a basic pH. Cys₅₂-SOH immediately reacts with Cys₁₇₃ of the other subunit to form an intermolecular disulfide, leading to impaired peroxidase activity. Woo *et al.* studied peroxiredoxin 1 expression during H₂O₂-induced ROS stress and the following recovery phase in a set of cellular models (Woo *et al.*, 2003). Fast and effective regeneration of peroxiredoxin 1 was apparent in all three human cell lines. For A549 cells, the “acidic” shift was observed within the first 10 min of H₂O₂ exposure, but after 2-4 h of recovery, no more difference in abundance of peroxiredoxin 1 isoforms compared to controls was evident. Furthermore and in line with the here presented observations, the appearance of an additional peroxiredoxin spot was detected in the basic region of the 2D gel. Thus, treatment of A549 cells with the used concentrations of CB or 1,2-DCB may initially have caused oxidative stress, followed by a recovery phase which is marked by an enhanced abundance of reduced peroxiredoxin 1 isoform (accounting for the spot seen in the basic pH range) and a concomitant depletion of less oxidized isoforms, compared to control cells.

The observed increases in expression of **biliverdin reductase A**, **Chloride intracellular channel protein 1** as well as of enzymes of the pentose phosphate pathway (PPP) support the hypothesis of augmented cellular ROS formation. Recovery of reduced glutathione from its oxidized form is dependent on NADPH mainly produced by the pentose phosphate pathway (Banki *et al.*, 1996; Rho *et al.*, 2005). **6-phosphogluconate dehydrogenase** (PGD), being involved in NADPH synthesis (see Figure 4-13), was significantly upregulated by a factor of 2 when exposed to the higher concentrations (1-10 g/m³) of styrene, whereas no regulation was seen in response to lower concentrations. In contrast, in cells exposed to only 10⁻³ g/m³ of 1,2-DCB, the spot was upregulated compared to control cells. Kozar *et al.* observed stimulation of the PPP, including activation of PGD, during the recovery period from acute, oxidant-mediated lung injury and concluded that both the PPP and the GSH system contribute to the recovery process (Kozar *et al.*, 2000).

Formation of reactive oxygen species and activation of oxidative stress proteins on transcript as well as on protein level following A549 cell exposure to CB were investigated and published by members of the Department of Environmental Immunology of the Helmholtz-Centre for Environmental Research Leipzig (Feltens *et al.*, 2010; Roder-Stolinski

et al., 2008a). They found that mRNA expression of heme oxygenase 1, glutathione S-transferase P, superoxide dismutase 1, prostaglandin-endoperoxide synthase 2 (PTGS2) and dual specificity phosphatase 1 were elevated in A549 cells in the presence of CB. Likewise, intracellular reactive oxygen species were found to be increased in response to CB exposure, as has been demonstrated for styrene above (Figure 4-9). In the presence of antioxidants, CB-induced upregulation of marker proteins and release of the inflammatory mediator MCP-1 were suppressed. Thus, an oxidative-stress response observed in these investigations is in accordance with the proteomics-based results presented here.

Finally, a relatively high number (15) of the identified proteins that have been differentially regulated in response to chlorinated benzenes are connected to cellular metabolism such as lactate dehydrogenase, alpha-enolase or glyceraldehyde-3-phosphate dehydrogenase. However, not much is known about the functional consequences of these changes or the molecular mechanism connecting these two areas (Kondoh *et al.*, 2007; Lelli *et al.*, 2005). Based on numerous studies demonstrating that glucose metabolism is implicated in cell death and survival, it has been speculated that these two crucial processes – glucose metabolism and apoptosis – are linked. There is further need to consider the non-enzymatic functions of enzymes in proteomic studies of cells and tissues (Kim *et al.*, 2005).

As an example, decreased expression of **glycogen phosphorylase** (as reported above for CB-treated A549 cells) was also observed by Lelli *et al.* when Wistar rats were exposed to the porphyrinogenic drug 2-allyl-2-isopropylacetamide. In parallel, cytosolic protein carbonyl content and lipid peroxidation increased significantly. Based on these results, the researchers speculated that the alterations observed in glucose metabolism enzymes might be related to the damage caused by ROS on their enzymatic protein structures (Lelli *et al.*, 2005).

Further, it has been suggested that pro-oxidant species such as H₂O₂ and OH· lead to sufficient alterations in protein structure and/or function to trigger heat shock protein induction (Polla *et al.*, 1996). Heat shock proteins such as HSP beta 1 that mediates the inhibition of cytochrome c-dependent activation of caspase 3, can prevent apoptotic cell death (Pandey *et al.*, 2000; Whitlock *et al.*, 2005). In contrast to that finding, impaired protein quality control function has been observed here. Nearly all differentially expressed proteasomal, ribosomal proteins as well as chaperones including HSPB1 showed decreased abundance hinting to apoptotic degradation.

In conclusion, significant changes in abundance and phosphorylation of total soluble proteins of A549 cells have been found detected in response to subtoxic concentrations of CB and 1,2-DCB. For most of the proteins, main cellular functions could be assigned. The results indicate two main pathways to be affected in the presence of chlorinated benzenes,

cell death signaling and oxidative stress response. Induction of apoptosis (cleavage of caspase 3) has been confirmed for both treatments.

6 *Common Mechanisms of Aromatic VOCs on Cellular Protein Expression*

The overall objective of this thesis is the characterization of molecular effects of aromatic VOCs in a human lung cell model with a focus on the modulation of the cellular proteome at VOC concentrations comparable to exposure scenarios below current occupational limits in order to provide further comprehension of VOC-caused adverse health effects. After discussing detailed effects as provided in the sections before, common mechanisms (regulated proteins) of A549 cells in response to the applied VOCs will be discussed in the following paragraphs.

Three aromatic VOCs, styrene, monochlorobenzene (CB) and 1,2-dichlorobenzene (1,2-DCB) have been investigated for their potential to alter protein expression in A549 cells employing proteomic techniques. The effects of styrene, CB and 1,2-DCB have been studied in response to 0.23-2,300 ppm, 2.2 ppm and 0.17 ppm, respectively. For all three compounds differential protein expression has been observed in A549 cells at concentrations that are below the ones that yielded significant cell toxicity and even below current German occupational limits (AGW) for CB, 1,2-DCB (each 10 ppm) and styrene (20 ppm).

As mentioned before, 4.6-6.9% of all quantified protein spots showed differential expression ($p < 0.05$) following cell exposure to styrene, CB or 1,2-DCB. This is in accordance with the general assumption that not more than 10% of all protein species will be significantly altered in response to subtoxic treatments.

Identified differentially expressed protein species of the three experiments have been compared, thus indicating similar and dissimilar regulation. A general overview is given in a Venn diagram (Figure 6-1). Detailed information on protein species that were affected by more than one VOC are listed in Table 6-1. In total, 174 protein spots have been detected with altered abundance ($p < 0.1$) for all treatments. Regarding single compounds, styrene caused 46 changes in expression, while CB and 1,2-DCB were responsible for 37 and 35 effects, respectively, that were not observed following treatment with any other VOC.

The greatest similarity was observed for CB and 1,2-DCB treatment. In addition to the three spots that were altered in response to all three VOCs, 31 protein spots showed similar alteration in response to both chlorinated compounds while effects induced by styrene and CB correlated the least (only 4 protein spots). Thus, 26.5% of all spots that were affected by either CB or 1,2-DCB were influenced by both compounds in the same way. These similar cellular reactions in response to both chlorinated compounds may be explained by their structural chemical similarity and cellular bioactivation. However, it should be noted, that exposure to a 10-fold lower 1,2-DCB concentration caused an about 16% higher total

number of altered spots (87) compared to CB-treatment (75) when considering all spots including the ones that are regulated for more than one VOC. This finding is in good agreement with the reported increasing toxicity of aromatic VOCs that depends upon the degree of chlorination (Ait-Aissa *et al.*, 2000; Croute *et al.*, 2002; Croute *et al.*, 2000).

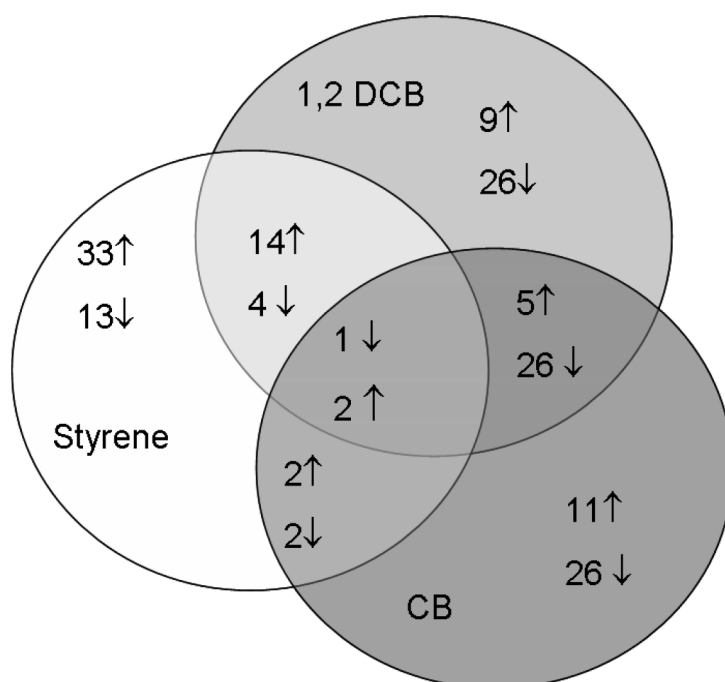


Figure 6-1 Venn diagram of differential protein expression following exposure to styrene, monochlorobenzene (CB) and 1,2-dichlorobenzene (1,2-DCB). Areas of overlap of 2 or more VOCs display the observed number of protein spots with similar modulation (direction) whereas in areas of each of the three compounds only the protein spots are included that were different in their expression exclusively in the cells exposed to this compound. Arrows indicate up- or downregulation in response to the treatment. Differential expression data were included in the analysis if relative expression compared to control was either higher than 1.5 or lower than 0.67 (styrene data set) and higher than 1.3 or lower than 0.77 (DIGE CB, 1,2-DCB data set) and $p < 0.1$. Included expression data is listed in Table 4-1 (styrene) and Table 5-1 (CB and 1,2-DCB). Differential expression of one spot in response to different styrene concentrations was included in the analysis as one effect. When more than one styrene concentration resulted in modulated expression of the same protein species the direction (up- or downregulation) that was induced by most of the concentrations was displayed in the diagram. Three protein spots showed significant regulation in the same direction for all three compounds: VDAC2 (↓), peroxiredoxin 1 (↑) and elongation factor 2 (↑).

As mentioned before and becoming apparent from the Venn-diagram and the corresponding Table 6-1, chlorinated benzenes induced predominantly (>70% of all protein species) a downregulation of most of the identified target proteins hinting at protein degradation or even induced apoptotic proteolysis. The set of protein species altered by CB and 1,2-DCB includes important cell death-associated proteins such as heterogeneous nuclear ribonucleoproteins C1/C2, voltage dependent anion-selective channel protein 2, prohibitin, mitochondrial isocitrate dehydrogenase 3A and WD-repeat containing protein 1 (for detailed information on protein function see section 5.3).

Strikingly, styrene and 1,2-DCB treatment shared a number (18) of alterations in protein copy number. In most cases, oxidative stress-related proteins such as biliverdin reductase A, aldose reductase and 6-phosphogluconate dehydrogenase were induced by 1,2-DCB and styrene. In addition, both compounds in concert modulated the expression of famous cell death-related proteins such as heat-shock protein beta and voltage dependent anion-selective channel protein 2. The similarity (15.6%) in the cellular response to both compounds was quite unexpected since no such effect was observed for CB and styrene. Therefore, the results may hint to a so far unknown similar toxic effect of styrene and 1,2-DCB, despite their significant differences in the chemical structure.

Based on the observed similarities in response to 1,2-DCB and styrene as well as the similarities between CB- and 1,2-DCB-regulated proteins one hypothesis could be drawn. It may be possible, that the bioactivation of 1,2-DCB causes oxidative stress to a much greater extent than the bioactivation of CB (at the same exposure concentration) does. Consequently, the resulting oxidative environment might be rather comparable to the one provoked by styrene treatment yielding the observed common molecular response mechanism. Furthermore, in contrast to styrene that seems to initiate an early apoptotic process as a result of increased cellular oxidative stress CB may induce apoptosis predominantly via a different mechanism (that may not be oxidatively triggered). It seems likely that the strong apoptotic process that is induced in response to an even 10-fold lower concentration of 1,2-DCB might be due to a cumulative effect of both pro-apoptotic signals, the oxidative and the non-oxidative one.

Finally, not more than three protein spots showed significant regulation in the same direction for all three volatile compounds: voltage-dependent anion-selective channel protein 2 (↓), peroxiredoxin 1 (↑) and elongation factor 2 (↑). They are important molecular targets in stress- and cell death-related signaling pathways (see sections 4.3 and 5.3). The small number of common alterations supports the hypothesis of two different sets of differentially expressed proteins, one shared by styrene/1,2-DCB treatment and one shared by CB/1,2-DCB treatment. However, since the response to each single compound altered about 40 protein species that were not affected by any other compound, in addition to the common response, each aromatic compound seems to interact with a compound-specific set of proteins. Most probably, VOC-specific alterations are due to the corresponding different physicochemical properties such as the vapor pressure and the octanol/water partition coefficient (see Table 3-1).

Table 6-1 Common effects of styrene, monochlorobenzene (CB) and 1,2-dichlorobenzene (1,2-DCB) exposure on protein expression of A549 cells.

Protein altered in response to VOC	Number of Spots	Regulation
CB-, 1,2-DCB- and styrene-treatment		
Voltage-depend. anion-sel. channel prot. 2	1	↓
Peroxiredoxin-1	1	↑
Elongation factor 2	1	↑
CB- and 1,2-DCB-treatment		
Elongation factor 2	5	↑
60S ribosomal protein L12	1	↓
Carbamoylphosphate synthetase I	4	↓
Electron transfer flavoprotein subunit alpha	1	↓
Elongation factor 1-alpha 1	2	↓
Heterog. nuclear ribonucleoprotein H	1	↓
Isocitrate dehydrogenase 3A1	1	↓
Heterog. nuclear ribonucleoproteins C1/C2	6	↓
Neutral alpha-glucosidase AB	5	↓
Prohibitin	1	↓
Reticulocalbin 1 precursor	1	↓
WD repeat-containing protein 1	3	↓
1,2-DCB- and styrene-treatment		
60S ribosomal protein L5	1	↑
6-phosphogluconate dehydrogenase	1	↑
Aldose reductase	1	↑
Alpha-enolase	3	↑
Annexin A1	1	↑
Annexin A2	1	↑
Annexin A4	2	↑
Annexin A5	1	↑
Biliverdin reductase A	1	↑
Chloride intracellular channel protein 1	1	↑
Phosphoglycerate mutase 1	1	↑
ATP synthase subunit alpha, mitochondrial	1	↓
Actin, cytoplasmic 2	1	↓
Heat shock protein beta-1	1	↓
Voltage-depend. anion-sel. channel protein 1	1	↓
CB- and styrene-treatment		
Glycogen phosphorylase	2	↓
Vimentin	2	↑

Arrows indicate up- or downregulation in response to the treatment. Differential expression data were included in the analysis if relative expression compared to control was either higher than 1.5 or lower than 0.67 (styrene data set) or higher than 1.3/lower than 0.67 (DIGE CB, 1,2-DCB data set) and $p < 0.1$. Included expression data is listed in Table 4-1 (styrene) and Table 5-1 (CB and 1,2-DCB).

In a second step, protein species that had been identified to be affected by the tested VOCs have been analyzed for protein-protein interactions using the STRING (Search Tool for the Retrieval of Interacting Genes/Proteins) database and web resource. STRING includes both, physical and functional interactions. It weights and integrates information from numerous sources including experimental repositories and computational prediction methods. Thus it acts as a meta-database that maps all interaction evidence onto a common set of genomes and proteins and provides the most comprehensive view on protein-protein interactions currently available (Jensen *et al.*, 2009).

Protein-protein interactions have been predicted for differentially expressed and differentially phosphorylated proteins for each VOC-treatment. The corresponding images are shown in the appendix (Figure 8-3 (styrene), Figure 8-4 (CB), Figure 8-5 (1,2-DCB)). When comparing these three images, it is obvious that there are much more different proteins in the network of the styrene treatment compared to the other images. That greater number of affected proteins may be explained by the broad range of styrene concentrations that has been used in the 2D experiments in contrast to only one single concentration used in the experiments with the chlorinated compounds. Moreover, in most cases, treatment with CB or 1,2-DCB affected not only single spots but spot chains of one protein (up to 6 spots differing in posttranslational modifications), resulting in a relatively small number of altered proteins. However, 1,2-DCB treatment yielded the greatest number of differential spots (as mentioned before).

Figure 6-2 presents a cumulative image of predicted protein-protein interactions including all protein species and phosphorylations that were detected following exposure to any of the three VOC-treatments. Predicted interactions are expressed as lines colored according to the source of information (see figure legend). The image shows a large network of protein connections albeit the settings of STRING have been restricted to the usage of direct protein-protein interactions based on experimental data (see color code of the connecting lines in the figures expressing the data source). Two proteins, elongation factor 1-alpha 1 (EEF1A1) and beta-actin (ACTB), are connected with each other in the middle of the network and develop two “signaling subnetworks”, one to each side of the image. The larger “beta actin-subnetwork” is composed of at least seven main axes of interacting proteins that arise all from ACTB. The “elongation factor 1-alpha 1 subnetwork” groups the interacting proteins predominantly around its central protein, the elongation factor 2 (EEF2). This second subnetwork shows much more cross-links between the signaling pathways making it challenging to identify distinct axes.

Both “signaling subnetworks” are also found in the STRING predictions for the styrene- and 1,2-DCB-treatment (Figure 8-3 and Figure 8-5) even though with a differing

number of departing signaling axes. In contrast, the CB-network does include the EEF1A1/EEF2 subnetwork but not the one arising from of beta-actin.

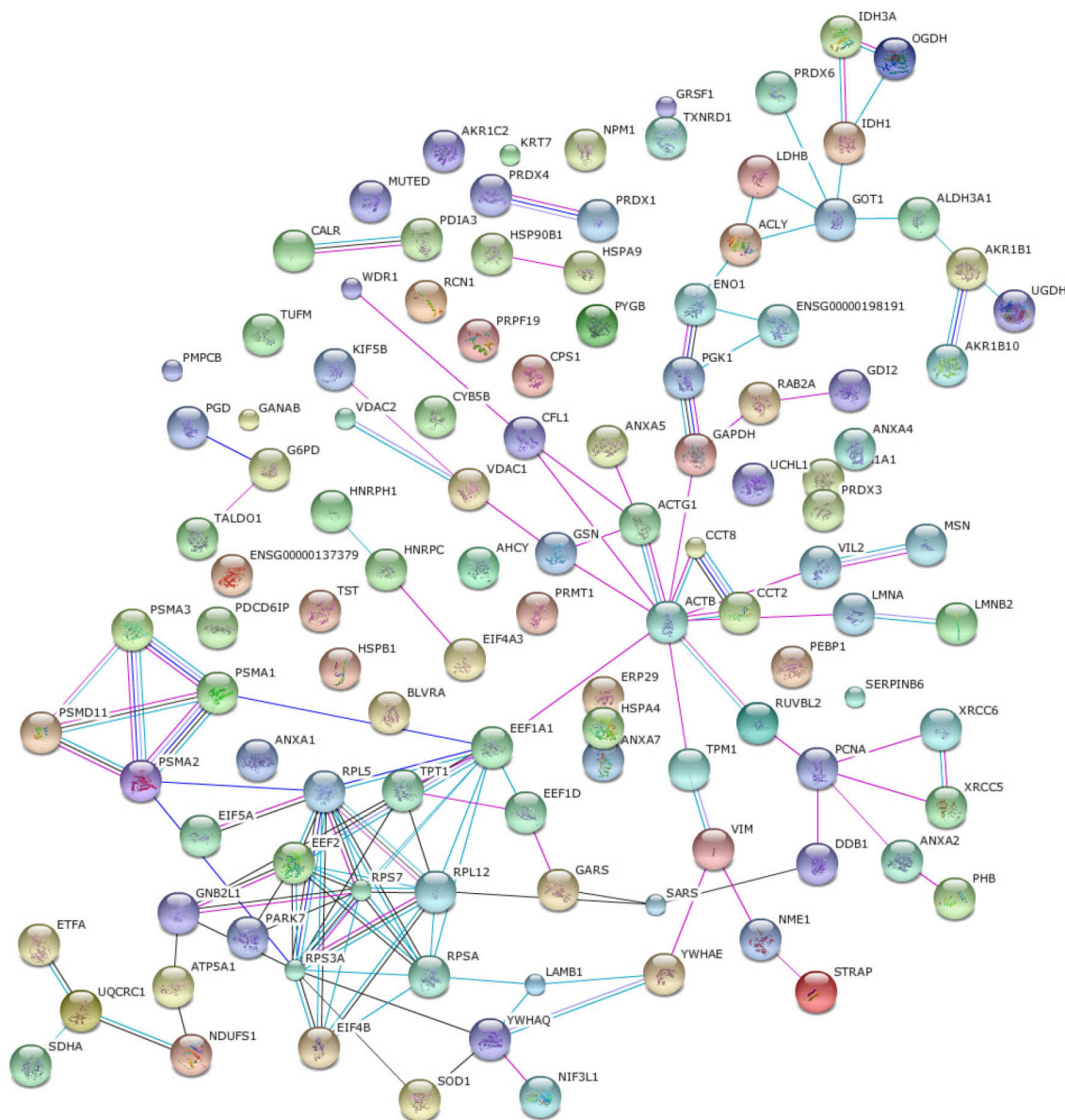


Figure 6-2 Potential protein-protein interactions of all differentially expressed ($p < 0.1$) protein species (including differential phosphorylations) for styrene, monochlorobenzene and 1,2-dichlorobenzene suggested by STRING 8.3 database and web resource. Uni-Prot Accessions were loaded in the STRING tool (<http://string-db.org/>) and analyzed by using the standard settings (medium confidence, network depth 1, no additional white nodes). The prediction methods “textmining and neighborhood” were excluded. The color of the connecting lines between two protein species encodes the source of the information: experimental data (rose), databases (light blue), coexpression data (black), cooccurrence data (dark blue). Gene names are listed in Table 8-4.

Of note, two of the three proteins (VDAC2 and EEF2) that were regulated concomitantly for all of the analyzed VOCs (see Table 6-1), have been predicted to be linked to one of the subnetworks. However, according to STRING prediction, the third protein, peroxiredoxin 1, shows no direct interaction with any other protein than peroxiredoxin 4. This may be due to a lacking differential expression of the direct interacting partners or incomplete coverage of the proteome using 2D SDS-PAGE. In particular, low-abundant proteins that account for numerous important signaling molecules as well as proteins with extreme *p*/values are only rarely detected in classical proteomic approaches. Finally, for the majority of identified protein species only basic information on function and posttranslational modifications is available in scientific databases, limiting the derivation of interactions and the biological relevance of the observed effects.

This thesis provides first insights into the complex protein network that is affected by aromatic VOCs. Naturally, the results do not allow delineation of the exact chain of events following exposure of human alveolar cells to aromatic VOCs. Particularly since no comparable investigation studying differential protein expression in response to these compounds has been carried out so far, it is difficult to deduce and discuss the overall significance of the observed effects. However, the results show that exposure of a stable cell line to aromatic VOCs in concentrations below current occupational limits causes significant molecular effects in these cells. Thus, occupational VOC standards should be critically evaluated and questioned as it could be assumed that primary human lung cells are even more sensitive.

The developed proteomic methods and the proteomic map of the model cell line A549 can be used for further projects. Moreover, the study illustrates the strengths and weaknesses of classical proteomic analyses. Regardless of the analytical techniques that are used, a major challenge for coming proteomic experiments will be the assignment of proteins to specific biological (signaling) pathways. Currently large gaps exist in the knowledge of cellular response mechanisms and the involved proteins making it difficult to identify the major pathways that are affected. Therefore, in future, genome-wide analyses of susceptibility genes (genomics), gene expression (transcriptomics) and protein expression (proteomics) in response to xenobiotics are crucial to understand gene-environment interactions, providing the ability to develop biomarkers for exposure, early effect and susceptibility. The data may be used to populate a large database that will help to understand the interactions among toxicity, susceptibility genes and mRNA (Zhang *et al.*, 2010a).

7 *Summary*

The widespread usage of products containing volatile organic compounds (VOC) has led to a general human exposure to these chemicals in work places or homes being suspected to contribute to the growing incidence of environmental diseases. Since the causal molecular mechanisms for the development of these disorders are not completely understood, the overall objective of this thesis was to investigate VOC-mediated molecular effects on human lung cells *in vitro* at VOC concentrations comparable to exposure scenarios below current occupational limits.

Cellular stress in response to VOCs is proposed to be triggered by different mechanisms of toxicity, among which impaired protein function seems to be a common link. Although differential expression of single proteins in response to VOCs has been reported, effects on complex protein networks (proteome) have not been investigated. However, this information is indispensable when trying to ascertain a mechanism for VOC action on the cellular level and establishing preventive strategies.

For this study, the alveolar epithelial cell line A549 has been used. This cell line, cultured in a two-phase (air/liquid) model allows the most direct exposure and had been successfully applied for the analysis of inflammatory effects in response to VOCs. As a first challenge, this exposure system has been adapted according to the requirements of proteomic techniques (**Chapter 3**). Cell culturing, exposure and harvesting procedures have been modified. Basic proteomic techniques such as high-resolution two-dimensional gel electrophoresis combined with pre-separation fluorescent labeling of proteins have been introduced. Mass spectrometric identification of 266 protein spots provided the first proteomic map of A549 cell line to this extent that may foster future work with this frequently used cellular model. The distribution of three typical air contaminants, monochlorobenzene (CB), styrene and 1,2 dichlorobenzene (1,2-DCB), between gas and liquid phase of the exposure model has been analyzed by gas chromatography. The obtained VOC partitioning was in agreement with available literature data.

Subsequently the adapted *in vitro* system has been successfully employed to characterize the effects of the aromatic compound styrene on the proteome of A549 cells (**Chapter 4**). Initially, the cell toxicity has been assessed in order to ensure that most of the concentrations used in the following proteomic approach were not cytotoxic. Significant changes in abundance and phosphorylation in the total soluble protein fraction of A549 cells have been detected following styrene exposure. All proteins have been identified using mass spectrometry and the main cellular functions have been assigned. Validation experiments on protein and transcript level confirmed the results of the 2-DE experiments. From the results, two main cellular pathways have been identified that were induced by styrene: the cellular oxidative stress response combined with moderate pro-apoptotic signaling. Measurement of

cellular reactive oxygen species (ROS) as well as the styrene-mediated induction of oxidative stress marker proteins confirmed the hypothesis of oxidative stress as the main molecular response mechanism. Finally, adducts of cellular proteins with the reactive styrene metabolite styrene 7,8 oxide (SO) have been identified. Especially the SO-adducts observed at both the reactive centers of thioredoxin reductase 1, which is a key element in the control of the cellular redox state, may be involved in styrene-induced ROS formation and apoptosis.

A similar proteomic approach has been carried out with the halobenzenes CB and 1,2-DCB (**Chapter 5**). In accordance with previous findings, cell toxicity assessment showed enhanced toxicity compared to the one caused by styrene. Significant changes in abundance and phosphorylation of total soluble proteins of A549 cells have been detected following exposure to subtoxic concentrations of CB and 1,2-DCB. All proteins have been identified using mass spectrometry and the main cellular functions have been assigned. As for the styrene experiment, the results indicated two main pathways to be affected in the presence of chlorinated benzenes, cell death signaling and oxidative stress response. The strong induction of pro-apoptotic signaling has been confirmed for both treatments by detection of the cleavage of caspase 3. Likewise, the induction of redox-sensitive protein species could be correlated to an increased cellular level of ROS observed following CB treatment.

Finally, common mechanisms in the cellular response to aromatic VOCs have been investigated (**Chapter 6**). A similar number (4.6-6.9%) of all quantified protein spots showed differential expression ($p < 0.05$) following cell exposure to styrene, CB or 1,2-DCB. However, not more than three protein spots showed significant regulation in the same direction for all three volatile compounds: voltage-dependent anion-selective channel protein 2, peroxiredoxin 1 and elongation factor 2. However, all of these proteins are important molecular targets in stress- and cell death-related signaling pathways. The greatest similarity in protein expression pattern was observed for CB- and 1,2-DCB-treatment. In addition, a quite unexpected similarity in the cellular response to 1,2-DCB and styrene has been observed that may hint to a so far unknown common molecular pathway. Nevertheless, each compound induced a VOC-specific pattern of alterations in the proteome.

In conclusion, differential protein expression has been observed in A549 cells in response to all three VOCs at subtoxic concentrations that are below current German occupational limits (AGW) for CB, 1,2-DCB (each 10 ppm) and styrene (20 ppm). Thus, occupational VOC standards should be critically evaluated and questioned as it could be assumed that primary human lung cells will be even more sensitive.

A major challenge for coming proteomic experiments will be the assignment of proteins to specific biological (signaling) pathways. Currently large gaps exist in the knowledge of cellular response mechanisms and the involved proteins making it difficult to identify the major pathways that are affected by toxic compounds.

Zusammenfassung

Die vermehrte Verwendung von Produkten, welche flüchtige organische Substanzen (VOC - volatile organic compound) enthalten, hat eine generelle Exposition der Bevölkerung mit diesen Substanzen an Arbeitsplätzen aber auch in Wohnräumen bedingt. VOCs stehen im Verdacht, zur zunehmenden Inzidenz umweltbedingter Erkrankungen beizutragen. Da die molekularen Ursachen dieser Erkrankungen bisher noch unverstanden sind, war es ein übergeordnetes Ziel dieser Arbeit, VOC-vermittelte molekulare Effekte in menschlichen Lungenepithelzellen anhand eines *in vitro* Modells zu untersuchen. Dabei sollten vor allem Konzentrationen unterhalb der gültigen Arbeitsplatzgrenzwerte untersucht werden.

Die zelluläre Stressantwort ausgelöst durch VOC-Exposition wird durch verschiedene Mechanismen gesteuert von denen die Einschränkung der Funktionalität der zellulären Proteine ein grundlegendes Phänomen zu sein scheint. Obwohl Effekte auf einzelne Proteine bekannt sind, wurden bisher keine Effekte der VOC-Exposition auf das komplexe Netzwerk der zellulären Proteine (Proteom) untersucht. Dieses Wissen ist essentiell, um induzierte zelluläre Mechanismen zu verstehen und Strategien zu deren Vermeidung zu entwickeln.

Für die hier durchgeführten Untersuchungen wurde die Lungenepithelzelllinie A549 in einem Zweiphasenexpositionsmodell eingesetzt. Dieses ermöglichte eine möglichst direkte zelluläre Exposition und wurde bereits erfolgreich verwendet, um durch VOC hervorgerufene Entzündungseffekte zu identifizieren.

Zunächst mußte das etablierte Expositionsmodell den Anforderungen proteomischer Analysemethoden angepaßt werden (**Kapitel 3**). Die Methoden der Zellkulturtechnik, der Zellexposition und Zellernte wurden modifiziert. Grundlegende proteomische Techniken wie die hochauflösende zweidimensionale Gelelektrophorese (2-DE) in Kombination mit einer Fluoreszenzmarkierung der zu trennenden Proteine wurden etabliert. Die massenspektrometrische Identifikation von 266 Proteinflecken lieferte die erste umfassende Proteomkarte der A549 Zelllinie, welche nachfolgende Untersuchungen mit diesem häufig verwendeten Zelltyp erleichtern wird. Zusätzlich wurde die Verteilung der drei gängigen Luftkontaminanten Chlorbenzol (CB), Styrol and 1,2-Dichlorobenzol (1,2-DCB) zwischen den beiden Phasen (gas/flüssig) des Expositionsmodells gaschromatographisch bestimmt. Die Verteilung entsprach den verfügbaren Literaturdaten.

Anschließend wurde das modifizierte Expositionsmodell erfolgreich eingesetzt, um styrol-vermittelte Effekte auf das Proteom der A549 Zellen zu charakterisieren (**Kapitel 4**). Zu Beginn erfolgte die Erfassung der Zelltoxizität der Substanz, um sicher zu stellen, daß der überwiegende Teil der späteren Expositionsexperimente mit subtoxischen Konzentrationen durchgeführt wird. Es konnte eine signifikant veränderte Expression und Phosphorylierung der löslichen Proteinfraction der A549 Zellen als Reaktion auf die Styrolexposition festgestellt

werden. Die regulierten Proteine wurden massenspektrometrisch identifiziert und ihre wichtigsten Funktionen wurden zugewiesen. Validierungsexperimente auf Protein- und auf Transkriptebeine bestätigten die 2-DE Ergebnisse. Insgesamt konnte die zelluläre Reaktion durch die styrol-vermittelte Induktion zweier zentraler Mechanismen erklärt werden: oxidativer zellulärer Stress und beginnende Apoptose. Folgeexperimente wie die Messung der Menge der zellulären reaktiven Sauerstoffspezies (ROS) und die Induktion von redox-sensitiven Markerproteinen konnte die Hypothese eines styrol-induzierten oxidativen Milieus bestätigen.

Schließlich wurden Proteinaddukte des reaktiven Styrolmetaboliten Styrol 7,8 epoxide (SO) identifiziert. Besonders die SO-Addukte, welche an den beiden aktiven Zentren der Thioredoxin Reduktase 1 gefunden wurden könnten eine wichtige Rolle bei der styrol-induzierten ROS-Bildung sowie der beginnenden Apoptose spielen.

In Analogie zum Styrolexperiment wurden die Effekte der halogenierten Benzole CB und 1,2-DCB untersucht (**Kapitel 5**). In Übereinstimmung mit schon publizierten Daten zeigten beide Substanzen eine deutlich stärkere Zelltoxizität. Die Exposition der A549 Zellen mit subtoxischen Konzentrationen von CB und 1,2-DCB führte zu signifikanten Veränderungen der Expression und Phosphorylierung zellulärer Proteine. Es konnten ebenfalls sämtliche Proteine identifiziert und die wichtigsten zellulären Funktionen zugewiesen werden. Diese Substanzen modulierten ebenfalls apoptotische Signalwege und die zelluläre Antwort auf oxidativen Stress. Der beobachtete starke pro-apoptotische Effekt konnte für beide Substanzen mit der Spaltung der Caspase 3 nachgewiesen werden. Weiterhin konnte für CB die Induktion redox-sensitiver Proteinspezies mit einem beobachteten höherem Gehalt an ROS erklärt werden.

Schließlich wurden ähnliche Mechanismen der zellulären Antwort auf die Exposition mit den drei untersuchten aromatischen VOCs diskutiert (**Kapitel 6**). Alle getesteten VOCs verursachten eine vergleichbare differentielle Expression ($p < 0,05$) von 4,6-6,9% aller quantifizierten Proteinspezies. Nur drei Proteinspots wurden dabei gemeinsam für alle VOCs reguliert: voltage-dependent anion-selective channel protein 2, peroxiredoxin 1 and elongation factor 2. Allerdings gehören diese drei Proteine zu wichtigen zellulären Zielstrukturen der Signalwege für Stressantwort und Zelltod. Die größte Übereinstimmung der regulierten Proteinspezies wurde zwischen CB und 1,2-DCB beobachtet. Zusätzlich trat eine eher unerwartete Ähnlichkeit der zellulären Antwort auf 1,2-DCB und Styrol auf, welche auf ein bisher unbekanntes, ähnliches toxisches Prinzip hinweisen könnte. Allerdings induzierte jedes der untersuchten VOCs auch ein ihm eigenes Muster an Proteomveränderungen.

Insgesamt konnte für alle drei VOCs in Konzentrationen unterhalb der gültigen Arbeitsplatzgrenzwerte (AGW) für CB, 1,2-DCB (jeweils 10 ppm) und Styrol (20 ppm) eine

differentielle Proteinexpression in A549 Zellen nachgewiesen werden. Diese Standards sollten kritisch geprüft und hinterfragt werden, da die Vermutung nahe liegt, dass primäre Lungenepithelzellen wesentlich sensitiver auf die getesteten VOCs reagieren.

Zum jetzigen Zeitpunkt ist das Verständnis zellulärer Reaktionsmechanismen noch sehr lückenhaft, was die eindeutige Zuordnung der durch Exposition beeinträchtigten Signalwege erschwert. Daher besteht die größte Herausforderung zukünftiger proteomischer Untersuchungen in der korrekten Zuordnung von Proteinen zu spezifischen biologischen Signalwegen.

References

1. ACGIH. Documentation of the threshold limit values and biological exposure indices (Cincinnati, OH, American Conference of Governmental Industrial Hygienists)(1991)
2. Adler, KB, Cheng, PW and Kim, KC. Characterization of guinea pig tracheal epithelial cells maintained in biphasic organotypic culture: cellular composition and biochemical analysis of released glycoconjugates. *Am J Respir Cell Mol Biol* 1990;2:145-154.
3. Ahmad, Z, Salim, M and Maines, MD. Human biliverdin reductase is a leucine zipper-like DNA-binding protein and functions in transcriptional activation of heme oxygenase-1 by oxidative stress. *J Biol Chem* 2002;277:9226-9232.
4. Ait-Aissa, S, Porcher, J, Arrigo, A and Lambre, C. Activation of the hsp70 promoter by environmental inorganic and organic chemicals: relationships with cytotoxicity and lipophilicity. *Toxicology* 2000;145:147-157.
5. Altirriba, J, Barbera, A, Del Zotto, H, Nadal, B, Piquer, S, Sanchez-Pla, A, Gagliardino, JJ and Gomis, R. Molecular mechanisms of tungstate-induced pancreatic plasticity: a transcriptomics approach. *BMC Genomics* 2009;10:406.
6. Altraja, S, Jaama, J, Valk, E and Altraja, A. Changes in the proteome of human bronchial epithelial cells following stimulation with leucotriene E4 and transforming growth factor-beta1. *Respirology* 2009;14:39-45.
7. Anderson, L and Seilhamer, J. A comparison of selected mRNA and protein abundances in human liver. *Electrophoresis* 1997;18:533-537.
8. Anonymous. Ortho-, meta-, and para-dichlorobenzene. *Rev Environ Contam Toxicol* 1988;106:51-68.
9. Antoine, SR, DeLeon, IR and O'Dell-Smith, RM. Environmentally significant volatile organic pollutants in human blood. *Bull Environ Contam Toxicol* 1986;36:364-371.
10. ARB. Toxic Air Contaminant Identification Report - Chlorobenzene, (Air Resources Board)(1997)
11. Ardakani, MD. Human-experimentelle Untersuchungen zur Toxikokinetik von 1,2-Dichlorbenzol nach standardisierten Expositionen. In Fachbereich Medizin, Gießen, Justus-Liebig-Universität (2007)
12. Arif, AA and Shah, SM. Association between personal exposure to volatile organic compounds and asthma among US adult population. *Int Arch Occup Environ Health* 2007;80:711-719.
13. ATSDR. Toxicological profile for chlorobenzene (Atlanta, GA, US Department of Health and Human Services, Public Health Service)(1990)
14. ATSDR. Toxicological profile for dichlorobenzenes, P.H.S. U.S. Department of Health and Human Services, ed. (Atlanta, GA, Agency for Toxic Substances and Disease Registry)(2006)
15. ATSDR. Toxicological profile for styrene (Atlanta, GA, US Department of Health and Human Services, Public Health Service)(2007), pp.
16. Ban, M, Hettich, D, Goutet, M and Binet, S. Serum-borne factor(s) of 1,1-dichloroethylene and 1,2-dichlorobenzene-treated mice inhibited in vitro antibody forming cell response and natural killer cell activity. *Toxicol Lett* 1998;94:93-101.
17. Ban, M, Langonne, I, Huguet, N, Pepin, E and Morel, G. Inhaled chemicals may enhance allergic airway inflammation in ovalbumin-sensitized mice. *Toxicology* 2006;226:161-171.
18. Banki, K, Hutter, E, Colombo, E, Gonchoroff, NJ and Perl, A. Glutathione levels and sensitivity to apoptosis are regulated by changes in transaldolase expression. *J Biol Chem* 1996;271:32994-33001.
19. Baranano, DE, Rao, M, Ferris, CD and Snyder, SH. Biliverdin reductase: a major physiologic cytoprotectant. *Proc Natl Acad Sci U S A* 2002;99:16093-16098.
20. Bardales, RH, Xie, SS, Schaefer, RF and Hsu, SM. Apoptosis is a major pathway responsible for the resolution of type II pneumocytes in acute lung injury. *Am J Pathol* 1996;149:845-852.
21. Basile, A, Ferranti, P, Mamone, G, Manco, I, Pocsfalvi, G, Malorni, A, Acampora, A and Sannolo, N. Structural analysis of styrene oxide/haemoglobin adducts by mass spectrometry: identification of suitable biomarkers for human exposure evaluation. *Rapid Commun Mass Spectrom* 2002;16:871-878.
22. Beliveau, M and Krishnan, K. Concentration dependency of rat blood: air partition coefficients of some volatile organic chemicals. *J Toxicol Environ Health A* 2000;60:377-389.
23. Benndorf, D, Balcke, GU, Harms, H and von Bergen, M. Functional metaproteome analysis of protein extracts from contaminated soil and groundwater. *Isme J* 2007;1:224-234.

24. Berth, M, Moser, FM, Kolbe, M and Bernhardt, J. The state of the art in the analysis of two-dimensional gel electrophoresis images. *Appl Microbiol Biotechnol* 2007;76:1223-1243.
25. Bialik, S, Berissi, H and Kimchi, A. A high throughput proteomics screen identifies novel substrates of death-associated protein kinase. *Mol Cell Proteomics* 2008;7:1089-1098.
26. Bieche, I, Narjoz, C, Asselah, T, Vacher, S, Marcellin, P, Lidereau, R, Beaune, P and de Waziers, I. Reverse transcriptase-PCR quantification of mRNA levels from cytochrome (CYP)1, CYP2 and CYP3 families in 22 different human tissues. *Pharmacogenet Genomics* 2007;17:731-742.
27. Blank, F, Rothen-Rutishauser, BM, Schurch, S and Gehr, P. An optimized in vitro model of the respiratory tract wall to study particle cell interactions. *J Aerosol Med* 2006;19:392-405.
28. Blom, N, Gammeltoft, Sand Brunak, S. Sequence and structure-based prediction of eukaryotic protein phosphorylation sites. *J Mol Biol* 1999;294:1351-1362.
29. Boccellino, M, Cuccovillo, F, Napolitano, M, Sannolo, N, Balestrieri, C, Acampora, A, Giovane, A and Quagliuolo, L. Styrene-7,8-oxide activates a complex apoptotic response in neuronal PC12 cell line. *Carcinogenesis* 2003;24:535-540.
30. Bogaards, JJ, van Ommen, B, Wolf, CR and van Bladeren, PJ. Human cytochrome P450 enzyme selectivities in the oxidation of chlorinated benzenes. *Toxicol Appl Pharmacol* 1995;132:44-52.
31. Bond, JA. Review of the toxicology of styrene. *Crit Rev Toxicol* 1989;19:227-249.
32. Boogaard, PJ, de Kloe, KP, Wong, BA, Sumner, SC, Watson, WP and van Sittert, NJ. Quantification of DNA adducts formed in liver, lungs, and isolated lung cells of rats and mice exposed to (14)C-styrene by nose-only inhalation. *Toxicol Sci* 2000;57:203-216.
33. Brondeau, MT, Bonnet, P, Guenier, JP, Simon, P and de Ceaurriz, J. Adrenal-dependent leucopenia after short-term exposure to various airborne irritants in rats. *J Appl Toxicol* 1990;10:83-86.
34. Burczynski, ME, Lin, HK and Penning, TM. Isoform-specific induction of a human aldo-keto reductase by polycyclic aromatic hydrocarbons (PAHs), electrophiles, and oxidative stress: implications for the alternative pathway of PAH activation catalyzed by human dihydrodiol dehydrogenase. *Cancer Res* 1999;59:607-614.
35. Burke-Gaffney, A, Callister, ME and Nakamura, H. Thioredoxin: friend or foe in human disease? *Trends Pharmacol Sci* 2005;26:398-404.
36. Byun, HO, Han, NK, Lee, HJ, Kim, KB, Ko, YG, Yoon, G, Lee, YS, Hong, SI and Lee, JS. Cathepsin D and eukaryotic translation elongation factor 1 as promising markers of cellular senescence. *Cancer Res* 2009;69:4638-4647.
37. Caohuy, H and Pollard, HB. Activation of annexin 7 by protein kinase C in vitro and in vivo. *J Biol Chem* 2001;276:12813-12821.
38. Casas, C, Ribera, J and Esquerda, JE. Antibodies against c-Jun N-terminal peptide cross-react with neo-epitopes emerging after caspase-mediated proteolysis during apoptosis. *J Neurochem* 2001;77:904-915.
39. Casey, J, Kaplan, J, Atochina-Vasserman, EN, Gow, AJ, Kadire, H, Tomer, Y, Fisher, JH, Hawgood, S, Savani, RC and Beers, MF. Alveolar surfactant protein D content modulates bleomycin-induced lung injury. *Am J Respir Crit Care Med* 2005;172:869-877.
40. Castell, JV, Donato, MT and Gomez-Lechon, MJ. Metabolism and bioactivation of toxicants in the lung. The in vitro cellular approach. *Exp Toxicol Pathol* 2005;57 Suppl 1:189-204.
41. Chan, DW, Ye, R, Veillette, CJ and Lees-Miller, SP. DNA-dependent protein kinase phosphorylation sites in Ku 70/80 heterodimer. *Biochemistry* 1999;38:1819-1828.
42. Chan, K, Jensen, NS, Silber, PM and O'Brien, PJ. Structure-activity relationships for halobenzene induced cytotoxicity in rat and human hepatocytes. *Chem Biol Interact* 2007;165:165-174.
43. Chander, A, Chen, XL and Naidu, DG. A role for diacylglycerol in annexin A7-mediated fusion of lung lamellar bodies. *Biochim Biophys Acta* 2007;1771:1308-1318.
44. Chatterjee, D, Bai, Y, Wang, Z, Beach, S, Mott, S, Roy, R, Braastad, C, Sun, Y, Mukhopadhyay, A, Aggarwal, BB *et al*. RKIP sensitizes prostate and breast cancer cells to drug-induced apoptosis. *J Biol Chem* 2004;279:17515-17523.
45. Chen, J, Jiang, J, Zhang, F, Yu, H and Zhang, J. Cytotoxic effects of environmentally relevant chlorophenols on L929 cells and their mechanisms. *Cell Biol Toxicol* 2004;20:183-196.
46. Cheng, EH, Sheiko, TV, Fisher, JK, Craigen, WJ and Korsmeyer, SJ. VDAC2 inhibits BAK activation and mitochondrial apoptosis. *Science* 2003;301:513-517.
47. Christian, KJ, Lang, MA and Raffalli-Mathieu, F. Interaction of heterogeneous nuclear ribonucleoprotein C1/C2 with a novel cis-regulatory element within p53 mRNA as a response to cytostatic drug treatment. *Mol Pharmacol* 2008;73:1558-1567.

48. Chuang, CY, Chen, TL and Chen, RM. Molecular mechanisms of lipopolysaccharide-caused induction of surfactant protein-A gene expression in human alveolar epithelial A549 cells. *Toxicol Lett* 2009;191:132-139.
49. Chung, JK, Yuan, W, Liu, G and Zheng, J. Investigation of bioactivation and toxicity of styrene in CYP2E1 transgenic cells. *Toxicology* 2006;226:99-106.
50. Colacci, A, Bartoli, S, Bonora, B, Niero, A, Silingardi, P and Grilli, S. In vivo and in vitro interaction of 1,2-dichlorobenzene with nucleic acids and proteins of mice and rats. *Tumori* 1990;76:339-344.
51. Cooke, TF. Indoor air pollutants. A literature review. *Rev Environ Health* 1991;9:137-160.
52. Cordwell, SJ, Nouwens, AS, Verrills, NM, Basseal, DJ and Walsh, BJ. Subproteomics based upon protein cellular location and relative solubilities in conjunction with composite two-dimensional electrophoresis gels. *Electrophoresis* 2000;21:1094-1103.
53. Cox, AG, Pullar, JM, Hughes, G, Ledgerwood, EC and Hampton, MB. Oxidation of mitochondrial peroxiredoxin 3 during the initiation of receptor-mediated apoptosis. *Free Radic Biol Med* 2008;44:1001-1009.
54. Croute, F, Poinot, J, Gaubin, Y, Beau, B, Simon, V, Murat, JC and Soleilhavoup, JP. Volatile organic compounds cytotoxicity and expression of HSP72, HSP90 and GRP78 stress proteins in cultured human cells. *Biochim Biophys Acta* 2002;1591:147-155.
55. Croute, F, Poinot, J, Gaubin, Y, Beau, B, Simon, V, Torres, L and Soleilhavoup, J. Evaluation of the cytotoxic threshold of benzene and its chlorinated derivatives and related stress protein expression (HSP72, HSP90, GRP78) in human cells in vitro *Fresenius Environmental Bulletin* 2000;9:373-380.
56. Crump, D. Volatile organic compounds in indoor air. *Issues Environ Sci Technol* 1995;4:109-124.
57. Cruzan, G, Carlson, GP, Johnson, KA, Andrews, LS, Banton, MI, Bevan, C and Cushman, JR. Styrene respiratory tract toxicity and mouse lung tumors are mediated by CYP2F-generated metabolites. *Regul Toxicol Pharmacol* 2002;35:308-319.
58. Cruzan, G, Cushman, JR, Andrews, LS, Granville, GC, Miller, RR, Hardy, CJ, Coombs, DW and Mullins, PA. Subchronic inhalation studies of styrene in CD rats and CD-1 mice. *Fundam Appl Toxicol* 1997;35:152-165.
59. Csanady, GA, Kessler, W, Hoffmann, HD and Filser, JG. A toxicokinetic model for styrene and its metabolite styrene-7,8-oxide in mouse, rat and human with special emphasis on the lung. *Toxicol Lett* 2003;138:75-102.
60. Damdimopoulos, AE, Miranda-Vizueté, A, Treuter, E, Gustafsson, JA and Spyrou, G. An alternative splicing variant of the selenoprotein thioredoxin reductase is a modulator of estrogen signaling. *J Biol Chem* 2004;279:38721-38729.
61. Dammeyer, P, Damdimopoulos, AE, Nordman, T, Jimenez, A, Miranda-Vizueté, A and Arner, ES. Induction of cell membrane protrusions by the N-terminal glutaredoxin domain of a rare splice variant of human thioredoxin reductase 1. *J Biol Chem* 2008;283:2814-2821.
62. Dare, E, Tofighi, R, Vettori, MV, Momoi, T, Poli, D, Saido, TC, Mutti, A and Ceccatelli, S. Styrene 7,8-oxide induces caspase activation and regular DNA fragmentation in neuronal cells. *Brain Res* 2002;933:12-22.
63. Davis, ME, Blicharz, AP, Hart, JE, Laden, F, Garshick, E and Smith, TJ. Occupational exposure to volatile organic compounds and aldehydes in the U.S. trucking industry. *Environ Sci Technol* 2007;41:7152-7158.
64. De Ceaurriz, J, Gagnaire, F, Ban, M and Bonnet, P. Assessment of the relative hazard involved with airborne irritants with additional hepatotoxic or nephrotoxic properties in mice. *J Appl Toxicol* 1988;8:417-422.
65. Debret, R, El Btaouri, H, Duca, L, Rahman, I, Radke, S, Haye, B, Sallenave, JM and Antonicelli, F. Annexin A1 processing is associated with caspase-dependent apoptosis in BZR cells. *FEBS Lett* 2003;546:195-202.
66. DeJongh, J, Verhaar, HJ and Hermens, JL. Role of kinetics in acute lethality of nonreactive volatile organic compounds (VOCs). *Toxicol Sci* 1998;45:26-32.
67. Dejournett, RE, Kobayashi, R, Pan, S, Wu, C, Etkin, LD, Clark, RB, Bogler, O and Kuang, J. Phosphorylation of the proline-rich domain of Xp95 modulates Xp95 interaction with partner proteins. *Biochem J* 2007;401:521-531.
68. den Besten, C, Brouwer, A, Rietjens, IM and van Bladeren, PJ. Biotransformation and toxicity of halogenated benzenes. *Hum Exp Toxicol* 1994;13:866-875.
69. den Besten, C, Ellenbroek, M, van der Ree, MA, Rietjens, IM and van Bladeren, PJ. The involvement of primary and secondary metabolism in the covalent binding of 1,2- and 1,4-dichlorobenzenes. *Chem Biol Interact* 1992;84:259-275.

70. den Besten, C, Vet, JJ, Besselink, HT, Kiel, GS, van Berkel, BJ, Beems, R and van Bladeren, PJ. The liver, kidney, and thyroid toxicity of chlorinated benzenes. *Toxicol Appl Pharmacol* 1991;111:69-81.
71. Dhar, SK and St Clair, DK. Nucleophosmin blocks mitochondrial localization of p53 and apoptosis. *J Biol Chem* 2009;284:16409-16418.
72. Diez, U, Kroessner, T, Rehwagen, M, Richter, M, Wetzig, H, Schulz, R, Borte, M, Metzner, G, Krumbiegel, P and Herbarth, O. Effects of indoor painting and smoking on airway symptoms in atopy risk children in the first year of life results of the LARS-study. Leipzig Allergy High-Risk Children Study. *Int J Hyg Environ Health* 2000;203:23-28.
73. Diez, U, Rehwagen, M, Rolle-Kampczyk, U, Wetzig, H, Schulz, R, Richter, M, Lehmann, I, Borte, M and Herbarth, O. Redecoration of apartments promotes obstructive bronchitis in atopy risk infants--results of the LARS Study. *Int J Hyg Environ Health* 2003;206:173-179.
74. Diodovich, C, Bianchi, MG, Bowe, G, Acquati, F, Taramelli, R, Parent-Massin, D and Gribaldo, L. Response of human cord blood cells to styrene exposure: evaluation of its effects on apoptosis and gene expression by genomic technology. *Toxicology* 2004;200:145-157.
75. Dongre, AR, Opitck, G, Cosand, WL and Hefta, SA. Proteomics in the post-genome age. *Biopolymers* 2001;60:206-211.
76. Dreger, M. Subcellular proteomics. *Mass Spectrom Rev* 2003;22:27-56.
77. Droz, PO and Guillemin, MP. Human styrene exposure. V. Development of a model for biological monitoring. *Int Arch Occup Environ Health* 1983;53:19-36.
78. Dubois, T, Rommel, C, Howell, S, Steinhussen, U, Soneji, Y, Morrice, N, Moelling, K and Aitken, A. 14-3-3 is phosphorylated by casein kinase I on residue 233. Phosphorylation at this site in vivo regulates Raf/14-3-3 interaction. *J Biol Chem* 1997;272:28882-28888.
79. EHC. Styrene (EHC 26, 1983) (International Safety Programme on Chemical Safety Environmental Health Criteria)(1983)
80. EPA. Health and environmental effects profile for styrene (Cincinnati, OH, U.S. Environmental Protection Agency, Environmental Criteria and Assessment Office)(1984)
81. EPA. Drinking water criteria document for styrene. Final draft. (Cincinnati, OH, U.S. Environmental Protection Agency, Office of Health and Environmental Assessment)(1985)
82. EPA. Broad scan analysis of the FY82 national human adipose tissue survey specimens (Washington, DC, U.S. Environmental Protection Agency, Office of Toxic Substances)(1986)
83. EPA. The Total Exposure Assessment Methodology (TEAM) study: Summary and analysis. (Washington, DC, U.S. Environmental Protection Agency, Office of Research and Development)(1987)
84. EPA. Exposure factors handbook (Washington, DC, U.S. Environmental Protection Agency, Office of Health and Environmental Assessment)(1989)
85. EPA. Integrated Risk Information System (IRIS) on Styrene (Washington, DC, U.S. Environmental Protection Agency, National Center for Environmental Assessment, Office of Research and Development)(1999)
86. EPA, Sick Building Syndrome. In *Indoor Air Facts No 4* (revised) (United States Environmental Protection Agency)(1991)
87. EPA, 2005 TRI Public Data Release eReport (New York)(2007)
88. Eriksson, JE, He, T, Trejo-Skalli, AV, Harmala-Brasken, AS, Hellman, J, Chou, YH and Goldman, RD. Specific in vivo phosphorylation sites determine the assembly dynamics of vimentin intermediate filaments. *J Cell Sci* 2004;117:919-932.
89. Escuder-Gilabert, L, Villanueva-Camañas, RM, Sagrado, S and Medina-Hernandez, MJ. Permeability and toxicological profile estimation of organochlorine compounds by biopartitioning micellar chromatography. *Biomed Chromatogr* 2008;23:382-389.
90. Estey, T, Piatigorsky, J, Lassen, N and Vasiliou, V. ALDH3A1: a corneal crystallin with diverse functions. *Exp Eye Res* 2007;84:3-12.
91. Fan, Z, Beresford, PJ, Oh, DY, Zhang, D and Lieberman, J. Tumor suppressor NM23-H1 is a granzyme A-activated DNase during CTL-mediated apoptosis, and the nucleosome assembly protein SET is its inhibitor. *Cell* 2003;112:659-672.
92. Feltens, R, Mogel, I, Roder-Stolinski, C, Simon, JC, Herberth, G and Lehmann, I. Chlorobenzene induces oxidative stress in human lung epithelial cells in vitro. *Toxicol Appl Pharmacol* 2010;242:100-108.
93. Filser, JG, Schwegler, U, Csanady, GA, Greim, H, Kreuzer, PE and Kessler, W. Species-specific pharmacokinetics of styrene in rat and mouse. *Arch Toxicol* 1993;67:517-530.

94. Fischäder, G. Dissertation 02/2007. In vitro Modelle zur Untersuchung von immunmodulierenden und inflammatorischen Effekten durch flüchtige organische Verbindungen (Leipzig, Universität Leipzig)(2006), pp. 1-132.
95. Fischader, G, Roder-Stolinski, C, Wichmann, G, Nieber, K and Lehmann, I. Release of MCP-1 and IL-8 from lung epithelial cells exposed to volatile organic compounds. *Toxicol In Vitro* 2008;22:359-366.
96. Fisher, RL, Gandolfi, AJ, Sipes, IG and Brendel, K. Culture medium composition affects the relative toxicities of chlorobenzenes in rat liver slices and the isolated perfused liver. *Drug Chem Toxicol* 1993;16:321-339.
97. Fisher, RL, Hasal, SJ, Sipes, IG, Gandolfi, AJ and Brendel, K. Comparative metabolism and toxicity of dichlorobenzenes in Sprague-Dawley, Fischer-344 and human liver slices. *Hum Exp Toxicol* 1995;14:414-421.
98. Fleming-Jones, ME and Smith, RE. Volatile organic compounds in foods: a five year study. *J Agric Food Chem* 2003;51:8120-8127.
99. Forbus, J, Spratt, H, Wiktorowicz, J, Wu, Z, Boldogh, I, Denner, L, Kurosky, A, Brasier, RC, Luxon, B and Brasier, AR. Functional analysis of the nuclear proteome of human A549 alveolar epithelial cells by HPLC-high resolution 2-D gel electrophoresis. *Proteomics* 2006;6:2656-2672.
100. Fritz-Wolf, K, Urig, S and Becker, K. The structure of human thioredoxin reductase 1 provides insights into C-terminal rearrangements during catalysis. *J Mol Biol* 2007;370:116-127.
101. Fusaro, G, Dasgupta, P, Rastogi, S, Joshi, B and Chellappan, S. Prohibitin induces the transcriptional activity of p53 and is exported from the nucleus upon apoptotic signaling. *J Biol Chem* 2003;278:47853-47861.
102. Fustinoni, S, Colosio, C, Colombi, A, Lastrucci, L, Yeowell-O'Connell, K and Rappaport, SM. Albumin and hemoglobin adducts as biomarkers of exposure to styrene in fiberglass-reinforced-plastics workers. *Int Arch Occup Environ Health* 1998;71:35-41.
103. Gargas, ML and Andersen, ME. Determining kinetic constants of chlorinated ethane metabolism in the rat from rates of exhalation. *Toxicol Appl Pharmacol* 1989;99:344-353.
104. Gell, D and Jackson, SP. Mapping of protein-protein interactions within the DNA-dependent protein kinase complex. *Nucleic Acids Res* 1999;27:3494-3502.
105. Gerin, M, Siemiatycki, J, Desy, M and Krewski, D. Associations between several sites of cancer and occupational exposure to benzene, toluene, xylene, and styrene: results of a case-control study in Montreal. *Am J Ind Med* 1998;34:144-156.
106. Gorlatov, SN and Stadtman, TC. Human thioredoxin reductase from HeLa cells: selective alkylation of selenocysteine in the protein inhibits enzyme activity and reduction with NADPH influences affinity to heparin. *Proc Natl Acad Sci U S A* 1998;95:8520-8525.
107. Gorreta, F, Runfola, TP, VanMeter, AJ, Barzaghi, D, Chandhoke, V and Del Giacco, L. Identification of thioredoxin reductase 1-regulated genes using small interference RNA and cDNA microarray. *Cancer Biol Ther* 2005;4:1079-1088.
108. Gourlay, CW and Ayscough, KR. A role for actin in aging and apoptosis. *Biochem Soc Trans* 2005;33:1260-1264.
109. Graves, PR and Haystead, TA. Molecular biologist's guide to proteomics. *Microbiol Mol Biol Rev* 2002;66:39-63
110. Green, T, Toghiani, A and Foster, JR. The role of cytochromes P-450 in styrene induced pulmonary toxicity and carcinogenicity. *Toxicology* 2001;169:107-117.
111. Groisman, R, Polanowska, J, Kuraoka, I, Sawada, J, Saijo, M, Drapkin, R, Kisselev, AF, Tanaka, K and Nakatani, Y. The ubiquitin ligase activity in the DDB2 and CSA complexes is differentially regulated by the COP9 signalosome in response to DNA damage. *Cell* 2003;113:357-367.
112. Grosshans, BL, Ortiz, D and Novick, P. Rabs and their effectors: achieving specificity in membrane traffic. *Proc Natl Acad Sci U S A* 2006;103:11821-11827.
113. Gündel, U. PhD Dissertation 03/2009. Proteomics Approach for Toxicity Assessment in Zebrafish (*Danio rerio*) Embryos (Leipzig, Humboldt-Universität zu Berlin)(2009), pp. 1-138.
114. Guengerich, F. Human Cytochrome P450 Enzymes. In *Cytochrome P450: Structure, Mechanism, and Biochemistry* (New York, Plenum Press)(1995), p. 473-535.
115. Guerin, TF. Ex-situ bioremediation of chlorobenzenes in soil. *J Hazard Mater* 2008;154:9-20.
116. Han, JH, Choi, CS, Kim, MY and Chun, YJ. Differential gene expression by styrene in rat reproductive tissue. *J Toxicol Environ Health A* 2007;70:1259-1263.
117. Hanczko, R, Fernandez, DR, Doherty, E, Qian, Y, Vas, G, Niland, B, Telarico, T, Garba, A, Banerjee, S, Middleton, FA *et al.* Prevention of hepatocarcinogenesis and increased susceptibility to

- acetaminophen-induced liver failure in transaldolase-deficient mice by N-acetylcysteine. *J Clin Invest* 2009;119:1546-1557.
118. Handler, JS, Green, N and Steele, RE. Cultures as epithelial models: porous-bottom culture dishes for studying transport and differentiation. *Methods Enzymol* 1989;171:736-744.
119. Hansch, C, Leo, A and Hoekman, D. Exploring QSAR. Hydrophobic, electronic, and steric constants. (Washington, DC, American Chemical Society)(1995)
120. Harvilchuck, JA and Carlson, GP. Effect of multiple doses of styrene and R-styrene oxide on CC10, bax, and bcl-2 expression in isolated Clara cells of CD-1 mice. *Toxicology* 2009a;259:149-152.
121. Harvilchuck, JA, Pu, X, Klaunig, JE and Carlson, GP. Indicators of oxidative stress and apoptosis in mouse whole lung and Clara cells following exposure to styrene and its metabolites. *Toxicology* 2009b;264:171-178.
122. Hashimoto, S, Amaya, F, Matsuyama, H, Ueno, H, Kikuchi, S, Tanaka, M, Watanabe, Y, Ebina, M, Ishizaka, A, Tsukita, S *et al.* Dysregulation of lung injury and repair in moesin-deficient mice treated with intratracheal bleomycin. *Am J Physiol Lung Cell Mol Physiol* 2008; 295: L566-L574
123. Heinisch, E, Kettrup, A, Bergheim, W, Martens, D and Wenzel, S. Persistend chlorinated hydrocarbons (PCHC), Source-orientated monitoring in aquatic media. 4. The chlorobenzenes. *Fresenius Environmental Bulletin* 2006;15:148-169.
124. Heinrich-Ramm, R, Jakubowski, M, Heinzow, B, Molin Christensen, J, Olsen, E and Hertel, E. Biological monitoring for exposure to volatile organic compounds (VOCs) - (IUPAC Recommendations 2000). *Pure Appl Chem*, 2000;72:385-436.
125. Herbarth, O and Rehwagen, M. VOC-Untersuchungen zur indoor- und outdoorexposition. Präsentation erster Ergebnisse einer umweltepidemiologischen Studie in Leipzig 1994-1997. *Umweltmed Forsch Prax* 1998;3:281-286.
126. Herberth, G, Gubelt, R, Roder, S, Kramer, U, Schins, RP, Diez, U, Borte, M, Heinrich, J, Wichmann, HE, Herbarth, O *et al.* Increase of inflammatory markers after indoor renovation activities: the LISA birth cohort study. *Pediatr Allergy Immunol* 2009;20:563-570.
127. Herberth, G, Weber, A, Roder, S, Elvers, HD, Kramer, U, Schins, RP, Diez, U, Borte, M, Heinrich, J, Schafer, T *et al.* Relation between stressful life events, neuropeptides and cytokines: results from the LISA birth cohort study. *Pediatr Allergy Immunol* 2008;19(8):722-729.
128. Herrmann, M. Identification and characterization of type III-secreted chlamydial pathogenicity factors and their impact on the infected host cell. Department of Biology. University of Konstanz(2004)
129. Hetland, RB, Schwarze, PE, Johansen, BV, Myran, T, Uthus, N and Refsnes, M. Silica-induced cytokine release from A549 cells: importance of surface area versus size. *Hum Exp Toxicol* 2001;20:46-55.
130. Hippelein, M. Background concentrations of individual and total volatile organic compounds in residential indoor air of Schleswig-Holstein, Germany. *J Environ Monit* 2004;6:745-752.
131. Hirasawa, F, Kawagoe, M, Arany, S, Koizumi, Y, Ueno, Y and Sugiyama, T. Styrene monomer primarily induces CYP2B1 mRNA in rat liver. *Xenobiotica* 2005;35:1089-1099.
132. Hirsch, J, Hansen, KC, Burlingame, AL and Matthay, MA. Proteomics: current techniques and potential applications to lung disease. *Am J Physiol Lung Cell Mol Physiol* 2004;287:L1-23.
133. Hissink, AM, Van Ommen, B, Kruse, J and Van Bladeren, PJ. A physiologically based pharmacokinetic (PB-PK) model for 1,2-dichlorobenzene linked to two possible parameters of toxicity. *Toxicol Appl Pharmacol* 1997;145:301-310.
134. Hissink, AM, Van Ommen, B and Van Bladeren, PJ. Dose-dependent kinetics and metabolism of 1,2-dichlorobenzene in rat: effect of pretreatment with phenobarbital. *Xenobiotica* 1996;26:89-105.
135. Hodgson, A, Wooley, J and Daisey, J. Emissions of volatile organic compounds from new carpet measured in a large scale environmental chamber. *J Air Waste Manage Assoc* 1993;43:316-324.
136. Hofmann, H and Plieninger, P. Bereitstellung einer Datenbank zum Vorkommen von flüchtigen organischen Verbindungen in der Raumluft. Publikationen des Umweltbundesamtes 2008;1-157.
137. Hoglen, NC, Younis, HS, Hartley, DP, Gunawardhana, L, Lantz, RC and Sipes, IG. 1,2-Dichlorobenzene-induced lipid peroxidation in male Fischer 344 rats is Kupffer cell dependent. *Toxicol Sci* 1998;46:376-385.
138. Holcik, M, Gordon, BW and Korneluk, RG. The internal ribosome entry site-mediated translation of antiapoptotic protein XIAP is modulated by the heterogeneous nuclear ribonucleoproteins C1 and C2. *Mol Cell Biol* 2003;23:280-288.
139. Howard, P. Large Production and Priority Pollutants. Handbook of Environmental Fate and Exposure Data for Organic Chemicals., Vol Volume 1, Boca Raton, CRC Press)(1989).

140. Hukkanen, J, Lassila, A, Paivarinta, K, Valanne, S, Sarpo, S, Hakkola, J, Pelkonen, O and Raunio, H. Induction and regulation of xenobiotic-metabolizing cytochrome P450s in the human A549 lung adenocarcinoma cell line. *Am J Respir Cell Mol Biol* 2000;22:360-366.
141. IARC. Styrene, polystyrene and styrene-butadiene copolymers. IARC monographs on the evaluation of the carcinogenic risk of chemicals to humans. (Geneva, Switzerland, International Agency for Research on Cancer, World Health Organization)(1979), pp. 231-274.
142. IARC. IARC monographs on the evaluation of the carcinogenic risk of chemicals to humans (Lyon, France, International Agency for Research on Cancer)(1994a), pp. 233-320.
143. IARC. International Agency for Research on Cancer (IARC) - Summaries & Evaluations, Styrene (IPCS-INCHEM)(1994b), pp. 233.
144. Jennings, GT, Sechi, S, Stevenson, PM, Tuckey, RC, Parmelee, D and McAlister-Henn, L. Cytosolic NADP(+)-dependent isocitrate dehydrogenase. Isolation of rat cDNA and study of tissue-specific and developmental expression of mRNA. *J Biol Chem* 1994;269:23128-23134.
145. Jensen, LJ, Kuhn, M, Stark, M, Chaffron, S, Creevey, C, Muller, J, Doerks, T, Julien, P, Roth, A, Simonovic, M *et al.* STRING 8--a global view on proteins and their functional interactions in 630 organisms. *Nucleic Acids Res* 2009;37:D412-416.
146. Jia, C, Batterman, S and Godwin, C. Continuous, intermittent and passive sampling of airborne VOCs. *J Environ Monit* 2007;9:1220-1230.
147. Jiang, H, Wang, XF, Fang, L, Tang, C, Zhu, Y and Wang, X. Upregulation of aldose reductase by homocysteine in type II alveolar epithelial cells. *Biochem Biophys Res Commun* 2005;337:1084-1091.
148. Jin, DY, Chae, HZ, Rhee, SG and Jeang, KT. Regulatory role for a novel human thioredoxin peroxidase in NF-kappaB activation. *J Biol Chem* 1997;272:30952-30961.
149. Jin, M, Diaz, PT, Bourgeois, T, Eng, C, Marsh, CB and Wu, HM. Two-dimensional gel proteome reference map of blood monocytes. *Proteome Sci* 2006;4:16.
150. Johanson, G and Filser, JG. Experimental data from closed chamber gas uptake studies in rodents suggest lower uptake rate of chemical than calculated from literature values on alveolar ventilation. *Arch Toxicol* 1992;66:291-295.
151. Jung, H, Seong, HA and Ha, H. NM23-H1 tumor suppressor and its interacting partner STRAP activate p53 function. *J Biol Chem* 2007;282:35293-35307.
152. Jung, H, Seong, HA, Manoharan, R and Ha, H. Serine-threonine kinase receptor-associated protein inhibits apoptosis signal-regulating kinase 1 function through direct interaction. *J Biol Chem* 2010;285:54-70.
153. Kagi, N, Fujii, S and Horiba, Y. Indoor air quality for chemical and ultrafine particle contaminants from printers. *Build Environ* 2007;42:1949-1954.
154. Kanemaki, M, Kurokawa, Y, Matsu-ura, T, Makino, Y, Masani, A, Okazaki, K, Morishita, T and Tamura, TA. TIP49b, a new RuvB-like DNA helicase, is included in a complex together with another RuvB-like DNA helicase, TIP49a. *J Biol Chem* 1999;274:22437-22444.
155. Kaufmann, W, Mellert, W, van Ravenzwaay, B, Landsiedel, R and Poole, A. Effects of styrene and its metabolites on different lung compartments of the mouse--cell proliferation and histomorphology. *Regul Toxicol Pharmacol* 2005;42:24-36.
156. Kaul, R, Verma, SC, Murakami, M, Lan, K, Choudhuri, T and Robertson, ES. Epstein-Barr virus protein can upregulate cyclo-oxygenase-2 expression through association with the suppressor of metastasis Nm23-H1. *J Virol* 2006;80:1321-1331.
157. Kenaga, EE. Predicted bioconcentration factors and soil sorption coefficients of pesticides and other chemicals. *Ecotoxicol Environ Safety* 1980;4:26-38.
158. Kile, BT, Panopoulos, AD, Stirzaker, RA, Hacking, DF, Tahtamouni, LH, Willson, TA, Mielke, LA, Henley, KJ, Zhang, JG, Wicks, IP *et al.* Mutations in the cofilin partner Aip1/Wdr1 cause autoinflammatory disease and macrothrombocytopenia. *Blood* 2007;110:2371-2380.
159. Kim, JW and Dang, CV. Multifaceted roles of glycolytic enzymes. *Trends Biochem Sci* 2005;30:142-150.
160. Kinney, PL, Chillrud, SN, Ramstrom, S, Ross, J and Spengler, JD. Exposures to multiple air toxics in New York City. *Environ Health Perspect* 2002;110 Suppl 4:539-546.
161. Klose, J. Protein mapping by combined isoelectric focusing and electrophoresis of mouse tissues. A novel approach to testing for induced point mutations in mammals. *Humangenetik* 1975;26:231-243.
162. Kolstad, HA, Juel, K, Olsen, J and Lynge, E. Exposure to styrene and chronic health effects: mortality and incidence of solid cancers in the Danish reinforced plastics industry. *Occup Environ Med* 1995;52:320-327.

163. Kondoh, H, Leonart, ME, Bernard, D and Gil, J. Protection from oxidative stress by enhanced glycolysis; a possible mechanism of cellular immortalization. *Histol Histopathol* 2007;22:85-90.
164. Kozar, RA, Weibel, CJ, Cipolla, J, Klein, AJ, Haber, MM, Abedin, MZ and Trooskin, SZ. Antioxidant enzymes are induced during recovery from acute lung injury. *Crit Care Med* 2000;28:2486-2491.
165. Krebs, J and Klemenz, R. The ALG-2/AIP-complex, a modulator at the interface between cell proliferation and cell death? A hypothesis. *Biochim Biophys Acta* 2000;1498:153-161.
166. Krewet, E, Muller, G and Norpoth, K. The excretion of chlorophenylmercapturic acid, chlorophenols and a guanine adduct in the urine of chlorobenzene-treated rats after phenobarbital pretreatment. *Toxicology* 1989;59:67-79.
167. Kubo, E, Hasanova, N, Tanaka, Y, Fatma, N, Takamura, Y, Singh, DP and Akagi, Y. Protein expression profiling of lens epithelial cells from Prdx6-depleted mice and their vulnerability to UV radiation exposure. *Am J Physiol Cell Physiol* 2010;298:C342-354.
168. Kulkarni, SG, Duong, H, Gomila, R and Mehendale, HM. Strain differences in tissue repair response to 1,2-dichlorobenzene. *Arch Toxicol* 1996;70:714-723.
169. Kumagai, S and Matsunaga, I. Effect of variation of exposure to airborne chlorobenzene on internal exposure and concentrations of urinary metabolite. *Occup Environ Med* 1995;52:65-70.
170. Kusters, E and Lauwerys, R. Biological monitoring of exposure to monochlorobenzene. *Int Arch Occup Environ Health* 1990;62:329-331.
171. Kwon, KD, Jo, WK, Lim, HJ and Jeong, WS. Volatile pollutants emitted from selected liquid household products. *Environ Sci Pollut Res Int* 2008;15:521-526.
172. Lachaise, F, Martin, G, Drougard, C, Perl, A, Vuillaume, M, Wegnez, M, Sarasin, A and Daya-Grosjean, L. Relationship between posttranslational modification of transaldolase and catalase deficiency in UV-sensitive repair-deficient xeroderma pigmentosum fibroblasts and SV40-transformed human cells. *Free Radic Biol Med* 2001;30:1365-1373.
173. Lamberti, A, Longo, O, Marra, M, Tagliaferri, P, Bismuto, E, Fiengo, A, Viscomi, C, Budillon, A, Rapp, UR, Wang, E *et al.* C-Raf antagonizes apoptosis induced by IFN-alpha in human lung cancer cells by phosphorylation and increase of the intracellular content of elongation factor 1A. *Cell Death Differ* 2007;14:952-962.
174. Lanosa, MJ, Willis, DN, Jordt, S and Morris, JB. Role of metabolic activation and the TRPA1 receptor in the sensory irritation response to styrene and naphthalene. *Toxicol Sci* 2010;115:589-595.
175. Lazrak, A, Samanta, A and Matalon, S. Biophysical properties and molecular characterization of amiloride-sensitive sodium channels in A549 cells. *Am J Physiol Lung Cell Mol Physiol* 2000;278:L848-857.
176. Lee, E, Jeong, J, Kim, SE, Song, EJ, Kang, SW and Lee, KJ. Multiple functions of Nm23-H1 are regulated by oxido-reduction system. *PLoS One* 2009;4:e7949.
177. Lee, HZ, Wu, CH and Chang, SP. Release of nucleophosmin from the nucleus: Involvement in aloe-emodin-induced human lung non small carcinoma cell apoptosis. *Int J Cancer* 2005;113:971-976.
178. Lee, JH, Kim, SY, Kil, IS and Park, JW. Regulation of ionizing radiation-induced apoptosis by mitochondrial NADP⁺-dependent isocitrate dehydrogenase. *J Biol Chem* 2007;282:13385-13394.
179. Lee, SM, Koh, HJ, Park, DC, Song, BJ, Huh, TL and Park, JW. Cytosolic NADP(+)-dependent isocitrate dehydrogenase status modulates oxidative damage to cells. *Free Radic Biol Med* 2002;32:1185-1196.
180. Lehmann, I, Rehwagen, M, Diez, U, Seiffart, A, Rolle-Kampczyk, U, Richter, M, Wetzig, H, Borte, M and Herbarth, O. Enhanced in vivo IgE production and T cell polarization toward the type 2 phenotype in association with indoor exposure to VOC: results of the LARS study. *Int J Hyg Environ Health* 2001;204:211-221.
181. Lehmann, I, Roder-Stolinski, C, Nieber, K and Fischader, G. In vitro models for the assessment of inflammatory and immuno-modulatory effects of the volatile organic compound chlorobenzene. *Exp Toxicol Pathol* 2008;60:185-193.
182. Lehmann, I, Thielke, A, Rehwagen, M, Rolle-Kampczyk, U, Schlink, U, Schulz, R, Borte, M, Diez, U and Herbarth, O. The influence of maternal exposure to volatile organic compounds on the cytokine secretion profile of neonatal T cells. *Environ Toxicol* 2002a;17:203-210.
183. Lehmann, I, Thielke, A, Weiss, M, Schlink, U, Schulz, R, Diez, U, Sierig, G, Emmrich, F, Jacob, B, Belcredi, P *et al.* T cell reactivity in neonates from an East and a West German city--results of the LISA study. *Allergy* 2002b;57:129-136.

184. Lekmine, F, Sassano, A, Uddin, S, Smith, J, Majchrzak, B, Brachmann, SM, Hay, N, Fish, EN and Plataniias, LC. Interferon-gamma engages the p70 S6 kinase to regulate phosphorylation of the 40S S6 ribosomal protein. *Exp Cell Res* 2004;295:173-182.
185. Lelli, SM, San Martin de Viale, LC and Mazzetti, MB. Response of glucose metabolism enzymes in an acute porphyria model. Role of reactive oxygen species. *Toxicology* 2005;216:49-58.
186. Lentsch, AB and Ward, PA. The NFkappaB/IkappaB system in acute inflammation. *Arch Immunol Ther Exp (Warsz)* 2000;48:59-63.
187. Leovic, KW, Sheldon, LS and Whitaker, DA. Measurement of indoor air emissions from dryprocess photocopy machines. *J Air Waste Manage Assoc* 1996;46:821-829.
188. Li, X, Zhuang, Z, Liu, J, Huang, H, Wei, Q and Yang, X. Proteomic analysis to identify the cellular responses induced by hydroquinone in human embryonic lung fibroblasts. *Toxicol Mech Methods* 2006;16:1-6.
189. Linke, T, Doraiswamy, S and Harrison, EH. Rat plasma proteomics: effects of abundant protein depletion on proteomic analysis. *J Chromatogr B Analyt Technol Biomed Life Sci* 2007;849:273-281.
190. Lopachin, RM and Decaprio, AP. Protein adduct formation as a molecular mechanism in neurotoxicity. *Toxicol Sci* 2005;86:214-225.
191. MacCoss, MJ, McDonald, WH, Saraf, A, Sadygov, R, Clark, JM, Tasto, JJ, Gould, KL, Wolters, D, Washburn, M, Weiss, A *et al.* Shotgun identification of protein modifications from protein complexes and lens tissue. *Proc Natl Acad Sci U S A* 2002;99:7900-7905.
192. Maddika, S and Chen, J. Protein kinase DYRK2 is a scaffold that facilitates assembly of an E3 ligase. *Nat Cell Biol* 2009;11:409-419.
193. Mahul-Mellier, AL, Strappazzon, F, Petiot, A, Chatellard-Causse, C, Torch, S, Blot, B, Freeman, K, Kuhn, L, Garin, J, Verna, JM *et al.* Alix and ALG-2 are involved in tumor necrosis factor receptor 1-induced cell death. *J Biol Chem* 2008;283:34954-34965.
194. Manini, P, Andreoli, R, Poli, D, De Palma, G, Mutti, A and Niessen, WM. Liquid chromatography/electrospray tandem mass spectrometry characterization of styrene metabolism in man and in rat. *Rapid Commun Mass Spectrom* 2002;16:2239-2248.
195. Marczynski, B, Peel, M and Baur, X. Changes in high molecular weight DNA fragmentation following human blood exposure to styrene-7,8-oxide. *Toxicology* 1997;120:111-117.
196. Martin, HJ, Breyer-Pfaff, U, Wsol, V, Venz, S, Block, S and Maser, E. Purification and characterization of akr1b10 from human liver: role in carbonyl reduction of xenobiotics. *Drug Metab Dispos* 2006;34:464-470.
197. Matsuoka, S, Ballif, BA, Smogorzewska, A, McDonald, ER, 3rd, Hurov, KE, Luo, J, Bakalarski, CE, Zhao, Z, Solimini, N, Lerenthal, Y *et al.* ATM and ATR substrate analysis reveals extensive protein networks responsive to DNA damage. *Science* 2007;316:1160-1166.
198. McDermott, C, O'Donoghue, MH and Heffron, JJ. n-Hexane toxicity in Jurkat T-cells is mediated by reactive oxygen species. *Arch Toxicol* 2008;82:165-171.
199. McIntosh, JM and Heffron, JJA. Modelling alterations in the partition coefficient in in vitro biological systems using headspace gas chromatography. *Journal of Chromatography B: Biomedical Sciences and Applications* 2000;738:207-216.
200. Mehlen, P, Schulze-Osthoff, K and Arrigo, AP. Small stress proteins as novel regulators of apoptosis. Heat shock protein 27 blocks Fas/APO-1- and staurosporine-induced cell death. *J Biol Chem* 1996;271:16510-16514.
201. Melnick, RL. Carcinogenicity and mechanistic insights on the behavior of epoxides and epoxide-forming chemicals. *Ann N Y Acad Sci* 2002;982:177-189.
202. Mendell, MJ. Indoor residential chemical emissions as risk factors for respiratory and allergic effects in children: a review. *Indoor Air* 2007;17:259-277.
203. Merrick, BA and Witzmann, FA. The role of toxicoproteomics in assessing organ specific toxicity. *EXS* 2009;99:367-400.
204. Merz, T. VOC – komplexe Krankheitsbilder durch zelluläre Multifunktionsstörungen. *Umwelt-Medizin-Gesellschaft* 2004;17:46-56.
205. Meyer, U, Schweim, P, Fracella, F and Rensing, L. Close Correlation between Heat Shock Response and Cytotoxicity in *Neurospora crassa* Treated with Aliphatic Alcohols and Phenols. *Appl Environ Microbiol* 1995;61:979-984.
206. Michalowicz, J and Sicinska, P. Chlorophenols and chlorocatechols induce apoptosis in human lymphocytes (in vitro). *Toxicol Lett* 2009;191:246-252.

207. Migita, T, Narita, T, Nomura, K, Miyagi, E, Inazuka, F, Matsuura, M, Ushijima, M, Mashima, T, Seimiya, H, Satoh, Y *et al.* ATP citrate lyase: activation and therapeutic implications in non-small cell lung cancer. *Cancer Res* 2008;68:8547-8554.
208. Moore, DJ, Dawson, VL and Dawson, TM. Lessons from *Drosophila* models of DJ-1 deficiency. *Sci Aging Knowledge Environ* 2006;2006:pe2.
209. Morita, M. Chlorinated benzenes in the environment. *Ecotoxicol Environ Saf* 1977;1:1-6.
210. Mourtada-Maarabouni, M, Kirkham, L, Farzaneh, F and Williams, GT. Functional expression cloning reveals a central role for the receptor for activated protein kinase C 1 (RACK1) in T cell apoptosis. *J Leukoc Biol* 2005;78:503-514.
211. Mustacich, D and Powis, G. Thioredoxin reductase. *Biochem J* 2000;346 Pt 1:1-8.
212. Myung, JK, Afjehi-Sadat, L, Felizardo-Cabatic, M, Slavc, I and Lubec, G. Expressional patterns of chaperones in ten human tumor cell lines. *Proteome Sci* 2004;2:pp 8.
213. Nakajima, T, Elovaara, E, Gonzalez, FJ, Gelboin, HV, Raunio, H, Pelkonen, O, Vainio, H and Aoyama, T. Styrene metabolism by cDNA-expressed human hepatic and pulmonary cytochromes P450. *Chem Res Toxicol* 1994;7:891-896.
214. Nedelcheva, V, Gut, I, Soucek, P and Frantik, E. Cytochrome P450 catalyzed oxidation of monochlorobenzene, 1,2- and 1,4-dichlorobenzene in rat, mouse, and human liver microsomes. *Chem Biol Interact* 1998;115:53-70.
215. Neuhaus-Steinmetz, U and Rensing, L. Heat shock protein induction by certain chemical stressors is correlated with their cytotoxicity, lipophilicity and protein-denaturing capacity. *Toxicology* 1997;123:185-195.
216. Neuhoff, V, Arold, N, Taube, D and Ehrhardt, W. Improved staining of proteins in polyacrylamide gels including isoelectric focusing gels with clear background at nanogram sensitivity using Coomassie Brilliant Blue G-250 and R-250. *Electrophoresis* 1988;9:255-262.
217. NIOSH. NIOH and NIOSH basis for an occupational standard: Chlorobenzene, ed. (Cincinnati, OH, National Institute for Occupational Safety and Health)(1993)
218. Nordberg, J, Zhong, L, Holmgren, A and Arner, ES. Mammalian thioredoxin reductase is irreversibly inhibited by dinitrohalobenzenes by alkylation of both the redox active selenocysteine and its neighboring cysteine residue. *J Biol Chem* 1998;273:10835-10842.
219. NTP. NTP Toxicology and Carcinogenesis Studies of 1,2-Dichlorobenzene (o-Dichlorobenzene) (CAS No. 95-50-1) in F344/N Rats and B6C3F1 Mice (Gavage Studies). *Natl Toxicol Program Tech Rep Ser* 1985;255:1-195.
220. Nunez, A, Franco, A, Madrid, M, Soto, T, Vicente, J, Gacto, M and Cansado, J. Role for RACK1 orthologue Cpc2 in the modulation of stress response in fission yeast. *Mol Biol Cell* 2009;20:3996-4009.
221. O'Farrell, PH. High resolution two-dimensional electrophoresis of proteins. *J Biol Chem* 1975;250:4007-4021.
222. Odabaei, G, Chatterjee, D, Jazirehi, AR, Goodglick, L, Yeung, K and Bonavida, B. Raf-1 kinase inhibitor protein: structure, function, regulation of cell signaling, and pivotal role in apoptosis. *Adv Cancer Res* 2004;91:169-200.
223. OECD. Screening Information DataSet (SIDS), Initial Assessment Report For SIAM 13: 1,2-Dichlorobenzene (Bern, United Nations Environment Programme)(2005)
224. Orsatti, L, Forte, E, Tomei, L, Caterino, M, Pessi, A and Talamo, F. 2-D Difference in gel electrophoresis combined with Pro-Q Diamond staining: a successful approach for the identification of kinase/phosphatase targets. *Electrophoresis* 2009;30:2469-2476.
225. Palackal, NT, Lee, SH, Harvey, RG, Blair, IA and Penning, TM. Activation of polycyclic aromatic hydrocarbon trans-dihydrodiol proximate carcinogens by human aldo-keto reductase (AKR1C) enzymes and their functional overexpression in human lung carcinoma (A549) cells. *J Biol Chem* 2002;277:24799-24808.
226. Panasyuk, G, Nemazanyy, I, Filonenko, V, Negrutskii, B and El'skaya, AV. A2 isoform of mammalian translation factor eEF1A displays increased tyrosine phosphorylation and ability to interact with different signalling molecules. *Int J Biochem Cell Biol* 2008;40:63-71.
227. Pandey, P, Farber, R, Nakazawa, A, Kumar, S, Bharti, A, Nalin, C, Weichselbaum, R, Kufe, D and Kharbanda, S. Hsp27 functions as a negative regulator of cytochrome c-dependent activation of procaspase-3. *Oncogene* 2000;19:1975-1981.
228. Papakonstanti, EA and Stournaras, C. Association of PI-3 kinase with PAK1 leads to actin phosphorylation and cytoskeletal reorganization. *Mol Biol Cell* 2002;13:2946-2962.

229. Pappas, GP, Herbert, RJ, Henderson, W, Koenig, J, Stover, B and Barnhart, S. The respiratory effects of volatile organic compounds. *Int J Occup Environ Health* 2000;6:1-8.
230. Park, KJ, Gaynor, RB and Kwak, YT. Heat shock protein 27 association with the I kappa B kinase complex regulates tumor necrosis factor alpha-induced NF-kappa B activation. *J Biol Chem* 2003;278:35272-35278.
231. Pellizzari, ED, Hartwell, TD, Harris, BS, 3rd, Waddell, RD, Whitaker, DA and Erickson, MD. Purgeable organic compounds in mother's milk. *Bull Environ Contam Toxicol* 1982;28:322-328.
232. Penning, TM and Drury, JE. Human aldo-keto reductases: Function, gene regulation, and single nucleotide polymorphisms. *Arch Biochem Biophys* 2007;464:241-250.
233. Petranovic, D, Grangeasse, C, Macek, B, Abdillatef, M, Gueguen-Chaignon, V, Nessler, S, Deutscher, J and Mijakovic, I. Activation of *Bacillus subtilis* Ugd by the BY-kinase PtkA proceeds via phosphorylation of its residue tyrosine 70. *J Mol Microbiol Biotechnol* 2009;17:83-89.
234. Phillips, DH and Farmer, PB. Evidence for DNA and protein binding by styrene and styrene oxide. *Crit Rev Toxicol* 1994;24 Suppl:S35-46.
235. Ping, P. Identification of novel signaling complexes by functional proteomics. *Circ Res* 2003;93:595-603.
236. Polla, BS and Cossarizza, A. Stress proteins in inflammation. *EXS* 1996;77:375-391.
237. Prieto-Castello, MJ, Cardona, A, Marhuenda, D, Roel, JM and Corno, A. Use of the CYP2E1 genotype and phenotype for the biological monitoring of occupational exposure to styrene. *Toxicol Lett* 2010;192:34-39.
238. Prosperi, E, Scovassi, AI, Stivala, LA and Bianchi, L. Proliferating cell nuclear antigen bound to DNA synthesis sites: phosphorylation and association with cyclin D1 and cyclin A. *Exp Cell Res* 1994;215:257-262.
239. Rahman, I and MacNee, W. Oxidative stress and regulation of glutathione in lung inflammation. *Eur Respir J* 2000;16:534-554.
240. Rehwagen, M, Schlink, U and Herbarth, O. Seasonal cycle of VOCs in apartments. *Indoor Air* 2003;13:283-291.
241. Rhee, HJ, Kim, GY, Huh, JW, Kim, SW and Na, DS. Annexin I is a stress protein induced by heat, oxidative stress and a sulfhydryl-reactive agent. *Eur J Biochem* 2000;267:3220-3225.
242. Rho, HK, Park, J, Suh, JH and Kim, JB. Transcriptional regulation of mouse 6-phosphogluconate dehydrogenase by ADD1/SREBP1c. *Biochem Biophys Res Commun* 2005;332:288-296.
243. Rietjens, IM, den Besten, C, Hanzlik, RP and van Bladeren, PJ. Cytochrome P450-catalyzed oxidation of halobenzene derivatives. *Chem Res Toxicol* 1997;10:629-635.
244. Roder-Stolinski, C, Fischader, G, Oostingh, GJ, Eder, K, Duschl, A and Lehmann, I. Chlorobenzene induces the NF-kappa B and p38 MAP kinase pathways in lung epithelial cells. *Inhal Toxicol* 2008a;20:813-820.
245. Roder-Stolinski, C, Fischader, G, Oostingh, GJ, Feltens, R, Kohse, F, von Bergen, M, Morbt, N, Eder, K, Duschl, A and Lehmann, I. Styrene induces an inflammatory response in human lung epithelial cells via oxidative stress and NF-kappaB activation. *Toxicol Appl Pharmacol* 2008b;231:241-247.
246. Roggen, EL, Soni, NK and Verheyen, GR. Respiratory immunotoxicity: an in vitro assessment. *Toxicol In Vitro* 2006;20:1249-1264.
247. Roth, J, Yam, GH, Fan, J, Hirano, K, Gaplovska-Kysela, K, Le Fourn, V, Guhl, B, Santimaria, R, Torossi, T, Ziak, M *et al.* Protein quality control: the who's who, the where's and therapeutic escapes. *Histochem Cell Biol* 2008;129:163-177.
248. Rothen-Rutishauser, BM, Kiama, SG and Gehr, P. A three-dimensional cellular model of the human respiratory tract to study the interaction with particles. *Am J Respir Cell Mol Biol* 2005;32:281-289.
249. Rousseau, B, Menard, L, Haurie, V, Taras, D, Blanc, JF, Moreau-Gaudry, F, Metzler, P, Hugues, M, Boyault, S, Lemièrre, S *et al.* Overexpression and role of the ATPase and putative DNA helicase RuvB-like 2 in human hepatocellular carcinoma. *Hepatology* 2007;46:1108-1118.
250. Rumchev, K, Spickett, J, Bulsara, M, Phillips, M and Stick, S. Association of domestic exposure to volatile organic compounds with asthma in young children. *Thorax* 2004;59:746-751.
251. Rush, J, Moritz, A, Lee, KA, Guo, A, Goss, VL, Spek, EJ, Zhang, H, Zha, XM, Polakiewicz, RD and Comb, MJ. Immunoaffinity profiling of tyrosine phosphorylation in cancer cells. *Nat Biotechnol* 2005;23:94-101.
252. Samet, JM, Marbury, MC and Spengler, JD. Respiratory effects of indoor air pollution. *J Allergy Clin Immunol* 1987;79:685-700.

253. Samoto, H, Fukui, Y, Ukai, H, Okamoto, S, Takada, S, Ohashi, F, Moriguchi, J, Ezaki, T and Ikeda, M. Field survey on types of organic solvents used in enterprises of various sizes. *International Archives of Occupational and Environmental Health* 2006;79:558-567.
254. Sanders, LC, Matsumura, F, Bokoch, GM and de Lanerolle, P. Inhibition of myosin light chain kinase by p21-activated kinase. *Science* 1999;283:2083-2085.
255. Sarma, SN, Kim, YJ and Ryu, JC. Gene expression profiles of human promyelocytic leukemia cell lines exposed to volatile organic compounds. *Toxicology* 2010;271:122-130.
256. Sato, A and Nakajima, T. Partition coefficients of some aromatic hydrocarbons and ketones in water, blood and oil. *Br J Ind Med* 1979;36:231-234.
257. Schaeffer, VH, Bhooshan, B and Chen, S-B. Characterization of volatile organic chemical emissions from carpet cushions. *J Air Waste Manage Assoc* 1996;46:813-820.
258. Scheele, GA. Two-dimensional gel analysis of soluble proteins. Characterization of guinea pig exocrine pancreatic proteins. *J Biol Chem* 1975;250:5375-5385.
259. Schmidt, MH, Dikic, I and Bogler, O. Src phosphorylation of Alix/AIP1 modulates its interaction with binding partners and antagonizes its activities. *J Biol Chem* 2005;280:3414-3425.
260. Schremmer, B, Manevich, Y, Feinstein, SI and Fisher, AB. Peroxiredoxins in the lung with emphasis on peroxiredoxin VI. *Subcell Biochem* 2007;44:317-344.
261. Sheets, PL, Yost, GS and Carlson, GP. Benzene metabolism in human lung cell lines BEAS-2B and A549 and cells overexpressing CYP2F1. *J Biochem Mol Toxicol* 2004;18:92-99.
262. Shen, S, Zhang, F, Zeng, S, Tian, Y, Chai, X, Gee, S, Hammock, BD and Zheng, J. Development of enantioselective polyclonal antibodies to detect styrene oxide protein adducts. *Anal Chem* 2009;81:2668-2677.
263. Shenton, D and Grant, CM. Protein S-thiolation targets glycolysis and protein synthesis in response to oxidative stress in the yeast *Saccharomyces cerevisiae*. *Biochem J* 2003;374:513-519.
264. Shisheva, A, Chinni, SR and DeMarco, C. General role of GDP dissociation inhibitor 2 in membrane release of Rab proteins: modulations of its functional interactions by in vitro and in vivo structural modifications. *Biochemistry* 1999;38:11711-11721.
265. Singer, R. *Neurotoxicity Guidebook*, Vol New York, Van Nostrand Reinhold(1990).
266. Singh, H and Ashley, RH. Redox regulation of CLIC1 by cysteine residues associated with the putative channel pore. *Biophys J* 2006;90:1628-1638.
267. Slaughter, DE and Hanzlik, RP. Identification of epoxide- and quinone-derived bromobenzene adducts to protein sulfur nucleophiles. *Chem Res Toxicol* 1991;4:349-359.
268. Slebos, DJ, Ryter, SW and Choi, AM. Heme oxygenase-1 and carbon monoxide in pulmonary medicine. *Respir Res* 2003;4:7.
269. Slebos, DJ, Ryter, SW, van der Toorn, M, Liu, F, Guo, F, Baty, CJ, Karlsson, JM, Watkins, SC, Kim, HP, Wang, X *et al*. Mitochondrial localization and function of heme oxygenase-1 in cigarette smoke-induced cell death. *Am J Respir Cell Mol Biol* 2007;36:409-417.
270. Sripathi, CE and Cuny, M. Phosphorylation of a 40S ribosomal subunit protein in *Tetrahymena*. Lack of correlation with cellular growth and ribosome stability. *Eur J Biochem* 1987;162:669-674.
271. Stearns, RC, Paulauskis, JD and Godleski, JJ. Endocytosis of ultrafine particles by A549 cells. *Am J Respir Cell Mol Biol* 2001;24:108-115.
272. Stehfest, E, Torky, A, Glahn, F and Foth, H. Non-destructive micromethod for MRP1 functional assay in human lung tumor cells. *Arch Toxicol* 2006;80:125-133.
273. Steinemann, AC. *Fragranced consumer products and undisclosed ingredients Environmental Impact Assessment Review* 2009;29:32-38.
274. Stone, JR, Maki, JL and Collins, T. Basal and hydrogen peroxide stimulated sites of phosphorylation in heterogeneous nuclear ribonucleoprotein C1/C2. *Biochemistry* 2003;42:1301-1308.
275. Sumner, SC, Cattley, RC, Asgharian, B, Janszen, DB and Fennell, TR. Evaluation of the metabolism and hepatotoxicity of styrene in F344 rats, B6C3F1 mice, and CD-1 mice following single and repeated inhalation exposures. *Chem Biol Interact* 1997;106:47-65.
276. Sur, R, Lyte, PA and Southall, MD. Hsp27 regulates pro-inflammatory mediator release in keratinocytes by modulating NF-kappaB signaling. *J Invest Dermatol* 2008;128:1116-1122.
277. Tähti, H. *The Neurotoxicity of Organic Solvents, Studied with In vitro models*. *ATLA* 1992;20:290-296.
278. Takeoko, GR, Flath, RA and Guntert, M. Nectarine volatiles: Vacuum steam distillation versus headspace. *J Agric Food Chem* 1988;36:553-560.

279. Tang, J, Jin, QZ and Shen, GH. Isolation and identification of volatile compounds from fried chicken. *J Agric Food Chem* 1983;31:1287-1292.
280. Tang, W, Hemm, I and Eisenbrand, G. Estimation of human exposure to styrene and ethylbenzene. *Toxicology* 2000;144:39-50.
281. Taylor, CA, Sun, Z, Cliche, DO, Ming, H, Eshaque, B, Jin, S, Hopkins, MT, Thai, B and Thompson, JE. Eukaryotic translation initiation factor 5A induces apoptosis in colon cancer cells and associates with the nucleus in response to tumour necrosis factor alpha signalling. *Exp Cell Res* 2007;313:437-449.
282. Teixeira, JP, Gaspar, J, Roma-Torres, J, Silva, S, Costa, C, Roach, J, Mayan, O, Rueff, J and Farmer, PB. Styrene-oxide N-terminal valine haemoglobin adducts in reinforced plastic workers: possible influence of genetic polymorphism of drug-metabolising enzymes. *Toxicology* 2007;237:58-64.
283. Tian, Q, Stepaniants, SB, Mao, M, Weng, L, Feetham, MC, Doyle, MJ, Yi, EC, Dai, H, Thorsson, V, Eng, J *et al.* Integrated genomic and proteomic analyses of gene expression in Mammalian cells. *Mol Cell Proteomics* 2004;3:960-969.
284. Timbrell, JA. Biomarkers in toxicology. *Toxicology* 1998;129:1-12.
285. Tisdale, EJ, Azizi, F and Artalejo, CR. Rab2 utilizes glyceraldehyde-3-phosphate dehydrogenase and protein kinase C $\{\iota\}$ to associate with microtubules and to recruit dynein. *J Biol Chem* 2009;284:5876-5884.
286. Topouzová-Hristova, T, Hazarosova, R, Bandreva, B and Stephanova, E. Halothane Does Not Directly Interact with Genome DNA of A549 Cells. *Folia Biol (Praha)* 2007;53:176-182.
287. Tuck, SA, Ramos-Barbon, D, Campbell, H, McGovern, T, Karmouty-Quintana, H and Martin, JG. Time course of airway remodelling after an acute chlorine gas exposure in mice. *Respir Res* 2008;9:61.
288. UBA. Hintergrundinformation: Sommersmog (Berlin, Umweltbundesamt)(2005), pp. 1-25.
289. Urban, B. Current assessment of targetd and theories of anaesthesia. *Br J Anaesth* 2004;89:167-183.
290. Vaghef, H and Hellman, B. Demonstration of chlorobenzene-induced DNA damage in mouse lymphocytes using the single cell gel electrophoresis assay. *Toxicology* 1995;96:19-28.
291. van Wijk, D, Thompson, RS, De Rooij, C, Garny, V, Lecloux, A and Kanne, R. 1,2-dichlorobenzene marine risk assessment with special reference to the OSPARCOM region: North Sea. *Environ Monit Assess* 2004;97:87-102.
292. Vettori, MV, Caglieri, A, Goldoni, M, Castoldi, AF, Dare, E, Alinovi, R, Ceccatelli, S and Mutti, A. Analysis of oxidative stress in SK-N-MC neurons exposed to styrene-7,8-oxide. *Toxicol In Vitro* 2005;19:11-20.
293. Vlaanderen, J, Moore, LE, Smith, MT, Lan, Q, Zhang, L, Skibola, CF, Rothman, N and Vermeulen, R. Application of OMICS technologies in occupational and environmental health research; current status and projections. *Occup Environ Med* 2010;67:136-143.
294. Vodicka, P, Koskinen, M, Stetina, R, Soucek, P, Vodickova, L, Matousu, Z, Kuricova, M and Hemminki, K. The role of various biomarkers in the evaluation of styrene genotoxicity. *Cancer Detect Prev* 2003;27:275-284.
295. Vodicka, PE, Linhart, I, Novak, J, Koskinen, M, Vodickova, L and Hemminki, K. 7-Alkylguanine adduct levels in urine, lungs and liver of mice exposed to styrene by inhalation. *Toxicol Appl Pharmacol* 2006;210:1-8.
296. Voellmy, R. Sensing stress and responding to stress. *EXS* 1996;77:121-137.
297. Von Burg, R. Monochlorobenzene. *J Appl Toxicol* 1981;1:50-51.
298. Wagner, PD and Vu, ND. Histidine to aspartate phosphotransferase activity of nm23 proteins: phosphorylation of aldolase C on Asp-319. *Biochem J* 2000;346 Pt 3:623-630.
299. Wallace, L, Pellizzari, E, Hartwell, TD, Perritt, R and Ziegenfus, R. Exposures to benzene and other volatile compounds from active and passive smoking. *Arch Environ Health* 1987;42:272-279.
300. Wang, CJ, Shao, H, Shang, M and Zhang, W. [Association between CYP2B6, CYP2D6, GSTP1 genetic polymorphisms and urinary styrene metabolites in professional workers.]. *Zhonghua Lao Dong Wei Sheng Zhi Ye Bing Za Zhi* 2009;27:589-592.
301. Wang, JY. DNA damage and apoptosis. *Cell Death Differ* 2001;8:1047-1048.
302. Wang, SC, Nakajima, Y, Yu, YL, Xia, W, Chen, CT, Yang, CC, McIntush, EW, Li, LY, Hawke, DH, Kobayashi, R *et al.* Tyrosine phosphorylation controls PCNA function through protein stability. *Nat Cell Biol* 2006;8:1359-1368.

303. Ware, JH, Spengler, JD, Neas, LM, Samet, JM, Wagner, GR, Coultas, D, Ozkaynak, H and Schwab, M. Respiratory and irritant health effects of ambient volatile organic compounds. The Kanawha County Health Study. *Am J Epidemiol* 1993;137:1287-1301.
304. Wetmore, BA and Merrick, BA. Toxicoproteomics: proteomics applied to toxicology and pathology. *Toxicol Pathol* 2004;32:619-642.
305. Wheelock, AM, Boland, BC, Isbell, M, Morin, D, Wegesser, TC, Plopper, CG and Buckpitt, AR. In vivo effects of ozone exposure on protein adduct formation by 1-nitronaphthalene in rat lung. *Am J Respir Cell Mol Biol* 2005;33:130-137.
306. Whilite, CC and Book, SA. Toxicology update. Monochlorobenzene. *J Appl Toxicol* 1990;10:307-310.
307. White, CW, Avraham, KB, Shanley, PF and Groner, Y. Transgenic mice with expression of elevated levels of copper-zinc superoxide dismutase in the lungs are resistant to pulmonary oxygen toxicity. *J Clin Invest* 1991;87:2162-2168.
308. White, SR, Williams, P, Wojcik, KR, Sun, S, Hiemstra, PS, Rabe, KF and Dorscheid, DR. Initiation of apoptosis by actin cytoskeletal derangement in human airway epithelial cells. *Am J Respir Cell Mol Biol* 2001;24:282-294.
309. Whitlock, NA, Lindsey, K, Agarwal, N, Crosson, CE and Ma, JX. Heat shock protein 27 delays Ca²⁺-induced cell death in a caspase-dependent and -independent manner in rat retinal ganglion cells. *Invest Ophthalmol Vis Sci* 2005;46:1085-1091.
310. Wieczorek, H. Evaluation of low exposure to styrene. II. Dermal absorption of styrene vapours in humans under experimental conditions. *Int Arch Occup Environ Health* 1985;57:71-75.
311. Wieslander, G, Janson, C, Norback, D, Bjornsson, E, Stalenheim, G and Edling, C. Occupational exposure to water-based paints and self-reported asthma, lower airway symptoms, bronchial hyperresponsiveness, and lung function. *Int Arch Occup Environ Health* 1994;66:261-267.
312. Wieslander, G, Norback, D, Bjornsson, E, Janson, C and Boman, G. Asthma and the indoor environment: the significance of emission of formaldehyde and volatile organic compounds from newly painted indoor surfaces. *Int Arch Occup Environ Health* 1997a;69:115-124.
313. Wieslander, G, Norback, D and Edling, C. Airway symptoms among house painters in relation to exposure to volatile organic compounds (VOCs)--a longitudinal study. *Ann Occup Hyg* 1997b;41:155-166.
314. Wilkins, MR, Sanchez, JC, Gooley, AA, Appel, RD, Humphery-Smith, I, Hochstrasser, DF and Williams, KL. Progress with proteome projects: why all proteins expressed by a genome should be identified and how to do it. *Biotechnol Genet Eng Rev* 1996;13:19-50.
315. Witzmann, F, Lee, K, Wang, M, Yemane, Y and Witten, M. Pulmonary effects of JP-8 jet fuel exposure – Label-free quantitative analysis of protein expression in alveolar type II epithelial cells using LC/MS. *Toxicol Sci* 2007;96:102.
316. Wolters, DA, Washburn, MP and Yates, JR, 3rd. An automated multidimensional protein identification technology for shotgun proteomics. *Anal Chem* 2001;73:5683-5690.
317. Woo, HA, Chae, HZ, Hwang, SC, Yang, KS, Kang, SW, Kim, K and Rhee, SG. Reversing the inactivation of peroxiredoxins caused by cysteine sulfinic acid formation. *Science* 2003;300:653-656.
318. Wood, MA, McMahon, SB and Cole, MD. An ATPase/helicase complex is an essential cofactor for oncogenic transformation by c-Myc. *Mol Cell* 2000;5:321-330.
319. Woods Ignatoski, KM, Grewal, NK, Markwart, SM, Vellaichamy, A, Chinnaiyan, AM, Yeung, K, Ray, ME and Keller, ET. Loss of Raf kinase inhibitory protein induces radioresistance in prostate cancer. *Int J Radiat Oncol Biol Phys* 2008;72:153-160.
320. Wu, HM, Jin, M and Marsh, CB. Toward functional proteomics of alveolar macrophages. *Am J Physiol Lung Cell Mol Physiol* 2005;288:L585-595.
321. Wullner, U, Neef, I, Eller, A, Kleines, M, Tur, MK and Barth, S. Cell-specific induction of apoptosis by rationally designed bivalent aptamer-siRNA transcripts silencing eukaryotic elongation factor 2. *Curr Cancer Drug Targets* 2008;8:554-565.
322. Yang, WP, Hu, BH, Chen, GD, Bielefeld, EC and Henderson, D. Protective effect of N-acetyl-L-cysteine (L-NAC) against styrene-induced cochlear injuries. *Acta Otolaryngol* 2008;1-8.
323. Yang, YH, Xi, ZG, Chao, FH and Yang, DF. Effects of formaldehyde inhalation on lung of rats. *Biomed Environ Sci* 2005;18:164-168.
324. Yano, CL and Marcondes, MC. Cadmium chloride-induced oxidative stress in skeletal muscle cells in vitro. *Free Radic Biol Med* 2005;39:1378-1384.

325. Yeowell-O'Connell, K, Jin, Z and Rappaport, SM. Determination of albumin and hemoglobin adducts in workers exposed to styrene and styrene oxide. *Cancer Epidemiol Biomarkers Prev* 1996;5:205-215.
326. Young, LC, Campling, BG, Cole, SP, Deeley, RG and Gerlach, JH. Multidrug resistance proteins MRP3, MRP1, and MRP2 in lung cancer: correlation of protein levels with drug response and messenger RNA levels. *Clin Cancer Res* 2001;7:1798-1804.
327. Younis, HS, Parrish, AR and Glenn Sipes, I. The role of hepatocellular oxidative stress in Kupffer cell activation during 1,2-dichlorobenzene-induced hepatotoxicity. *Toxicol Sci* 2003;76:201-211.
328. Yuan, W, Chung, J, Gee, S, Hammock, BD and Zheng, J. Development of polyclonal antibodies for the detection of styrene oxide modified proteins. *Chem Res Toxicol* 2007;20:316-321.
329. Zhang, JY, Wang, Y and Prakash, C. Xenobiotic-metabolizing enzymes in human lung. *Curr Drug Metab* 2006;7:939-948.
330. Zhang, L, McHale, CM, Rothman, N, Li, G, Ji, Z, Vermeulen, R, Hubbard, AE, Ren, X, Shen, M, Rappaport, SM *et al.* Systems biology of human benzene exposure. *Chem Biol Interact* 2010a;184:86-93.
331. Zhang, Z, Huang, L, Zhao, W and Rigas, B. Annexin 1 induced by anti-inflammatory drugs binds to NF-kappaB and inhibits its activation: anticancer effects in vitro and in vivo. *Cancer Res* 2010b;70:2379-2388.
332. Zhu, K, Zhao, J, Lubman, DM, Miller, FR and Barder, TJ. Protein pI shifts due to posttranslational modifications in the separation and characterization of proteins. *Anal Chem* 2005;77:2745-2755.
333. Zolotarjova, N, Martosella, J, Nicol, G, Bailey, J, Boyes, BE and Barrett, WC. Differences among techniques for high-abundant protein depletion. *Proteomics* 2005;5:3304-3313.

8 Appendix

Table 8-1 Mass spectrometric data of identified protein spots of A549 cell line (see map with ID numbers in Figure 3-2)

ID ^a	Identification ^b	Mascot score	MW [Da] ^b	pI ^b	Sequ. cov [%]	Matching peptides	Access. number ^b
1	MCM7 minichromosome maintenance deficient 7	348	81,308	6.08	13	9	A4D2A1
2	Chloride intracellular channel protein 1	461	26,923	5.02	31	12	O00299
3	Eukaryotic translation initiation factor 3	360	37,564*	5.24	28	10	O00303
4	ATP-dependent RNA helicase DDX3X	658	73,243	6.73	20	14	O00571
5	Cytochrome b5 type B	133	16,322	4.88	13	4	O43169
6	Alpha-actinin-4	329	104,854	5.27	30	29	O43707
7	Alpha-actinin-4	328	104,854	5.27	39	35	O43707
8	UDP-glucose 6-dehydrogenase	708	55,024	6.73	27	18	O60701
9	UDP-glucose 6-dehydrogenase	135	55,024	6.73	15	5	O60701
10	WD repeat-containing protein 1	66	66,194	6.17	17	6	O75083
11	WD repeat-containing protein 1	108	66,194	6.17	19	7	O75083
12	Acyl-protein thioesterase 1	130	24,670	6.05	14	3	O75608
13	Isocitrate dehydrogenase (NADP)	640	46,659	6.53	35	15	O75874
14	Isocitrate dehydrogenase (NADP)	969	46,659	6.19	43	27	O75874
15	Glutaredoxin-3	248	37,432*	5.25	16	5	O76003
16	Glutaredoxin-3	172	37,432*	5.25	14	4	O76003
17	6-phosphogluconolactonase	249	27,547	5.70	27	6	O95336
18	L-lactate dehydrogenase A chain	101	36,689	8.46	26	13	P00338
19	Retinal dehydrogenase 1	322	54,862	6.29	29	15	P00352
20	Retinal dehydrogenase 1	325	54,862	6.29	29	15	P00352
21	Retinal dehydrogenase 1	844	54,862	6.29	33	20	P00352
22	Superoxide dismutase [Cu-Zn]	230	15,936	5.70	30	8	P00441
23	Phosphoglycerate kinase 1	1,073	44,615	8.30	48	30	P00558
24	Lamin A/C isoform 2	794	65,153	6.40	32	18	P02545
25	Lamin A/C isoform 1	841	74,139	6.57	29	21	P02545
26	Lamin A/C isoform 2	1,161	65,153	6.40	34	29	P02545
27	Lamin A/C isoform 1	501	74,139	6.57	16	10	P02545
28	Lamin A/C isoform 2	562	65,153	6.40	20	13	P02545
29	Catalase	881	59,756	6.95	31	19	P04040
30	Fructose-bisphosphate aldolase	789	39,420	8.30	36	26	P04075
31	Annexin A1	469	38,714	6.64	28	12	P04083
32	Annexin A1	815	38,714	6.64	38	23	P04083
33	Ornithine aminotransferase, OAT	432	48,535	6.39	22	11	P04181
34	Glyceraldehy.-3-phosph. Dehydrogen.	158	36,053	8.58	38	11	P04406
35	Glyceraldehy.-3-phosph. Dehydrogen.	456	36,053	8.58	38	16	P04406
36	Heat shock protein beta-1	232	22,783	5.98*	19	5	P04792
37	60S acidic ribosomal protein P0	390	34,274	5.71*	26	9	P05388
38	Vimentin	343	53,652	5.06*	55	24	P08670
39	Gelsolin precursor	290	85,698	5.90*	7	6	P06396
40	Alpha-enolase	464	47,169	6.99	19	10	P06733
41	Alpha-enolase	682	47,169	6.99	32	17	P06733
42	Alpha-enolase	437	47,169	6.99	20	12	P06733
43	Alpha-enolase	894	47,169	6.99	41	18	P06733
44	Alpha-enolase	850	47,169	6.99	42	26	P06733
45	Nucleophosmin	263	32,575*	4.67	29	10	P06748
46	Tropomyosin alpha-3 chain	81	32,819	4.68	17	5	P06753
47	L-lactate dehydrogenase B chain	498	36,638	5.71	31	13	P07195
48	L-lactate dehydrogenase B chain	278	36,638	5.71	17	5	P07195
49	L-lactate dehydrogenase B chain	365	36,638	5.71	27	10	P07195
50	L-lactate dehydrogenase B chain	585	36,638	5.71	37	16	P07195

Appendix

51	L-lactate dehydrogenase B chain	605	36,638	5.71	38	13	P07195
52	Protein disulfide-isomerase precursor	611	57,116*	4.76	31	22	P07237
53	Tubulin beta chain	583	49,671	4.78	57	37	P07437
54	Tubulin beta chain	577	49,671	4.78	52	36	P07437
55	Heat shock protein HSP 90-alpha	1,338	84,660	4.94	32	32	P07900
56	Heterogeneous nuclear Ribonucleoprotein C1/C2	223	33,670*	4.95	16	6	P07910
57	Laminin subunit beta-1 [Precursor]	1,108	66,653	4.70	38	27	P07942
58	Heat shock 70 kDa protein 1	728	70,052	5.48	30	23	P08107
59	Vimentin	662	53,652	5.06	40	21	P08670
60	Vimentin	1,075	53,652	5.06	45	25	P08670
61	Keratin, type II cytoskeletal 7	406	51,418	5.50	41	20	P08729
62	Keratin, type II cytoskeletal 7	133	51,418	5.50	20	7	P08729
63	Annexin A5	734	35,937	4.94	47	21	P08758
64	40S ribosomal protein SA	712	32,854*	4.79	46	13	P08865
65	Glutathione S-transferase P	212	23,356	5.43	31	6	P09211
66	Glutathione S-transferase P	622	23,356	5.43	50	20	P09211
67	Annexin A4	903	35,883*	5.85	46	19	P09525
68	Annexin A4	425	35,883*	5.85	26	10	P09525
69	Annexin A4	830	35,883*	5.85	52	28	P09525
70	Annexin A4	866	35,883*	5.85	37	17	P09525
71	Small nuclear ribonucleoprotein polypeptide A	393	28,512	8.72*	33	9	P09661
72	Leukotriene A4 hydrolase	639	69,285	5.80	26	18	P09960
73	60 kDa heat shock protein	1,220	61,055	5.70*	40	30	P10809
74	60 kDa heat shock protein	924	61,055	5.70*	35	22	P10809
75	Pyruvate dehydrogenase E1 subunit beta	364	36,807	5.38	24	7	P11177
76	Glycogen phosphorylase	626	96,696	6.26	16	16	P11216
77	Glucose-6-phosphate 1-dehydrogenase	753	59,257	6.39	34	20	P11413
78	C-1-tetrahydrofolate synthase	223	101,559	6.94	32	27	P11586
79	C-1-tetrahydrofolate synthase	176	101,559	6.94	25	22	P11586
80	Annexin A3	790	36,375*	5.63	42	20	P12429
81	Xaa-Pro dipeptidase	463	54,548	5.64	21	11	P12955
82	ATP-dependent DNA helicase 2 subunit 1	809	69,843	6.23	35	21	P12956
83	ATP-dependent DNA helicase 2 subunit 1	439	69,843	6.23	16	12	P12956
84	ATP-dependent DNA helicase 2 subunit 2	475	82,705	5.55	16	13	P13010
85	ATP-dependent DNA helicase 2 subunit 2	429	82,705	5.55	16	13	P13010
86	Elongation factor 2	957	95,338	6.42	30	31	P13639
87	Electron transfer flavoprotein subunit alpha	136	35,080	8.62*	9	2	P13804
88	Electron transfer flavoprotein subunit alpha	186	35,080	8.62*	15	4	P13804
89	Alcohol dehydrogenase [NADP+]	615	36,573*	6.32	44	18	P14550
90	Pyruvate kinase isozymes M1/M2	154	57,937	7.95	21	11	P14618
91	Pyruvate kinase isozymes M1/M2	1,383	57,937	7.95	55	34	P14618
92	Pyruvate kinase isozymes M1/M2	938	57,937	7.95	38	23	P14618
93	Aldose reductase	352	35,853	6.52	18	9	P15121
94	Ezrin	574	69,413*	5.94	19	14	P15311
95	Ezrin	707	69,413*	5.94	26	19	P15311
96	Ezrin	901	69,413*	5.94	30	23	P15311
97	NAD(P)H dehydrogenase [quinone] 1	317	30,868	8.91	25	11	P15559
98	Vinculin	1,490	123,799	5.51	26	29	P18206
99	Phosphoglycerate mutase 1	296	28,804	6.75	21	7	P18669
100	Voltage-depend. anion-selective channel protein 1	427	30,773	8.62	25	8	P21796
101	Voltage-depend. anion-selective channel protein 1	144	30,773	8.62	47	9	P21796
102	Protein-glutamine gamma-glutamyltransferase 2	698	77,329*	5.11	24	20	P21980
103	Heterogeneous nuclear ribonucleoproteins A2/B1	121	37,430	8.97	34	12	P22626
104	Thioredoxin reductase 1 isoform 5	602	54,754	6.07	40	17	Q16881
105	Cofilin-1	136	18,502	8.26	53	9	P23528
106	ATP synthase subunit alpha, mitochondrial	462	59,751	9.07	15	11	P25705
107	Proteasome alpha 1 subunit isoform 2	742	29,556	6.15	58	24	P25786
108	Proteasome subunit alpha type-2	194	25,899	6.92	26	4	P25787
109	Moesin	707	67,820	6.09	26	19	P26038

Appendix

110	NADH-ubiquinone oxidoreductase 75 kDa subunit	538	79,468	5.89	16	13	P28331
111	Transketolase	236	67,878	7.58	29	14	P29401
112	Transketolase	546	67,878	7.58	24	18	P29401
113	Transketolase	451	67,878	7.58	40	25	P29401
114	Endoplasmic reticulum protein ERp29 precursor	104	28,993	6.77*	15	4	P30040
115	Peroxioredoxin 6	528	25,035	6.00	48	12	P30041
116	60S ribosomal protein L12	665	17,819	9.40*	71	18	P30050
117	Thioredoxin-dependent peroxide reductase	288	27,693*	7.67*	26	4	P30048
118	Phosphatidylethanolamine-binding protein 1	65	21,057	7.10	22	3	P30086
119	Protein disulfide-isomerase A3	476	56,782	5.98*	24	15	P30101
120	Protein disulfide-isomerase A3	996	56,782	5.98*	42	25	P30101
121	Protein disulfide-isomerase A3	114	56,782	5.98*	7	3	P30101
122	Aldehyde dehydrogen., dimeric NADP-preferring	358	50,379	5.99	21	12	P30838
123	Aldehyde dehydrogen., dimeric NADP-preferring	810	50,379	5.99	37	20	P30838
124	Succinate dehydrogenase flavoprotein	152	72,692*	7.06*	20	9	P31040
125	Cytochrome b-c1 complex subunit 1, mitochondrial	317	52,646	5.94*	13	7	P31930
126	Heterogeneous nuclear ribonucleoprotein H	236	49,229	5.89	14	5	P31943
127	14-3-3 protein beta/alpha	460	28,082	4.76	40	14	P31946
128	Kinesin-1 heavy chain	208	109,685	6.12	4	4	P33176
129	Kinesin-1 heavy chain	163	109,685	6.12	2	3	P33176
130	Prohibitin	117	29,804	5.57	23	5	P35232
131	Prohibitin	263	29,804	5.57*	40	8	P35232
132	26S protease regulatory subunit 7	1,334	48,634	5.72	35	27	P35998
133	Transaldolase	634	37,540	6.35	35	15	P37837
134	Electron transfer flavoprotein subunit beta	572	27,844	8.29	44	15	P38117
135	Stress-70 protein, mitochondrial	444	73,680	6.03*	17	12	P38646
136	Stress-70 protein, mitochondrial	1,332	73,680	6.03*	45	40	P38646
137	Eukaryotic initiation factor 4A-III	100	46,871	6.30	16	6	P38919
138	Eukaryotic initiation factor 4A-III	703	46,871	6.30	38	18	P38919
139	Macrophage capping protein	149	38,518	5.88	12	3	P40121
140	T-complex protein 1 subunit zeta	138	58,024	6.25	36	21	P40227
141	Malate dehydrogenase, cytoplasmic	477	36,426	6.91*	27	10	P40925
142	Glycyl-tRNA synthetase	158	83,140	5.88	6	5	P41250
143	Glycyl-tRNA synthetase	354	83,140	5.88	11	8	P41250
144	Glycyl-tRNA synthetase	265	83,140	5.88	5	5	P41250
145	Glycyl-tRNA synthetase	657	83,140	5.88	34	18	P41250
146	Aldo-keto reductase family 1 member C3	222	36,844	8.05	20	8	P42330
147	Leucine-rich PPR motif-containing protein	581	157,905	5.81	8	15	P42704
148	Matrin-3	119	94,623*	5.87	2	2	P43243
149	Voltage-depend. anion-selective channel protein 2	396	31,567	8.00	34	9	P45880
150	60S ribosomal protein L5	416	34,363	9.70*	33	13	P46777
151	Cytosolic NADP(+)-dependent malic enzyme	346	64,150	5.88	16	10	P48163
152	Glutathione synthetase	639	52,385	5.67	29	17	P48637
153	Elongation factor Tu	750	49,542	7.26	36	18	P49411
154	Elongation factor Tu	861	49,542	7.26	37	20	P49411
155	Seryl-tRNA synthetase	268	59,226	6.05*	10	8	P49591
156	Seryl-tRNA synthetase	306	59,226	6.05*	14	8	P49591
157	Proteasome subunit beta type-3	138	22,949	6.14	11	2	P49720
158	Isocitrate dehydrogenase	481	39,592	5.71*	26	16	P50213
159	T-complex protein 1 subunit theta	989	59,621	5.42	36	21	P50990
160	T-complex protein 1 subunit theta	1,069	59,621	5.42	40	25	P50990
161	6-phosphogluconate dehydrogen., decarboxylating	316	53,140*	6.88	18	9	P52209
162	6-phosphogluconate dehydrogen., decarboxylating	234	53,140*	6.88	32	16	P52209
163	Aldo-keto reductase family 1 member C2	226	36,735	7.13	13	7	P52895
164	Aldo-keto reductase family 1 member C2	400	36,735	7.13	18	11	P52895
165	Biliverdin reductase A	229	33,428	6.06	15	4	P53004
166	ATP-citrate synthase	928	120,839	6.95	18	22	P53396
167	ATP-citrate synthase	899	120,839	6.95	15	19	P53396
168	ATP-citrate synthase	604	120,839	6.95	11	13	P53396

Appendix

169	Transitional endoplasmic reticulum ATPase	240	89,322	5.14	42	26	P55072
170	Triosephosphate isomerase	97	26,669	6.51	31	7	P60174
171	Triosephosphate isomerase	753	26,669	6.51	56	17	P60174
172	Dextrin isoform a	533	18,506	8.06	53	16	P60981
173	Chain A, Crystal Structure Of 14-3-3 Gamma	162	28,303	4.80	15	4	P61981
174	GTP-binding nuclear protein Ran	128	24,423	7.20	50	12	P62826
175	Peptidyl-prolyl cis-trans isomerase A	258	18,012	7.68	31	8	P62937
176	Translation initiation factor eIF-5A	271	16,832	5.08	37	8	P63241
177	Actin, cytoplasmic 2	292	41,793	5.31	19	7	P63261
178	Tropomyosin alpha-4 chain	113	28,522	4.67	34	9	P67936
179	Elongation factor 1-alpha 1	63	50,141	9.10	4	2	P68104
180	T-complex protein 1 subunit beta	737	57,488*	6.02	29	18	P78371
181	Protein SET	451	33,489*	4.12	29	9	Q01105
182	Lamin B2	948	67,689	5.29	27	9	Q03252
183	Aldo-keto reductase family 1 member C1	309	36,788	8.02	20	17	Q04828
184	Peroxiredoxin-1	182	22,110	8.27	19	5	Q06830
185	Peroxiredoxin-1	449	22,110	8.27	52	13	Q06830
186	Peroxiredoxin-1	382	22,110	8.27	49	12	Q06830
187	Peroxiredoxin-1	704	22,110	8.27	58	24	Q06830
188	Complement compon. 1 Q subcompon.-bind. Prot.	345	31,362	4.32	32	8	Q07021
189	Splicing factor, arginine/serine-rich 1 isoform 2	275	31,899	5.61	21	5	Q07955
190	Peroxiredoxin-4	389	30,540	5.86	29	9	Q13162
191	Heterogeneous nuclear ribonucleoprotein D isof. a	262	38,434*	7.62	13	6	Q14103
192	Neutral alpha-glucosidase AB	1,298	106,874	5.71	25	37	Q14697
193	Septin-2	159	41,487	6.15	9	4	Q15019
194	Lysyl-tRNA synthetase	436	68,048	5.94	19	15	Q15046
195	Platelet-activat. factor acetylhydrolase IB subun. γ	299	25,734	6.33	35	9	Q15102
196	Reticulocalbin 1 precursor	464	38,890*	4.83	22	10	Q15293
197	Dihydropyrimidinase-like 2	457	62,294	5.95*	19	10	Q16555
198	Thiosulfate sulfurtransferase	131	33,429	6.77	25	6	Q16762
199	Mitochondrial inner membrane protein	1,005	83,678	6.08	28	33	Q16891
200	HSPA5 protein	1,437	72,422	5.07	44	37	Q2KHP4
201	Heat shock 70kDa protein 4	269	94,381	5.11	12	9	P34932
202	Glyceraldehyde 3-phosphate dehydrogenase	324	36,049	8.57*	19	9	Q2TSD0
203	Eukaryotic translation initiation factor 4B	123	69,151*	5.49	6	3	P23588
204	ACLY variant protein	587	124,557	8.24	9	11	Q4LE36
205	Putative uncharacterized protein UCHL1	344	24,824	5.33	43	11	Q4W5K6
206	Proteasome 26S non-ATPase subunit 11	615	47,535	6.08	30	13	Q53FT5
207	Calreticulin variant	287	46,919*	4.30	16	11	Q53G71
208	Tumor rejection antigen	719	65,953	5.08	22	21	Q59FC6
209	Tumor rejection antigen	1,368	92,340*	4.77	31	33	Q5CAQ5
210	Carbamoylphosphate synthetase I	899	164,907	6.30	13	22	Q5R208
211	Annexin A7	582	50,316	6.25	32	14	P20073
212	Heterogeneous nuclear ribonucleoprotein K	605	47,557	5.46	27	13	Q5T6W5
213	Tumor protein	149	21,526	5.34*	20	4	Q5W0H4
214	IDH1 protein	336	46,659	6.53	21	10	Q6FHQ6
215	Putative riboflavin biosynthesis protein	605	36,719	7.12	42	19	Q6GHG3
216	GDI2 protein	548	50,663	6.10	32	17	Q6IAT1
217	GDI2 protein	647	50,663	6.10	40	19	Q6IAT1
218	HNRPH1 protein	405	49,229	5.79	19	9	Q6IBM4
219	PDCD6IP protein	1,081	96,023*	6.13	26	26	Q8WUM4
220	Beta-actin	520	41,737	5.29	32	14	P60709
221	Importin 5	510	125,588	4.80	11	12	Q86XC7
222	Nucleoside diphosphate kinase	345	19,654	5.42	36	8	Q86XQ2
223	Elongation factor 2b	132	58,148*	6.51	5	2	Q8TA90
224	Annexin A2	725	38,576	7.57*	39	16	Q8TBV2
225	Annexin A2	975	38,576	7.57	52	32	Q8TBV2
226	ATP-dependent RNA helicase DDX1	573	82,432*	7.97	13	12	Q92499
227	DJ-1 protein	517	19,891	6.33	44	14	Q99497

Appendix

228	DJ-1 protein	410	19,891	6.33	36	9	Q99497
229	Synapt. vesicle membr. Prot. VAT-1	533	41,920	5.88	27	11	Q99536
230	3-Hydroxyacyl-CoA dehydrogen.type-2	730	26,923	7.86	55	14	Q99714
231	Protein arginine N-methyltransferase 1	224	41,516	5.46	14	5	Q99873
232	Acetyl-CoA acetyltransf., cytosolic	222	41,351	6.27	14	7	Q9BWD1
233	Aminopeptidase B	493	72,596	5.51	27	16	Q9H4A4
234	Adipocyte plasma membr.-associat. Prot.	454	46,480	5.78	18	10	Q9HDC9
235	Septin 11	448	49,398	6.36	24	12	Q9NVA2
236	Pyridoxine 5'-phosphate oxidase	224	29,988	6.62	9	2	Q9NVS9
237	2-Oxoglutarate dehydrog. E1 compon.	385	115,935	6.40	8	9	Q02218
238	Protein disulfide-isomerase A3	226	56,640	5.80	10	5	Q9UHG3
239	Prenylcysteine oxidase 1	416	56,640	5.80	16	12	Q9UHG3
240	Stomatin-like protein 2	97	38,534	5.80	32	6	Q9UJZ1
241	Pre-mRNA-processing factor 19	204	55,181	6.14	10	5	Q9UMS4
242	Heat shock protein 70 kDa	1,052	70,898	5.37	32	27	P11142
243	Ribosomal protein S3a	401	29,975	9.74*	40	14	Q6NXR8
244	60S ribosomal protein L5	358	34,363	9.70*	36	13	P46777
245	Thioredoxin reductase 1 isoform 5	211	54,754	6.07	9	5	Q16881
246	Poly(rC)-binding protein	296	37,498	6.66	20	6	Q15365
247	Proteasome subunit beta type-2	254	22,836	6.51	34	8	P49721
248	Flavin reductase	213	22,119	7.13	25	6	P30043
249	Flavin reductase	242	22,119	7.13	39	10	P30043
250	Phosphatidylethanolamine-bind. Prot. 1	266	21,057	7.01	31	5	P30086
251	Proteasome subunit beta type-1	208	26,489	7.77	31	5	P20618
252	Transgelin-2	434	22,391	8.40	40	17	P37802
253	Moesin	130	67,820	6.08	12	7	P26038
254	Actin, cytoplasmic 1	155	41,737	5.29	32	8	P60709
255	Elongation factor 1-delta	155	31,122*	4.9	33	9	P29692
256	Proliferating cell nuclear antigen	174	28,769*	4.57	20	6	P12004
257	Retinal dehydrogenase 1	578	54,862	6.30	25	16	P00352
258	G-rich sequence factor 1	66	53,126	5.67	5	2	Q12849
259	Elongation factor 1-alpha 1	248	50,141	9.10*	7	12	P68104
260	Elongation factor 1-alpha 1	115	50,141	9.10*	4	12	P68104
261	Elongation factor 1-alpha 1	315	50,141	9.10*	9	16	P68104
262	Protein disulfide-isomerase A6	423	48,121	4.95	21	11	Q15084
263	Tropomyosin alpha-1	673	32,709	4.69	45	40	P09493
264	Peroxisredoxin-1	557	22,110*	8.27	71	27	Q06830
265	Heterog. Nucl. Ribonucleoprot. C1/C2	776	33,670	4.95	40	35	P07910
266	Guanine nucleot.-bind. Prot. subunit b-2-like 1	732	35,511	7.57	45	20	P63244

a) Spot ID from figure 2A

b) ^b Values taken from UniProtKB/TrEMBL database

* Experimental mass or pI values differ from values on UniProtKB/TrEMBL database. Posttranslational modifications especially known (www.uniprot.org) and predicted (NetPhos (Blom *et al.*, 1999)) phosphorylations could possibly explain the pI shift for ID38, ID71, ID150, ID243, ID244, ID259-61

Experimental difference in pI as noticed in this study was already published for database entries of ID73,

ID74 ID119-21 (Zhu *et al.*, 1999). Molecular weight and/or pI shifts for spots ID104, ID245, ID189 indicate occurrence of specific isoforms and was confirmed by peptide mass fingerprint analysis.

Table 8-2 Mass spectrometric data of identified phosphoprotein spots of A549 cell line following styrene treatment.

Spot	Identification ^b	Mascot score	MW [Da] ^a	pI ^a	Sequ. Cov [%]	Match . pept.	Access. Number ^a
P1	DNA damage-binding protein 1	439	126,887	5.14	9	12	Q16531
P2	Heat shock 70 kDa protein 4	1,587	94,271	5.11	44	41	P34932
P3	Isocitrate dehydrogenase [NADP] cytoplasmic	464	46,639	6.53	31	13	O75874
P4	ATP-dependent DNA helicase 2 subunit 2	194	82,652	5.55	8	6	P13010
P5	Protein disulfide-isomerase	1,389	57,081	4.76	51	55	P07237
P6	UDP-glucose 6-dehydrogenase	429	54,989	6.72	20	11	O60701
P7	Vimentin	998	53,619	5.06	45	20	P08670
P8	Thioredoxin domain-containing protein 5	292	47,599	5.63	14	6	Q8NBS9
P9	RuvB-like 2	180	51,125	5.49	10	4	Q9Y230
P10	Actin, cytoplasmic 1	887	41,710	5.29	52	27	P60709
P11	40S ribosomal protein SA	324	32,833	4.79	25	7	P08865
P12	ATP-citrate synthase	1,350	120,762	6.95	26	29	P53396
P13	Glyceraldehyde-3-phosphate dehydrogenase	342	36,030	8.58	15	9	P04406
P14	Mitochondrial-process. peptidase subunit beta	401	54,331	6.38	19	11	O75439
P15	Heterogen. nuclear ribonucleoproteins C1/C2	559	33,650	4.95	28	12	P07910
P16	Heterogen. nuclear ribonucleoproteins C1/C2	208	33,650	4.95	15	8	P07910
P17	NIF3-like protein 1	206	41,942	6.19	9	3	Q9GZT8
P18	Proliferating cell nuclear antigen	750	28,750	4.57	52	38	P12004
P19	14-3-3 protein epsilon	346	29,155	4.63	34	11	P62258
P20	14-3-3 protein theta	148	27,747	4.68	13	3	P27348
P21	Proteasome subunit alpha type-3	423	28,415	5.19	25	11	P25788
P22	Programmed cell death 6-interacting protein	253	65,963	6.14	12	5	Q8WUM4
P23	Aspartate aminotransferase, cytoplasmic	664	46,219	6.52	35	16	P17174
P24	Aldo-keto reductase family 1 member B10	439	35,998	7.12	21	9	O60218
P25	Ras-related protein Rab-2A	207	23,531	6.08	25	4	P61019
P26	40S ribosomal protein S7	228	22,113	10.09	23	6	P62081
P27	Alpha-enolase	249	47,139	7.01	16	6	P06733
P28	Transaldolase	93	37,516	6.36	7	2	P37837

a) Values taken from UniProtKB/TrEMBL database

Table 8-3 Mass spectrometric data of identified phosphoprotein spots of A549 cell line following treatment with chlorinated benzenes.

Spot	Identification ^b	Mascot score	MW [Da] ^a	pI ^a	Sequ. Cov [%]	Match . pept.	Access. Number ^a
A	Aldehyde dehydrogenase	565	50,378	6.11	31	7	P30838
B	Adenosylhomocysteinase	784	47,584	5.92	45	14	P23526
C	Ser.-threon. kinase recept.-assoc. prot.	373	38,438	4.98	51	5	Q9Y3F4
D	Transaldolase	559	37,540	6.36	40	11	P37837
E	Transaldolase	474	37,540	6.36	35	7	P37837
F	L-lactate dehydrogenase B chain	498	36,900	5.71	31	13	P07195
G	L-lactate dehydrogenase B chain	365	36,900	5.71	27	10	P07195
H	L-lactate dehydrogenase B chain	605	36,900	5.71	38	13	P07195
I	Translationally-controlled tumor protein	175	19,595	4.84	30	5	P13693
J	Proliferating cell nuclear antigen	399	28,768	4.57	46	10	P12004
K	Serpin B6	373	42,621	5.18	39	9	P35237
L	Heterog. nuclear ribonucleoprot. C1/C2	197	33,538	4.95	26	7	P07910
M	Aldo-keto red. family 1 member B10	853	36,020	7.12	68	5	O60218
N	Translationally-controlled tumor protein	145	19,595	4.84	23	3	P13693
O	Cytochrome b5 type B	187	15,354	5.07	27	3	O43169
P	Calreticulin	649	46,466	4.29	52	12	P27797
Q	Alpha-enolase	408	47,037	6.99	45	9	P06733
R	Annexin A5	240	35,805	4.94	44	3	P08758
S	Elongation factor 1-alpha 1	315	50,900	9.10	9	5	P68104
T	Actin, cytoplasmic	666	41,736	5.29	49	9	P60709
U	Tubulin beta chain	156	49,670	4.78	34	7	P07437
V	Tubulin beta chain	1,718	49,670	4.78	71	25	P07437
W	Tubulin beta chain	372	49,670	4.78	47	7	P07437

a) Values taken from UniProtKB/TrEMBL database

Table 8-4 Gene names and corresponding protein names

Gene name	Protein	Gene name	Protein
ACTB	Actin, cytoplasmic 1	MUTED	Thioredoxin domain-containing protein 5
ACTG1	Actin, cytoplasmic 2	NDUFS1	NADH-ubiquinone oxidoreductase
AHCY	Adenosylhomocysteinase	NIF3L1	NIF3-like protein 1
AKR1B1	Aldose reductase	NME1	Nucleoside diphosphate kinase B
AKR1B10	Aldo-keto reductase 1 B10	NPM1	Nucleophosmin
AKR1C2	Aldo-keto reductase family 1 C2	OGDH	2-oxoglutarate dehydrog. E1
ALDH1A1	Retinal dehydrogenase 1	PARK7	Protein DJ-1
ALDH3A1	Aldehyde dehydrogenase,	PCNA	Proliferating cell nuclear antigen
ANXA1	Annexin A1	PDCD6IP	Programmed cell death 6-interacting protein
ANXA2	Annexin A2	PDIA3	Protein disulfide-isomerase A3 precursor
ANXA4	Annexin A4	PEBP1	Phosphatidylethanolamine-binding protein 1
ANXA5	Annexin A5	PGD	6-phosphogluconate dehydrogenase
ANXA7	Annexin A7	PGK1	Phosphoglycerate kinase 1
ATP5A1	ATP synthase alpha	PHB	Prohibitin
BLVRA	Biliverdin reductase	PMPCB	Mitochondrial-process. peptid. subunit beta
CALR	Calreticulin	PRDX1	Peroxiredoxin-1
CCT2	T-complex protein 1 subunit beta	PRDX3	Thioredoxin-dependent peroxide reductase
CCT8	T-complex protein 1 subunit theta	PRDX4	Peroxiredoxin-4
CFL1	Cofilin-1	PRDX6	Peroxiredoxin-6
CPS1	Carbamoyl-phosphate synthase	PRMT1	Protein arginine N-methyltransferase 1
CYB5B	Cytochrome b5 type B precursor	PRPF19	Pre-mRNA-processing factor 19
DDB1	DNA damage-binding protein 1	PSMA1	Proteasome subunit alpha type 1
EEF1A1	Elongation factor 1-alpha 1	PSMA2	Proteasome subunit alpha type 2
EEF1D	Elongation factor 1-delta	PSMA3	Proteasome subunit alpha type 3
EEF2	Elongation factor 2	PSMD11	26S proteasome non-ATPase subunit 11
EIF4A3	Eukaryotic initiation factor 4A-III	PYGB	Glycogen phosphorylase
EIF4B	Eukaryotic transl. initiation factor 4B	RAB2A	Ras-related protein Rab-2A
EIF5A	Eukary. Transl. initiation fact. 5A-1	RCN1	Reticulocalbin-1
ENO1	Alpha-enolase	RPL12	60S ribosomal protein L12
ENSG00000096238	Chloride intracell. channel protein 1	RPL5	60S ribosomal protein L5
ENSG00000137379	Tubulin beta chain	RPS3A	40S ribosomal protein S3a
ENSG00000198191	Phosphoglycerate mutase 1	RPS7	40S ribosomal protein S7
ERP29	Endoplasmic reticulum protein	RPSA	40S ribosomal protein SA
ETFA	Electron transfer flavoprotein alpha,	RUVBL2	RuvB-like 2
G6PD	Glucose-6-phosphate 1-dehydrog.	SARS	Seryl-tRNA synthetase, cytoplasmic
GANAB	Neutral alpha-glucosidase AB	SDHA	Succinate dehydrogenase [
GAPDH	Glyceraldehyde-3-phosphate dehyd..	SERPINB6	Serpin B6
GARS	Glycyl-tRNA synthetase	SOD1	Superoxide dismutase [Cu-Zn]
GDI2	Rab GDP dissociation inhibitor beta	STRAP	Serine-threo. kinase receptor-assoc. protein
GNB2L1	Guanine nucleot.-bind. Prot. beta 2	TALDO1	Transaldolase
GOT1	Aspartate aminotransferase	TPM1	Tropomyosin-1 alpha chain
GRSF1	G-rich sequence factor 1	TPT1	Translationally-controlled tumor protein
GSN	Gelsolin precursor	TST	Thiosulfate sulfurtransferase
HNRPC	Heterog. Nucl. Ribonucleoprot. C1/C2	TUFM	Elongation factor Tu
HNRPH1	Heterog. Nuclear Ribonucleoprot. H	TXNRD1	Thioredoxin reductase 1, cytoplasmic
HSP90B1	Endoplasmic precursor	UCHL1	Ubiquitin carboxyl-terminal hydrolase L1
HSPA4	Heat shock 70 kDa protein 4	UGDH	UDP-glucose 6-dehydrogenase
HSPA9	Stress-70 protein, mitochondrial	UQCRC1	Ubiquinol-cytochrome-c reduct. complex 1
HSPB1	Heat-shock protein beta-1	VDAC1	Voltage-depend. anion-sel. channel prot. 1
IDH1	Isocitrate dehydrogenase [NADP]	VDAC2	Voltage-depend. anion-sel. channel prot. 2
IDH3A	Isocitrate dehydrogenase [NAD]	VIL2	Ezrin
KIF5B	Kinesin heavy chain	VIM	Vimentin
KRT7	Keratin, type II cytoskeletal 7	WDR1	WD repeat protein 1
LAMB1	Laminin subunit beta-1 precursor	XRCC5	ATP-dependent DNA helicase 2 subunit 2
LDHB	L-lactate dehydrogenase B chain	XRCC6	ATP-dependent DNA helicase 2 subunit 1
LMNA	Lamin-A/C	YWHAE	14-3-3 protein epsilon
MSN	Lamin-B2	YWHAQ	14-3-3 protein theta

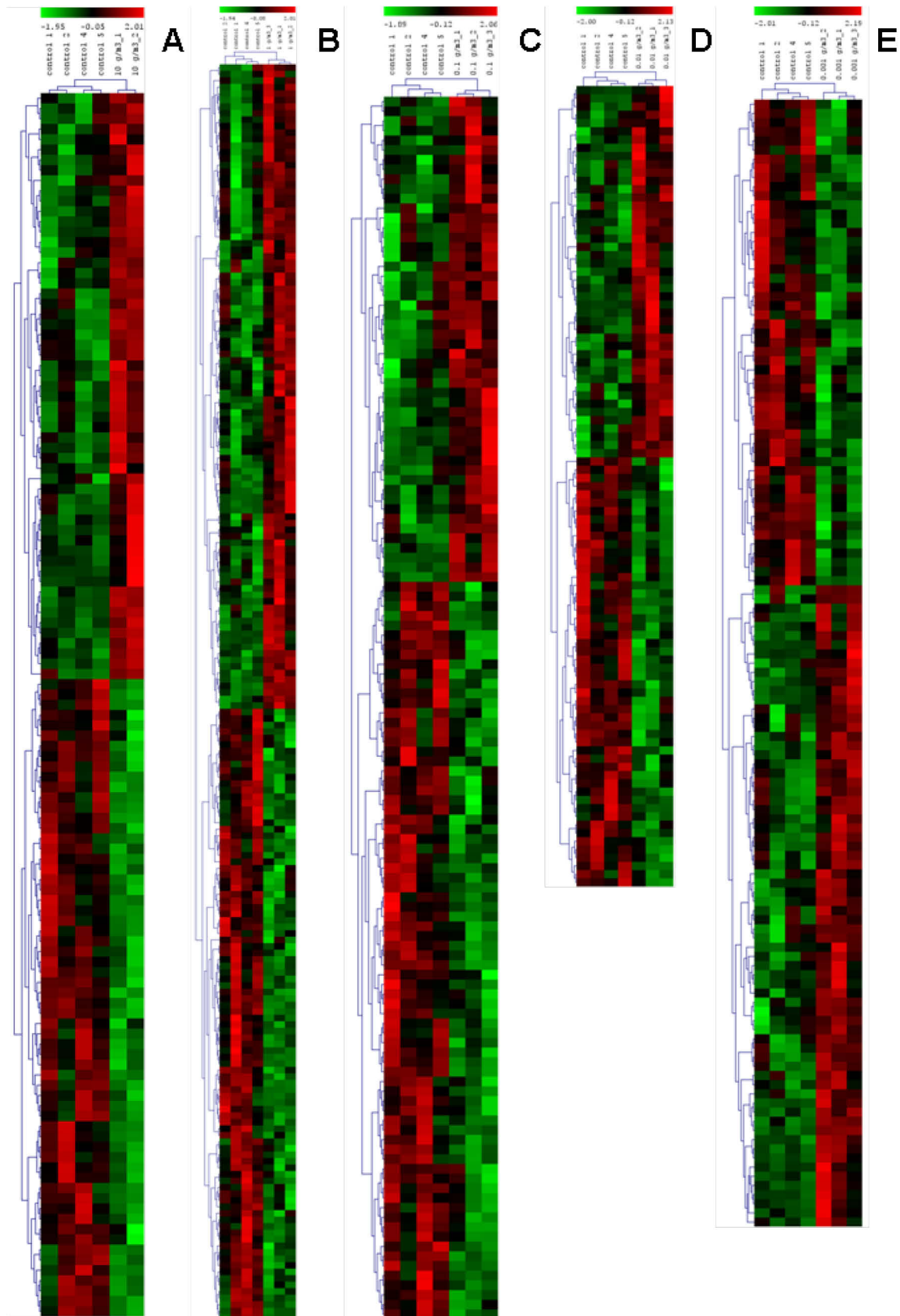


Figure 8-1 Unsupervised clustering illustrating differential protein expression following exposure to styrene. The figure exhibits close-ups of a dendrogram using Delta 2D 3.6 software's integrated statistical tool (TIGR). The clustered protein spots are displayed on the y-axis. On the x-axis, 2-4 gel replicates of exposure concentrations 10^1 g/m³ (A), 10^0 g/m³ (B), 10^{-1} g/m³ (C), 10^{-2} g/m³ (D), 10^{-3} g/m³ (E) and 4 controls (left side) are clustered using the settings of "Euclidean distance" and "average linkage".

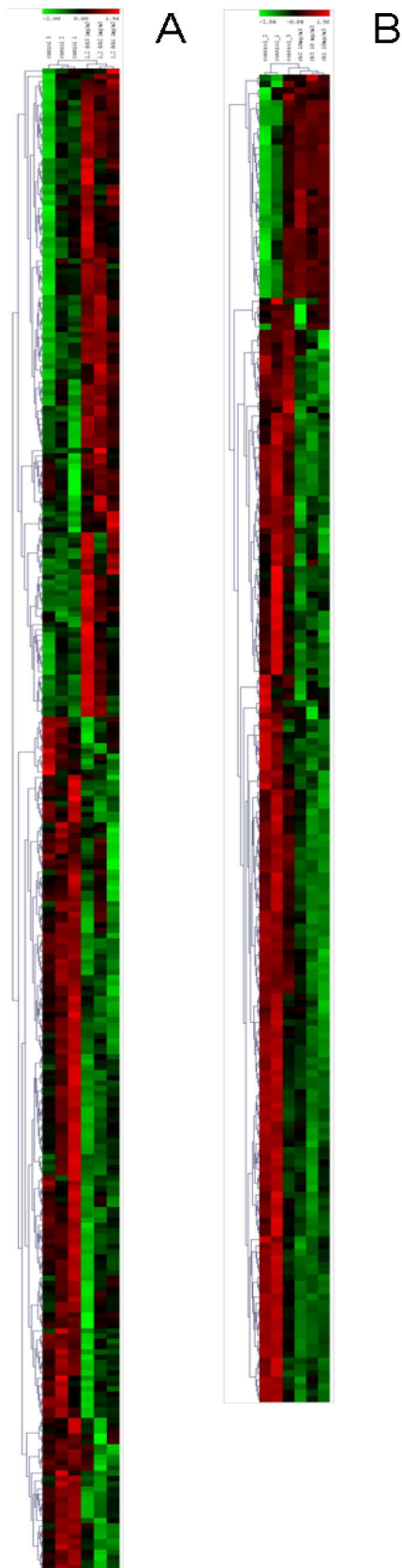


Figure 8-2 Unsupervised clustering illustrating differential protein expression following exposure to chlorinated benzenes. The figure exhibits close-ups of a dendrogram using Delta 2D 3.6 software's integrated statistical tool (TIGR). The clustered protein spots are displayed on the y-axis. On the x-axis, 3 gel replicates of exposure concentrations 10^{-3} g/m^3 1,2-DCB (A) and 10^{-2} g/m^3 CB (B) and controls (left side) are clustered using the settings of "Euclidean distance" and "average linkage".

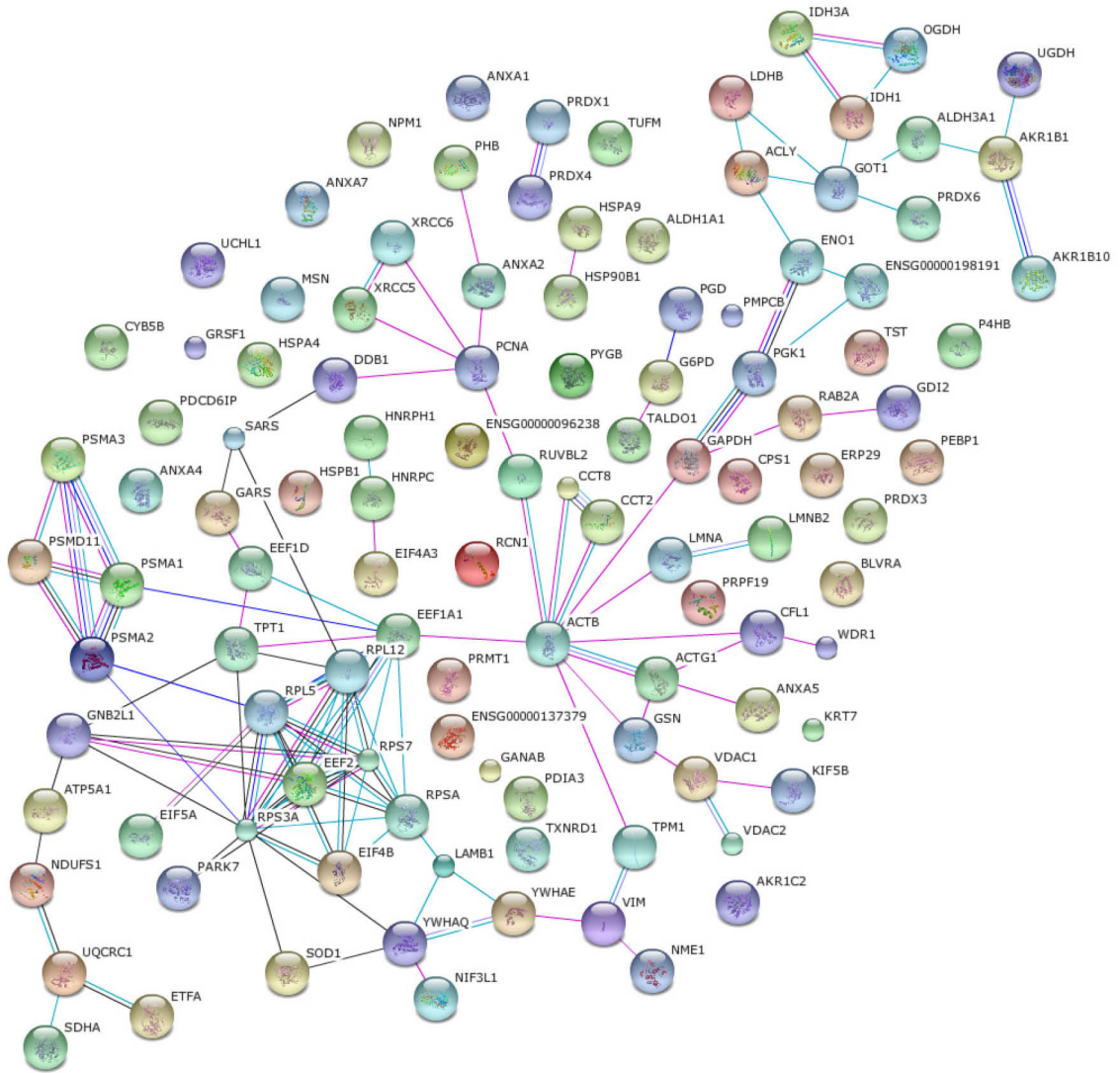


Figure 8-3 Potential protein-protein interactions of differential expressed ($p < 0.1$) protein species (including differential phosphorylations) for styrene treatment of A549 cells suggested by STRING 8.3 database and web resource. UniProt accessions were loaded in the STRING tool (<http://string-db.org/>) and analyzed by using the standard settings (medium confidence, network depth 1, no additional white nodes). The prediction methods “textmining and neighborhood” were excluded. The color of the connecting lines between two protein species encodes the source of the information: experimental data (rose), databases (light blue), coexpression data (black), cooccurrence data (dark blue). Gene names are listed in Table 8-4.

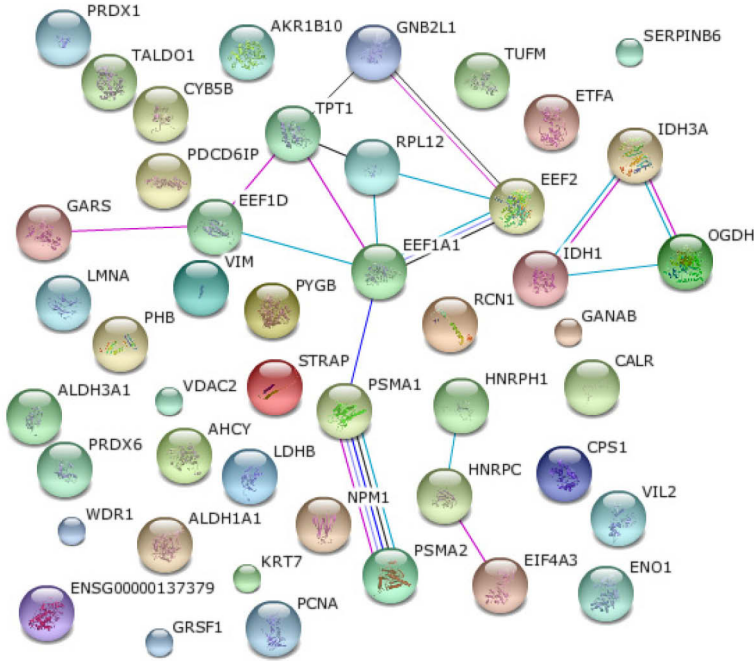


Figure 8-4 Potential protein-protein interactions of differential expressed ($p < 0.1$) protein species (including differential phosphorylations) for mono-chlorobenzene treatment of A549 cells suggested by STRING 8.3 database and web resource. For further details, see legend of Figure 8-3. Gene names are listed in Table 8-4.

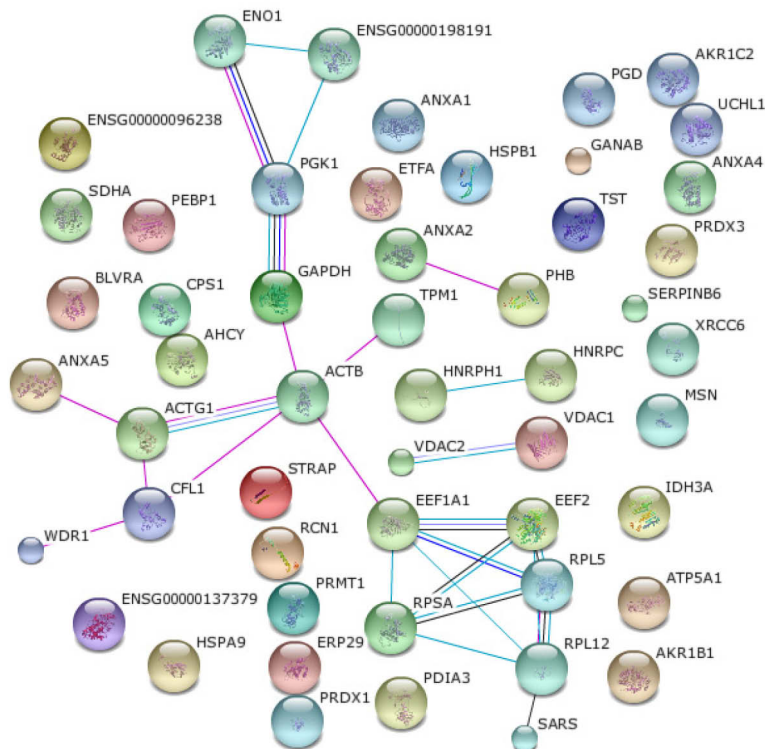


Figure 8-5 Potential protein-protein interactions of differential expressed ($p < 0.1$) protein species (including differential phosphorylations) for 1,2-dichlorobenzene treatment of A549 cells suggested by STRING 8.3 database and web resource. For further details, see legend of Figure 8-3. Gene names are listed in Table 8-4.

Publications and Conference Contributions

PUBLICATIONS

Mörbt N., Feltens R., Tomm J., Kalkhof S., Vogt C., Lehmann I. and von Bergen M. Chlorinated benzenes cause concomitantly oxidative stress and apoptosis in lung epithelial cells (A549) at non acute toxic concentrations. *Submitted*

Mörbt N., Mögel I., Kalkhof S., Feltens R., Röder-Stolinski C., Zheng J., Vogt C., Lehmann I., von Bergen M. Proteome changes in human bronchoalveolar cells following styrene exposure indicate involvement of oxidative stress in the molecular-response mechanism. *Proteomics*. 2009, 9, 4920-4933.

Röder-Stolinski C., Fischäder G., Oostingh G. J., Feltens R., Kohse F., von Bergen M., Mörbt N., Eder K., Duschl A., Lehmann I. Styrene induces an inflammatory response in human lung epithelial cells *via* oxidative stress and NF-kappa B activation. *Toxicol. Appl. Pharmacol.* 2008, 231, 241–247.

Ullmann K., Reiche K., Mörbt N., Kretzschmar A. K., Tomm J., Verhaegh G., Schalken J., von Bergen M., Horn F., Hackermüller J. miRNAs 130a, 203, and 205 are lost in prostate carcinoma and inhibit androgen receptor trans-activation. *Submitted*

CONFERENCE CONTRIBUTIONS

Mörbt N., Röder-Stolinski C., Fischäder G., Lehmann I., von Bergen M. Differential Proteome Analysis Of Human Alveolar Cells Following Styrene Exposure Research Festival Leipzig, 2007, Poster prize Category Cell Biology

Mörbt N., Röder-Stolinski C., Fischäder G., Feltens R., Lehmann I., von Bergen M. Indoor air exposure of volatile organic compounds on human alveolar cells 17th Annual HUPO World Congress, Amsterdam, 2008

Ullmann K., Reiche K., Kretzschmar A., Mörbt N., Tomm J., von Bergen M., Verhaegh G., Schalken G., Horn F., Hackermüller J. MicroRNAs lost during prostate carcinoma pathogenesis cooperatively regulate mRNAs and expression of proteins involved in Androgen Receptor signaling. 14th Annual Meeting of the RNA Society 2009

Blumert C., Kalkhof S., Mörbt N., von Bergen M., Horn F. Expanding the STAT3 - protein SILAC network using SILAC.

Ullmann K., Kretzschmar A., Horn F., Schutt K., Mörbt N., von Bergen M., Verhaegh G., Schalken J., Schreiber S., Hackermüller J. MicroRNAs lost during prostate carcinoma pathogenesis cooperatively regulate mRNAs involved in Androgen Receptor signaling. Cambridge University 2009

Erklärung zur Dissertation

Diese Arbeit entstand während meiner Tätigkeit als Doktorandin am Helmholtz-Zentrum für Umweltforschung, Leipzig, im Department Proteomik unter der Leitung von Herrn PD Dr. Martin von Bergen.

Hiermit versichere ich, dass ich die vorliegende Arbeit selbstständig und ausschließlich unter Verwendung der aufgeführten Mittel angefertigt habe. Diese Arbeit wurde bisher an keiner anderen Hochschule eingereicht.

Dresden, den 07.06.2010

Nora Mörbt

Danksagung

An dieser Stelle sei all jenen, die zum Gelingen dieser Arbeit beigetragen haben, ganz herzlich gedankt.

Mein ganz besonderer Dank gilt Herrn Prof. Steinberg sowie Herrn Prof. Püschel.

Meinem Betreuer am Helmholtz-Zentrum in Leipzig, PD Dr. Martin von Bergen möchte ich für die Vergabe des Themas, die Betreuung während der Zeit am UFZ sowie für die Unterstützung meiner Weiterbildung zur Fachtoxikologin danken.

Frau Dr. Irina Lehmann danke ich für die Möglichkeit, die Laborräume und Methoden des Departments Umweltimmunologie zu nutzen.

Dr. Ralph Feltens danke ich für die interessanten wissenschaftlichen Diskussionen, die vielen Tipps und Tricks und das kritische Korrekturlesen dieser Arbeit.

Ein großes Dankeschön geht auch an Dr. Carsten Vogt und Frau Hinke für die freundliche Unterstützung bei den gaschromatographischen Messungen.

Dr. Stefan Kalkhof danke ich herzlich für die Hilfe bei der Identifizierung der Styroloxidproteinaddukte.

Carmen Röder-Stolinski und Iljana Mögel möchte ich für die Unterstützung bei den Styrol-Validierungsexperimenten, Kerstin Krist für die Anleitung bei den QPCR Messungen und Susanne Arnold für die zuverlässige Pflege und Bereitstellung der Zellkulturen danken.

Zudem möchte ich Yvonne Kullnick, Michaela Öhler und Christine Schumann danken, die immer ein Auge auf Ordnung und Sauberkeit im Labor hatten und dafür sorgten, dass alles in ausreichender Menge am rechten Platz zu finden war.

Ein lieber Dank geht auch an Nico, Jayaseelan und Yvonne für gemeinsames Freud' und Leid im täglichen Laboralltag.

Meiner Familie danke ich für die uneingeschränkte Unterstützung während des Studiums und der Promotionszeit.

Lebenslauf

Nora Mörbt

Geboren am 07.02.1981 in Dresden

WEITERBILDUNG

Seit 09/2006 Weiterbildung zur Fachtoxikologin (DGPT)

BERUFLICHER WERDEGANG

seit 08/2009 Wiss. Mitarbeiterin, WALA Heilmittel GmbH, Arzneimittelsicherheit,
Bad Boll

05/2006-07/2009 Doktorandin im Department Proteomik, Helmholtz-Zentrum für
Umweltforschung Leipzig-Halle GmbH, Leipzig

01-03/2006 Wiss. Assistent, Schering AG, Enabling
Technologies/Proteinchemie, Berlin

03-12/2005 Student. Hilfskraft am Deutschen Institut für Ernährungsforschung
(DIfE) in Potsdam, Abteilung Ernährungstoxikologie

HOCHSCHULSTUDIUM

01-12/2005 Diplomarbeit am DIfE, Abteilung Ernährungstoxikologie, Potsdam

10/2000-12/2005 Studium Ernährungswissenschaft an den Universitäten Jena und
Potsdam, Gesamtnote: Sehr gut

01-09/2000 Auslandsaufenthalt, Université de Rouen/Frankreich

STUDIENBEGLEITENDE TÄTIGKEITEN

06-07/2004 Praktikum, Medizinische Akademie, Pädiatrische Hämatologie und
Onkologie/Molekulare Diagnostik, Dresden

02-03/2004 Praktikum in der Abteilung Ernährungstoxikologie des Instituts für
Ernährungswissenschaft der Universität Potsdam

08/2003 Lebensmittelchemisches Praktikum, Landesuntersuchungsamt,
Standort Dresden, Abteilung Bedarfsgegenstände

PREISE/GRANTS

2007 Posterpreis, Cell Biology, Leipziger Research Festival

2007-2009 3 DAAD RISE Sommer-Forschungsstipendien

07/2002-12/2005 Stipendiatin der Friedrich-Ebert-Stiftung

SCHULAUSSBILDUNG

1992-1999 Gymnasiale Ausbildung am Vitzthumgymnasium in Dresden
Gesamtnote: Sehr gut

MITGLIEDSCHAFTEN

Seit 04/2010 Deutsche Gesellschaft für Toxikologie e. V. in der DGPT